

Gas-phase electronic spectroscopy of highly unsaturated hydrocarbons by resonance enhanced multiphoton ionization

Inauguraldissertation

zur Erlangung der Würde eines Doktors der Philosophie vorgelegt der Philosophisch-Naturwissenschaftlichen Fakultät der Universität Basel

von

Andrey E. Boguslavskiy
aus Novosibirsk, Russland

Basel, 2006

Genehmigt von der Philosophisch-Naturwissenschaftlichen Fakultät

auf Antrag von

Prof. Dr. John P. Maier und Prof. Dr. Hanspeter Huber

Basel, den 5. Juli 2006

Prof. Dr. Jakob Wirz

Dekan

Dedicated to my father.

Acknowledgements

I would like to thank Prof. John Maier for giving me the opportunity to work in his group and develop my interest in molecular spectroscopy. I would also like to thank Prof. Hanspeter Huber for his courteous agreement to act as my co-referee and for introducing me into the complicated world of computational chemistry.

During my PhD study I was lucky to meet and work with a whole wealth of very good worthy people. I would like to express my gratitude to Dr. Thomas Pino and Dr. Timothy Schmidt for their guidance and invaluable assistance during the first few years of my study. They showed what it means to be motivated and what is to be smart in science.

I indeed enjoyed the time when Prof. Michael Morse was on his sabbatical in Basel. I am enchanted by his openness and willingness to spend his time thinking on your question. I also haven't yet seen a teacher who would explain scientific concepts so clear and easy to follow.

I am grateful to Dr. Przemyslaw Kolek for giving me feeling and intuition on electronic conjugation. I enjoyed the "periods of peace" with Dr. Hongbin Ding especially while he was not a Dr. yet. Numerous scientifically oriented discussions we had together have a great impact on me.

Of course I cannot forget mentioning Alexey Denisov. I am indebted to him for all time we spend in discussions. The time devoted to scientific topics, especially in the last few years, overwhelms that spent on any other subjects excluding perhaps women.

My special thanks are especially directed to Dr. Evan Johnowitz for his unlimited friendliness, patience, permanent willingness to help, and perfect English.

I am grateful to the mechanical workshop headed with Mr. Dieter Wild for constructing a great piece of experimental equipment.

I express my profound gratitude to Georg Holderied for his extraordinary skills in constructing electronic devices without which our experiment would never even "stand up", let alone to "run". Also I am indebted to him and to Esther Stalder for their guidance through the chaos and confusions of living in foreign country.

Basel, Switzerland
July 5, 2006

Andrey Boguslavskiy

Contents

1	Introduction	5
1.1	Relevance and motivation of the study	6
1.1.1	Diffuse interstellar bands	7
	Formation considerations	12
	Observational constraints	13
	Bibliography	15
2	”Methodology”: Overview of experimental methods	19
2.1	REMPI	20
2.2	TOF mass spectrometer	24
2.3	VUV generation in gases. Background.	28
2.3.1	Introduction	28
2.3.2	Theoretical background	28
	Bibliography	34
3	Experimental	39
3.1	Molecular source	40
3.1.1	Discharge source	40
3.1.2	Ablation source	40
3.2	Vacuum system	42
3.3	Light sources	43
3.4	Ion detection	43
3.5	Data handling	46
	Bibliography	48
4	Spectroscopy of C_{4n+2} carbon rings	50
	Foreword	51
	Introduction	53
	Experiment	53
	Observations	54
	A. Spectra	54
	B. Bandwidths	54
	C. Rotational and vibrational cooling	55
	Ab-initio calculations	56
	Discussion	57

A. Isomer structure	57
B. Electronic transitions	57
1. C ₁₈	57
2. C ₂₂	58
Astrophysical implications	58
References	58
Gas-phase electronic spectroscopy of the C ₁₄ ring	60
Bibliography	63
5 VUV generation in gases for the benefit of REMPI	64
5.1 Implementation of Resonant Difference-Frequency Mixing (RDFM)	65
5.1.1 Motivation	65
5.1.2 Implementation	67
First test application: mass spectroscopy with 9.75 eV photons	71
Second test application: Determining ionization threshold	72
5.1.3 Implications	74
5.2 Implementation of third harmonic generation (THG) in Xe	75
5.2.1 Introduction	75
5.2.2 Implementation	76
First test application: mass spectroscopy with 10.5 eV photons	77
Second test application: $A^1\Pi_u \leftarrow X^1\Sigma_g^+$ electronic transition in C ₃	77
5.2.3 Implications	79
Bibliography	80
6 Gas phase electronic spectra of the carbon chains C₅, C₆, C₈, and C₉	82
6.1 Abstract	83
6.2 Introduction	83
6.3 Experimental	84
6.4 Observations and Discussion	86
6.4.1 Electronic transitions of C ₅	86
6.4.2 Decay of C ₅ electronic states	87
6.4.3 The $A^1\Pi_u \leftarrow X^1\Sigma_g^+$ transition of C ₅	88
6.4.4 UV band of C ₅	89
6.4.5 Electronic spectra of C ₆ , C ₈ , and C ₉	90
6.5 Concluding remarks	91
6.6 Acknowledgement	92
Bibliography	98
7 Gas-phase electronic spectra of C₆NH₂ and C₈NH₂	102
Introduction	103
Experiment	104
Results and discussion	104
1. Observations	104
2. Structural considerations	105
Concluding remarks	106

References	106
8 Optical detection of C₉H₃, C₁₁H₃, and C₁₃H₃	107
Introduction	108
Experimental	110
Results and discussion	111
1. Overview of vibronic structure	111
2. Structural considerations	112
3. Chemical implications	113
Concluding remarks	114
References	114
9 Appendix	116
Sellmeier formula and refraction indices for Ar, Kr, and Xe	117
Bibliography	119
Other publications contributed during PhD study	120
9.1 <i>Electronic spectra of carbon chains, rings and ions of relevance to astrophysics</i>	121
9.2 <i>The gas phase spectrum of cyclic C₁₈ and the diffuse interstellar bands</i> . .	129
9.3 <i>Gas phase electronic spectra of two C₅H₅ radical isomers</i>	133
9.4 <i>Gas phase electronic spectrum of the nitrogen terminated nanowire NC₁₆N</i>	137
9.5 <i>New laboratory data on a molecular band at 4429 Å</i>	141
9.6 <i>Sulfur terminated nanowires in the gas phase: laser spectroscopy and mass spectrometry</i>	147
9.7 <i>Methyl substitution in hydrocarbon discharge chemistry: Diagnosis by laser spectroscopy</i>	153
9.8 <i>Gas phase electronic spectra of the linear carbon chains HC_{2n+1}H (n=3-6,9)</i>	157
List of publications during PhD study	163
Curriculum vitae of the author	164

Chapter 1

Introduction

1.1 Relevance and motivation of the study

Spectroscopy, the study of the dependence of physical quantities on frequency, is the primary tool for remote sensing of physical conditions. Through the spectra emitted or absorbed, substances can be identified, and detailed information about structure and intramolecular dynamics can be inferred. If all of the relevant molecular processes are understood, the observed rotational/vibrational/electronic excitation can provide valuable information about the density, kinetic temperature, and the intensity of the radiation field in the probed volume. This structural and dynamical information is not only of fundamental interest, but is also valuable in many branches of physical, organic, inorganic, and astrochemistry. It gives insight into the chemical processes occurring in the probe by providing information on the composition of the matter.

Plasmas, flames, and chemical vapor deposition processes are all prominent examples of environments. Given the hydrocarbon nature of the precursors usually used in these fields it is not surprising that these environments are rich in carbon containing compounds. The study of these (often transient) species is necessary for acquiring a thorough understanding of these complex chemical environments, and a detailed knowledge of their physical and chemical properties is important for understanding a large variety of chemical systems. In addition to such practical considerations, carbon clusters are fascinating examples of the richness and variety of carbon chemistry in itself. Due to the enormous bonding flexibility of carbon, namely its unique ability to form stable single, double, or triple bonds, carbon clusters appear in a wide range of structural forms that are synthesized spontaneously in hot carbon plasmas. For example, researchers have been puzzling for more than a decade over the ability of a molecule as symmetric as the icosahedral C_{60} cluster to form in such a spontaneous way [1]. Elucidating the evolution of carbon cluster structure, from linear chains to rings to closed spheroidal cages to nanotubes, that takes place as the cluster size increases constitutes a major scientific challenge and requires an intimate interplay of state of the art experimental and theoretical techniques. While great progress has been made in recent years many unanswered questions still remain [2].

Another field taking advantage of remote sensing is astronomy. Here spectroscopy serves as the only probe of the physical and chemical conditions of interstellar clouds, which represent the starting material for the formation of stars and planetary systems. Diagnostics of the ongoing processes in the Universe, its evolution, composition, and physical properties should provide us with essential information for the verification of fundamental theories in physics, such as general relativity theory, and refining our understanding (or aggravating our incomprehension) of nature. With laboratory spectra obtained in the gas-phase at low temperatures in hand one can use the techniques of

astronomical spectroscopy to measure the concentrations of molecular ions and neutral molecules in the interstellar medium using powerful ground-based and space-based telescopes. The observed concentrations can then be interpreted using models based on chemical kinetics to serve as a remote probe of both the chemical and physical conditions in interstellar clouds [3].

The most abundant element in the Universe is hydrogen. It is followed by helium which is 10 times less abundant. These were supposedly produced in the first 17 minutes after the Big Bang [4]. The rest of the elements have been formed inside of stars billions of years later [4], and their presence in space is considerably lower in fractional abundances. Next most abundant elements - oxygen, carbon, and nitrogen - are represented by another two orders of magnitude less. However they play an important role in the interstellar chemistry.

More than 130 molecules have been detected in the interstellar medium or circumstellar shells, ranging in complexity from molecular hydrogen (H_2), through other familiar ones, such as water, hydrogen cyanide (HCN), nitrous oxide or "laughing gas" (N_2O), and ethanol ($\text{CH}_3\text{CH}_2\text{OH}$), to esoteric carbon-chains known as cyano-polyynes, the biggest known of which is HC_{11}N (figure 1.1). About 100 of these (i.e. $\approx 75\%$) contain carbon. The percentage increases among the polyatomics: $\approx 88\%$ of molecules larger than diatomic, and $\approx 96\%$ - larger than triatomic. This must be related to the peculiarity of the carbon atoms in their ability to create easily covalent bonds with themselves and form chains, and hints that the others, yet unidentified molecules, could also possess carbon skeleton, (capped, terminated, or) augmented by other members of the periodic table.

Yet perhaps one of the most astonishing developments in astronomy in the past twenty years has been the realization that very large organic molecules may be highly abundant in diffuse clouds. "Large" refers to molecules containing tens or hundreds of atoms, rather than the diatomics and several-atom molecules discussed above - and in fact much more massive than the largest species yet identified in dense molecular clouds [5]. Demonstrating a serious gap in our understanding of space chemistry, this assertion is based on the existence of so-called diffuse interstellar bands (DIBs).

1.1.1 Diffuse interstellar bands

Diffuse interstellar bands are absorption features seen in the spectra of astronomical objects in the Galaxy (figure 1.2). They are caused by the absorption of light by the interstellar medium. Their interstellar nature was shown by the fact that the strength of the

Molecules in the Interstellar Medium or Circumstellar Shells (as of 09/2005)

2 atoms	3 atoms	4 atoms	5 atoms	6 atoms	7 atoms	8 atoms	9 atoms	10 atoms
H ₂	C ₃ *	c-C ₃ H	C ₅ *	C ₃ H	C ₆ H	CH ₃ C ₃ N	CH ₃ C ₄ H	CH ₃ C ₅ N 2005
AlF	C ₂ H	l-C ₃ H	C ₄ H	l-H ₂ C ₄	CH ₂ CHCN	HCOOCH ₃	CH ₃ CH ₂ CN	(CH ₃) ₂ CO
AlCl	C ₂ O	C ₃ N	C ₄ Si	C ₂ H ₄ *	CH ₃ C ₂ H	CH ₃ COOH	(CH ₃) ₂ O	(CH ₂ OH) ₂ (?)
C ₂ **	C ₂ S	C ₃ O	l-C ₃ H ₂	CH ₃ CN	HC ₅ N	C ₇ H	CH ₃ CH ₂ OH	H ₂ NCH ₂ COOH
CH	CH ₂	C ₃ S	c-C ₃ H ₂	CH ₃ NC	CH ₃ CHO	H ₂ C ₆	HC ₇ N	Glycine ? 2005
CH ⁺	HCN	C ₂ H ₂ *	CH ₂ CN	CH ₃ OH	CH ₃ NH ₂	CH ₂ OHCHO	C ₈ H	CH ₃ CH ₂ CHO
CN	HCO	NH ₃	CH ₄ *	CH ₃ SH	c-C ₂ H ₄ O	2004		2004
CO	HCO ⁺	HCCN	HC ₃ N	HC ₃ NH ⁺	H ₂ CCHOH	CH ₂ CHCHO		
CO ⁺	HCS ⁺	HCNH ⁺	HC ₂ NC	HC ₂ CHO		(?) 2004		
CP	HOC ⁺	HNCO	HCOOH	NH ₂ CHO				
SiC	H ₂ O	HNCS	H ₂ CNH	C ₃ N				
HCl	H ₂ S	HOCO ⁺	H ₂ C ₂ O	l-HC ₄ H* (?)				
KCl	HNC	H ₂ CO	H ₂ NCN	l-HC ₄ N				
NH	HNO	H ₂ CN	HNC ₃	2004				
NO	MgCN	H ₂ CS	SiH ₄ *					
NS	MgNC	H ₃ O ⁺	H ₂ COH ⁺					
NaCl	N ₂ H ⁺	c-SiC ₃						
OH	N ₂ O	CH ₃ *						
PN	NaCN					11 atoms	12 atoms	13 atoms
SO	OCS					HC ₉ N	C ₆ H ₆ * (?)	HC ₁₁ N
SO ⁺	SO ₂							
SiN	c-SiC ₂							
SiO	CO ₂ *							
SiS	NH ₃							
CS	H ₃ ⁺ *							
HF	H ₂ D ⁺ ,							
SH*	HD ₂ ⁺ 2004							
HD	SiCN							
FeO (?)	AlNC							
O ₂ ?	SiNC 2004							
CF ⁺ 2005								

http://www.ph1.uni-koeln.de/vorhersagen/molecules/main_molecules.html

Figure 1.1: All molecules have been detected by rotational spectroscopy in the radiofrequency to far-infrared regions unless indicated otherwise (* indicates those detected by their rotation-vibration spectrum, ** detected by electronic spectroscopy only). As of May 2006, there are 134 molecules listed as detected in the interstellar medium or circumstellar shells.

observed absorption was roughly proportional to the extinction¹, and that in objects with widely differing radial velocities the absorption bands were not affected by Doppler shifts, implying that the absorption was not occurring in or around the object concerned. The name diffuse interstellar band was coined to reflect the fact that the absorption features are much broader than the normal absorption lines seen in stellar spectra and interstellar in origin [6].

The first notice given to diffuse unidentified features in the spectra of distant stars came in 1922, when Heger reported [8] a pair of 'stationary' features at 5780 and 5797 Å in spectroscopic binaries. More than a decade later Merrill [9, 10] began the first of many systematic studies of these features, by then dubbed 'diffuse interstellar bands' or DIBs. Later spectroscopic studies at higher spectral resolution and sensitivity revealed more and more DIBs; a catalogue of them in 1975 contained 25 [11], and a decade later the number known had more than doubled. Today over 300 have been detected in the optical region between 0.4 and 1.3 μm , but none - identified. The great problem with DIBs, apparent from the earliest observations, was that their central wavelengths did not correspond with any known spectral lines of any ion or molecule, and so the material which was responsible for the absorption could not be identified. A large number of theories were advanced as the number of known DIBs grew, and determining the nature of the absorbing material (the 'carrier') became a crucial problem in astrophysics.

At typical diffuse interstellar cloud densities (1–100 particles per cm^3), it was thought very unlikely that any significant population of even triatomics could be maintained, much less the larger species that seemed to be required. For this reason the most popular theories in the interval between the 1930s and the 1970s considered dust grains with impurity centers instead of gas-phase molecules as the most rational explanation. However with the emergence of more precise and higher resolution observational data it has been recognized that dust cannot be the carrier. The most powerful arguments favoring gas-phase carriers are the observed constancy of DIB wavelengths and profiles from sightline² to sightline (these should vary if solid state transitions were responsible) [12] and the existence of fine structure in some DIBs [13]. Concurrently it was realized that rapid molecular formation through ion-neutral reactions was possible and the notion that DIBs are formed by molecules regained favor.

As many of the molecules proposed as possible carriers have accessible electronic tran-

¹extinction - the reduction of the intensity of radiation as a consequence of absorption and scattering. Interstellar extinction varies with wavelength resulting in blue light more strongly absorbed than red light. The longer the path through the dust, and the denser the dust, the more the starlight is dimmed and reddened.

²sightline - An imaginary straight line between the earth and the star absorption of which light by interstellar matter is studied(/whose light become absorbed by interstellar mater)

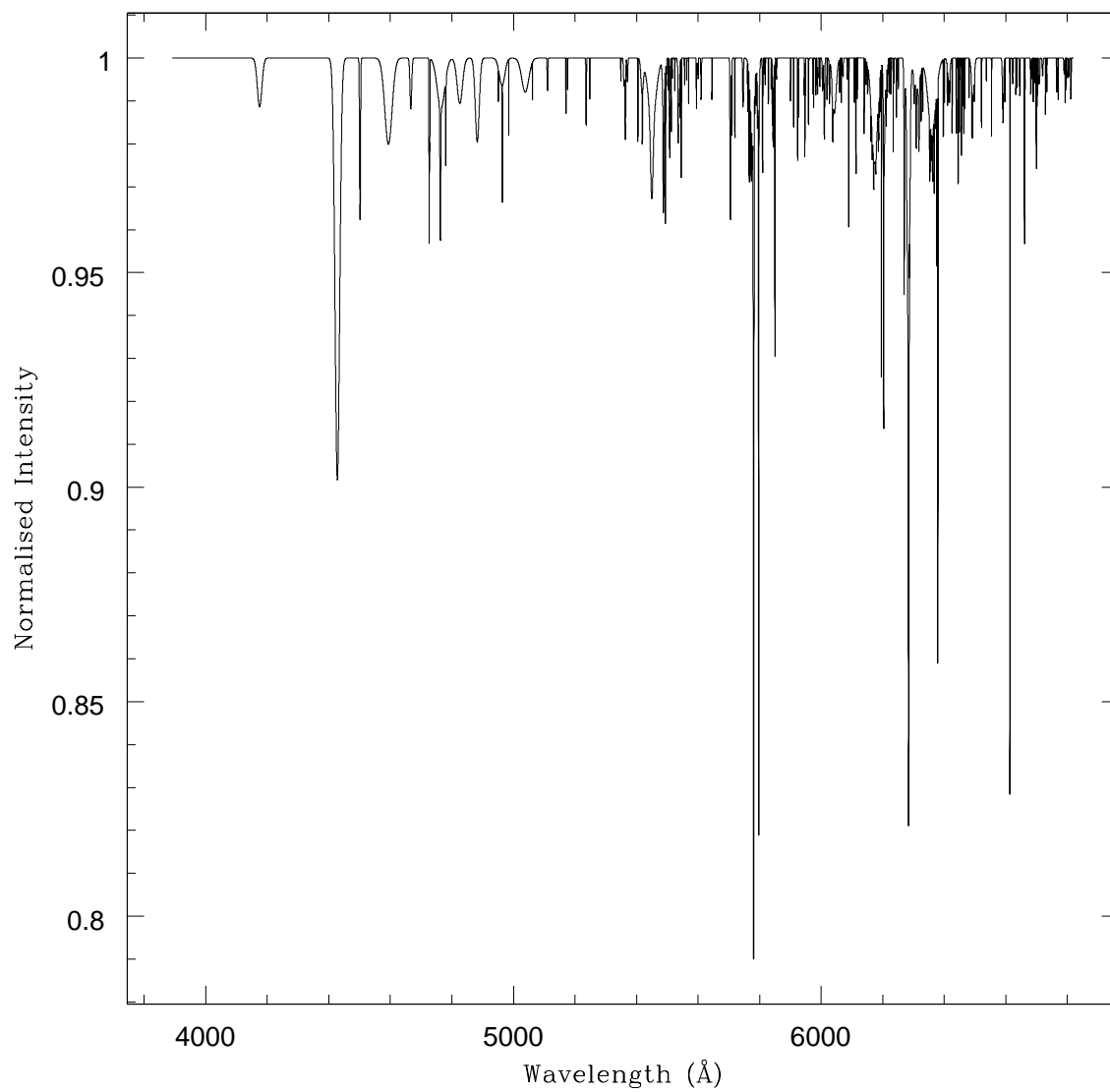


Figure 1.2: A synthetic spectrum of 226 DIBs confirmed towards BD+63° 1964 between 3906 Å and 6812 Å. Stellar lines have been removed through division by the spectrum of a similar star having little foreground absorption. This object has the strongest DIBs yet measured, and is cited as a prototype for the DIB spectrum (taken from [7]).

sitions in the UV, useful insight into the nature of the DIB carriers may be gained by extending the study of DIBs to ultraviolet wavelengths. However, several obstacles make this difficult: far-UV extinction rise limits studies to much lower total visual extinctions than optical observations; hot stars have intrinsically complex UV spectra; and other atomic and molecular interstellar lines create confusion, especially below 1108 Å where strong H₂ bands begin to dominate the spectra of reddened stars. Two general searches for UV DIBs have been carried out [14, 15] without any significant detections [16].

Although the exact nature of the molecules responsible for the DIBs is still not known, some clues can be gleaned from observational evidence. The salient characteristics of the DIBs in short are [5, 17]:

- There are at least 300 DIBs (200 in October 1998 [7]) within the 0.4 to 1.3 μm range;
- the DIBs are definitely interstellar;
- their wavelengths and profiles are invariant (except possibly for fine structure features);
- they do not correlate perfectly with each other;
- the density of DIBs increases towards the red and near-IR;
- the line widths are not uniform; some DIBs show fine structure that is best explained as due to rotational and vibrational substructure [13, 18, 19];
- a few DIBs have been seen in emission in special environments [20].

It is widely assumed that the DIB carriers are composed of cosmically abundant elements (such as H, C, O, and N), out of concern that molecules containing trace elements may not be abundant enough to account for the large number of DIBs [7] and their overall strength. It is also widely assumed that DIBs are 'organic' in nature, because carbon has a sufficiently rich chemistry to support the wide variety of individual species probably needed to explain the DIBs [16].

Much of the speculation about which specific molecules form the DIBs is centered on two classes of molecules: polycyclic aromatic hydrocarbons (PAHs) [21] and carbon chains [22–24]. The speculation about PAHs is motivated by the likely aromatic nature of the UIB³ carriers and their probable presence in diffuse clouds; while the speculation about

³UIB - Unidentified Infrared Bands are observed in emission toward sources in which interstellar dust is irradiated with UV light. The general mechanism invoked to explain the UIBs is, absorption of a UV photon, followed by relaxation to an excited vibrational state of the ground electronic state, and subsequent emission of IR photons as the molecule transitions to the ground vibrational state [25].

carbon chains is motivated by the fact that many of the molecular species observed (see figure 1.1) in cold dense molecular clouds are carbon chains⁴. None of these propositions can be preferred at the time as they both have weak aspects (some of which will be highlighted below) and are used (while) lacking something better. Therefore, "...we should keep in mind the rich diversity of chemistry, and consider the likelihood that we have simply not yet thought of the best candidates for the DIB carriers" [16].

Eventually our understanding should include the names and structures of those species, their concentrations, and their mechanisms of formation and maintaining steady state equilibrium. As such the solution should be approached on all of these fronts simultaneously and success on any of them will assist the others.

Formation considerations

So far a "complete" model of a diffuse cloud - that is, one where the complete physical and chemical structure is solved self-consistently - has not yet been attempted. Such a model would require treating the equations of hydrostatic equilibrium, thermal balance, radiative transfer, ionization balance, and chemical processes [16]. The first comprehensive model of a diffuse cloud [26] in many ways came close to the "complete" model, in that it utilized pressure, thermal, electrical, and chemical balance equations. Yet, like most of the models that followed, it was a one-dimensional model and it assumed steady state (that the formation rate for each species equals its destruction rate). It did not make an assumption for the total number density but instead treated it as a free parameter, subject to pressure balance with an assumed external pressure. Although modern models of gas-phase chemistry of diffuse clouds [27–29] are quite advanced in terms of their treatment of physical processes (especially radiative processes), they are still in a relatively immature state in terms of the number of chemical species and reactions considered.

They do not address the formation of large species such as PAHs or carbon chains though some work on modeling their effects on the chemistry and heating of clouds has been done [30, 31]. One possibility is that these large organic species form in the gas phase in dense molecular clouds, and are then cycled back into the diffuse ISM (e.g., [32]). But it is not clear if sufficient quantities of these species, to account for the DIBs, can be produced in this way. Another possibility is that the large organics are formed in the outflows from carbon-rich giant stars late in their evolution [33–36]. Under highly constrained conditions (density, velocity law of the outflow, and initial temperature) it may be possible to form the observed quantities in this way, and it is widely accepted

⁴though carbon chains represent only a small fraction of the total molecular mass in these clouds - the apparent preponderance of carbon chains is in part a selection effect, because these species have high dipole moments and are therefore more likely to be detectable than other classes of molecules [16]

that carbon star atmospheres may be a major source of large organics in the general ISM. Yet another closely related possibility is that large molecules in the diffuse ISM are the result of shock-induced destruction of graphitic or carbonaceous grains, some of which may have initially formed in carbon star outflows. For example, graphite essentially consists of stacked layers of fused carbon rings with very weak bonding between layers. When such a grain is shattered in a shock, the fragments will be planar fused carbon ring species, which, if they acquire peripheral hydrogen atoms, would become PAHs. Any discussion of the origin of the large organics in diffuse clouds is necessarily speculative at this point [16]. The models are hampered by our lack of a good physical understanding of clouds, and especially of processes such as turbulence and their coupling to the chemistry. Therefore all their consequences could be treated only as advisory but not binding.

In order to unravel a knot we need to find a beginning of a rope - several molecules which have an established presence and carry some of the DIBs. Once 'the ice will begin to break' then the full solution will be inevitable. Rigorous identification will only come through laboratory studies showing precise and specific spectral matches with the observed astronomical features.

Observational constraints

Blind laboratory searches are unlikely to work. There are about 10^7 organic molecules known on Earth and $\sim 10^{200}$ stable molecules of weight < 750 containing only C, H, N, O, S could exist in isolated conditions (under vacuum) [37]. To reduce the number of possibilities additional constraints should be placed based on observations. These (criteria) could be formulated as follows:

- Composing elements should be abundant.
- They (or one of them) should be able to make covalent bond with itself to build a skeleton
- Finite number of carriers $\sim 10^2$ (300 DIBs are generally not correlated with each other)
- Carriers should have electronic transitions in the optical range (0.4 to 1.3 μm)
- Robustness against UV radiation (photostability)
- Carriers have molecular rather than atomic nature (lines are 1–100 cm^{-1} broad)
- Lifetimes of its excited states should not be too short. Generally not shorter than ~ 1 –10 ps to comply with the uncertainty principle and absorption linewidth. As a consequence of that:

- An electronic transition involved will likely be the lowest possible electronic transition in this molecule. This should normally minimize effects like non-adiabatic coupling of electronic and vibrational degrees of freedom (caused by proximity of other electronic states) that lead to fast intramolecular energy redistribution processes and, hence, lifetime broadening.
- This electronic transition should probably be dipole-allowed to ensure maximum absorption with minimal concentration.

Interesting implications could be formulated here. Thus, for example, many carbon chains fail to meet these requirements. The C_{2n} family of linear chains can be eliminated because of the absence of electronic transitions in the visible for reasonable chain sizes. In turn, odd-numbered chains C_{2n+1} can be ruled out since the strong transition ${}^1\Sigma_u^+ \leftarrow X{}^1\Sigma_g^+$ proposed to cause the enigmatic absorptions is far from being the first one and thus will be likely lifetime broadened in larger extent than necessary. Generalized partially hydrogenated chains or/and capped (or doped) with non-carbon elements are still within the play as there are not enough experimental data on their account. (Though some combination, for example, $C_{2n}H$, $C_{2n}H^-$, C_{2n+1}^- , $HC_{2n}H$, $HC_{2n+1}H$ were already tried and rejected, vast number of them are still ahead.)

On the other hand, the "PAH theory" also has its weaknesses. Thus, for example, the requirement of restricted set (~ 300) of generally homotypic molecules may not agree with virtually infinite number of PAH, PAH^+ , PAH^- , $H-PAH^+$, etc. Other criteria, like the requirement of "first electronic transition - allowed" and/or "photostability" could help. Indeed not all of PAHs are photostable [38–40]. Presumably produced in the circumstellar envelopes of carbon-rich red giants [33], PAHs spread out in interstellar space and become exposed to harsh UV radiation. Under that, depending on the photon flux, many of them may lose some of (or all) their hydrogens, fall apart, etc. This will result in a wealth of unsaturated PAH skeletons that will be subjected to ring-openings, ring-loss, etc. reactions (see introduction to the chapter about rings ($C_{14,18,22}$) and discussion in experimental section of the C_5 chapter) and will eventually end up in a variety of linear and quasilinear, bare and partially hydrogenated chains, rings (monocyclic and polycyclic), PAHs (ionized, protonated, and partially dehydrogenated), and fullerenes.

These molecular radicals, both neutral and ionic, are highly reactive in normal terrestrial conditions and can be difficult to produce in the laboratory in the quantities necessary for spectroscopic study. Much work was done using frozen rare gas matrices (where large number densities could be accumulated), but such "matrix spectra" suffer from wavelength shifts and band broadening which are difficult to quantify with sufficient precision to unambiguously compare with interstellar (gas-phase) absorption features.

Identification of the bands in space will only come through gas-phase laboratory studies showing spectral matches with the observed astronomical features. This involves cutting-edge laboratory laser spectroscopy techniques combining supersonic expansions molecular beam techniques (to produce cold molecules) with ultra-sensitive spectroscopic methods (which will approach the limit of single-molecule absorption spectroscopy).

Results of the powerful combination of the REMPI technique with supersonic beam expansion, time-of-flight mass spectrometry, and nonlinear generation of coherent UV radiation towards neutrals rings $C_{14,18,22}$ and chains C_5 , $C_{6,8}NH_2$, $C_{9,11,13}H_3$ compose the body of this thesis.

Bibliography

- [1] H. W. Kroto, J. R. Heath, S. C. O'Brien, R. F. Curl, and R. E. Smalley. C_{60} buckminsterfullerene. *Nature*, 318: 162–163, 1985.
- [2] A. Van Orden and R. J. Saykally. Small carbon clusters: Spectroscopy, structure, and energetics. *Chem. Rev.*, 98: 2313–2357, 1998.
- [3] B. J. McCall. The McCall Group homepage: Research. <http://bjm.scs.uiuc.edu/research.php>.
- [4] Lawrence Berkeley National Laboratory's Physics Division. Project Universe Adventure. http://www.universeadventure.org/universe_fusion.html.
- [5] T. P. Snow. The unidentified diffuse interstellar bands as evidence for large organic molecules in the interstellar medium. *Spectrochimica Acta Part A-Molecular And Biomolecular Spectroscopy*, 57: 615–626, 2001.
- [6] Wikipedia, the free encyclopedia. http://en.wikipedia.org/wiki/Diffuse_interstellar_band.
- [7] S. O. Tuairisg, J. Cami, B. H. Foing, P. Sonnentrucker, and P. Ehrenfreund. A deep echelle survey and new analysis of diffuse interstellar bands. *Astronomy & Astrophysics Supplement Series*, 142: 225–238, 2000.
- [8] M.L. Heger. Further study of the sodium lines in class B stars; The spectra of certain class B stars in the regions 5630Å–6680Å and 3280 Å–3380 Å; Note on the spectrum of γ Cassiopeiae between 5860 Å and 6600 Å. *Lick Observatory Bull.*, 337: 141–148, 1922.
- [9] P. W. Merrill. *Publ. Astron. Soc. Pacific*, 46: 206–207, 1934.
- [10] P. W. Merrill. Unidentified interstellar lines. *Phys. Rev.*, 52: 0761–0762, 1937.

- [11] G. H. Herbig. Diffuse interstellar bands. 4. Region 4400–6850 Å. *Astrophys. J.*, 196: 129–137, 1975.
- [12] W. H. Smith, T. P. Snow, and D. G. York. Comments on origins of diffuse interstellar bands. *Astrophys. J.*, 218: 124–132, 1977.
- [13] P. J. Sarre, J. R. Miles, T. H. Kerr, R. E. Hibbins, S. J. Fossey, and W. B. Somerville. Resolution of intrinsic fine-structure in spectra of narrow diffuse interstellar bands. *Monthly notices of the royal astronomical society*, 277: L41–L43, 1995.
- [14] T. P. Snow, D. G. York, and M. Resnick. Search for diffuse interstellar bands in far ultraviolet wavelengths. *Publications of the astronomical society of the pacific*, 89: 758–764, 1978.
- [15] G. C. Clayton, K. D. Gordon, F. Salama, L. J. Allamandola, P. G. Martin, T. P. Snow, D. C. B. Whittet, A. N. Witt, and M. J. Wolff. The role of polycyclic aromatic hydrocarbons in ultraviolet extinction. I. Probing small molecular polycyclic aromatic hydrocarbons. *Astrophys. J.*, 592: 947–952, 2003.
- [16] T. P. Snow and B. J. McCall. Diffuse atomic and molecular clouds. *Annual Review of Astronomy & Astrophysics*, 44: 367–414, 2006.
- [17] G. H. Herbig. The diffuse interstellar bands. *Annual review of astronomy and astrophysics*, 33: 19–73, 1995.
- [18] P. Ehrenfreund and B. H. Foing. Resolved profiles of diffuse interstellar bands: evidence for rotational contours of gas-phase molecules. *Astronomy And Astrophysics*, 307: L25–L28, 1996.
- [19] J. Krelowski and M. Schmidt. Intrinsic profiles of strong diffuse interstellar bands. *Astrophys. J.*, 477: 209–217, 1997.
- [20] P. J. Sarre, J. R. Miles, and S. M. Scarrott. Molecular diffuse interstellar band carriers in the red rectangle. *Science*, 269: 674–676, 1995.
- [21] R. Ruiterkamp, N. L. J. Cox, M. Spaans, L. Kaper, B. H. Foing, F. Salama, and P. Ehrenfreund. PAH charge state distribution and DIB carriers: Implications from the line of sight toward HD 147889. *Astronomy and Astrophysics*, 432: 515–+, 2005.
- [22] A. E. Douglas. Origin of diffuse interstellar lines. *Nature*, 269: 130–132, 1977.
- [23] J. P. Maier, G. A. H. Walker, and D. A. Bohlender. On the possible role of carbon chains as carriers of diffuse interstellar bands. *Astrophys. J.*, 602: 286–290, 2004.

- [24] J. P. Maier, A. E. Boguslavskiy, H. B. Ding, G. A. H. Walker, and D. A. Bohlender. The gas phase spectrum of cyclic C₁₈ and the diffuse interstellar bands. *Astrophys. J.*, 640: 369–372, 2006.
- [25] K. Sellgren. The near-infrared continuum emission of visual reflection nebulae. *Astrophys. J.*, 277: 623–633, 1984.
- [26] A. E. Glassgold and W. D. Langer. Model calculations for diffuse molecular clouds. *Astrophys. J.*, 193: 73–91, 1974.
- [27] B. E. Turner. A common gas-phase chemistry for diffuse, translucent, and dense clouds? *Astrophys. J.*, 542: 837–860, 2000.
- [28] E. F. van Dishoeck and J. H. Black. Comprehensive models of diffuse interstellar clouds: physical conditions and molecular abundances. *Astrophysical Journal Supplement Series*, 62: 109–145, 1986.
- [29] F. Le Petit, E. Roueff, and E. Herbst. H₃⁺ and other species in the diffuse cloud towards ζ Persei: A new detailed model. *Astronomy and Astrophysics*, 417: 993–1002, 2004.
- [30] S. Lepp and A. Dalgarno. Polycyclic aromatic-hydrocarbons in interstellar chemistry. *Astrophys. J.*, 324: 553–556, 1988.
- [31] S. Lepp, A. Dalgarno, E. F. Vandishoeck, and J. H. Black. Large molecules in diffuse interstellar clouds. *Astrophys. J.*, 329: 418–424, 1988.
- [32] R. P. A. Bettens and E. Herbst. The abundance of very large hydrocarbons and carbon clusters in the diffuse interstellar medium. *Astrophys. J.*, 468: 686–693, 1996.
- [33] M. Frenklach and E. D. Feigelson. Formation of polycyclic aromatic-hydrocarbons in circumstellar envelopes. *Astrophys. J.*, 341: 372–384, 1989.
- [34] W. B. Latter. Large molecule production by mass-losing carbon stars: the primary source of interstellar polycyclic aromatic-hydrocarbons. *Astrophys. J.*, 377: 187–191, 1991.
- [35] I. Cherchneff, J. R. Barker, and A. G. G. M. Tielens. Polycyclic aromatic hydrocarbon formation in carbon-rich stellar envelopes. *Astrophys. J.*, 401: 269–287, 1992.
- [36] M. Giard, J. M. Lamarre, F. Pajot, and G. Serra. The large-scale distribution of pahs in the galaxy. *Astronomy And Astrophysics*, 286: 203–210, 1994.

- [37] S. D. Friedman L. M. Hobbs T. Oka B. L. Rachford T. P. Snow P. Sonnentrucker J. A. Thorburn D. E. Welty B. J. McCall, T. Fishman and D. G. York. Status of the Diffuse Interstellar Band Problem. In *American Astronomical Society 206th Meeting, Minneapolis, Minnesota, May 29 - June 2, 2005*.
- [38] P. Boissel, G. Lefèvre, and P. Thiébot. Photofragmentation of PAH Ions: Laboratory Experiments on Long Timescales. In I. Nenner, editor, *AIP Conf. Proc. 312: Molecules and Grains in Space*, pages 667–674, 1994.
- [39] S. P. Ekern, A. G. Marshall, J. Szczepanski, and M. Vala. Photon-induced complete dehydrogenation of putative interstellar polycyclic aromatic hydrocarbon cations: coronene and naphtho[2,3-a]pyrene. *Astrophys. J.*, 488: L39–L41, 1997.
- [40] S. P. Ekern, A. G. Marshall, J. Szczepanski, and M. Vala. Photodissociation of gas-phase polycyclic aromatic hydrocarbon cations. *J. Phys. Chem. A*, 102: 3498–3504, 1998.

Chapter 2

”Methodology”: Overview of experimental methods

2.1 REMPI

The realization that an atom or molecule can undergo a coherent (i.e. simultaneous) multi-photon transition if placed in a sufficiently intense radiation field is almost as old as the original ideas of quantum mechanics [1]. However it was not until the discovery of the laser in 1960 that sufficiently high optical fluxes were available to compensate for the intrinsic weakness of these transitions. Another 20 years passed before lasers themselves were sufficiently robust and stable enough to allow multiphoton excitation experiments to become commonplace [2].

The first experiments to illustrate at least some applications of MPI methods in molecular spectroscopy appeared in the mid-1970s. Specifically, it was shown that the MPI spectra (i.e. the excitation spectra for forming positive ions and/or photoelectrons) of diatomics such as NO [3] and I₂ [4], obtained using visible laser radiation, were structured. This structure arises because at the appropriate wavelengths the MPI probability is enhanced by the presence of resonant intermediate excited states of the neutral molecule. This is what constitutes resonance-enhanced multiphoton ionization (REMPI). Such processes are often described as an [n+m] MPI, implying that the excitation involves a coherent n-photon absorption to reach the resonant intermediate state of the neutral and that a further m photons is needed to cause the ionization process. This intermediate state does not have to be particularly stable; even predissociated excited states will provide significant resonance enhancement provided the rate of the final ionization step is comparable to, or greater than, the rate of all other population loss processes from the resonant intermediate state. In this respect the REMPI technique is far less dependent than, say, LIF upon the lifetime of the excited state giving rise to the resonance enhancement.

Like most spectroscopies, the technique is also highly species specific. In a well designed experiment MPI will occur only at those frequencies which correspond to a one- (or multi-) photon resonance in the neutral molecule. This specificity can be further enhanced if the experiment is coupled to a mass spectrometer thereby allowing determination of the mass of the ions resulting from the REMPI process. Another advantage of REMPI as a detection method is its sensitivity. This is due to the eventual products arising in a REMPI process are charged particles (ions and electrons) which, unlike photons, can be detected with unit efficiency.

However, compared with most one-photon transitions, multiphoton ones are inherently improbable, i.e. their cross-sections are small. Typical cross-sections σ for two- and three-photon absorption are 10^{-50} cm⁴s and 10^{-82} cm⁶s², respectively [5]. In comparison, a typical value for the cross-section of an electric dipole allowed one-photon excitation between two bound states of a molecule is 10^{-17} cm² [2]. Very high light fluxes I [$\frac{\text{photons}}{\text{cm}^2\text{sec}}$]

are needed in order to achieve a significant transition probability, σI^N , therefore lasers are the only real option to use as light sources. Typical modern pulsed dye lasers have powers of around 1 mJ/10 ns pulse (10^5 watts in 10^{-8} s, or about 10^{23} photons/s or 10^{16} photons/pulse). These powers within a 1 mm² spot will give only $\sim 10^{-8}$ transition probability in each laser pulse for two-photon resonance. In turn, focusing to a focal radius of about 100 μm increases the probability of a two photon absorption to 10^{-2} in each laser pulse, whereas a typical one photon transition is already saturated by two orders of magnitude.

Such intensities are normally achieved by focussing the output of conventional (nanosecond pulse duration) tunable dye lasers. Side effect of it is the localization of the multiphoton excitation events in small space region (i.e. the focal volume) which makes the technique ideally suited to use with molecular beams.

The photoelectrons formed in the REMPI process may also carry certain information. Their kinetic energies can be measured, as in conventional photoelectron spectroscopy (PES), and information derived about the energy levels of the partner cation. One distinction should be noted: in cases involving a bound resonance-enhancing state, the REMPI-PES experiment [6–9] will yield the photoelectron spectrum of the resonant intermediate state, not of the ground state as in the more traditional one-photon photoelectron spectroscopy.

Another form of photoelectron spectroscopy - zero kinetic energy (ZEKE) photoelectron spectroscopy [10,11], may also benefit from REMPI. The difference from REMPI-PES is that photoelectrons are formed with zero kinetic energy. For that electrons detected in such an experiment are actually produced by pulsed field ionization of very high Rydberg states belonging to a series converging toward the threshold of interest [12–15]. Detecting the appearance of electrons instead of their kinetic energy distribution can be done much more accurately and offers typically an order (or more) of magnitude improvement in energy resolution (i.e. cm^{-1} resolution) however this also requires a tunable coherent light source. Excitation of the Rydberg states requires high photon energies, and therefore is often done via resonance multiphoton excitation (or one-photon, if tunable vacuum ultraviolet radiation is available).

Detecting the threshold ion instead of threshold electrons constitutes the mass analyzed threshold ionization (MATI) spectroscopy [16,17] - an alternative and high resolution route to measuring ionization thresholds and deriving information about the internal energy states of cations. In contrast to ZEKE-PES, this technique offers both wavelength and mass information and finds particular application in the study of cations of radicals, clusters and complexes where, because of the production method, species identification might be ambiguous [2, 18, 19].

REMPI is an especially suitable tool for studying the spectroscopy of the atoms and diatomic molecules. A multiphoton excitation provides means of populating an excited state lying at energies that, in one-photon absorption, would fall in the technically more demanding vacuum ultraviolet spectral region. It also provides access to a manifold of states complementary to those allowed by selection rules for electronic dipole transitions and that can be accessed via one-photon absorption spectroscopy.

Though, as it was already mentioned, the resonant intermediate state does not have to be particularly stable, the efficiency of the ionization step still depends on the relative magnitudes of the ionization rate and the rates for all other population loss processes affecting the resonant intermediate level. Obviously in those cases where the excited state of the neutral molecule predissociates at a rate comparable to, or greater than, the ionization rate, this competition must lead to a reduced ionization probability and a relative diminution of the eventual ion yield. Thus, multiphoton excitations proceeding via such predissociated levels will appear with reduced relative intensity in the REMPI spectrum. In extreme cases the lines may show lifetime broadening as well. Careful analysis of such discrepancies between observed REMPI transition intensities and those predicted through use of the appropriate multiphoton rotational line strengths have provided much insight into the detailed predissociation dynamics of a range of hydrides, e.g. H₂O [20,21], H₂S [22], CH₃ [23], and NH [24].

As a molecule's size and mass increase, dynamical aspect becomes more and more important. Middle sized closed shell stable molecules often possess relatively large energy gaps between their ground and first excited states. Therefore nonradiative decay is slow. Particularly popular systems for study using REMPI techniques were substituted benzenes. Their first excited (S_1) singlet states are generally stable; they have low first IPs - less than twice the S_1 - S_0 energy separation (the S_1 - S_0 transition is thus well suited to study by [1+1] REMPI); and the S_1 - S_0 transition has a large oscillator strength and falls in an experimentally convenient wavelength range. However spectroscopic study of already S_2 is restricted in relatively low resolution due to lifetime broadening. The situation generally worsens with every next electronic state. Increasing density of vibronic states, generated by lower lying electronic energy levels, leads to increasingly efficient intramolecular processes that removing the molecule's excitation induced by the tunable laser at the first step of REMPI. In extreme cases this depletion may occur on time scales shorter than delay before arrival of next laser photons and REMPI effectively proceeds on N-scheme (figure 2.1) [25].

Through use of a variable time delay between the excitation step and the subsequent photoionization, it is possible to derive kinetic information about intramolecular vibrational redistribution and vibrational predissociation in selected vibronic levels of the

excited state of the molecule (like in chapter 6). Often, however, the timescale provided by conventional (nanosecond) pulsed lasers is not appropriate. To compete effectively with these ultrafast energy redistribution processes a change from nanosecond to sub-picosecond time scales is required. One of the first such attempts were made while studying nonradiative decay processes in the aniline-CH₄ van der Waals complex [26]. Now, more often in the form of PES, this field has "exploded" under the femtosecond time resolved photoelectron spectroscopy (TR-PES) name - a useful tool for the study of non-adiabatic dynamics in isolated polyatomic molecules [27,28].

In astronomical/DIBs observation relevant context (see previous chapter) a few lowest, if not the only one, electronic transitions of middle sized and large molecules are of interest (since the rest are lifetime broadened). The electronic transitions in the visible and near infrared regions become readily accessible with one photon of a conventional dye laser. In turn their subsequent ionization often requires more energy. The speed of this step should not be limiting [5] and thus resonant processes that govern it should be of no higher order resonance than was the excitation. Therefore it is necessary to do [1+1'] REMPI with second photon in UV or even VUV (vacuum ultraviolet) spectral region. Thus, the studies described in this thesis were done using an [1+1'] scheme with 5.8 eV (212 nm), 6.4 eV (193 nm), 7.9 eV (157 nm), and as high as 10.5 eV (118 nm) ionizing photons.

Another reason for using the [1+1'] scheme for a space relevant study comes from the fact that, apart from regions in stars proximity, the photons flux in interstellar space is low enough to expect mainly one-photon absorption processes. Therefore one attempting the laboratory "simulation" of the moieties in space should probably be concerned mostly by the one photon processes governed by corresponding selection rules.

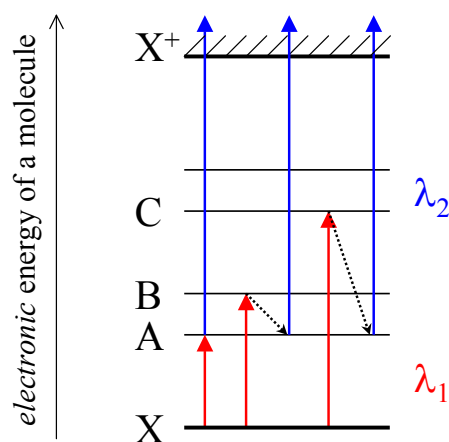


Figure 2.1: REMPI in polyatomic molecules.

2.2 TOF mass spectrometer

Time-of-flight mass spectrometry (TOF-MS) is a *separation-in-time* technique, unlike magnetic sector and quadrupole mass analyzers in which ions are spatially separated.

A time-of-flight mass spectrometer uses the differences in transit time through a drift region to separate ions of different masses. It operates in a pulsed mode so ions must be produced or extracted in pulses. An electric field accelerates all ions into a field-free drift region with a kinetic energy of qV , where q is the ion charge and V is the applied voltage. Since the ion kinetic energy is $\frac{1}{2}mv^2$, lighter ions have a higher velocity than heavier ions and reach the detector at the end of the drift region sooner.

$$\text{K.E.} = qV$$

$$\frac{1}{2}mv^2 = qV$$

$$v = \sqrt{(2qV/m)}$$

The transit time (t) through the drift tube is D/v where D is the length of the drift tube.

$$t = D / \sqrt{(2qV/m)} = \frac{D}{\sqrt{2V}} * \sqrt{m/q}$$

Thus the mass-to-charge ratios can be determined from this equation if the exact drift length and acceleration potential are known. Unlike magnetic sector and quadrupole calibrations, though, the direct relation is rarely used. In most cases, calibration of the TOF spectrometer is performed through empirical determination of the time-of-flight of a pair of known masses. This allows constants a and b in the equation $t_i = a\sqrt{(m/q)_i} + b$ to be determined and, afterwards, any experimental time-of-flights t to be converted to a m/q value to identify the unknown ions.

The resolution of the mass spectrometer is defined broadly as the ability to distinguish

Criteria	Notes
sensitivity	higher mass analyzer efficiency than scanning MS (scan mode)
speed	hundreds of spectra per second may be acquired
mass range	analyzer transmits ions of very high m/z
mass accuracy	very stable calibration in many cases
selectivity	resolution of $\sim 10\,000$ FWHM now attainable without loss in sensitivity
versatility	many ion sources may be coupled with TOF MS
performance/cost	digital control and processing

Table 2.1: The key strengths [29] of TOF are the reason why its adoption has proceeded. However, only in recent times many of these strengths have become tangible due to the availability of supporting technologies.

two ions of adjacent masses, and is usually scaled to the mass range under consideration, such that

$$R = \frac{m}{\Delta m}$$

where R is the resolution, Δm is the difference in mass of the species, and m is the average mass of the two ions.

If all ions were formed in a plane parallel to the electrodes (i.e. in the same plane perpendicular to the TOF tube) and with zero initial velocity the flight time would be same for all ions which had the same m/q , and the resolution would be limited by the detecting equipment. In practice, however, the resolving power of a TOF spectrometer depends on its ability to reduce the time spread caused by the ever-present initial space and initial kinetic energy distribution [30].

Ions of the same mass formed at the same time with the same initial kinetic energy, but at different locations in the extraction field will receive different kinetic energies from the electric field. This initial spacial distribution will therefore result in different arrival times for otherwise identical ions.

Yet ions formed at the back of the source will reside under the accelerating potential longer, acquire larger velocities, and even though they will enter the field-free region later, they will eventually pass the ions formed closer to the extraction grid. It can be shown that there exist a plane, called "spatial focus" where all the ions arrive at the same time at the detector independent of their starting positions. Ideally the detector should be placed at this location. Yet this approach does not give one much flexibility in designing a spectrometer.

$$t_a = \frac{v}{a} = \sqrt{\frac{sdm}{qV}}$$

$$t_D = D/v = D\sqrt{\frac{dm}{sqV}}$$

$$T = t_a + t_D = v/a + D/v = \sqrt{\frac{m}{q}} \frac{d}{V} \left(\frac{D}{\sqrt{s}} + \sqrt{s} \right)$$

then the space focus requirement can be expressed by setting the first derivative to zero

$$\frac{\partial T}{\partial s} = 0$$

which results in the constraint: $s = D$ independent of mass of the ion. This is a very disadvantageous trade off. The drift chamber D has to be long in order to gain resolution but the acceleration region should be short to allow for uniform electric field and for using reasonably low voltage.

A much better solution for space-focusing employs a more complex, dual-stage ionization region of three electrodes, (figure 2.3) as was proposed by Wiley and McLaren [30]. This type of spectrometer possesses two acceleration regions (separated by a grid) and a drift region. Using a second grid and an appropriate potential distribution of the ion extraction field allows one to move the spatial focus plane at any given distance (figure 2.4). The position of the space focus is a function of the ratio of the extraction and acceleration

fields. Keeping total voltage fixed by powering all grids via a potential divider (figure 3.7 in chapter 3) and varying the ratio allows one to match the space focus position with the detector without changing the times of flight and, hence, mass calibration.

Higher order space focusing ($\frac{\partial T}{\partial s} = 0$, $\frac{\partial^2 T}{\partial s^2} = 0$, etc.) can be achieved by using more than two field regions. A general solution for a n-order space focusing in an m-field regime can be found in [31]. There they demonstrated quantitatively that if higher orders of space focus are employed a significant improvement in the mass resolution can be achieved, provided that the initial velocity distribution of the ions is sufficiently narrow.

The double stage acceleration scheme is also less sensitive to the distribution of initial kinetic energy of ions. A double-field system brings the ions to their maximum energies in about 5% of the flight time compared with 50% in the focused single-field source. Thus, the disturbing effect of U_0 is reduced because U_0 is a smaller percentage, on the average, of the energy which determines the velocity at each point. Further improvement in minimizing this effect could be gained by utilizing longer field-free regions (a longer drift length increases the magnitude of the time-of-flight; this reduces the effect of turn-around time on resolution) or, more radically, by employing reflection type TOF spectrometer [32–34]. In our experiments, however, this last pivotal arrangement is unnecessary as in the supersonically expanded and skimmed molecular beam of neutral molecules advancing in the direction orthogonal to the TOF spectrometer axis the spread in velocities parallel to the TOF tube axis is low enough.

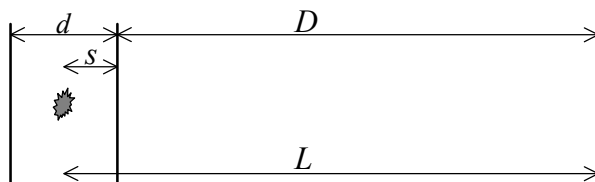


Figure 2.2: Basic geometry of TOF mass spectrometer.

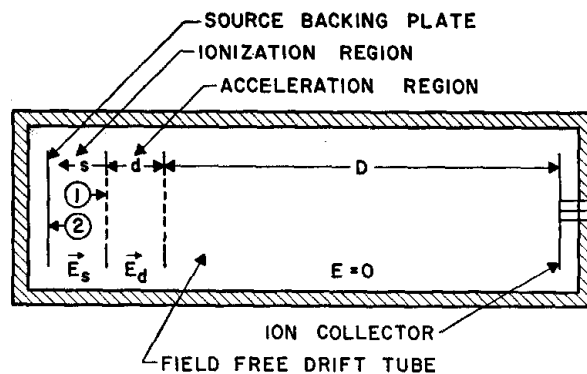


Figure 2.3: Basic geometry of the Wiley-McLaren TOF mass spectrometer [30].

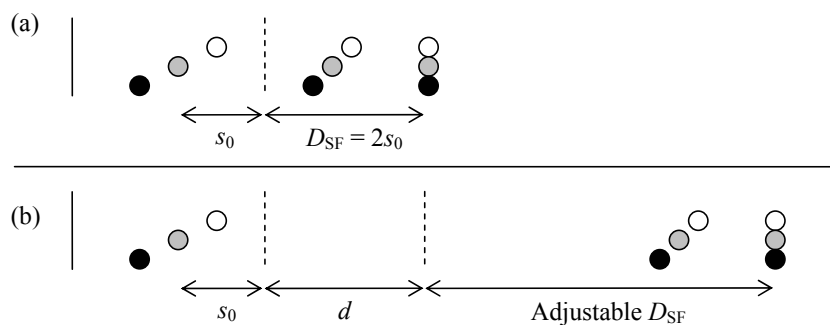


Figure 2.4: Space focus for (a) single-stage and (b) dual-stage TOF. The focus condition for the single field system is the purely geometric condition, $D_{SF} = 2s_0$. In dual-field configuration, position of SF plane depends on the voltage applied to the extraction/acceleration grids. Illustration from [35]

2.3 Vacuum Ultraviolet¹(VUV) generation in gases. Background.

2.3.1 Introduction

The REMPI technique uses photons to promote an atom or molecule above its ionization potential to create an ion. Through being an extremely sensitive method, yet with the vanishing concentrations of the studied transient molecules the resonance enhanced multiphoton ionization method is restricted almost exclusively to the [1+1] (i.e. one color, two photons) or [1+1'] (two different photons with different colors) resonant processes involving one or two lasers correspondingly. The typical IP of the small molecules studied varies from 8–12 eV. Therefore studies in the visible and, especially, near-infrared spectroscopic region (1.5–2 eV) require the flexibility of choice for the second-photon energy in the range 6–10.5 eV to be able to ionize the excited molecules. The most energetic source we have in our laboratory is a F₂-excimer laser which provides 7.9 eV photons (157 nm). Probably the only commercially available source of more energetic coherent radiation would be a synchrotron radiation light source, which, though existing (for example, Advanced Light Source (ALS) in Berkeley), was not considered here (our machine should have been built in the proximity of such a source, not vice versa). Therefore alternative approaches must be considered.

Coherent light can be generated via nonlinear up-conversion (harmonics generation, mixing, etc.) of the available laser sources in nonlinear media. Whereas in the visible and the infrared spectral regions this is generally done by sum- or difference-frequency mixing in suitable nonlinear crystals (widely available commercially), in the vacuum ultraviolet spectral region most solids become opaque and can no longer be employed since the generated wave of interest is absorbed and cannot escape the nonlinear medium. It is for this reason frequency mixing in the vuv region is generally carried out in gaseous media.

2.3.2 Theoretical background

The principle of harmonic generation is often visualized in terms of the classical Lorentz model where the bonding of an electron to the atomic nucleus is pictured by a spring, which to a first approximation, i.e. for small displacements of the electron away from its equilibrium position with respect to the nucleus, gives rise to a harmonic binding potential [36]. An electron bound this way and experiencing an oscillating monochromatic electric field will, if the field is sufficiently weak, respond by carrying out a harmonic

¹VUV, Vacuum UV, ultraviolet radiation that is absorbed by air. ($\lambda < 200$ nm)

motion which, by Maxwells equations, will give rise to emission of light at the driving frequency. If the magnitude of the driving field amplitude is large enough for the electronic motion to become anharmonic, the light emitted by this oscillating dipole will, in addition to the driving (or fundamental) frequency component, contain the second-, third- or higher order multipla of this frequency.

Formally, this can be expressed through the polarization \mathbf{P} of the medium by the electric field \mathbf{E} . When an electromagnetic wave \mathbf{E} travels through a medium it influences the bound electrons of the atoms or molecules. Electrons displaced from their equilibrium positions give rise to a net polarization of the medium. For small electric fields $\mathbf{E}(\omega)$, the polarization $\mathbf{P}(\omega)$ of a medium is proportional to the incident electric field $\mathbf{E}(\omega)$ via the susceptibility $\chi^{(1)}$

$$\mathbf{P}^L(\omega) = N\chi^{(1)}\mathbf{E}(\omega)$$

where N is the number density of atoms or molecules and the proportionality constant $\chi^{(1)}$. For high-intensity fields, however, the response of the medium will be non-linear and the induced polarization can be expressed in a power series of incident fields \mathbf{E} :

$$\mathbf{P}(\omega) = N(\chi^{(1)}\mathbf{E}(\omega) + \chi^{(2)}\mathbf{E}(\omega)\mathbf{E}(\omega) + \chi^{(3)}\mathbf{E}(\omega)\mathbf{E}(\omega)\mathbf{E}(\omega) + \dots)$$

Whereas the second-order term gives rise to the well-known processes of second harmonic generation, optical parametric oscillation, and sum and difference frequency mixing in crystals, it may exist only in the nonlinear medium without center of symmetry. In isotropic gaseous media the nonlinear polarization must be unaffected by reflection of the coordinate system at its origin. This requirement (i.e. $\mathbf{P}(\omega, \mathbf{r}) = -\mathbf{P}(\omega, -\mathbf{r})$) gives

$$(\chi^{(1)}\mathbf{E} + \chi^{(2)}\mathbf{E}\mathbf{E} + \chi^{(3)}\mathbf{E}\mathbf{E}\mathbf{E} + \dots) = -(-\chi^{(1)}\mathbf{E} + \chi^{(2)}\mathbf{E}\mathbf{E} - \chi^{(3)}\mathbf{E}\mathbf{E}\mathbf{E} + \dots)$$

which can be satisfied for any \mathbf{E} only if all the even-order terms $\chi^{(2)}, \chi^{(4)} \dots$ vanish. Therefore for an isotropic medium, first nonzero non-linear response of isotropic medium is described by $\chi^{(3)}$ and since the third-order response is proportional to the product of three oscillating electric fields - three photons should be involved to the process of generation of fourth one. Four electric fields are oscillating in the nonlinear medium simultaneously, three fundamental $\omega_1, \omega_2, \omega_3$ and one generated $\omega_g = \omega_1 \pm \omega_2 \pm \omega_3$ give the so-called "four-wave mixing" process.

Of the different possible combinations of how to compose the 4th wavelength from the three initial ones, two cases could generally lead to the generation of the coherent light at shorter wavelength is the sum $\omega_g = \omega_1 + \omega_2 + \omega_3$ and difference frequency mixing $\omega_g = \omega_1 + \omega_2 - \omega_3$ (provided that $\omega_3 < \omega_1, \omega_2$).

For practical application, however, one is more interested in situations where either two or all three of the incident beams have identical frequencies. The simplest type of four-wave mixing uses only one fundamental frequency, and the generated wave is at three times the fundamental frequency $\omega_g = 3\omega_1$. This process is called third harmonic

generation. For this case the intensity of the generated third harmonic is described by [37]

$$I_{3\omega} = N^2 |\chi^{(3)}(3\omega)|^2 I_{\omega}^3 F(b\Delta k) \quad (2.1)$$

intensity of the fundamental, N is the number density of the nonlinear medium, and $\chi^{(3)}(3\omega)$ is the third-order susceptibility for third harmonic generation. The function $F(b\Delta k)$, where b is the path length and Δk the the wave vector mismatch, depends on the macroscopic properties of the medium and the focusing of the fundamental, and represents the phase matching between the input light and the generated VUV.

Phase matching stands for the constructive interference of the contributions generated in different volume elements of the medium to the output wave. This is described by a generally sophisticated function, which could be written for the limiting case of a plane wave in a small signal limit regime and neglecting absorption as [38]:

$$F(L\Delta k) \simeq \left(\frac{\sin(L\Delta k/2)}{L\Delta k/2} \right)^2$$

which is similar to the second-order processes in nonlinear crystals [39]. This gives unity as the upper limit on the $F(L\Delta k)$ factor in the expression (2.1). However, intensity of the generated light is the third power of the incident one, and it is often (if not always) advantageous to focus the fundamental in order to increase the conversion efficiency of a nonlinear medium. This, in turn, affects the phase-matching which for a tight focused gaussian beam (the case of laser beam) at same other assumptions will be [38]:

$$F(\Delta kb, b/L \ll 1) = \begin{cases} 0 & \text{for } \Delta kL \geq 0 \\ \frac{\pi^2}{4} \left(\frac{b}{L}\right)^2 (\Delta kb)^2 e^{\Delta kb} & \text{for } \Delta kL < 0 \end{cases}$$

The latter function goes through a maximum for $\Delta kb = -2$, where the phase-matching factor takes on the value

$$F(\Delta kb, b/L \ll 1) = \left(\frac{\pi}{e} \frac{b}{L}\right)^2.$$

now far less then unity. Furthermore, in the tight focusing limit $b/L \ll 1$ the power $Pwr \propto I \cdot R^2 \sim I \cdot b$ conversion efficiency becomes independent of confocal parameter b and, thus, independent of particular focusing [38]

$$PowerConversionEfficiency = Power_{3\omega} / Power_{\omega} \propto (I_{3\omega} b / I_{\omega} b \propto I_{\omega}^3 b^2 b / I_{\omega} b = I_{\omega}^2 b^2) \propto (Power_{\omega})^2$$

The higher intensity upon tighter focusing is "compensated" by a shorter effective length of the nonlinear medium. Therefore any excessive focusing will no longer raise the power conversion efficiency, but will only lead to additional perturbing nonlinear polarizations as a consequence of the increased intensity. As the rule of thumb the optimum power conversion efficiency in a phase matched system is given typically for $b \simeq L$ [38].

The demand of negative value for Δkb (where $\Delta k = k_g - 3k_1$) has serious implications. This limits the third harmonic generation with focused lasers to the cases when the refractive index n at 3ω is less than the refractive index at ω .

$$k_\omega = \omega n_\omega / c$$

$$\Delta k = k_g - 3k_1 = k_{3\omega} - 3k_\omega = 3\omega n_{3\omega} / c - 3(\omega n_\omega / c) = \frac{3\omega}{c}(n_{3\omega} - n_\omega) < 0$$

Since the refractive index normally increases with frequency, this behavior ($n_{3\omega} < n_\omega$) is called *negative dispersion*. For rare gases where the refractive index is close to 1, the simplified Sellmeier expression could be used [40]

$$n - 1 \simeq \frac{Ne^2}{8\pi^2\epsilon_0 mc^2} \sum_i \frac{f_i}{\lambda_i^{-2} - \lambda^{-2}}$$

where N is the number density of atoms or molecules, e and m are charge and mass of electron respectively, and ϵ_0 is the vacuum permittivity. The summation is to be taken over electronic transitions of wavelengths λ_i with the absorption oscillator strengths f_i . Thus the regions of negative dispersion could be found only to the blue of resonance lines in gases. As an example, if we consider Xe gas as the nonlinear medium. Figure 2.5 represent the refractive index for Xe in the 110–200 nm region. The graph is calculated using above mentioned formula and information [41] on dipole allowed electronic transitions in xenon. (More information on the calculating refraction indices in Ar, Ne, Kr and Xe gases, could be found in Appendix.) The first resonance line is at 146.961 nm, meaning that there is no THG possible in Xe for wavelengths longer than about 146 nm. The region of negative dispersion extends to about 140 nm. The next resonance in Xe is at 129.549 nm and this gives rise to just a narrow window from about 127.5–129 nm and the next region for THG is below 125 nm. Thus THG in a given gas could be produced only in relatively restricted range with numerous gaps. However, by choosing between, say, Ar, Kr, or Xe, it is possible to generate third harmonic light over a broad range of frequency from 90 to 147 nm with a few gaps [37].

Other possibilities to increase efficiency could be seen in the formula (2.1). These are:

- increasing the number density. In a one component mixture the density is governed by the phase matching condition. However a two component gas mixture would allow an increase in the number density and recover the phase matching conditions by compensating the excess of negative dispersion with another, positively dispersive gas. Yet, the optical depth of the order of unity should not be exceeded in order to avoid attenuation due to absorption.
- Intensity of generated light increases as the third power of incident intensity. This is true, however, only in small signal limit. At higher intensities saturation will eventually occur. Increasing the intensity of the incident beams is only advantageous as long as higher-order nonlinearities do not reduce the conversion efficiency and cause additional perturbing parametric processes to occur [38]. Thus, at high laser intensities effects like dielectric gas breakdown in the focus of the laser light [42] and

nonlinear intensity-dependent changes of the refractive index [43], which destroy the phase matching, become the major limitation on the efficiency [44].

- to increase the value of $|\chi^{(3)}|^2$ term in equation (2.1).

For the third harmonic generation third-order susceptibility has the form [37]

$$\chi^{(3)} = \frac{e^4}{\hbar^3} \sum_{i,j,k} \frac{d_{gi}d_{ij}d_{jk}d_{kg}}{(\Omega_{ig}-\omega)(\Omega_{jg}-2\omega)(\Omega_{kg}-3\omega)}$$

where d_{xy} are dipole matrix elements, Ω_{xg} are the complex transition frequencies for the $x \leftarrow g$ transitions, and summation is over all states. The resonant terms in this equation lead to a strong enhancement of $|\chi^{(3)}|^2$ when either ω , 2ω , or 3ω are resonant with a transition in the nonlinear medium. On the other hand, in minimizing the factor containing the dipole allowed transition one has to be careful because the one-photon resonance may lead to a strong absorption of the fundamental wave, whereas the three photon resonance leads to a strong absorption of the harmonic wave [38]. Detailed analysis is required to see if one gains or loses in signal strength when the single-photon resonances are approached. In general, if the absorption is relatively weak but nonlinearity is strongly resonantly enhanced by the proximity to this weak transition, then it is worth tuning to near resonance [45]. So, the electric dipole allowed transitions should be optimized only to the extent that the corresponding optical depth is smaller or comparable to unity [46,47]. Two photon resonance (figure 2.6) is the most effective and widely used enhancement scheme for VUV generation since it avoids significant absorption at the fundamental and VUV light frequencies.

With only one input frequency, fixing ω so that 2ω corresponded to a resonance would not allow for tuning of the generated coherent light. To have both tunability and resonant enhancement, two fundamental frequencies must be used: ω_1 and ω_2 . This allows the coherent light to be generated at either the sum or the difference frequency: $\omega_g = 2\omega_1 \pm \omega_2$. For general four-wave mixing there is no significant difference with respect to the physics [38], although the equations are much more cumbersome. Sum frequency mixing has the same conditions on phase-matching as its special case - third harmonic generation. In turn difference frequency mixing possess more relaxed phase matching conditions with optimum at

$$b\Delta k = 0$$

making it possible to do RDFM at essentially any wavelength. RDFM is generally more efficient than DSFM when the same two-photon resonance is used [37]. Typical conversion provides 10^{11} - 10^{12} photons per pulse when millijoule pulses of the fundamental are used [37]. This should give an order of 0.1 – 1 μ joules and 10^{-3} – 10^{-4} of efficiency to the 10 eV. Non-resonant THG is few orders of magnitude less efficient, yet the near-resonant THG conversion can be as good [48,49].

Experimental implementation of both RDFM and THG schemes were attempted by the author to be employed for the spectroscopic study of target highly unsaturated hydrocarbon molecules. The particular motivations, results, and implications are described in corresponding chapters of the thesis.

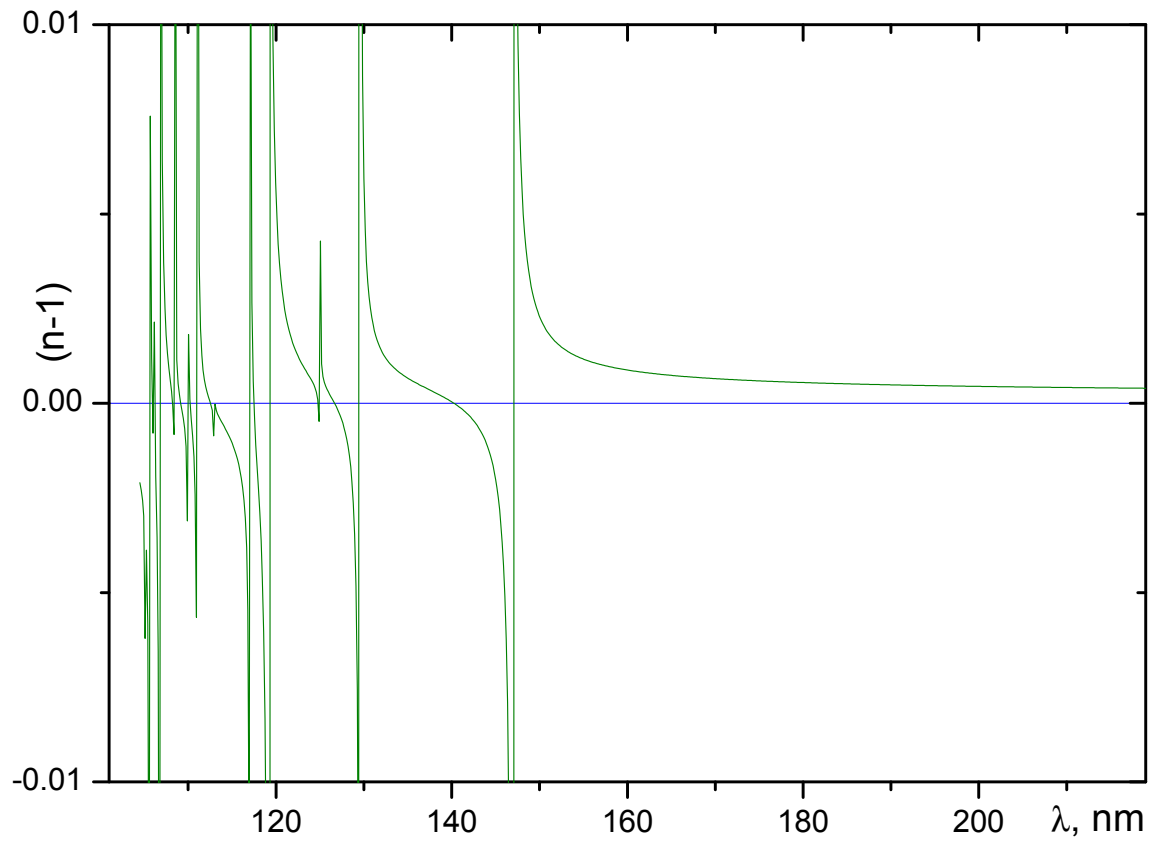


Figure 2.5: Xenon refractivity calculated using Sellmeier formula and atomic lines data from NIST database [41].

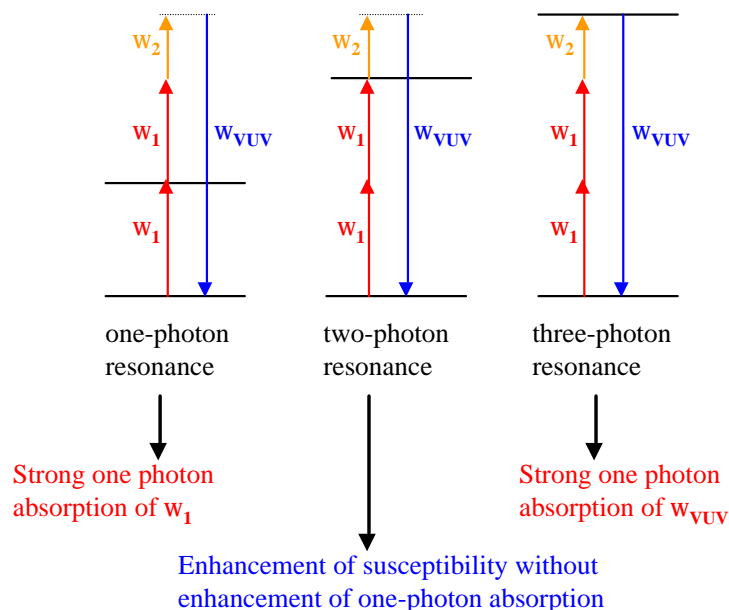


Figure 2.6: Two photon resonance is the most effective enhancement scheme for VUV generation since it avoids significant absorption at the fundamental and VUV light frequencies.

Bibliography

- [1] M. Goppert-Mayer. Elementary file with two quantum fissures. *Annalen Der Physik*, 9: 273–294, 1931.
- [2] M. N. R. Ashfold and J. D. Howe. Multiphoton spectroscopy of molecular-species. *Annu. Rev. Phys. Chem.*, 45: 57–82, 1994.
- [3] P. M. Johnson, M. R. Berman, and D. Zakheim. Nonresonant multiphoton ionization spectroscopy. 4-photon ionization spectrum of nitric-oxide. *J. Chem. Phys.*, 62: 2500–2502, 1975.
- [4] G. Petty, C. Tai, and F. W. Dalby. Nonlinear resonant photoionization in molecular iodine. *Phys. Rev. Lett.*, 34: 1207–1209, 1975.
- [5] P. M. Johnson and C. E. Otis. Molecular multi-photon spectroscopy with ionization detection. *Annu. Rev. Phys. Chem.*, 32: 139–157, 1981.
- [6] K. Kimura. Molecular dynamic photoelectron-spectroscopy using resonant multiphoton ionization for photophysics and photochemistry. *Int. Rev. Phys. Chem.*, 6: 195–226, 1987.

- [7] D. J. Leahy, K. L. Reid, H. K. Park, and R. N. Zare. Measurement of circular-dichroism in rotationally resolved photoelectron angular-distributions following the photoionization of NO $A^2\Sigma^+$. *J. Chem. Phys.*, 97: 4948–4957, 1992.
- [8] H. Park and R. N. Zare. Photoionization dynamics of the NO $A^2\Sigma^+$ state deduced from energy-resolved and angle-resolved photoelectron-spectroscopy. *J. Chem. Phys.*, 99: 6537–6544, 1993.
- [9] K. Kimura. Development of laser photoelectron spectroscopy based on resonantly enhanced multiphoton ionization. *J. Electron Spectrosc. Relat. Phenom.*, 100: 273–296, 1999.
- [10] K. Muller-Dethlefs and E. W. Schlag. High-resolution zero kinetic-energy (ZEKE) photoelectron-spectroscopy of molecular-systems. *Annu. Rev. Phys. Chem.*, 42: 109–136, 1991.
- [11] E. R. Grant and M. G. White. ZEKE threshold photoelectron-spectroscopy. *Nature*, 354: 249–250, 1991.
- [12] F. Merkt and T. P. Softley. Rotational line-intensities in zero kinetic-energy photoelectron-spectroscopy (ZEKE-PES). *Int. Rev. Phys. Chem.*, 12: 205–239, 1993.
- [13] I. Fischer, R. Lindner, and K. Muller-Dethlefs. State-to-state photoionization dynamics probed by zero kinetics energy (ZEKE) photoelectron-spectroscopy. *Journal Of The Chemical Society-Faraday Transactions*, 90: 2425–2442, 1994.
- [14] K. Muller-Dethlefs and E. W. Schlag. Chemical applications of zero kinetic energy (ZEKE) photoelectron spectroscopy. *Angewandte chemie-International edition*, 37: 1346–1374, 1998.
- [15] M. C. R. Cockett. Photoelectron spectroscopy without photoelectrons: twenty years of ZEKE spectroscopy. *Chem. Soc. Rev.*, 34: 935–948, 2005.
- [16] L. C. Zhu and P. Johnson. Mass analyzed threshold ionization spectroscopy. *J. Chem. Phys.*, 94: 5769–5771, 1991.
- [17] S. Sato and K. Kimura. Two-pulsed-field ionization method in zero kinetic energy photoelectron spectroscopy and mass analyzed threshold ionization spectroscopy. *Chem. Phys. Lett.*, 249: 155–161, 1996.
- [18] H. J. Neusser and H. Krause. Binding-energy and structure of van-der-Waals complexes of benzene. *Chem. Rev.*, 94: 1829–1843, 1994.

- [19] C. E. H. Dessent and K. Muller-Dethlefs. Hydrogen-bonding and van der Waals complexes studied by ZEKE and REMPI spectroscopy. *Chem. Rev.*, 100: 3999–4021, 2000.
- [20] M. N. R. Ashfold, J. M. Bayley, and R. N. Dixon. The $4s\leftarrow 1b_1$ and $3d\leftarrow 1b_1$ Rydberg States of H_2O and D_2O spectroscopy and predissociation dynamics. *Can. J. Phys.*, 62: 1806–1833, 1984.
- [21] A. Hodgson, J. P. Simons, M. N. R. Ashfold, J. M. Bayley, and R. N. Dixon. Quantum state-selected photodissociation dynamics in H_2O and D_2O . *Mol. Phys.*, 54: 351–368, 1985.
- [22] M. N. R. Ashfold, J. M. Bayley, R. N. Dixon, and J. D. Prince. Molecular predissociation dynamics revealed through multiphoton ionization spectroscopy. 3. New $1A_2$ and $1B_1$ Rydberg states in H_2S and D_2S . *Chem. Phys.*, 98: 289–313, 1985.
- [23] J. F. Black and I. Powis. Rotational structure and predissociation dynamics of the methyl $4p_z(v=0)$ Rydberg state investigated by resonance enhanced multiphoton ionization spectroscopy. *J. Chem. Phys.*, 89: 3986–3992, 1988.
- [24] M. N. R. Ashfold, S. G. Clement, J. D. Howe, and C. M. Western. Multiphoton ionization spectroscopy of free-radical species. *Journal of the chemical society-faraday transactions*, 89: 1153–1172, 1993.
- [25] A. E. Boguslavskiy, H. Ding, and J. P. Maier. Gas-phase electronic spectra of C_{18} and C_{22} rings. *J. Chem. Phys.*, 123: 034305, 2005.
- [26] J. M. Smith, X. Zhang, and J. L. Knee. Aniline- CH_4 S_1 vibrational dynamics studied with picosecond photoelectron-spectroscopy. *J. Chem. Phys.*, 99: 2550–2559, 1993.
- [27] A. Stolow. Femtosecond time-resolved photoelectron spectroscopy of polyatomic molecules. *Annu. Rev. Phys. Chem.*, 54: 89–119, 2003.
- [28] A. Stolow, A. E. Bragg, and D. M. Neumark. Femtosecond time-resolved photoelectron spectroscopy. *Chem. Rev.*, 104: 1719–1757, 2004.
- [29] M. Guilhaus. Time-of-flight mass spectrometry (Plenary lecture). In *Advances in Mass Spectrometry - Proceedings of the 15th International Mass Spectrometry Conference, Barcelona, August 27 - September 1, 2000*.
- [30] W. C. Wiley and I. H. McLaren. Time-of-flight mass spectrometer with improved resolution. *Rev. Sci. Instrum.*, 26: 1150–1157, 1955.

- [31] D. P. Seecombe and T. J. Reddish. Theoretical study of space focusing in linear time-of-flight mass spectrometers. *Rev. Sci. Instrum.*, 72: 1330–1338, 2001.
- [32] B. A. Mamyrin, V. I. Karataev, D. V. Shmikk, and V. A. Zagulin. Mass-reflectron a new nonmagnetic time-of-flight high-resolution mass-spectrometer. *Zhurnal Eksperimentalnoi I Teoreticheskoi Fiziki*, 64: 82–89, 1973.
- [33] B. A. Mamyrin, V. I. Karataev, D. V. Shmikk, and V. A. Zagulin. Mass-reflectron a new nonmagnetic time-of-flight high-resolution mass-spectrometer. *Sov. Phys. JETP*, 37: 45, 1973.
- [34] T. Bergmann, T. P. Martin, and H. Schaber. High-resolution time-of-flight mass spectrometers. 2. Reflector design. *Rev. Sci. Instrum.*, 61: 2592–2600, 1990.
- [35] D. Khoroshev. *Electronic spectroscopy of carbon chain radicals using cw cavity ring down in conjunction with mass detection*. PhD thesis, University of Basel, Basel, Switzerland, 2005.
- [36] Peter W. Milonni and Joseph H. Eberly. *Lasers*. (Wiley Series in Pure and Applied Optics). John Wiley & Sons, 1988. ISBN 0-471-62731-3.
- [37] J. W. Hepburn. *Laser Techniques in Chemistry*, chapter Generation of coherent vacuum ultraviolet radiation: applications to high-resolution photoionization and photoelectron spectroscopy, page 149183. Wiley, New York, 1995.
- [38] C. R. Vidal. *Tunable Lasers, Topics in Applied Physics, vol.59*, chapter Four wave frequency mixing in gases, pages 57–113. Springer, New York, 1987.
- [39] A. Yariv. *Quantum Electronics*. John Wiley & Sons, 3rd edition, 1988. ISBN 0-471-60997-8.
- [40] A. Bideau-Mehu, Y. Guern, R. Abjean, and A. Johannin-Gilles. Measurement of refractive-indexes of neon, argon, krypton and xenon in the 253.7-140.4 nm wavelength range. Dispersion-relations and estimated oscillator-strengths of the resonance lines. *J. Quant. Spectrosc. Radiat. Transfer*, 25: 395–402, 1981.
- [41] NIST. Atomic Spectra Database. http://physics.nist.gov/cgi-bin/AtData/main_asd.
- [42] R. Hilbig and R. Wallenstein. Enhanced production of tunable VUV radiation by phase-matched frequency tripling in krypton and xenon. *IEEE J. Quantum Electron.*, 17: 1566–1573, 1981.

- [43] H. Langer, H. Puell, and H. Rohr. Lyman-alpha (1216\AA) generation in krypton. *Opt. Commun.*, 34: 137–142, 1980.
- [44] R. Hilbig, G. Hilber, A. Lago, B. Wolff, and R. Wallenstein. Tunable coherent VUV radiation generated by nonlinear optical frequency conversion in gases. *Comments on Atomic and Molecular Physics*, 18: 157–180, 1986.
- [45] J. J. Wynne and P. P. Sorokin. *Nonlinear infrared generation, Topics Appl. Phys., Vol.16*, chapter Optical mixing in atomic vapors, pages 159–214. Springer, Berlin, Heidelberg, 1977.
- [46] H. Scheingraber, H. Puell, and C. R. Vidal. Quantitative-analysis of resonant 3rd-harmonic generation in strontium. *Phys. Rev. A*, 18: 2585–2591, 1978.
- [47] H. Puell, H. Scheingraber, and C. R. Vidal. Saturation of resonant 3rd-harmonic generation in phase-matched systems. *Phys. Rev. A*, 22: 1165–1178, 1980.
- [48] A. H. Kung, J. F. Young, and S. E. Harris. Generation of 1182\AA radiation in phase-matched mixtures of inert-gases. *Appl. Phys. Lett.*, 22: 301–302, 1973.
- [49] A. H. Kung. Correction. *Appl. Phys. Lett.*, 28: 239–239, 1976.

Chapter 3

Experimental

3.1 Molecular source

Two molecular sources were used in the experiments highlighted in this thesis: plasma discharge source and laser ablation source.

3.1.1 Discharge source

The discharge source, "our universal synthesizer"¹, is depicted in figure 3.1. Based on the design of Ohshima and Endo [1] it is indispensable for producing a great variety of both neutral and ionic hydrocarbon radicals. Nearly all carbon-chain-related spectroscopic gas phase studies in J.P. Maier group in Basel have been done using this "pinhole" discharge source or its slit modification [2–6]. A precursor diluted with buffer gas (Ar, Ne, He, N₂, etc.) down to 0.15–3% is expanded under 5–10 bar backing pressure into vacuum through the ceramic body. The gas burst generated by an electromagnetic valve (General Valve 106, \varnothing 0.7) is computer controlled. The amount of gas released is varied by manipulating the width of the valve opening pulse. Adjusting this in accord with the pressure in the source chamber allows one to keep the latter constant and thus ensuring stable source conditions. A 100–200 μ s long high voltage pulse (-700–900V) from a homebuilt power supply [7] is applied between the stainless steel electrodes placed on either side of the 10–20 mm thick insulating spacer. The channel is 1–1.2 mm thick all the way through the source, except for the insulator section where it is enlarged to 2 mm in order to create a localized plasma region. The inner electrode is simply a 1 mm thick disk with a 1 mm hole, and the outer one is 3–4 mm and possess a divergent conical exit channel through which plasma is expanded to the vacuum chamber. The mass distribution of the clusters can be influenced by increasing the thickness of the outer electrode. A lengthened electrode allows more time for "clustering" and generally results in a higher relative abundance of larger species. Source stability is better when the outer electrode is grounded while the inner one is negatively pulsed. The source is mounted on an XYZ translation system, which allows one to vary the solid angle sampled by the skimmer and thus a means to adjust the tolerance to the perpendicular velocity of the species in the beam. This gives control over the concentrations of species (both cold and hot) and their temperature characteristics during experiment. The typical distance was 50–70 mm.

3.1.2 Ablation source

This source (figure 3.2) was designed specifically to produce large pure-carbon chains. It relies on conventional laser vaporization of graphite [8–12]. The rod is rotated and

¹as it called by J.P. Maier

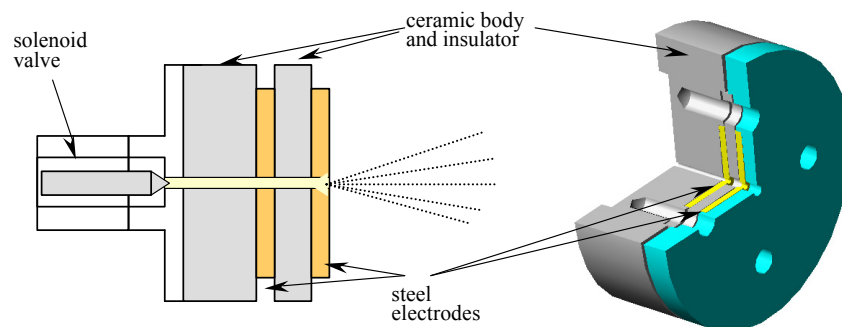


Figure 3.1: Discharge source.

translated so that a fresh surface is continuously exposed to the laser (25 mJ/5 ns pulse of 532 nm Nd:YAG, focused into 0.3 mm spot) which is fired to coincide with an inert gas flow over the target area. Vaporized carbon is swept through a 15 mm long and 3 mm diameter tube with a buffer gas under 3–10 bar backing pressure and expanded into a vacuum chamber. At the laser spot on the graphite rod the plasma is constricted at high buffer pressure. This makes clustering reactions in the plume of the carbon vapor rapid compared with the diffusion speed, which the production of results in large molecules [13] (figure 3.3). The distribution can be shifted down to smaller masses by shortening or removing the extender (effectively changing length of the interaction region from 20 to 5 mm). This reduces the time available for clustering, and smaller masses generally are produced. Typically Ar, Ne, or He is used as a buffer gas. The pressure can be varied from 10 to 3.5 bar in order to optimize production of a specific molecule. However, this will also affect the reaction products cooling efficiency, which should be kept in mind when doing such optimizations. Some discussion on the mechanism is given in the experimental section of the chapter 6.

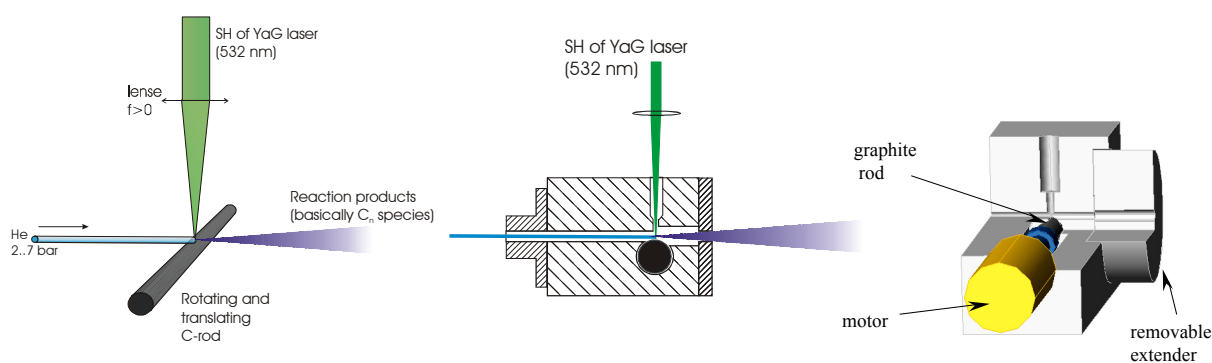


Figure 3.2: Ablation source.

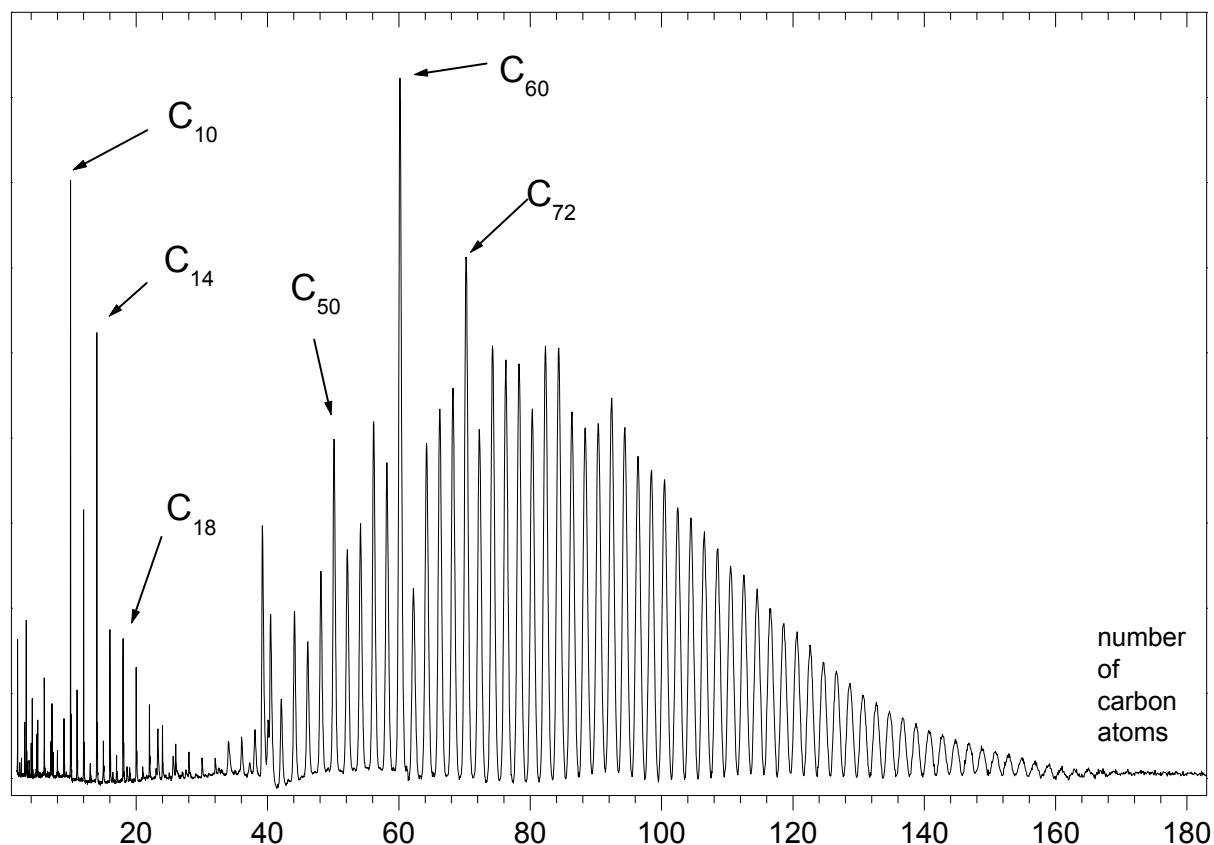


Figure 3.3: Neutral pure carbon moieties produced in the ablation source and ionized by 10.5 eV photons (9th harmonic of a Nd:YAG laser produced as described in the chapter 5.2)

3.2 Vacuum system

The vacuum system of the experimental apparatus consisted of two chambers - a source chamber and a TOF mass spectrometry chamber - separated by a 2 mm diameter skimmer (Beamline) and subjected to differential pumping. First, the source chamber consisted of a large stainless-steel cross-piece (25 cm in diameter and about 15 dm³ capacity) evacuated by a large diffusion pump (Edwards, EO6K, 2000 l/s with a baffle cooled by water) being backed with a 80 m³/h two-stage mechanical pump (Edwards E2M80). The pressure obtained in the chamber without operating the molecular source was at the level of $\sim 10^{-5}$ mbar, and typically $\sim 1.5 \times 10^{-4}$ mbar when operating the source at 20 Hz with a backing pressure of 8 bar. The second chamber hosted the TOF mass spectrometer and ion detector, and required vacuum on the order of 10^{-5} mbar. This requirement is achieved through the use of the turbo-molecular pumps: 210 l/s Pfeifer TMU261 (backed by a 12 m³/h mechanical pump Edwards RV12) is located near the region where the lasers interact with the molecules (extraction plates of TOF) and the second, smaller

pump (Balzers TPH190, 190 l/s backed by 10 m³/h mechanical pump Pfeifer DUO10) secures the MCP detector. A set of gauges are employed to indicate vacuum levels in the machine. Low vacuum, 1 bar–10⁻³ mbar, is monitored by Pirani-type gauges (Balzers TPR) whereas high vacuum in the range 10⁻³–10⁻⁷ mbar is diagnosed by Penning ionization gauges (Balzers IKR251). The pressure readings of the gauge in the source chamber are sent via RS232 port to a computer for feedback control of the valve driver program [14] to keep the pressure constant during the experiment.

3.3 Light sources

A summary of the coherent light sources used in the experiments is presented in figure 3.4(I). The most appropriate scheme for each experiment was chosen according to the energy constraints of ionizing photons, which should be able to ionize the studied molecule from an excited state and not from its ground state. The variety of tunable systems (figure 3.4(II)), in turn, is mostly stipulated by their inaccessibility on different stages of experiments.

To achieve maximum space overlap between laser and molecular beams, they were arranged in a way dictated by their dimensions (figure 3.5).

3.4 Ion detection

The ion detector used in the experiment is a Micro Channel Plate (MCP) detector. A microchannel plate (figure 3.6) consists of an array of glass capillaries (10–25 μ m inner diameter) that are coated on the inside with a electron-emissive material. The capillaries are biased at a high voltage and like the channeltron, an ion that strikes the inside wall one of the capillaries creates an avalanche of secondary electrons. This cascading effect creates a gain of 10³ to 10⁴ and produces a current pulse at the output. Two plate are stacked and connected in series (so-called Chevron configuration) so that the overall gain is 10⁶–10⁷. The MCP detectors provide high temporal resolution, direct conversion, high physical charge amplification, low noise, and pulse-counting capabilities. The fast response time (in 100 ps range) and flat geometry (effective area diameter of 25 mm) are particularly important for TOF mass spectrometric applications.

The detector is operated for positive ion detection (for the electrical arrangement see lower right corner of the figure 3.7). Following impact by the positive ion the first plate produces an electron output which is subsequently amplified to more electrons to provide a gain on the ion signal. The detector gain is governed by the potential applied to the plates (0–1 kV per plate). The gain selected is determined by the intensity of the ion signal

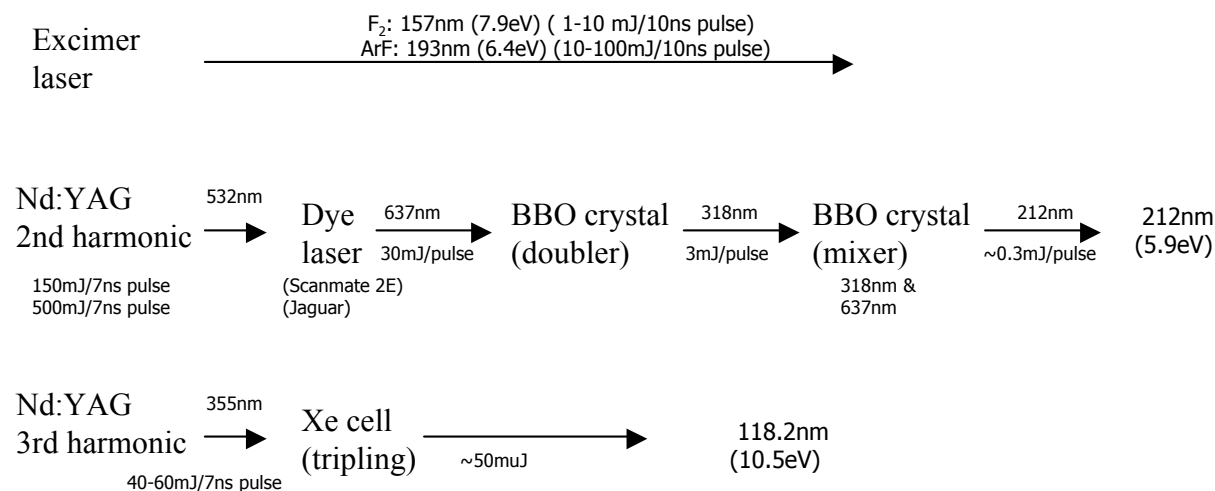
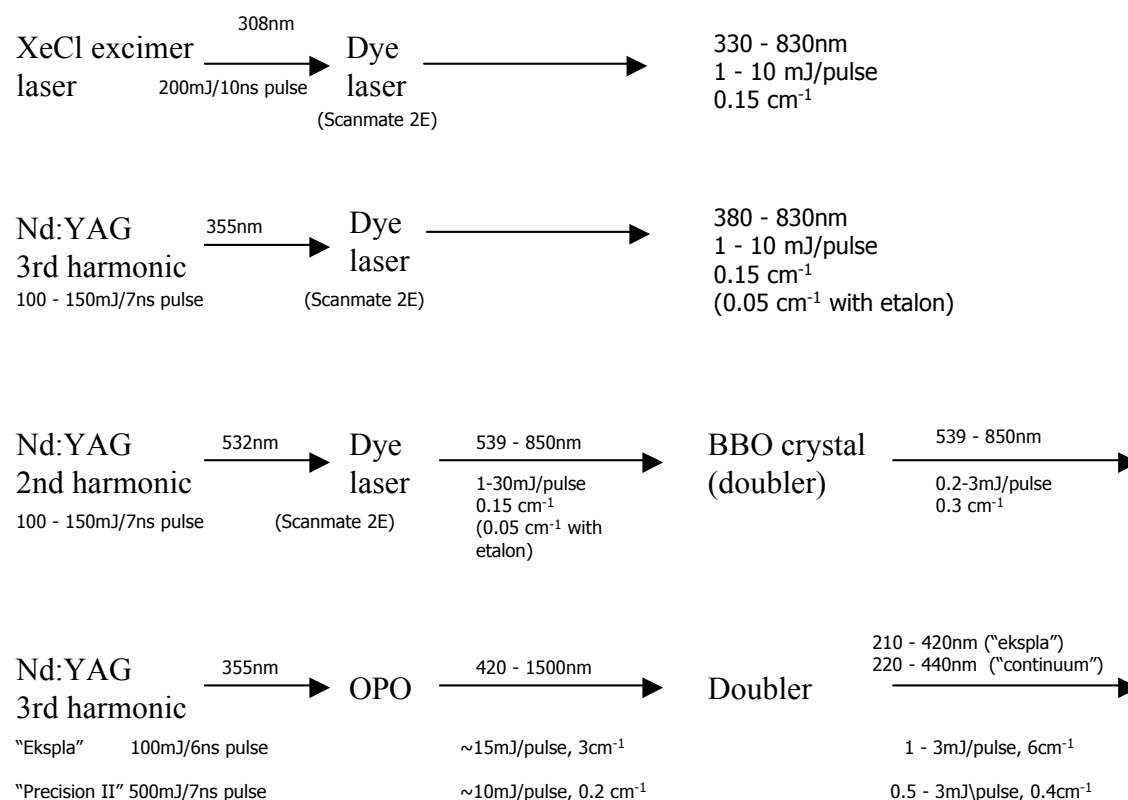
I. ionization:II. tunable:

Figure 3.4: Sources of coherent light used on different stages of experimental work described in the thesis.

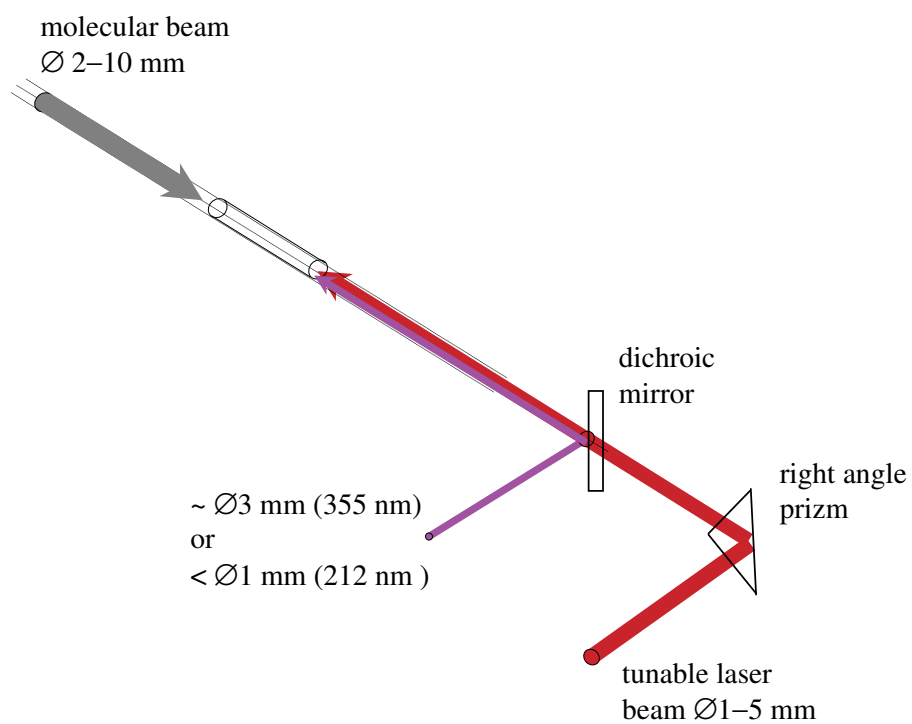
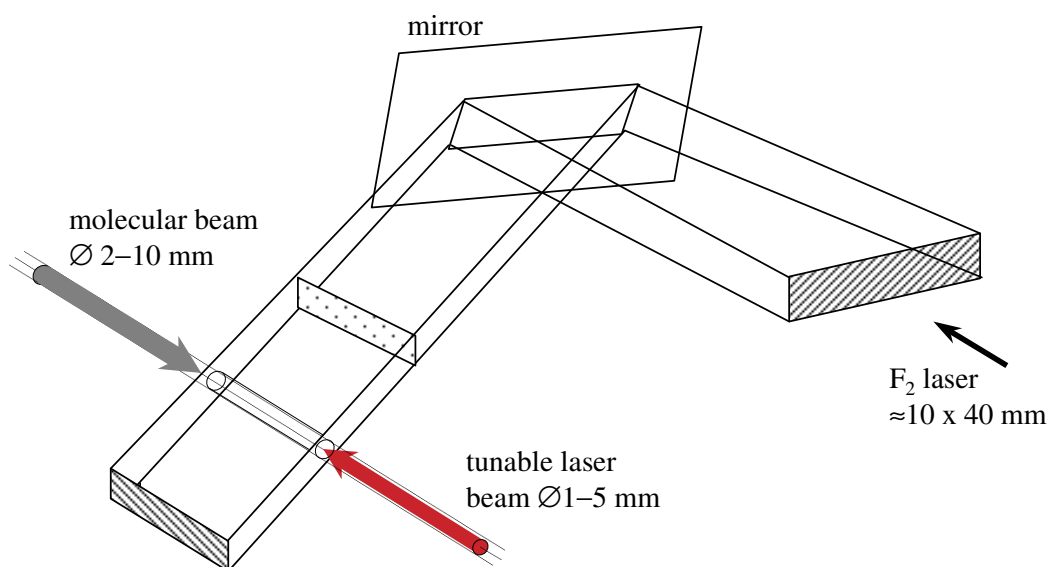


Figure 3.5: Combining molecular and laser beams for maximum overlap.

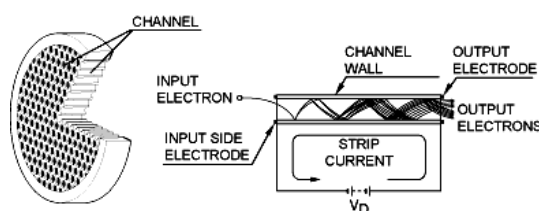


Figure 3.6: Schematic of a microchannel plate (from [15]).

observed on the oscilloscope and signal saturation is avoided by lowering the detector voltage when necessary. The detection efficiency² of the MCP varies considerably based on the velocity of the impinging ions. For positive ions with acceleration potential of ~ 3 kV the efficiency is approximately 40% [16]. The output of the detector is an electron current that is amplified by a fast, low-noise pre-amplifier and transmitted through a BNC cable to the oscilloscope (LeCroy LT342, 500MHz, 2 channels) where the accumulation and digitalization of the data takes place.

3.5 Data handling

Typically 30 laser shots were averaged by the oscilloscope before being transmitted via a GPIB interface to a PC computer. The whole data acquisition process is controlled by a program written in LabView.

The program can work in two main modes: mass spectrometer and REMPI spectrometer. The first mode allows the user to monitor the evolution of the mass spectrum in near real-time. The "master" computer interrogates the oscilloscope in cycle, requesting it to digitize and average a set number of laser shots, each of which is followed by a complete TOF cycle. The resulting waveform can replace the previous one on the screen of the PC or can be added to it when further signal accumulation is required. The mass calibration is defined by the operator through an empirical assignment of two time delays to the two masses. The calibration entered can be used immediately to convert the mass spectrum's abscissa axis to mass-to-charge (m/q) units. Assessment of correctness of calibration is usually done on base of integrality (integer value) of all observable mass-peaks.

The peak of interested can be marked and "gated" manually or automatically, based on the $M_0+i*M_1+j*M_2$ template(/expression). This is especially convenient when a certain family of molecules (for example like C_nH_3) is the focus of the study.

In the 'REMPI spectrometer' mode the program records the dependence of the mass-

²detection efficiency is defined as a measure of the ability of an incident particle to induce secondary electrons in a MCP detector.

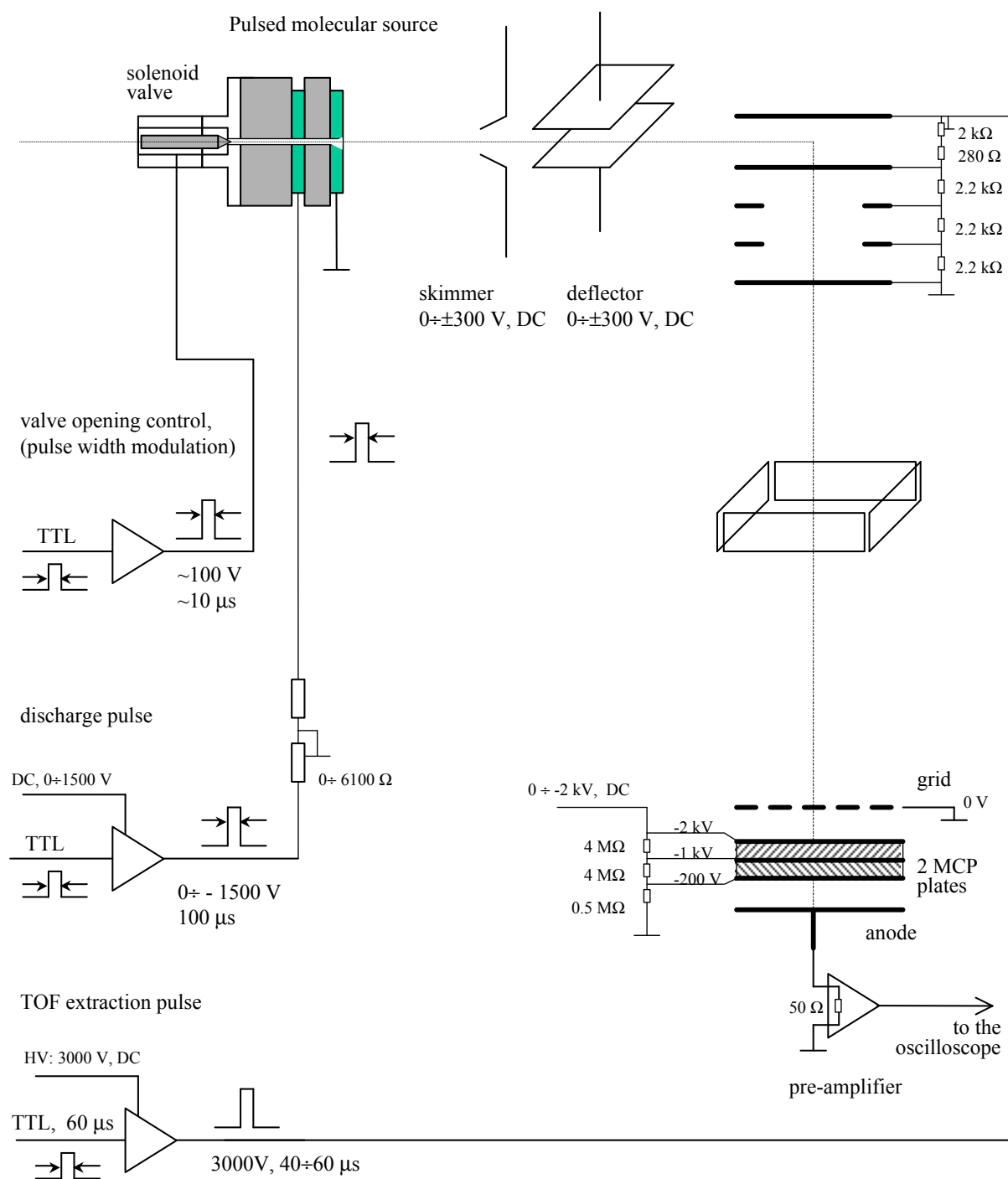


Figure 3.7: Electrical arrangement of the experiment.

spectrum on the laser wavelength. The master computer drives the scanning laser to the next wavelength, programs the oscilloscope on certain given number of accumulation cycles, and downloads the acquired waveform. The integral intensities of the gated peaks are calculated and stored. The cycle is looped and the laser is tuned to the next wavelength. Mass-peak area is proportional to the ion current of the ions with a specific mass, and, in turn, to the ionization efficiency of the corresponding neutral species. The variation of the peak area versus laser wavelength provides the REMPI spectrum of the molecule.

Bibliography

- [1] Y. Ohshima and Y. Endo. Structure of C_3S studied by pulsed-discharge-nozzle Fourier-transform microwave spectroscopy. *J. Mol. Spectrosc.*, 153: 627–634, 1992.
- [2] K. R. Comer and S. C. Foster. Infrared-spectroscopy of the products of a corona-excited supersonic expansion. *Chem. Phys. Lett.*, 202: 216–220, 1993.
- [3] D. T. Anderson, S. Davis, T. S. Zwier, and D. J. Nesbitt. An intense slit discharge source of jet-cooled molecular ions and radicals ($T_{rot} < 30K$). *Chem. Phys. Lett.*, 258: 207–212, 1996.
- [4] S. Davis, D. T. Anderson, G. Duxbury, and D. J. Nesbitt. Jet-cooled molecular radicals in slit supersonic discharges: Sub-Doppler infrared studies of methyl radical. *J. Chem. Phys.*, 107: 5661–5675, 1997.
- [5] J. Remy, L. Biennier, and F. Salama. Plasma structure in a pulsed discharge environment. *Plasma Sources Science & Technology*, 12: 295–301, 2003.
- [6] J. Remy, L. Biennier, and F. Salama. Plasma in a pulsed discharge environment. *IEEE Transactions On Plasma Science*, 33: 554–555, 2005.
- [7] Georg Holderied, Ing.HTL. Chemistry Department, University of Basel.
- [8] D. E. Powers, S. G. Hansen, M. E. Geusic, A. C. Pui, J. B. Hopkins, T. G. Dietz, M. A. Duncan, P. R. R. Langridgesmith, and R. E. Smalley. Supersonic metal cluster beams laser photo-ionization studies of Cu_2 . *J. Phys. Chem.*, 86: 2556–2560, 1982.
- [9] T. G. Dietz, M. A. Duncan, D. E. Powers, and R. E. Smalley. Laser production of supersonic metal cluster beams. *J. Chem. Phys.*, 74: 6511–6512, 1981.
- [10] P. Milani and W. A. Deheer. Improved pulsed laser vaporization source for production of intense beams of neutral and ionized clusters. *Rev. Sci. Instrum.*, 61: 1835–1838, 1990.

- [11] K. Laihing, R. G. Wheeler, W. L. Wilson, and M. A. Duncan. Photoionization dynamics and abundance patterns in laser vaporized tin and lead clusters. *J. Chem. Phys.*, 87: 3401–3409, 1987.
- [12] E. F. Rexer, M. P. Joshi, R. L. DeLeon, P. N. Prasad, and J. F. Garvey. A reactive laser ablation source for the production of thin films. *Rev. Sci. Instrum.*, 69: 3028–3030, 1998.
- [13] J. R. Heath, Q. Zhang, S. C. O'Brien, R. F. Curl, H. W. Kroto, and R. E. Smalley. The formation of long carbon chain molecules during laser vaporization of graphite. *J. Am. Chem. Soc.*, 109: 359–363, 1987.
- [14] T. Motylewski. *Cavity ringdown spectroscopy of transient species*. PhD thesis, Basel University, 2001.
- [15] Del Mar Ventures. Microchannel Plates and Microchannel Plate Detectors. <http://www.sciner.com/MCP/MCP.htm>.
- [16] Burle Industries, Inc. Scientific detectors products: Technical Brief No2 - Detection Efficiency. http://www.burle.com/dettechbrief_2.htm.

Chapter 4

Spectroscopy of C_{4n+2} carbon rings

Foreword

This chapter is devoted to the spectroscopic study of the C_{14} , C_{18} , C_{22} pure-carbon species in the gas phase. The molecules were synthesized using a graphite ablation source and detected by REMPI. Information on their masses allowed the chemical formula to be determined. Additional analysis was involved to draw conclusions about their cyclic nature. Linear and cyclic forms could be distinguished from the behavior of the absorptions on addition of hydrogen to the plasma discharge while monitoring the produced linear $HC_{4n+2}H$ species whose absorption spectrum is known. Knowledge concerning where the linear isomer absorbs, calculated ground state stabilities, and comparison with calculated excitation energies for the cyclic isomer helped assign the spectra.

Since the publication of the corresponding paper [1] in *Journal of Chemical Physics*, the importance of investigation of these sort of molecules was realized to an increased degree. Although immediate spectroscopic matches with known DIBs were not found in subsequent studies [2], the analysis of the C_{18} origin band profile revealed a striking resemblance to the observed structure of a number of DIBs at other wavelengths. This could suggest that platelike molecules or ions, comprising a couple of dozen to hundred carbon atoms, could be responsible for some of the latter absorptions.

This finding is especially interesting in the light of the issue of the questionable validity of the PAH hypothesis of the DIB carriers. This is because PAH cations are inherently unstable to photolysis [3–5]. Fragmentation patterns for two dozen polycyclic aromatic hydrocarbon (PAH) cations, the photostabilities of which have been tested in [4], fell into four groups: photostable, hydrogens loss only, hydrogens and carbons loss, and photodestroyed. Another study [3] concentrated on coronene cation $C_{24}H_{12}^+$ indicates that depending on photon flux, the molecule subjected to, partial and even complete dehydrogenation may occur.

It is unlikely that the resulting $C_{24}H_{n<12}^+$ would retain PAH-like form [4]. These losses must be followed by some structural reorganization and accompanied by one or more ring openings, suggesting that some bare neutral and ionic carbon rings of this size may be prevalent in the diffuse medium. Hence the relevance of the current study on cyclic carbon molecules.

Cyclic C_{18} is essentially a dehydrogenated PAH, also with singlet ground state, but is perhaps photochemically more robust because the hydrogens have already been removed and the $4n+2$ ring shows enhanced stability. Indeed, the bare carbon molecules demonstrate an enhanced photostability compare to PAH^+ . Thus, for example, the coronene study mentioned above indicates that the respective C_{24}^+ cations resist further dissociation. Isolated in matrix bare carbon cluster anions, C_{16}^- to C_{40}^- were also found to be stable, unlike the smaller carbon cluster anions, and were not photobleached when exposed to

broadband irradiation [6].

On the other hand, a good number of studies on the fragmentation patterns of pure-carbon moieties (both ionic and neutral) indicate losses of C_2 and C_3 , and, though in much less copious amounts, C_5 , $C_{10,14,18,22}$ (see discussion in experimental section of the chapter about C_5 and references therein). This may suggest that similar processes may occur with dehydrogenated PAHs in space. Though fully dehydrogenated coronene did not produce further fragmentation [3] under conditions of those experiments, it is not impossible that under higher photon flux or with other PAHs this would happen.

Gas-phase electronic spectra of C₁₈ and C₂₂ rings

A. E. Boguslavskiy, H. Ding, and J. P. Maier^{a)}

Department of Chemistry, University of Basel, Klingelbergstrasse 80, CH-4056 Basel, Switzerland

(Received 27 April 2005; accepted 27 May 2005; published online 28 July 2005)

The electronic spectra of C₁₈ and C₂₂ in the 15 150–36 900 cm⁻¹ range have been detected in the gas phase by a mass-selective resonant two-color two-photon ionization technique coupled to a laser ablation source. The spectra were assigned to several electronic systems of monocyclic cumulenic isomers with a *D*_{9h} symmetry for C₁₈ and *D*_{11h} for C₂₂, based on time-dependent-density-functional calculations and reactivity with respect to H₂. The best cooling conditions were achieved with Kr as the buffer gas, and the origin of the $\tilde{A}^1A_2'' \leftarrow \tilde{X}^1A_1'$ transition of C₁₈ at 592.89 nm shows a pair of 1 cm⁻¹ broadbands spaced by 1.5 cm⁻¹. The next electronic transitions exhibited much broader, ~30 (in the visible) to 200 cm⁻¹ (in ultraviolet range), features. The spectrum of C₂₂ exhibits an absorption pattern similar to C₁₈, except that the narrow features to the red are missing; the oscillator strength of the $\tilde{A} \leftarrow \tilde{X}$ transition is predicted to be low. © 2005 American Institute of Physics. [DOI: 10.1063/1.1961564]

I. INTRODUCTION

The study of pure carbon molecules has attracted interest for many decades.^{1,2} Following the discovery of C₆₀ (Ref. 3) and carbon nanotubes⁴ much effort has been devoted to comprehending the structures and properties of pure carbon molecules. These species are also present, for example, in hydrocarbon flames and as intermediates in the plasma chemistry taking place in vapor deposition systems for the production of diamond and silicon carbide films. Thus the study of their electronic structure and spectra is necessary for an understanding of these environments. However, the experimental measurements on neutral carbon species with more than a few atoms are still limited.

The linear isomers of C₄–C₁₀ have been identified by electron spin-resonance (ESR) measurements in neon matrices.⁵ Chains up to C₁₃ have been observed via infrared vibrational spectroscopy in rare-gas matrices^{6,7} and in the gas phase.^{8,9} The electronic absorption spectra in solid neon have identified linear chain structures for C_{2n} (*n*=2–7) (Refs. 10 and 11) and C_{2n+1} (*n*=2–10).^{12,13}

Though a variety of structures for the bare carbon entities, both cations and anions, have been established from ion mobility measurements,^{14,15} electronic transitions on rings have been detected so far only in low-temperature matrices. In the latter, some absorption bands of mass-selected C₁₀, C₁₂, and C₁₄ were assigned to transitions of monocyclic structures.¹⁶ The Raman spectra of matrix-isolated mass-selected C_{2n} (7 ≤ *n* ≤ 10) were assigned to linear isomers.^{17,18} However, the fluorescence spectra seen under the same conditions for C_{*n*} (*n*=14, 18) were attributed to cyclic isomers.¹⁸

In the recent years an effort has been made by our group to obtain the electronic spectra of carbon chains, particularly in an attempt to understand which species have strong transitions in the diffuse interstellar band (DIB) region. The

smallest linear polyatomics C_{3–5} have been searched for in diffuse interstellar clouds as their gas-phase electronic spectra are known. Because only C₃ could be detected,^{19,20} these studies led to the conclusion that only certain systems of the longer carbon chains seem to satisfy the criteria necessary to be DIB carriers.²¹

Among the bare carbon moieties, apart from fullerenes, species with 10, 14, 18, and 22 atoms attract special attention. These magic numbers manifest themselves in the mass spectra with 10.5 eV photon ionization of neutral molecules produced by laser ablation of graphite.²² They also appear to correspond to the size of preferential neutral loss by collision-induced dissociation according to the mobility experiments on relatively large carbon cations.^{14,15,23}

The measurement of gas-phase electronic spectra of larger carbon chains and rings is a challenge. For this purpose a laser ablation graphite source in conjunction with a resonance-enhanced multiphoton ionization (REMPI) detection scheme has been used. The gas-phase electronic spectra of C₁₈ and C₂₂ have been obtained using a mass-selective resonant two-color two-photon ionization (R2C2PI) spectroscopy under a supersonic molecular-beam condition. The theoretical calculations using density-functional theory were carried out to guide an assignment of the observed spectra.

II. EXPERIMENT

The apparatus consisted of a molecular beam combined with a linear time-of-flight (TOF) mass analyzer.²⁴ The source relied on a conventional laser vaporization of graphite coupled to a pulsed valve. The rod was rotated and translated so that a fresh surface was continuously exposed to the laser [25 mJ/5 ns pulse of 532 nm Nd:YAG, 0.3 mm spot] which was fired to coincide with the inert gas flow over the target area. Vaporized carbon was swept through a 15 mm-long and 3 mm diameter tube with helium or neon at 5–10 bars and expanded into a vacuum chamber. The carbon species produced passed through a skimmer into a differentially pumped

^{a)}Electronic mail: j.p.maier@unibas.ch

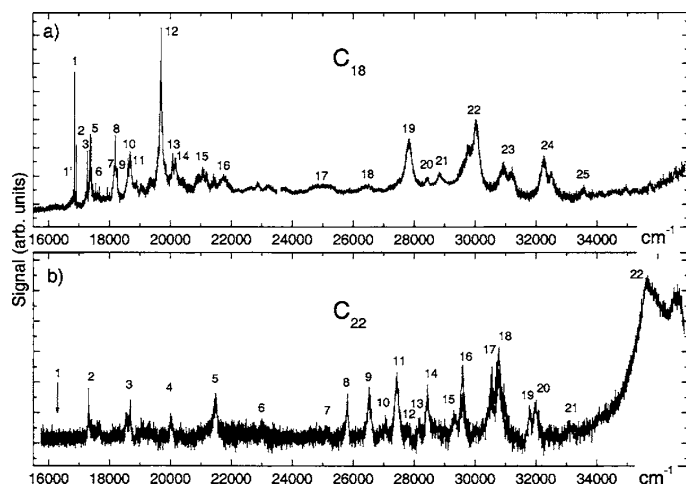


FIG. 1. Gas-phase electronic spectra of (a) C_{18} and (b) C_{22} detected by a resonant two-color two-photon ionization technique under supersonic molecular-beam conditions.

region where ions were removed by a perpendicular electrical field before entering the extraction zone of the TOF. The neutral molecules were then ionized by 7.9 eV photons of a F_2 laser. The ionization process is more efficient when the tunable laser is resonant with an allowed electronic transition. Ions were extracted and accelerated towards a dual microchannel plate detector. The excitation photons in the 278–341, 325–450, and 440–680 nm ranges were delivered by Nd:YAG, excimer-pumped dye laser, or an optical parametric oscillator system. The latter was anticollinear to the molecular beam, while the ionization laser was perpendicular, allowing for maximum overlap. Variation of the mass-peak amplitude as function of the laser wavelength gives the R2C2PI spectrum of the molecule with a defined mass. Separation of the ions in the drift tube after resonant excitation enables a large number of masses to be monitored simultaneously.

III. OBSERVATIONS

A. Spectra

Figure 1 shows the measured electronic excitation spectra of C_{18} [Fig. 1(a)] and C_{22} [Fig. 1(b)] in the 15150–36900 cm^{-1} range. Immediately noticeable is the broadness ($\sim 100 \text{ cm}^{-1}$) of all the bands except for the first two groups to the red which have widths $< 10 \text{ cm}^{-1}$. The spectra were recorded at different laser pulse energies, from tenths up to 15 mJ to test for power broadening. No noticeable changes in the widths of the bands were observed. Varying the backing pressure and the carrier gas of the supersonic expansion in an effort to modify the reaction products' cooling efficiency did not appear to influence the widths of the broad peak systems, implying that it is intrinsic. On the other hand changing the cooling conditions did have an influence on the narrower peaks (see Sec. III B).

Some similarities between the spectra of the two species are observed. Both possess a series of twin peaks in the 28 000–33 000 cm^{-1} range with those from C_{22} being almost a copy of those from C_{18} but shifted by $\sim 480 \text{ cm}^{-1}$ to the red. The growth started on the blue edge of the C_{18} spectrum

predicts the beginning of an analogous absorption in the spectrum of C_{22} , which lies outside the range scanned.

Yet there are differences between the two spectra. The strong progression starting at 27 830 cm^{-1} , with a spacing of 2205 cm^{-1} , apparent in the UV region of the C_{18} spectrum does not have a direct counterpart for C_{22} . Even though both spectra contain a twin pattern on the UV side, the linewidths of those in C_{18} were 1.5 times larger than in C_{22} . In contrast to C_{18} , C_{22} exhibits less pronounced features in the visible. The spread of the peaks and the complicated nature of the spectra indicate the presence of at least four but probably more electronic transitions.

The relative intensities of the bands in the spectrum were not calibrated in the UV (278–440 nm) range, where dye lasers were used. The maxima of the observed vibronic bands determined by single- and/or multi-Lorentzian fits are given in Tables I and II.

B. Bandwidths

The broadness of the majority of the spectroscopic features ($\sim 100 \text{ cm}^{-1}$) is striking. The rotational structure overlap for such molecules is estimated to be a few wave numbers. Thus the width corresponds to a 0.1 ps excited-state lifetime. This is five orders of magnitude smaller than the pulse width of the lasers used in the experiment. Predissociation can be excluded because no peaks were observed at the same wavelength for species of smaller masses. This behavior is similar to that seen for $HC_{2n}H$,²⁵ $C_{2n+1}H$,²⁶ and transitions into B state of $HC_{13}H$ and $HC_{19}H$ (Ref. 29) measured by the R2C2PI technique. Intramolecular processes were concluded to be responsible for this relaxation and are efficient due to the number of electronic states accessible. After excitation into the prepared state, internal conversion to an intermediate state occurs on a subpicosecond time scale. Experimental evidence for this was observed for C_{18} and C_{22} ; the signal did not change when the delay between the excitation and ionization laser was varied from a few up to 500 ns. For such a two-color signal to be detected, the Franck-Condon factor for the ionization step at 7.9 eV must

TABLE I. Maxima of the vibronic bands observed in the electronic spectrum of C₁₈ and the suggested assignment in *D*_{9h} symmetry.

Label	ν (cm ⁻¹)	$\Delta\nu$ (cm ⁻¹)	Transition
1'	16 806	-56	
1	16 862	0	$\tilde{A}^1A_2'' \leftarrow \tilde{X}^1A_1'$
2	16 919	57	
3	17 274	412	
4	17 347	485	
5	17 377	515	
6	17 401	539	
7	18 151	-55	
8	18 206	0	$\tilde{B}^1A_2'' \leftarrow \tilde{X}^1A_1'$
9	18 262	56	
10	18 612	406	
11	18 690	484	
12	19 695	0	$\tilde{C}^1E_1' \leftarrow \tilde{X}^1A_1'$
13	20 080	385	
14	20 170	475	
15	21 060	1365	
16	21 735	2040	
17	22 880	3185	
18	25 260	5565	
19	27 830	0	$\tilde{D}^1E_1' \leftarrow \tilde{X}^1A_1'$
20	28 420	590	
21	28 840	1010	
22	29 755 (& 30 035)	0	$\tilde{E}^1E_1' \leftarrow \tilde{X}^1A_1'$
23	30 940 (& 31 190)	~1170	
24	32 255 (& 32 495)	~2480	

be favorable. This will be the case for molecules with an ionization potential comparable to the photon energy.

In contrast, the two bands in the red part of spectrum are two orders of magnitude narrower than others (corresponding to 10 ps as the lower limit to the excited-state lifetime). Such a difference in the internal conversion rate can be rationalized assuming this state is the lowest excited one of this multiplicity and thus internal conversion is not efficient. This interpretation is in accord with the electronic spectra of polyacetylene chains. Absorptions to *B*, *C*, and *D* states of C_{2n+1}H and to *B* state of HC_{2n+1}H were seen as broad features with widths of hundreds of cm⁻¹ slowly dependent on chain size, whereas those to the *A* state were found to be orders of magnitude narrower.^{26,27}

C. Rotational and vibrational cooling

A supersonic jet expansion was used to remove the excess energy of the transient species. The rotational temperatures of the molecules was expected to be the same (20–40 K) to those attained with a discharge source in previous experiments^{25–27} because the gas flow parameters used in the laser vaporization source were similar. Vibrationally excited molecules, on the other hand, are not as efficiently cooled through adiabatic expansion. The achieved distribution is far from statistical, making vibrational temperature mode specific. In these experiments a number of carrier gases were used to study the collisional relaxation upon larger carbon chains such as C₁₈. Using nitrogen resulted in a much better vibrational cooling (Fig. 2) than with helium

TABLE II. Maxima of the vibronic bands observed in the electronic spectrum of C₂₂ and the suggested assignment in *D*_{11h} symmetry.

Label	ν (cm ⁻¹)	$\Delta\nu$ (cm ⁻¹)	Transition
1	16 114	0	$\tilde{C}^1E_1' \leftarrow \tilde{X}^1A_1'$
2	17 320	1206	
3	18 553	2439	
	18 688	2574	
4	20 020	3906	
5	21 490	5376	
6	22 980	6866	
7	25 120	0	$\tilde{D}^1E_1' \leftarrow \tilde{X}^1A_1'$
9	26 525	1405	
12	27 800	2680	
15	29 310	4190	
17	30 540	5420	
19	31 790	6670	
21	33 095	7975	
8	25 810	0	$\tilde{E}^1E_1' \leftarrow \tilde{X}^1A_1'$
10	27 060	1250	
13	28 160	2350	
16	29 575	3765	
18	30 780	4970	
20	31 990	6180	
11	27 430	0	$\tilde{F}^1E_1' \leftarrow \tilde{X}^1A_1'$
14	28 430	1000	

or neon, suppressing the broad red tails caused by sequence bands. Because low-energy vibrational modes, such as $\nu \sim 56$ cm⁻¹, were already sufficiently cooled ($T_{\text{vib}} \sim 60$ –70 K) using Ne, significant further relaxation with N₂ was not observed ($T_{\text{vib}} = 37$ K). Higher-frequency modes, on the other hand, are typically more resistant to cooling and therefore require a heavier carrier gas.

By using a proper buffer gas the width of origin band was decreased down to ~ 5 cm⁻¹. Higher-resolution scans reveal further substructure: three bands whose intensities and maxima depend on the carrier gas. The spectra shown in Fig. 3 are normalized to peak c. Upon changing the cooling gas, peak a gradually decreases and shifts slightly toward

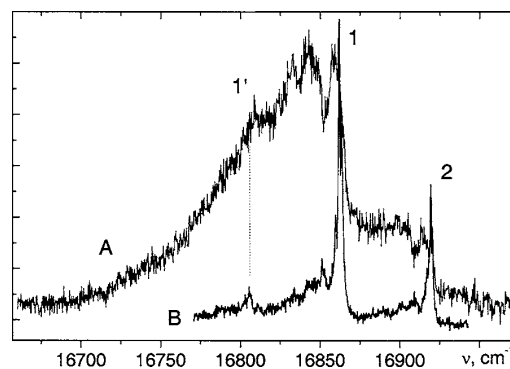


FIG. 2. The lowest-energy band in the electronic spectrum of C₁₈ recorded under different expansion conditions. Trace A was obtained using Ne as a buffer gas, whereas trace B was obtained using 10% N₂ in Ne. Incorporating N₂ into Ne led to more efficient cooling. Peak 1 is assigned to the origin of the electronic transition. 1' is a hot band $\nu(57 \text{ cm}^{-1})_0^0$ and 2 is a vibronic band $\nu'(56 \text{ cm}^{-1})_0^1$.

034305-4 Boguslavskiy, Ding, and Maier

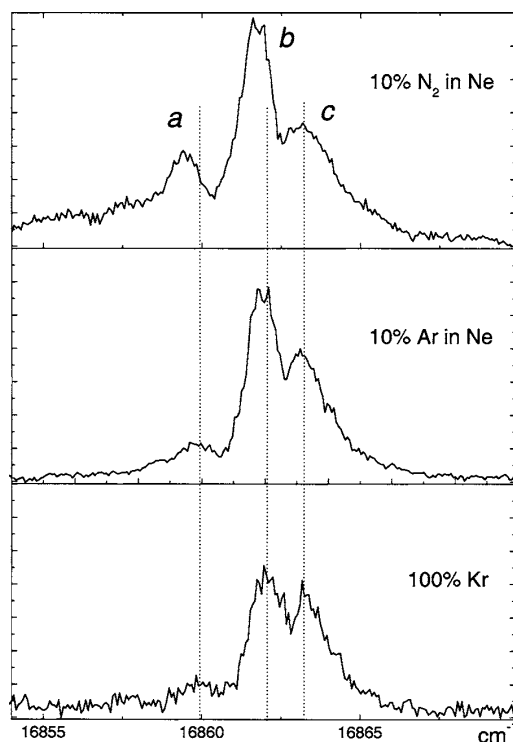
J. Chem. Phys. **123**, 034305 (2005)

FIG. 3. Closeup of the origin band of C_{18} showing three peaks whose intensity ratio is dependent on the internal temperature. The three spectra are normalized to peak c. Peak a gradually decreases and slightly shifts towards higher energy upon changing the cooling gas. At the same time the relative amplitude of peak b decreases.

higher energy. At the same time the relative amplitude of peak b reduces too. With the heaviest gas used (Kr) the profile evolves into a pair of equally strong, 1 cm^{-1} wide lines spaced by 1.5 cm^{-1} . This may be due to a level splitting in a double-well potential which is expected to take place in monocyclic molecules such as C_{18} along the even-odd bond-length alternation or analogous angle alternation normal coordinates (see Sec. IV). The residual bandwidth may be attributed to the overlap of rotational structure which is estimated to be about 1.5 cm^{-1} at 30 K rotational temperature.

IV. AB INITIO CALCULATIONS

Theoretical studies predict that the even-numbered C_n carbon molecules with less than ten atoms possess a linear geometry with triplet ground electronic state, whereas for $C_n > 10$ monocyclic structures are preferred.^{28,29} Measurements in neon matrices indicate that neutrals coexist in both linear and cyclic forms up to 14 atoms.^{11,16} According to ion chromatography, linears sustain at least up to 20 for anions but only up to 10 for cations.¹⁵ The relative linear-to-cyclic ratio of neutrals produced by a given source is apparently dependent on production pathways and both isomers need to be considered. The calculations for four isomers of each C_{18} and C_{22} were carried out at the B3LYP/6-31G* level using GAUSSIAN03. The optimized ground-state geometries and

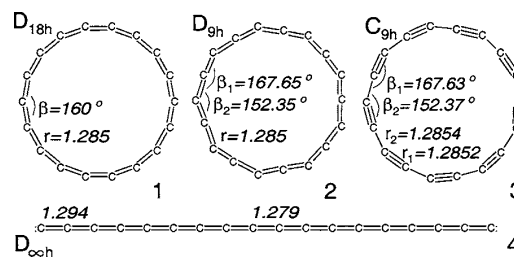


FIG. 4. Geometries of the ground states of the C_{18} isomers optimized at DFT-B3LYP/6-31G* level. The bond lengths are given in angstrom. The structure 3 (C_{9h}) is the only local minimum at the HF level, but effectively converges to cumulenic D_{9h} upon optimization at the DFT level.

relative energies of linear and three cyclic isomers are indicated in Fig. 4 and Table III. Among these the linear isomer has the highest relative energy, 3.5 eV above the cyclic structure with D_{18h} symmetry. The cyclic isomer is doubly aromatic because the valence electrons are delocalized in two perpendicular systems of π orbitals, one in the ring plane, another one out of it. Structures 2 (D_{9h}), 3 (C_{9h}), and 4 ($D_{\infty h}$) are local minima, whereas 1 (D_{18h}) is a high-order saddle point. Lowering the symmetry by splitting the carbon atoms into two equivalent subgroups via bond-angle alternation leads to a D_{9h} cumulenic cycle with an energy of 0.11 eV lower. Alternation of bond length instead gives an acetylenic D_{9h} structure which is a saddle point. Simultaneous alternation of distances and angles brings the molecule to C_{9h} symmetry. The last structure is the only local minimum at the HF level, but effectively converges to cumulenic D_{9h} upon optimization at the density-functional theory (DFT) level.

The excited states were calculated using the time-dependent DFT method³⁰ with a B3LYP functional and 6-31G* basis sets. To check if the approach is suitable, linear and cyclic C_{10} were used as a test because experimental values are available.^{11,16} This comparison indicates that the calculated vertical excitation energies of the allowed transitions of C_{10} are within 0.1–0.3 eV of the experiment (Table IV). Thus the TD-DFT calculations appear suitable to predict the electronic absorption spectrum of large carbon species where high-level electron correlation approaches [such as complete active space self-consistent field (CASSCF) or multireference configuration interaction (MRCI)] cannot easily be used.

Vertical electronic excitation energies of C_{18} and C_{22} were calculated at the optimized ground state geometries and are listed in Tables V and VI. The calculations predict ten dipole allowed electronic systems within the studied spectral

TABLE III. Calculated relative stabilities of C_{18} isomers.

C_{18}	HF/6-31G*	B3LYP/6-31G*	Ground state
	$\Delta E/\text{eV}$ (im. freq.)	$\Delta E/\text{eV}$ (im. freq.)	
$D_{\infty h}$	3.23 (6)	3.63 (0)	$X^3\Sigma_g^-$
D_{18h}	2.98 (2)	0.11 (5)	X^1A_{1g}
D_{9h}	1.41 (1)	0.00 (0)	$X^1A'_1$
C_{9h}	0 (0)	0 (0)	X^1A^1

TABLE IV. Calculated vertical transition energies (in eV) and oscillator strengths for the C₁₀ isomers using the TD-DFT-B3LYP/6-31G* level of theory and comparison with the experimental values.

Molecule	Transition	TD-DFT (<i>f</i>)	Expt. (Ref. 16)
<i>cyc</i> -C ₁₀ (<i>D</i> _{10h})	¹ E _{1u} ← \tilde{X} ¹ A _{1g}	3.932 (0.0229)	3.921
<i>lin</i> -C ₁₀ (<i>D</i> _{∞h})	³ Π _u ← \tilde{X} ³ Σ _g ⁻	1.540 (0.0015)	
	³ Σ _u ⁻ ← \tilde{X} ³ Σ _g ⁻	1.840 (0.0064)	
	³ Π _u ← \tilde{X} ³ Σ _g ⁻	3.355 (0.0013)	3.461
	³ Π _u ← \tilde{X} ³ Σ _g ⁻	4.097 (0.0098)	3.717
	³ Σ _g ⁻ ← \tilde{X} ³ Σ _g ⁻	4.321 (3.6348)	

range 1.55–4.5 eV for the linear structure of C₁₈ and C₂₂. The lowest-energy allowed transitions are predicted at 1.13 eV (C₁₈) and 0.96 eV (C₂₂), while the strongest band systems should lie at 2.8 and 2.45 eV. There is only one dipole-allowed electronic transition at 2.39 and 1.98 eV, respectively, for the highly symmetric cumulenic *D*_{18h} cyclic structure of C₁₈ and *D*_{22h} one of C₂₂. In contrast, for the lower symmetry cumulenic rings (*D*_{9h} and *D*_{11h}) five dipole-allowed electronic transitions are predicted for C₁₈ (*D*_{9h}) and six for C₂₂ (*D*_{11h}) in the same energy range (Tables V and VI).

V. DISCUSSION

A. Isomer structure

In order to discriminate between the ring and the chain structures of C₁₈ the reactivity with hydrogen was studied. The carrier gas was seeded with 10% of H₂ and the peak intensities were compared to those without H₂. While changes in mass peaks of other C_{*n*} molecules occurred, no visible variations in the amplitude of the C₁₈ mass peak were observed. At the same time the signals corresponding to the mono- and the dihydrogenated C₁₈ gradually grew. The absence of multihydrogen peaks is consistent with the expected lower reactivity of the cyclic-C₁₈ isomer compared to the linear one.³¹ Monocycles have a closed electron shell structure while the even-numbered linear chains are open shell

with the two terminal carbon atoms left unsaturated. Using these conditions the R2C2PI spectra of the C₁₈ and HC₁₈H were recorded simultaneously. The electronic transition of the linear polyynic chain HC₁₈H is known.²⁵ Thus there is no doubt that linear C₁₈ is present in the beam. On the other hand, the addition of hydrogen does not change the intensity of the C₁₈ spectral bands shown in Fig. 1. The same approach was applied to C₂₂ and HC₂₂H and gave an analogous result. Another consideration is that the linear carbon chain molecules should form C_{2*n*} homologous series whereas cycles comply with the (4*n*+2) Hückel aromaticity rule. In fact, the absorption of C₁₄ has also been observed, but not of C₁₆ nor C₂₀, which suggests that C₁₄, C₁₈, and C₂₂ belong to one family. The above arguments seem to indicate that the observed spectra arise from cyclic isomers of C₁₈ and C₂₂.

Further support for this interpretation is based on predictions made by theory (Sec. IV). The highly symmetric C₁₈ (*D*_{18h}) and C₂₂ (*D*_{22h}) isomers would lead to only one electronic transition in the measured range, whereas lowering the symmetry down to *D*_{9h} (*D*_{11h}) results in five (six) allowed ones, in agreement with experimental observations. In view of the predictions for the relative energetics, the *D*_{9h} (or *D*_{11h}) structures are expected to be the major contributors to the observed spectra.

The calculations employed were unable to discriminate between C_{4*N*+2/2*h*} and *D*_{4*N*+2/2*h*} structures. This would have helped to resolve the controversy surrounding the critical size in C_{4*n*+2} rings at which the Peierls transition from the aromatic (bond angle alternated) to dimerized (bond length alternated) ground state structures occurs.^{32–35} Where this crossover happens would provide a sensitive probe for the treatment of electron correlation in different theoretical approaches. The gas-phase spectroscopical data presented here could serve as a selection criterion for this with more rigorous electronic transition calculations.

B. Electronic transitions

1. C₁₈

The assignment of electronic transitions is guided by the calculations (Table V). The first strong vibronic band 1 to the

TABLE V. Calculated vertical transition energies (in eV) for the lowest dipole-allowed electronic transitions for three isomers of C₁₈ at the optimized ground-state geometries using the TD-DFT approach with 6-31G* basis sets.

State	<i>lin</i> -C ₁₈ (<i>D</i> _{∞h})		<i>cyc</i> -C ₁₈ (<i>D</i> _{18h})		<i>cyc</i> -C ₁₈ (<i>D</i> _{9h})	
	<i>T</i> ₀	<i>f</i>	<i>T</i> ₀	<i>f</i>	<i>T</i> ₀	<i>f</i>
\tilde{X}	0.000 (³ Σ _g ⁻)		0.000 (¹ A _{1g})		0.000 (¹ A ₁)	
\tilde{A}	1.130 (³ Σ _u ⁻)	0.0067	2.392 (¹ E _{1u})	0.0024	2.204 (¹ A ₂ ['])	0.0007
\tilde{B}	1.603 (³ Π _u)	0.0011			2.282 (¹ A ₂ ['])	0.0009
\tilde{C}	2.683 (³ Σ _u ⁻)	0.6813			2.435 (¹ E _{1g})	0.0013
\tilde{D}	2.828 (³ Π _u)	0.0008			4.521 (¹ E _{1g})	0.0292
\tilde{E}	2.876 (³ Σ _u ⁻)	7.2657			4.819 (¹ E _{1g})	0.1032
\tilde{F}	3.274 (³ Π _u)	0.004				
\tilde{G}	3.340 (³ Σ _u ⁻)	0.9156				
\tilde{H}	3.435 (³ Σ _u ⁻)	0.4524				
\tilde{I}	3.909 (³ Σ _u ⁻)	0.0794				

TABLE VI. Calculated vertical transition energies (in eV) for the lowest dipole-allowed electronic transitions for three isomers of C_{22} at the optimized ground-state geometries using the TD-DFT approach with 6-31G* basis sets.

State	lin- C_{22} (D_{2h})		cyc- C_{22} (D_{22h})		cyc- C_{22} (D_{11h})	
	T_0	f	T_0	f	T_0	f
\tilde{X}	0.000 (${}^3\Sigma_g^-$)		0.000 (${}^1A_{1g}$)		0.000 (${}^1A_1'$)	
\tilde{A}	0.962 (${}^3\Sigma_u^-$)	0.0059	1.977 (${}^1E_{1u}$)	0.0012	1.776 (${}^1A_2'$)	0.0003
\tilde{B}	1.462 (${}^3\Pi_u$)	0.0009			1.848 (${}^1A_2'$)	0.0004
\tilde{C}	2.321 (${}^3\Sigma_u^-$)	1.4047			1.996 (${}^1E_1'$)	0.0007
\tilde{D}	2.457 (${}^3\Sigma_u^-$)	7.2913			3.801 (${}^1E_1'$)	0.0116
\tilde{E}	2.521 (${}^3\Pi_u$)	0.0006			4.089 (${}^1E_1'$)	0.0400
\tilde{F}	2.891 (${}^3\Sigma_u^-$)	2.7568			4.270 (${}^1E_1'$)	0.0187
\tilde{G}	2.916 (${}^3\Pi_u$)	0.0033				
\tilde{H}	2.954 (${}^3\Sigma_u^-$)	0.3283				
\tilde{I}	3.388 (${}^3\Sigma_u^-$)	0.1691				
\tilde{J}	3.616 (${}^3\Sigma_u^-$)	0.0102				

red [Fig. 1(a)] is not temperature sensitive and is assigned as origin of the \tilde{A}^1A_2'' state. $1'$ is a hot band, implying a vibrational frequency of 56 cm^{-1} in the ground state. Band 3 corresponds to a frequency of 412 cm^{-1} in the \tilde{A}^1A_2'' state. The TD-DFT calculations predict that \tilde{B}^1A_2'' lies within 0.08 eV of the \tilde{A}^1A_2'' state. Because band 8 has a broader profile compared to 1-6, it is assigned as origin of the $\tilde{B}^1A_2'' \leftarrow \tilde{X}^1A_1'$ transition. Bands 7-10 belong to this system. The \tilde{C}^1E_1' state is predicted to be 0.15 eV higher than \tilde{B}^1A_2'' and thus band 12 could be the origin of the $\tilde{C}^1E_1' \leftarrow \tilde{X}^1A_1'$ transition. In the UV region bands 19-21 are attributed to the $\tilde{D}^1E_1' \leftarrow \tilde{X}^1A_1'$ system and 22-25 to $\tilde{E}^1E_1' \leftarrow \tilde{X}^1A_1'$ as the \tilde{E}^1E_1' state is predicted to be 0.3 eV above \tilde{D}^1E_1' .

2. C_{22}

The spectrum of C_{22} was recorded under the same conditions as that of C_{18} , and thus it was expected that the formation of the D_{11h} structure would be favored [Fig. 1(b)]. The origin band 1 at 620 nm is in good agreement with the prediction of the TD-DFT calculation for the $\tilde{C}^1E_1' \leftarrow \tilde{X}^1A_1'$ transition. Bands 2 through 6 are members of a progression with a vibrational frequency of $\sim 1370\text{ cm}^{-1}$. Band 7 at $25\,120\text{ cm}^{-1}$ is assigned as the origin of the $\tilde{D}^1E_1' \leftarrow \tilde{X}^1A_1'$ system based on calculations, and 9, 12, 15, 17, 19, and 21 are part of the system. The origin of the $\tilde{E}^1E_1' \leftarrow \tilde{X}^1A_1'$ transition is attributed to band 8 with peaks 10, 13, 16, 18, and 20 corresponding to vibrational excitation in the upper state. Band 11 is assigned as origin of the $\tilde{F}^1E_1' \leftarrow \tilde{X}^1A_1'$ system. Furthermore the TD-DFT calculations predict that the \tilde{A}^1A_2'' and \tilde{B}^1A_2'' states are located at 1.78 and 1.85 eV above the ground state. The transitions to these states were not observed perhaps because they are too weak. The absorption to the \tilde{C}^1E_1' state was already near the experimental detection limit, and the oscillator strengths to the \tilde{A} and \tilde{B} states are

predicted to be several times lower (Table VI). In addition the lower intensity of the excitation laser in the near-infrared limits the measurement.

VI. ASTROPHYSICAL IMPLICATIONS

Some of the observed electronic transitions of C_{18} and C_{22} are found in the region where diffuse interstellar absorptions are located. Among these only the relatively strong and narrow ones ($\sim 0.1\text{ nm}$), namely, the bands 1-6 of C_{18} , are of direct relevance for a comparison. Though band 1 (at 592.89 nm) is close to a DIB (592.59 nm) and has a similar bandwidth (0.1 nm), this is a chance coincidence because the other strong peak 2 at 590.80 nm does not have an interstellar absorption as counterpart. The other bands of C_{18} and those of C_{22} are too broad ($\sim 1\text{ nm}$) and do not match DIBs in a systematic way. Thus it appears that the cyclic bare carbon systems, with sizes exemplified by C_{18} , C_{22} are also not responsible for any of the stronger DIB absorptions.

ACKNOWLEDGMENTS

This work has been supported by the Swiss National Science Foundation (Grant No. 200020-107386), as well as the EU project "Molecular Universe" (Grant No. MRTN-CT-2004-512302). We wish to thank Professor Pavel Rosmus for advice concerning the calculations.

- J. W. Weltner and R. V. Zee, Chem. Rev. (Washington, D.C.) **89**, 1713 (1989).
- A. V. Orden and R. J. Saykally, Chem. Rev. (Washington, D.C.) **98**, 2313 (1998).
- H. W. Kroto, J. R. Heath, C. C. O'Brien, R. F. Curl, and R. E. Smalley, Nature (London) **318**, 162 (1985).
- S. Iijima, Nature (London) **354**, 56 (1991).
- R. J. V. Zee, R. F. Ferrante, K. J. Zeringue, J. W. Weltner, and D. W. Ewing, J. Chem. Phys. **88**, 3465 (1988).
- S. L. Wang, C. M. L. Rittby, and W. R. M. Graham, J. Chem. Phys. **107**, 7025 (1997).
- J. Szczepanski, S. Ekern, and M. Vala, J. Phys. Chem. A **101**, 1841 (1997).
- T. F. Giesen, A. V. Orden, H. J. Hwang, R. S. Fellers, R. A. Provencal, and R. J. Saykally, Science **265**, 756 (1994).

- ⁹P. Neubauer-Guenther, T. F. Giesen, U. Berndt, G. Fuchs, and G. Winnewisser, *Spectrochim. Acta, Part A* **59**, 431 (2002).
- ¹⁰P. Freivogel, M. Grutter, D. Forney, and J. P. Maier, *Chem. Phys. Lett.* **249**, 191 (1996).
- ¹¹P. Freivogel, J. Fulara, M. Jakobi, D. Forney, and J. P. Maier, *J. Chem. Phys.* **103**, 54 (1995).
- ¹²D. Forney, P. Freivogel, M. Grutter, and J. P. Maier, *J. Chem. Phys.* **104**, 4954 (1996).
- ¹³M. Wyss, M. Grutter, and J. P. Maier, *Chem. Phys. Lett.* **304**, 35 (1999).
- ¹⁴G. von Helden, N. G. Gotts, and M. T. Bowers, *J. Am. Chem. Soc.* **115**, 4363 (1993).
- ¹⁵G. von Helden, P. R. Kemper, N. G. Gotts, and M. T. Bowers, *Science* **259**, 1300 (1993).
- ¹⁶M. Grutter, M. Wyss, E. Riplov, J. P. Maier, S. D. Peyerimhoff, and M. Hanrath, *J. Chem. Phys.* **111**, 7397 (1999).
- ¹⁷A. K. Ott, G. A. Rechtsteiner, C. Felix, O. Hampe, M. F. Jarrold, R. P. Van duyne, and K. Raghavachari, *J. Chem. Phys.* **109**, 9652 (1998).
- ¹⁸G. A. Rechtsteiner, C. Felix, A. K. Ott, O. Hampe, R. Van duyne, M. F. Jarrold, and K. Raghavachari, *J. Phys. Chem. A* **105**, 3029 (2001).
- ¹⁹J. P. Maier, N. M. Lakin, G. A. H. Walker, and D. A. Bohlender, *Astrophys. J.* **553**, 267 (2001).
- ²⁰J. P. Maier, G. A. H. Walker, and D. A. Bohlender, *Astrophys. J.* **566**, 332 (2002).
- ²¹J. P. Maier, G. A. H. Walker, and D. A. Bohlender, *Astrophys. J.* **602**, 286 (2004).
- ²²K. Kaizu, K. Kohno, S. Suzuki, H. Shiromaru, T. Moriwaki, and Y. Achiba, *J. Chem. Phys.* **106**, 9954 (1997).
- ²³J. Hunter, J. Fye, and M. F. Jarrold, *J. Phys. Chem.* **97**, 3460 (1993).
- ²⁴F. Guethe, H. Ding, T. Pino, and J. P. Maier, *Chem. Phys.* **269**, 347 (2001).
- ²⁵T. Pino, H. Ding, F. Güthe, and J. P. Maier, *J. Chem. Phys.* **114**, 2208 (2001).
- ²⁶H. Ding, T. Pino, F. Güthe, and J. P. Maier, *J. Chem. Phys.* **117**, 8362 (2002).
- ²⁷H. Ding, T. W. Schmidt, T. Pino, A. E. Boguslavskiy, F. Güthe, and J. P. Maier, *J. Chem. Phys.* **119**, 814 (2003).
- ²⁸J. Hutter, H. P. Luethi, and F. Diederich, *J. Am. Chem. Soc.* **116**, 750 (1994).
- ²⁹J. M. L. Martin, J. El-Yazai, and J. P. Francois, *Chem. Phys. Lett.* **242**, 570 (1995).
- ³⁰R. E. Stratmann, G. E. Scuseria, and M. J. Frisch, *J. Chem. Phys.* **109**, 8218 (1998).
- ³¹J. R. Heath, Q. Zhang, S. C. O'Brien, R. F. Curl, H. W. Kroto, and R. E. Smalley, *J. Am. Chem. Soc.* **109**, 359 (1987).
- ³²M. Saito and Y. Okamoto, *Phys. Rev. B* **60**, 8939 (1999).
- ³³D. A. Plattner and K. N. Houk, *J. Am. Chem. Soc.* **117**, 4405 (1995).
- ³⁴T. Torelli and L. Mitas, *Phys. Rev. Lett.* **85**, 1702 (2000).
- ³⁵E. J. Bylaska, R. Kawai, and J. H. Weare, *J. Chem. Phys.* **113**, 6096 (2000).

Gas-phase electronic spectroscopy of the C_{14} ring

Another member of the $C_{(4n+2)}$ family detected with REMPI is C_{14} . Here, only experimental observations and tentative speculations will be presented. A more detailed analysis is needed.

The C_{14} molecule was produced and detected spectroscopically by the same approach applied towards the measurement of the ring species C_{18} and C_{22} . As in those cases, C_{14} is an abundant graphite ablation product and also demonstrates low reactivity with respect to hydrogen. According to DFT calculations (B3LYP/6-31G(d)), the ground state prefers a cyclic form by about 4 eV over the linear. Therefore the expected structure of C_{14} is cyclic.

However, the REMPI spectrum differs drastically from those of C_{18} and C_{22} (figure 4.1). Located solely in the visible region around 520 nm, it contains dozen of lines that could be attributed to just one or two close lying electronic transition bands. Such a small number of allowed electronic transitions suggests high symmetry in the carrier: for instance, a ring of D_{14h} symmetry has fewer allowed transitions than a ring with D_{7h} or C_{7h} (aside from $D_{\infty h}$).

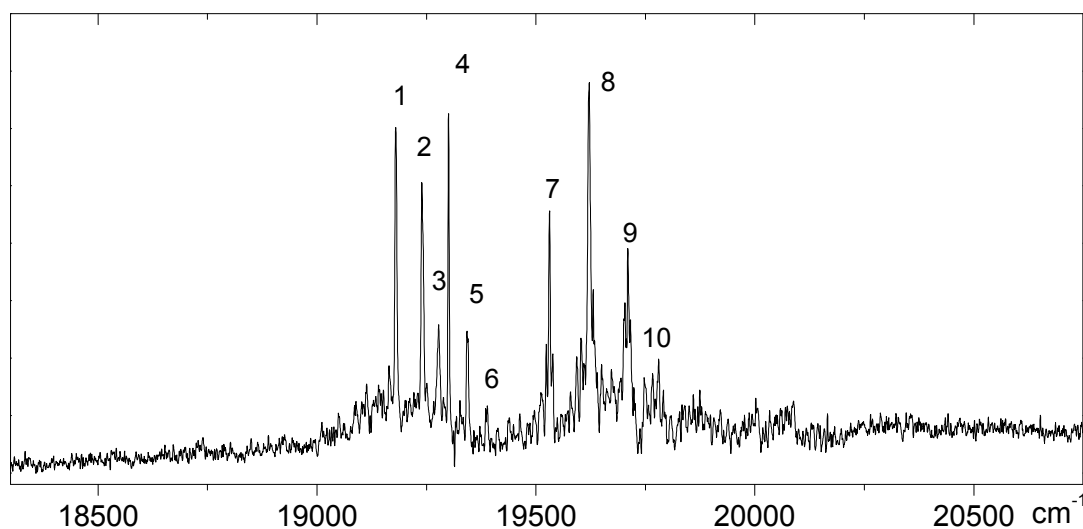


Figure 4.1: Gas-phase electronic spectrum of C_{14} detected by a resonant two-color two-photon ionization technique under supersonic molecular beam conditions. Broad background is due to sequence bands as its extent varies with source conditions. Band **1** appears to be the origin. Peaks' positions are listed in Table 4.1

The spectrum consists of about 11 distinct lines, 3–7 cm^{-1} broad, and with substructure. At least some of them are visibly split (figure 4.2). Contrary to the case of C_{18} , this substructure can be described as a sharp dip on top of a broad band rather than as being a

convolution of Lorentzian peaks. Neither can this splitting be due to an artefact from the incident coupling of a "bright state" with a "dark state". Such coupling would probably be isotope dependent ($^{12}\text{C}_{14}$ versus $^{12}\text{C}_{13}^{13}\text{C}$). Instead, the spectra of the two isotopomers appear very similar, with a small isotope shift. Perhaps, it could be a rotational band profile sophisticated by Coriolis couplings or a set of overlapping sequence bands.

The vibronic structure does not feature any obvious harmonic progressions. However if the upper state potential is assumed nonharmonic then the assignment of the first few bands as a progression in the lowest energy bending vibration would result in an extremely flat excited state surface.

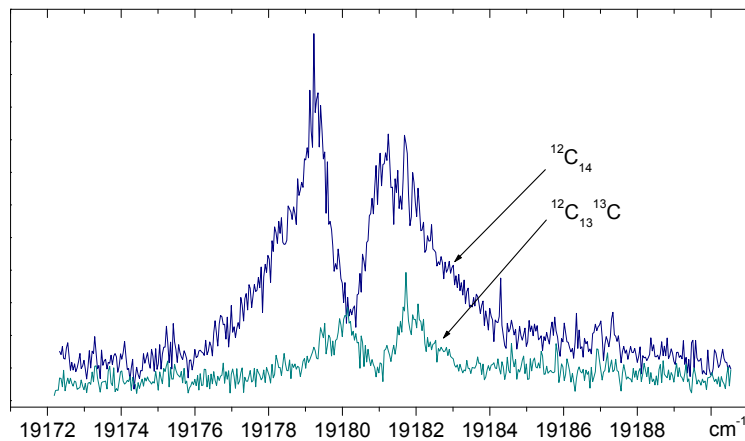


Figure 4.2: Close-up of band **1** of $^{12}\text{C}_{14}$ and its isotopomer $^{12}\text{C}_{13}^{13}\text{C}$, both showing non-trivial band profiles.

Although the natural isotope abundance of heavy carbon atom ^{13}C is only 1.109%, there is a $\approx 13.4\%$ probability that a C_{14} species will have one heavy atom. Unit mass resolution in the mass spectrometer allowed a separation of m/z 168 and m/z 169, and the laser resolution ($\approx 0.15 \text{ cm}^{-1}$) permitted the observation of the spectral isotopic shifts of the first few vibronic lines in the spectrum of the C_{14} (figure 4.2). Thus one observes the origin band in the spectrum of the heavy $^{12}\text{C}_{13}^{13}\text{C}$ isotopomer shifted $\approx 0.8 \text{ cm}^{-1}$ to the blue compare to that in normal $^{12}\text{C}_{14}$. The next few lines are shifted $\approx 0.3 \text{ cm}^{-1}$, $\approx 0.25 \text{ cm}^{-1}$, and $\approx 0.15 \text{ cm}^{-1}$, respectively. This decrease of the blue shift in the vibronic bands relative to that of the origin can be understood from a consistent increase in the vibrational red shift. The latter seems rational, as a vibrational energy lowers (hence the "red shift") upon increasing the mass of an oscillator ($E_{vib} \sim \sqrt{\frac{k}{\mu}}$) and does it proportionally to the vibrational frequency¹. The blue isotopic shift of the origin of the electronic transition in turn can be rationalized as due to a more shallow excited state

$${}^1\Delta\nu_{isotopic} \propto \left(\sqrt{\frac{k}{m+1}} - \sqrt{\frac{k}{m}} \right) = \sqrt{\frac{k}{m}} \left(\left(1 + \frac{1}{m}\right)^{-1/2} - 1 \right) \Big|_{m \gg 1} \approx -\frac{1}{2m} \sqrt{\frac{k}{m}} = -\frac{\nu}{2m}$$

potential surface (figure 4.3). In this case the isotopic substitution lowers the energy levels in the deeper and narrower ground state potential more than in the shallower excited state so that the transition energy overall increases. Relaxation of an electronic potential surface upon molecule excitation is common. Moving an electron from binding to the non-binding molecular orbital causes the molecule to swell slightly in the upper state.

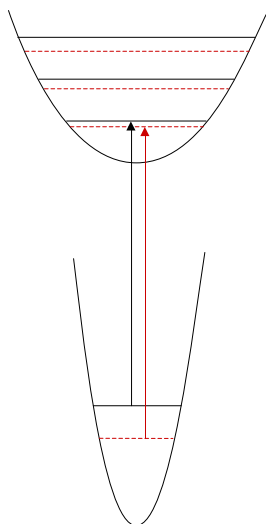


Figure 4.3: An illustration for the isotopic shift considerations. A one dimensional cut of the ground and excited electronic states potential energy surfaces. Solid lines indicate the energy levels of a normal isotopomer, dashed – the heavy ones.

Such a drastic change in spectral pattern from C_{22} and C_{18} to C_{14} is striking and probably indicates a structural change upon decreasing the size of the doubly aromatic ring. The decrease in symmetry (for the family $(4n+2)$) from the aromatic and fully symmetric $D_{(4n+2)h}$ to the aromatic but bond angle alternated $D_{(2n+1)h}$ and further to the dimerised $C_{(2n+1)h}$ with increasing ring size was predicted in several theoretical works [7–10]. They, however, disagree at which ring size these changes should occur.

Table 4.1: Maxima of the most prominent vibronic bands observed in the electronic spectrum of C_{14} .

Label	λ (nm)	$\Delta\nu$ (cm^{-1})
1	521.23	0 (19180.2)
2	519.58	61
3	518.61	97
4	517.99	120
5	516.84	163
6	515.67	207
7	511.86	351
8	509.49	442
9	507.22	530
10	505.50	597

Bibliography

- [1] A. E. Boguslavskiy, H. Ding, and J. P. Maier. Gas-phase electronic spectra of C_{18} and C_{22} rings. *J. Chem. Phys.*, 123: 034305, 2005.
- [2] J. P. Maier, A. E. Boguslavskiy, H. B. Ding, G. A. H. Walker, and D. A. Bohlender. The gas phase spectrum of cyclic C_{18} and the diffuse interstellar bands. *Astrophys. J.*, 640: 369–372, 2006.
- [3] S. P. Ekern, A. G. Marshall, J. Szczepanski, and M. Vala. Photon-induced complete dehydrogenation of putative interstellar polycyclic aromatic hydrocarbon cations: coronene and naphtho[2,3-a]pyrene. *Astrophys. J.*, 488: L39–L41, 1997.
- [4] S. P. Ekern, A. G. Marshall, J. Szczepanski, and M. Vala. Photodissociation of gas-phase polycyclic aromatic hydrocarbon cations. *J. Phys. Chem. A*, 102: 3498–3504, 1998.
- [5] P. Boissel, G. Lefèvre, and P. Thiébot. Photofragmentation of PAH Ions: Laboratory Experiments on Long Timescales. In I. Nenner, editor, *AIP Conf. Proc. 312: Molecules and Grains in Space*, pages 667–674, 1994.
- [6] J. Szczepanski, S. Ekern, and M. Vala. Vibrational spectroscopy of small matrix-isolated linear carbon cluster anions. *J. Phys. Chem. A*, 101: 1841–1847, 1997.
- [7] M. Saito and Y. Okamoto. Second-order Jahn-Teller effect on carbon $4N+2$ member ring clusters. *Phys. Rev. B*, 60: 8939–8942, 1999.
- [8] D. A. Plattner and K. N. Houk. C_{18} is a polyynes. *J. Am. Chem. Soc.*, 117: 4405–4406, 1995.
- [9] T. Torelli and L. Mitas. Electron correlation in C_{4n+2} carbon rings: Aromatic versus dimerized structures. *Phys. Rev. Lett.*, 85: 1702–1705, 2000.
- [10] E. J. Bylaska, R. Kawai, and J. H. Weare. From small to large behavior: The transition from the aromatic to the Peierls regime in carbon rings. *J. Chem. Phys.*, 113: 6096–6106, 2000.

Chapter 5

VUV generation in gases for the benefit of REMPI

5.1 Implementation of Resonant Difference-Frequency Mixing (RDFM)

5.1.1 Motivation

One dream of spectroscopists is the development of a high resolution, universal, and sensitive experimental technique. REMPI is a good step in presumably right direction.

It was already pointed out that the REMPI approach may suffer from lack of photons of appropriate energy. Figure 5.1 indicates the ionization potentials of some relevant known unsaturated hydrocarbons. Superimposed is the energy diagram for the two photon ionization of a hypothetical electronic transition at 700 nm with a 7.9 eV ionization step. It can be noted that many small molecules which have an absorption at 700 nm would escape detection.

Another problem may occur with large molecules in which the Born-Openheimer approximation is often violated and electronic and vibrational motions are coupled. This results in fast (compared to ns timescale) intramolecular energy conversion processes. Thus, after an electronic excitation from the ground state X to the A-state by absorption of λ_1 (figure 5.2), a fast internal conversion may occur and convert the electronic energy into vibrational energy of the molecule, before the latter absorbs a photon from the second laser. If this happen, the ionization from the second laser must occur from a highly vibrationally excited electronic ground state, i.e. one with a very small overlap integral between the vibrational wavefunctions of the neutral molecule and its cation. Two approaches seem possible here. Either lasers should be fast enough to compete with internal conversion processes; or λ_2 photons must lie just below the IP of studied molecule to enhance the FC-factor¹ while avoiding direct one-photon ionization.

With this in mind an attempt to employ resonant difference frequency mixing (RDFM) - the type of four-wave mixing most suitable for the generation of the tunable VUV - for the benefit of REMPI was endeavored.

¹FC(Franck-Condon) factor stands for the square of the overlap integral between the vibrational wavefunctions of the two states that are involved in the transition.

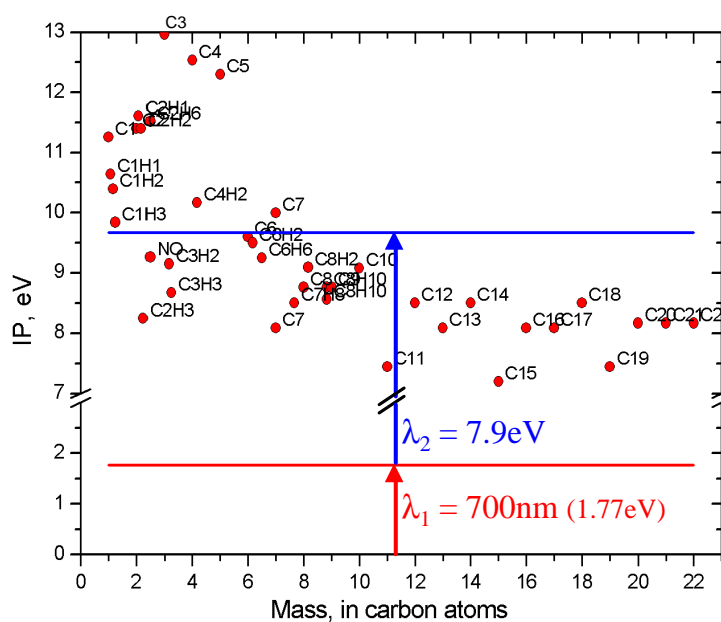


Figure 5.1: Ionization potentials (IPs) of some known unsaturated hydrocarbon and pure-carbon molecules (presumably chains).

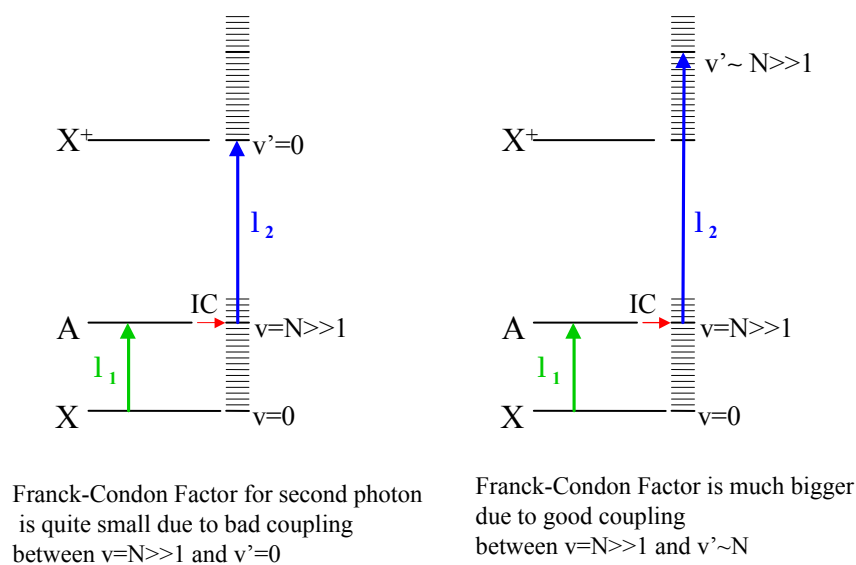


Figure 5.2: It is desirable for the λ_2 photon energy to be comparable with the IP of the molecule.

5.1.2 Implementation

Whereas the choice of a wave mixing scheme was relatively straightforward, the choice of nonlinear media, electronic transition, and exact pumping scheme was not as clear. Any gaseous media (and not only gaseous) could be turned into nonlinear media capable of mixing light frequencies. It is only a question of the intensity of the electromagnetic wave the media is exposed to. Nonlinear interaction intrinsically cannot be scaled to some standard conditions which would allow one to compare all combinations in order to choose the one most suitable for a given application. As such an ample amount of reported implementations do not give the whole integral picture but rather somewhat scattered. The aim here was to build an external coherent light source which could be easily attached to the REMPI machine and avoid serious modification. The important criteria were maximum efficiency, relative simplicity, robustness, and the possibility to pump with the range of nanosecond pulse lasers accessible in our laboratory. At this stage a very helpful expert in the field [1] recommended using a rare gas cell and the $4p^6 (1p_0) \rightarrow 5p4p^5 (2p_5)$ two photon resonance in krypton.

The corresponding 212 nm radiation was generated (figure 5.3) in two steps by first doubling the visible output of the Nd:Yag (532 nm, second harmonic) pumped dye laser in a BBO crystal (637 nm \rightarrow 318.5 nm) and then adding again one 637 nm photon to the doubled output of the dye laser in a second BBO crystal (637 nm + 318.5 nm \rightarrow 212 nm) thus effectively tripling the initial visible frequency. The UV pulse energy produced was between 0.1 and 1 mJ depending on the dye laser pump energy. ²

After separation from the dye fundamental the resulting beam was carefully aligned to the cell collinearly with the second color ω_2 (of 4–10 mJ energy). The resulting beam is focused in the krypton cell by a 200 mm focal length lens (fused silica, plano convex) to increase intensity and thus increase conversion efficiency. The chromatism of the lens was compensated by a mildly converging telescope (not shown) placed on the visible beam before it merges with the UV beam. The conversion cell (300 mm) was attached to the REMPI chamber but separated from it by a 200 mm focal length MgF₂-lens transparent down to 105 nm. After passing through the lens VUV-light meets the molecular beam and ionizes it just between the extraction plates of TOF-mass spectrometer.

By tuning the visible light in the interval of 400–800 nm while keeping the first

²More obvious possibility would be to use a dye laser to generate 424 nm and then double it with a BBO crystal, avoiding the mixing step. This approach however is less favorable as the laser dyes in the blue region should be pumped with at least the third harmonic (355 nm) of a Nd:Yag instead, which implies one more frequency conversion step and associated energy loss; then, the efficiency of these dyes is generally lower ('Stilbene 3' dye performs at halved efficiency compare to 'DCM' dye); but the biggest problem concerns the dye's lifetime which drops ~ 20 times (from 300 down to ~ 15 Wh) so that dyes should be changed on daily basis.

laser at the $94092.8557 \text{ cm}^{-1}$ $4p^6 (1p_0) \rightarrow 5p4p^5 (2p_5)$ two photon resonance of Kr, the $\sim 8.6\text{--}10.2 \text{ eV}$ ($\sim 145\text{--}123 \text{ nm}$) range could be accessed (figure 5.4). This extensive continuous range is characteristic of the difference frequency mixing process which has relaxed constraints concerning phase matching, in contrast to the sum frequency mixing of the third harmonic processes. In reality, the efficiency will vary significantly with the wavelength of tunable light containing numerous depletions corresponding to proximity to all sorts of $2\omega_{UV} + \omega_{vis}$ and $\omega_{VUV} + \omega_{uv}$, etc. resonances where either strong negative (at the blue side of a resonance or positive at the red side) dispersion will favor other conversion processes [2]; or newly generated light will be absorbed *ibidem* in the two photon resonance [3, 4].

To ensure that the fixed (doubling) laser is exactly on the $4p^6 (1p_0) \rightarrow 5p4p^5 (2p_5)$ two photon electronic transition in krypton, the $[2+1']$ REMPI spectrum of this transition was recorded (figure 5.5). The 2% Kr/Ar gas mixture was adiabatically expanded to the vacuum chamber and $\sim 212.5 \text{ nm}$ laser light was fed along with one of the fundamentals 318 nm towards the molecular beam. The resonance was located at 212.508 nm , which slightly differs from the NIST database [5] value (212.41568 nm), presumably due to the laser's calibration. Krypton's ionization potential (13.999 eV [5]) implies that resonant ionization occurs most likely via a $[2+1']$ process involving absorption of two quanta of 212 nm radiation followed by one quantum of 318 nm .

Absolute measurement of generated flux is usually done with a special solar blind photomultiplier or by monitoring the ionization current in a cell filled with gas of a known ionization yield (usually NO) [6]. In the geometry of our experiments calibration is hampered by the dependence of the ionization current on the overlap between the molecular beam and laser beams in the machine and on voltage on MCP detector (read as 'amplification'). For our application, where the ionization cross-section is unknown and varies from molecule to molecule, separate flux measurements were considered irrelevant and were not attempted. Beam alignment, focusing conditions, and the pressure of the krypton gas (typically $20\text{--}60 \text{ mbar}$) were optimized on the maximum of one photon ionization of a 0.25% benzene mixture in argon, which was adiabatically expanded into the chamber. Benzene has suitable IP (9.25 eV) so that ionization is only possible by vuv photons.

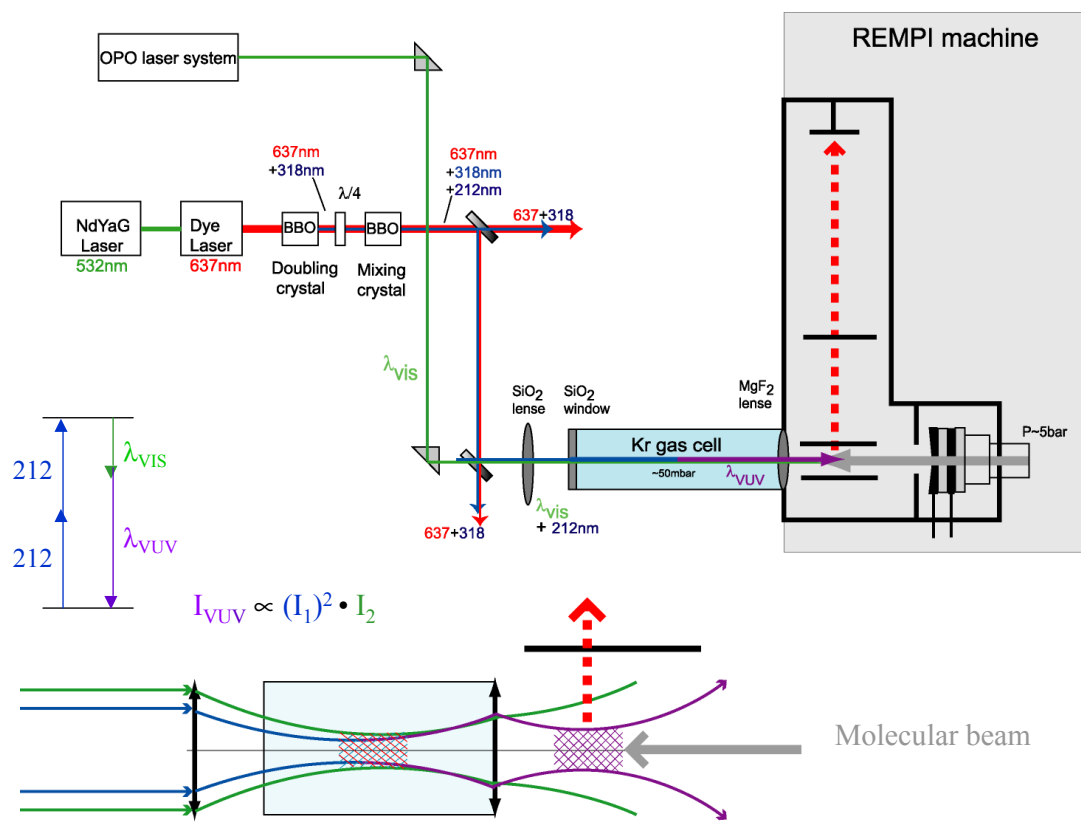


Figure 5.3: The experimental setup consists of two laser systems, a conversion cell filled with Kr gas at room temperature, and a REMPI machine with TOF mass-spectrometer. The 212 nm laser light for the two-photon transition λ_1 is synthesized by doubling the dye laser with a BBO-crystal and subsequently mixing it with a second BBO. After separating the dye's fundamental the resulting beam is carefully aligned to the cell collinearly with the second color λ_2 and focused inside the Kr cell. The conversion cell and the REMPI chamber are separated by a MgF₂ lens transparent down to 105 nm. After passing through the lens, the VUV photons face the molecular beam in the extraction region of TOF mass spectrometer ionizing ionize it.

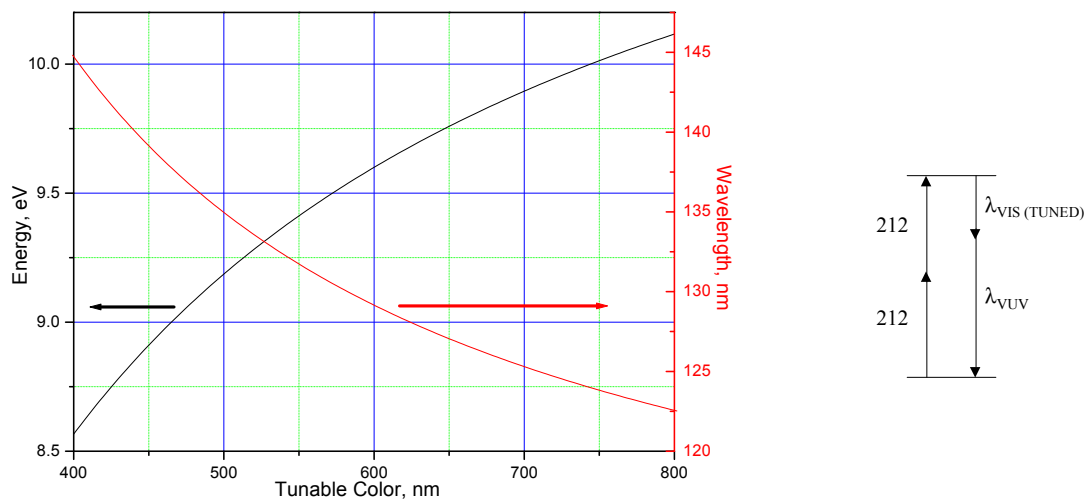


Figure 5.4: Graph demonstrates the expected available range of generated energies (left axis) and wavelengths (right) as functions of tunable wavelength.

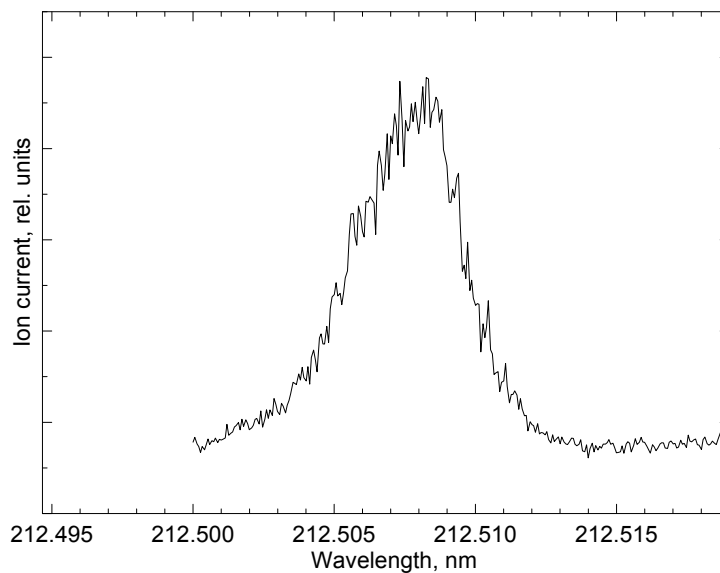


Figure 5.5: $[2+1']$ REMPI of $4p^6 (1p_0) \rightarrow 5p4p^5 (2p_5)$ two-photon electronic transition in krypton. Ordinate stands for the wavelength of one photon.

First test application: mass spectroscopy with 9.75 eV photons

As a test the mass spectrum of a typical (for our work) discharge of 0.5% butadiyne (HCCCCH) in Ar was used. The mass spectrum obtained is presented in figure 5.6 and is compared with the one obtained using 157 nm light produced by F₂ excimer laser. VUV photons of 9.75 eV (~ 127 nm) produced in $\omega_{VUV} = 2 \times \omega_{(212\text{ nm})} - \omega_{(637\text{ nm})}$ process in Kr gas cause direct one photon ionization of the otherwise neutral discharge products. In turn, the relatively high intensity of the 10 mJ/pulse of 7.9 eV (~ 157 nm) light leads to both one- and two-photon ionization processes³. There is a clear difference in distribution of the species for these two cases. F₂-laser ionization seems to favor the C_nH₃-series, especially for even number of carbons. In turn, in the VUV-cell case the C_nH₂-series is more common. The latter light source gives a more sensible impression about the relative abundances of species in the discharge, since most of the produced middle-sized species could be ionized with one photon. Thus, for example, the relative excess of C_nH₃ species in the 7.9 eV mass spectrum as compared to the one taken with 9.75 eV. This hints at the low IP of these moieties⁴.

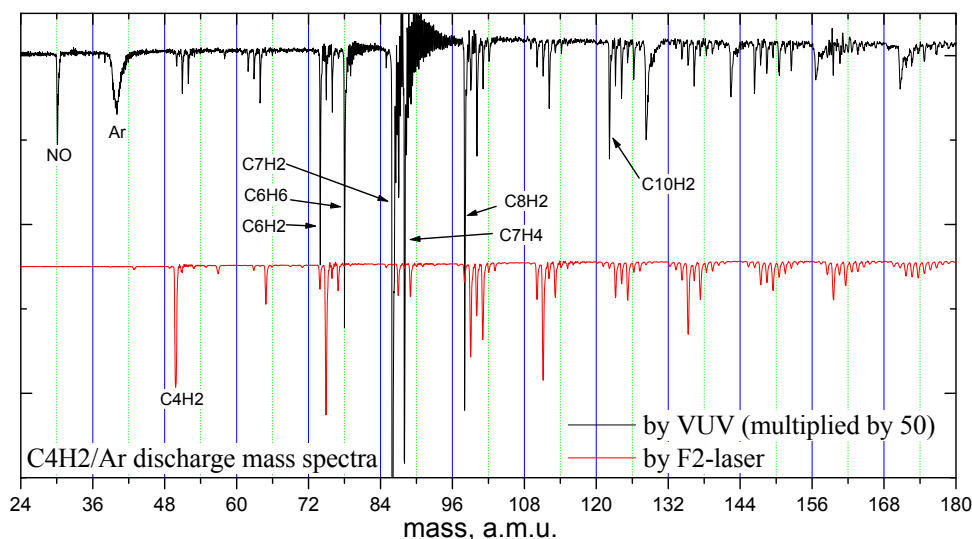


Figure 5.6: Discharge (0.5% C₄H₂/Ar) products ionized with VUV ($P \sim 1 \mu\text{J}$; $E_{h\nu} = 9.71$ eV direct one-photon ionization) (upper trace) and alternatively with F₂-laser ($P \sim 1$ mJ; $E_{2h\nu} = (7.9 + 7.9)$ eV two-photon ionization) (lower trace). The intensity of the peaks is a convolution of species abundance in the discharge and their ionization cross-sections. Though most species are Ar and C₄H₂ (precursor), the corresponding peaks are not prominent in the mass spectra as their IPs (15.76 eV for argon and 10.17 for C₄H₂) lie beyond the energies of ionizing photons used.

³Moreover, for F₂-case some mass peaks might be caused by dissociation of bigger molecules under exposure of relatively high laser intensity.

⁴This has eventually been exploited and led to the results presented in chapter 8

Second test application: Determining ionization threshold

To produce tunable VUV, external tunable radiation was combined collinearly with the 212 nm light which was filtered out from the fundamental beams (i.e. 637 and 318 nm radiation) using dichroic mirrors. A molecular beam of 0.25% C₆H₆/Ar was expanded into the source chamber. Benzene was chosen as the test molecule because it has an IP energy of 9.25 eV [7], which can be conveniently produced by scanning an external laser around ≈ 507 nm. Benzene has also relatively high vapor pressure and is readily available. Presence of the step function in the ionization yield signal (figure 5.7) in the corresponding mass channel confirms the tunability of generated light.

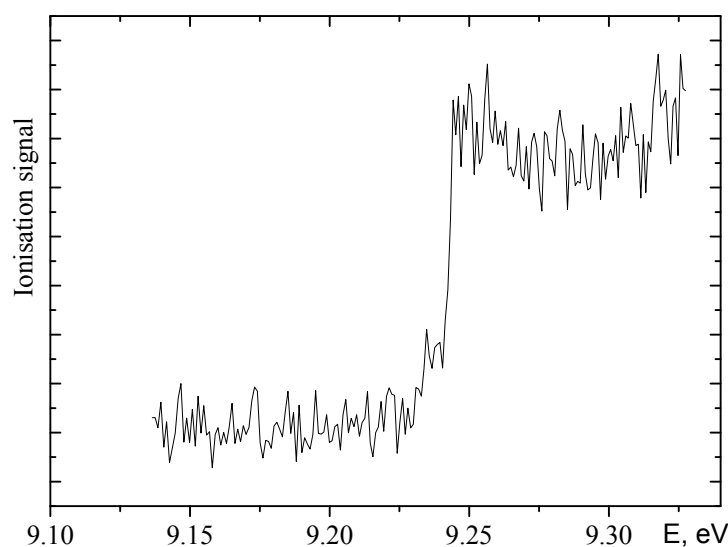


Figure 5.7: Ionization threshold of benzene seen as the step-like rise of ionization yield in the corresponding mass channel. VUV light faces the molecular beam of 0.5% C₆H₆/Ar inside vacuum chamber; produced ions are analyzed by TOF mass spectrometer. Reference book value for IP of benzene is 9.25 eV.

Ionization curves can be used to identify molecular species when mass (m/z) does not necessary resolve the question. For example, mass-to-charge 30 (figure 5.8), would appear in the mass spectrum regularly after opening the vacuum chamber. Since nothing was fed into the machine deliberately, the carrier had to had existed in only trace amounts. By obtaining the IP of the enigmatic m/z 30 species, the unknown could be identified as nitric oxide (figure 5.8).

Another example of determining the IP threshold of a species present in relatively low concentration is depicted on figure 5.9. Triacetylene was produced by discharging (the source is described in chapter 3) a 0.5% mixture of diacetylene in argon⁵. The observed

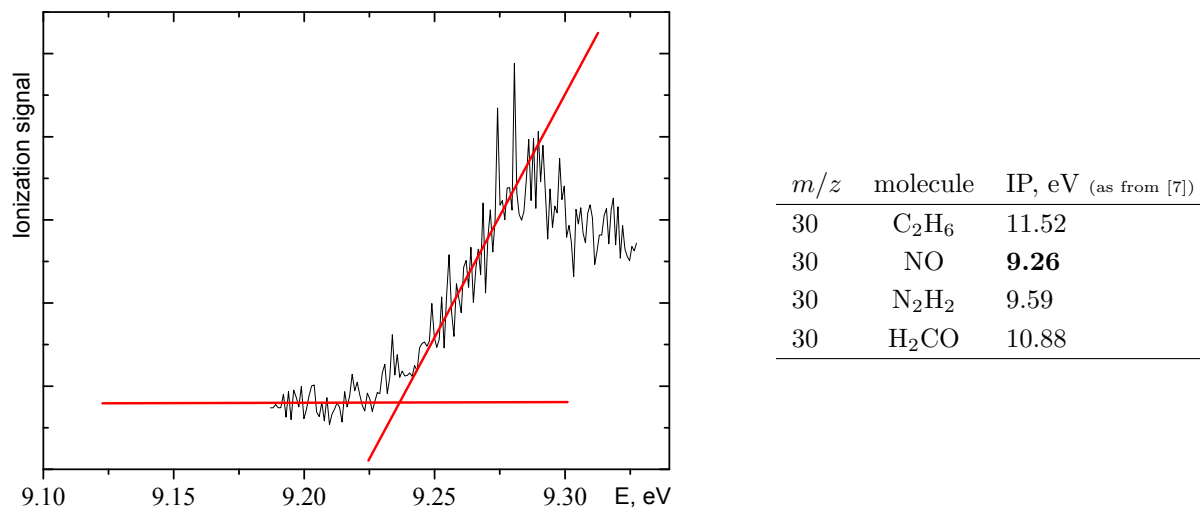


Figure 5.8: Ionization threshold for species with m/z 30. This result allowed the identification of trace amounts of nitric oxide in the chamber.

ionization threshold (9.5 eV) coincides with the reference value [7].

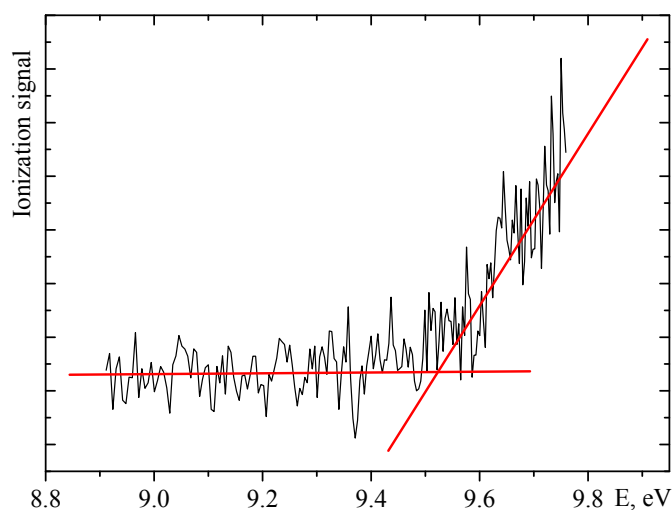


Figure 5.9: Ionization threshold for C₆H₂ in molecular beam produced from the discharge of C₄H₂/Ar=0.5%.

⁵It should be noted that the concentration of C₆H₂ is not trivial to estimate. The major part of the molecules expanded (apart from argon) are those of the precursor itself (C₄H₂), but these cannot be seen (detected) on the mass spectrum as its IP (10.17 eV) is higher than the energy of the ionizing photons used in the experiment (figure 5.6).

5.1.3 Implications

Despite its promising start, this project has been shelved for a number of reasons. Even though the generated intensities seemed sufficient and could perhaps be improved an order of magnitude by perfecting the alignment, optimizing the focusing conditions, varying gas composition and phase matching, the approach itself was very demanding and sensitive to the beam alignment, which is rather laborious without proper instruments. Combining the numerous fundamentals with tunable color of the first (resonant) step of REMPI and the subsequent beam separation, without touching the tunable laser beam and the one freshly generated, makes the generalized use for the REMPI purposes very tedious if feasible at all.

Intensity of the fundamentals from VUV generation (i.e. 212 nm and second (tunable) color) are orders of magnitude stronger than the resulting light. Their interaction with molecules in the beam create background which hinder the signal. Therefore the separation of generated light is requisite. Reflective diffraction gratings are commonly used for this purpose, however these have very low reflectivity for VUV wavelengths (R is an order of few percents). Such a losses of precious generated light are inadmissible when working with a trace amounts of unidentified species. Also, employing a diffraction grating for the harmonic separation would then imply a non axial combining of the generated VUV and the tunable step of REMPI which is again not favorable for sensitivity reasons.

However the idea should not be buried. The approach could be used for studying chosen molecules at specific wavelengths when relatively small regions of continuous tunability is sufficient. Yet before attempting to do so, some auxiliary devices like a removable pinhole⁶ and vuv sensitive in-chamber video camera⁷ should be implemented.

⁶which could be inserted into (and subsequently removed from) the heart of setup without breaking vacuum (extraction chamber) to define the alignment point in 3D space

⁷to visualize the in-chamber beam alignment

5.2 Implementation of third harmonic generation (THG) in Xe

5.2.1 Introduction

Failure to employ RDFM for REMPI was caused, first of all, by the need for laborious alignment of the fundamental beams and their subsequent filtering out. This, in turn, was complicated significantly by the need to keep the alignment wavelength independent. This was all accompanied by several steps of energy conversion from the fundamental radiation of the pumping laser (for example, from the 1064 nm from Nd:YAG laser). However if to omit the tunability requirement, then it is feasible to use a less sophisticated scheme. Thus, the 3rd, 4th, or 5th harmonic of the Nd:YAG laser could be effectively generated in nonlinear crystals. Yet, crystals become opaque further to the blue and the next conversion steps should be done in gas media as was mentioned before.

An aposite scheme is the generation of the 9th harmonic wavelength of a Nd:YAG laser. Herein up to third harmonic conversion is carried out in nonlinear crystals (doubling and subsequent mixing) and followed by tripling in xenon gas cell. The reason for the popularity of this arrangement comes from the fortunate coincidence of generated wavelength with the region of negative dispersion of xenon caused by the vicinity of the 5p-5d transition of Xe at 119.2 nm. Therefore, achieving the phase-matching condition is possible; these can be tuned by varying the Xe gas pressure. The lack of conversion efficiency due to non-optimal resonance match can be compensated by a high intensity of incident radiation. Energies of the order of 100–300 mJ per 7 ns pulse are common and commercially available and upon focusing are intense enough not only to induce the nonlinear response of the medium but even to cause its breakdown.

Resulting photons have an energy of 10.5 eV, which surpass the IPs of most pure-carbon species except those smaller than C₅. Because of the high ionization energies of the neutral carbon clusters and lack of a proper high energy ionization light source, the mass spectral measurements have been carried out previously by using multiphoton ionization with 7.9, 6.4 or 3.5 eV photons. This technique has the advantage of easy handling or use of a commercially available laser source, however, can lead to a misunderstanding of the real nascent mass distribution, because of the fragmentation and/or some resonance effects that lead to the special enhancement at specific sizes during multiphoton excitation processes. In turn, VUV radiation has similar single photon ionization cross sections for a variety of species, provided their ionization potentials are below the 10.5 eV. In this sense, a single photon ionization of clusters must be an ideal method to determine the size distribution in order to keep free from these complications.

On the other hand, it is also tempting to combine resulting VUV radiation within [1+1'] REMPI of small carbon molecules. Thus, for example, on C₅, which was virtually not studied spectroscopically in the gas phase. So far the gas-phase spectrum available [8] concerns only the origin and few vibronic bands of the $A^1\Pi_u \leftarrow X^1\Sigma_g^+$ transition around 511 nm. It was recorded using the CRDS technique [9], which is not mass selective, and therefore the spectrum recorded is subjected to an overlap with a number of C₂ absorption lines, thus preventing a rotational contour overlap band profile fit. To observe the rotational contour in the absence of such lines was another incentive of this project.

5.2.2 Implementation

The cell used was the same as in the RDFM experiments. A Continuum PL9020 pulsed Nd:YAG laser (fundamental wavelength 1064 nm) was used to generate vacuum ultraviolet (118 nm) photons. The repetition rate of the laser is 20 Hz and the diameter of the output beam is 0.8 cm with a divergence of 0.45 mrad. Typically 355 nm pulse energies of 40–50 mJ were used with pulse width is 5–7 ns. The 118 nm radiation was produced by focusing the third harmonic of the fundamental frequency (355 nm) into the center of an isolated 50-cm long stainless steel gas cell (figure 5.10). A quartz Brewster angle window was at the entrance of the gas cell, and a 15-cm focal length (at 200 nm) MgF₂ lens was located at the exit (vacuum chamber side). This lens also provided the high vacuum seal between the gas cell and the ionization chamber of the vacuum system. Pure Xe, or a mixture of inert gases (Ar and Xe), in the cell was used to triple the 355 nm output of the laser to attain the desired wavelength (118 nm).

The ionizing photons produced meet the molecular beam anti-collinearly allowing for maximum overlap. The efficiency of this non-resonant nonlinear conversion process is known to rise up to 10^{-4} – 10^{-3} [10, 11]. In spite of a slight defocusing of the fundamental light (because of chromatic dispersion property of the lens) in the TOF extraction region, the energy density (50 mJ of 355 nm in ~ 5 mm spot) is high enough to cause nonresonant multiphoton ionization and fragmentation in the molecular beam, producing background in the channel of interest. To overcome this without losing precious micro-joules of generated light with additional optical elements, the dispersive property of an off-axis penetrated lens was utilized (figure 5.10). The 355 nm light was carefully aligned so that it was dumped on the ceramic beam block inside the vacuum chamber while the generated 118.2 nm light enters the interaction region only slightly off-axis.

Approximately 5–10 Torr of Xe and roughly four times this pressure of Ar were used in the gas cell to give maximum ionization signal for benzene (IP=9.25 eV) or acetone (IP=9.70 eV), small concentrations of which were expanded into the chamber on the

alignment stage. The acetone molecular ion signal at m/z 58 was maximized, whereas the m/z 43 ion from acetone fragmentation was minimized to ensure complete separation of the two beams, since the presence of 355 nm radiation induced photodissociation.

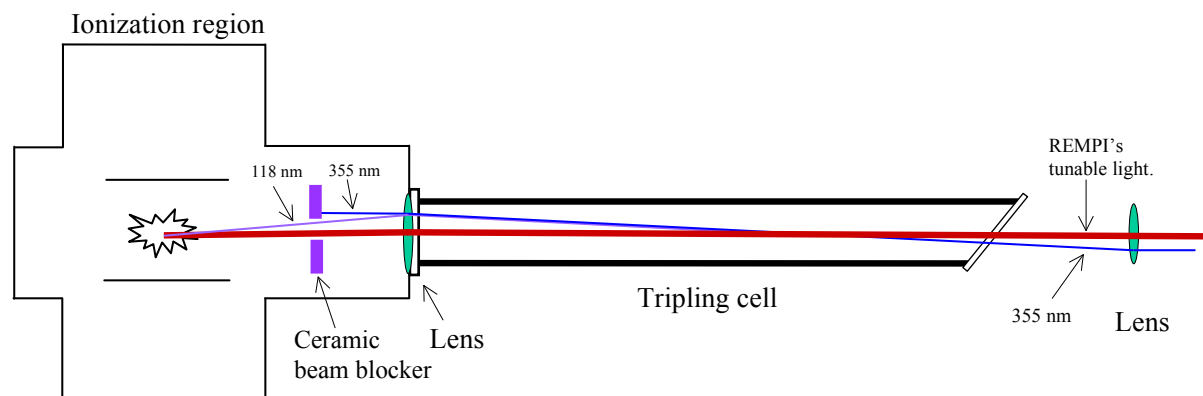


Figure 5.10: Tripling cell. The drawing is based on illustration in [12]

First test application: mass spectroscopy with 10.5 eV photons

The first test is a characterization of the graphite ablation source products. Figure 5.11 shows the mass distribution of the neutral carbon clusters ionized by the 7.9 eV (F_2 excimer laser) and 10.5 eV light in comparison. The upper mass spectrum (7.9 eV) features the prevalence of the odd-numbered species and magic numbers at $n=11, 15, 19, 23$, whereas the lower trace (10.5 eV) indicates the enhanced amounts of even-numbered pure-carbon moieties where numbers $n=10, 14, 18$ emphasize themselves at certain conditions.

Such a spectral pattern contrast is due to switching between single-photon and multiphoton-ionizations for different species that correspond to the peaks in the 7.9 eV mass spectrum. The magic numbers are in fact due to the low IPs of those species, which allow direct ionization. In turn, 10.5 eV photon energy provides the objective picture of relative abundances. The magic numbers in this case are "real" and must originate from the stability of these neutral clusters. Their stability and abundance support the idea that they are caused by the fragmentation of the initially formed neutral large carbon clusters [13].

Second test application: REMPI spectroscopy with 10.5 eV photons.

$A^1\Pi_u \leftarrow X^1\Sigma_g^+$ electronic transition in C_3

The second test involves combining the generated light with a second tunable color in REMPI. The molecule chosen, C_3 , is known to correspond to the one of the main fragmentation channel of the larger carbon species/clusters and therefore is expected to be

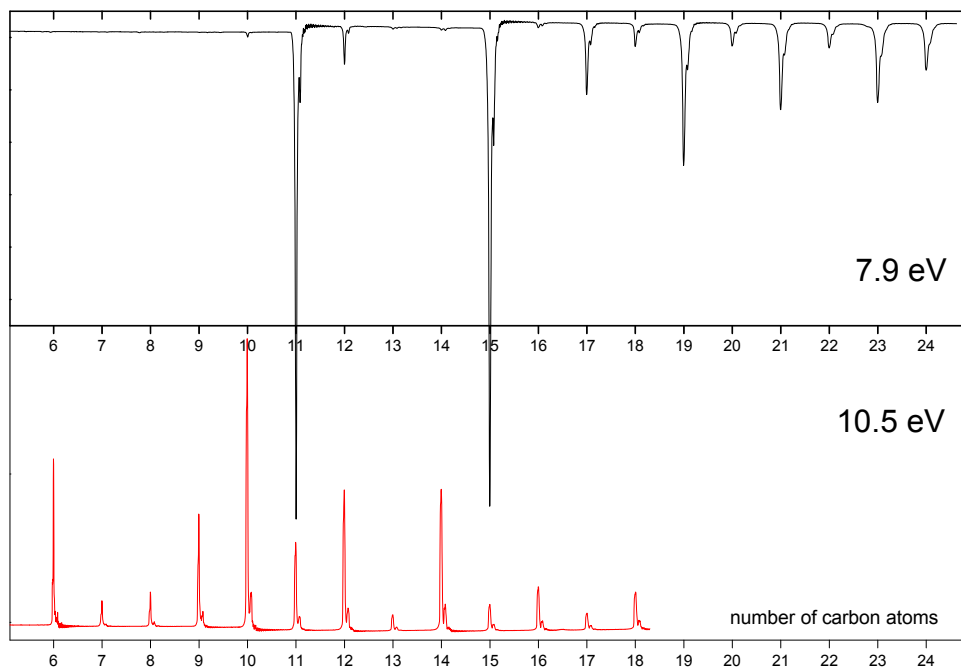


Figure 5.11: ms of ablation. 157 vs 118nm.

abundant among products in the graphite ablation source. It is also known to have stable long-lived excited states and a high IP (11.7 eV [14]). Because of the latter, spectroscopy of C_3 in the visible had been studied in the gas phase mainly by direct absorption methods, CRDS, and LIF; and only transitions (still unassigned because of strong mixing) in UV (like 266–320 nm) were done by REMPI ([15], for example). Thus it is a perfect candidate for the [1+1']REMPI with 10.5 eV photons at the ionization step.

Scanning of a tunable laser around 405 nm reveals the high resolution (0.05 cm^{-1}) rotationally resolved electronic spectrum of the famous "Comet band" (figure 5.12).

Despite the small size of the molecule and its long and rich spectroscopic history⁸, full assignment of its electronic (rovibronic) spectrum has not yet been attempted. The reason for this are the numerous perturbations that the molecule experiences. Thus, for example, the very recent in-depth LIF study of this transition [16] performed with rotational resolution (similar to the one employed here). In their paper the issue of an impossible full assignment of all lines by a single electronic transition was presented. Based on detailed analysis of those extra lines impeding the complete rotational fit, at least two long lived states were found to perturb the the $A^1\Pi_u, 000$ state. These perturbations appear to involve levels of lower-lying triplet states. One of these appears to be a $^3\Sigma_u^-$

⁸ $A^1\Pi_u$ emission spectrum of C_3 , near 4050 Å, was first observed from the tail of a comet by Huggins in 1882. These same bands were later observed in the laboratory by Herzberg in 1942, and were finally identified by Douglas in 1951.

vibronic state, which may possibly be a high vibrational level of the $b^3\Pi_g$ state, and the other appears to be a P=1 state with a low rotational constant B [16].

Therefore the spectrum is presented here for a demonstration of the VUV+REMPI in work. Specific band-to-band assignment was not attempted.

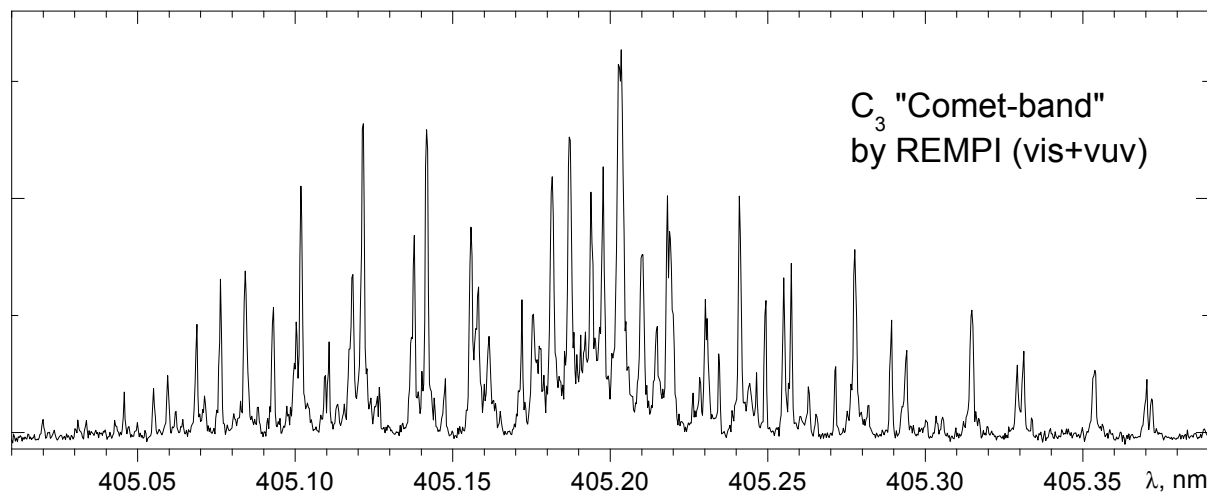


Figure 5.12: C_3 Comet band by REMPI.

5.2.3 Implications

The scheme for generating 10.5 eV photons proved itself as robust and fairly effective. The approach can and should be employed for the REMPI electronic spectroscopy of the molecules (not necessarily pure-carbons) with IP higher than 10.5 eV, as it was demonstrated convincingly through an example of C_3 here and of C_5 in the corresponding chapter of the thesis.

Subjective technical recommendations for possible implementations would include:

- Auxiliary devices like a removable pinhole and VUV-sensitive in-chamber video camera (as already mentioned for the case of RDFM) would be very helpful in alignment (though not as vital as when aligning tunable VUV).
- A longer gas cell would allow higher power and less focusing, avoiding a gas breakdown in the focus point, and would eventually allow the production of more VUV.
- Sufficient distance between the MgF_2 lens and the beam blocker should be provided to ensure dependable full separation of the generated third harmonic (118 nm) and fundamentals (355 nm). This becomes intensively important with rise in power of the incident laser (355 nm).

Bibliography

- [1] Frédéric Merkt. private communication, ETH Zurich, 2002.
- [2] K. Yamanouchi and S. Tsuchiya. Tunable vacuum-ultraviolet laser spectroscopy: excited-state dynamics of jet-cooled molecules and van-der-Waals complexes. *Journal of physics B-Atomic molecular and optical physics*, 28: 133–165, 1995.
- [3] R. Hilbig and R. Wallenstein. Tunable VUV radiation generated by 2-photon resonant-frequency mixing in xenon. *IEEE J. Quantum Electron.*, 19: 194–201, 1983.
- [4] R. Hilbig, G. Hilber, A. Lago, B. Wolff, and R. Wallenstein. Tunable coherent VUV radiation generated by nonlinear optical frequency conversion in gases. *Comments on Atomic and Molecular Physics*, 18: 157–180, 1986.
- [5] NIST. Atomic Spectra Database. http://physics.nist.gov/cgi-bin/AtData/main_asd.
- [6] A. Jolly, J. L. Lemaire, D. BelleOudry, S. Edwards, D. Malmasson, A. Vient, and F. Rostas. High resolution 'VUV laser' measurements of the band oscillator strengths of the CO $A^1\Pi (9 \leq v' \leq 17) \leftarrow X^1\Sigma^+ (v''=0)$ transition. *Journal Of Physics B-Atomic Molecular and Optical Physics*, 30: 4315–4337, 1997.
- [7] NIST. Chemistry WebBook. <http://webbook.nist.gov/chemistry/>.
- [8] T. Motylewski, O. Vaizert, T. F. Giesen, H. Linnartz, and J. P. Maier. The $^1\Pi_u \leftarrow -X^1\Sigma_g^+$ electronic spectrum of C_5 in the gas phase. *J. Chem. Phys.*, 111: 6161–6163, 1999.
- [9] A. Okeefe and D. A. G. Deacon. Cavity ring-down optical spectrometer for absorption-measurements using pulsed laser sources. *Rev. Sci. Instrum.*, 59: 2544–2551, 1988.
- [10] A. H. Kung, J. F. Young, and S. E. Harris. Generation of 1182 Å radiation in phase-matched mixtures of inert-gases. *Appl. Phys. Lett.*, 22: 301–302, 1973.
- [11] A. H. Kung. Correction. *Appl. Phys. Lett.*, 28: 239–239, 1976.
- [12] A. L. Brown, D. C. Dayton, M. R. Nimlos, and J. W. Daily. Characterization of biomass pyrolysis vapors with molecular beam, single photon ionization time-of-flight mass spectrometry. *Chemosphere*, 42: 663–669, 2001.
- [13] K. Kaizu, M. Kohno, S. Suzuki, H. Shiromaru, T. Moriwaki, and Y. Achiba. Neutral carbon cluster distribution upon laser vaporization. *J. Chem. Phys.*, 106: 9954–9956, 1997.

- [14] C. Nicolas, J. N. Shu, D. S. Peterka, M. Hochlaf, L. Poisson, S. R. Leone, and M. Ahmed. Vacuum ultraviolet photoionization of C_3 . *J. Am. Chem. Soc.*, 128: 220–226, 2006.
- [15] G. W. Lemire, Z. W. Fu, Y. M. Hamrick, S. Taylor, and M. D. Morse. New electronic band systems of jet-cooled C_3 : 266–302 nm. *J. Phys. Chem.*, 93: 2313–2319, 1989.
- [16] G. Q. Zhang, K. S. Chen, A. J. Merer, Y. C. Hsu, W. J. Chen, S. Shaji, and Y. A. Liao. The 4051Å band of C_3 ($A^1\Pi_u < -X^1\Sigma_g^+$, 000-000): Perturbed low-J lines and lifetime measurements. *J. Chem. Phys.*, 122: 244308, 2005.

Chapter 6

Gas phase electronic spectra of the carbon chains C_5 , C_6 , C_8 , and C_9

Foreword

This chapter contains manuscript submitted to the Journal of Chemical Physics. (*A.E. Boguslavskiy and J.P. Maier "Gas phase electronic spectra of the carbon chains C₅, C₆, C₈, and C₉."*)

6.1 Abstract

Three electronic absorption systems for C₅ at 511, 445, and 232 nm and one for C₆, C₈, and C₉ centered at 228, 259, and 288 nm have been observed in the gas phase. The C₅ chain was produced in both discharge and ablation sources and detected using resonant two-color two-photon ionization spectroscopy involving 10.5 eV photons. The decay of the excited singlet electronic states indicates fast intramolecular processes on a sub-ps time scale. The internal energy is assumed to be trapped in a triplet state for at least 15 μs. Hole-burning experiments on the $2\ ^3\Sigma_u^- \leftarrow X\ ^3\Sigma_g^-$ transition of C₆, C₈, and $1\ ^1\Sigma_u^+ \leftarrow X\ ^1\Sigma_g^+$ of C₉ confirm the predissociative nature of the excited electronic states.

6.2 Introduction

Bare carbon molecules, especially smaller ones, have been identified as reaction intermediates in combustion-, plasma-, and astro-chemistry [1]. Electron-spin resonance [2] and infrared absorption spectra [1, 3] of several C_n species had been obtained, allowing the deduction of their ground state symmetries and structures. The infrared spectra have permitted the identification of C₃ [4] along with C₅ [5] in the circumstellar shell of the carbon star IRC+10216. The photoelectron spectra of mass-selected anions complement the picture with information on the ground states vibrations and electron affinities of larger carbon species, indicating the appearance of rings beyond the C₁₀ size in addition to chains [6]. Also a number of low lying (below 1 eV) electronic states in C₄, C₆ and C₈ were revealed [7]. While the electronic absorption spectra in the visible and UV of many of C_n species in neon matrices have been reported [8], the gas phase electronic spectroscopy of these moieties is still in its infancy. Ultraviolet photoelectron spectroscopy of carbon anions was successfully applied for n=2-30 [9] and recently for n=10-41 [10], but obtained the energies of excited electronic states of the neutral C_n species only at low resolution. Apart from the thoroughly studied C₃ [1, 11], only one electronic transition has been identified in both C₄ [12] and C₅ [13] using cavity ringdown spectroscopy (CRDS). Observation of the C₅ electronic transition in the gas phase enabled a search for this absorption to be made through diffuse interstellar clouds. However only upper

limit to the column density of C_5 could be inferred [14, 15]. Other exceptions are the ring species C_{18} , C_{22} [16] and the fullerenes C_{60} and C_{70} [17] that were identified in the gas-phase using resonant enhanced multiphoton ionization (REMPI) techniques.

Because it is not possible to produce a given C_n species as a dominant product one should consider mass selective methods; the lack of this is the intrinsic weakness of CRDS. Even after the elemental formula is determined via isotopic substitutions, other species like C_2 and C_3 , which have absorptions just about everywhere at energies above 516 and 405 nm, respectively, are still present. Thus there remains a set of overlapping sharp peaks in the first detection of an electronic transition of C_5 in the gas phase by CRDS [13]. One of the incentives of this work was to observe the rotational contour in the absence of such lines. The REMPI technique, with its mass-selection and sensitivity was chosen for this survey.

Three main issues have been addressed. The first concerns an efficient method of production: the use of a graphite ablation source ensured that sufficient amounts of the studied molecules were generated. A discharge source was also capable of producing C_5 and proved particularly useful for spectroscopy in the UV where this mass gate is otherwise polluted with products of photofragmentation of larger carbon moieties produced by the ablation source. The second aspect is the large ionization potential (IP) of C_5 , 12.3 eV [18] which required vacuum UV radiation for the ionization. The third issue relates to the intramolecular dynamics, the fast part of which manifests itself in the spectroscopic linewidths and the slower step can be observed in some cases on a ns or longer timescale.

This contribution is devoted to the gas phase REMPI spectroscopy of the linear chains C_n , $n=5, 6, 8$, and 9. The first complete gas-phase electronic spectrum of C_5 in the 210–700 nm region is reported and intramolecular dynamics of the excited states are discussed. Also the spectra of the electronic transitions $2\ ^3\Sigma_u^- \leftarrow X\ ^3\Sigma_g^-$ of C_6 and C_8 , and $1\ ^1\Sigma_u^+ \leftarrow X\ ^1\Sigma_g^+$ of C_9 obtained by a dissociative hole-burning approach are presented.

6.3 Experimental

The setup consists of a molecular beam combined with a linear time-of-flight (TOF) mass analyzer [19]. Major modifications concerned the production of carbon chains and ionization photons. The source was a pulsed valve coupled to either an electric discharge or graphite laser vaporization. For the former, a gas pulse of 1% acetylene in Ar (backing pressure 8–10 bar) was expanded through a ceramic body. A high voltage pulse (100 μ s of ~ -700 –800 V at 1 k Ω) was applied between the electrodes placed on either side of the insulating spacer. In the laser vaporization source a graphite rod was rotated and translated so that a fresh surface was continuously exposed to a Nd:YAG laser (25 mJ/5 ns

pulse of 532 nm, focused to 0.3 mm) which was fired to coincide with the buffer gas flow over the target area.

The gas flow conditions optimized previously for monocyclic ring production [16] gave a maximum production of masses like C_{84} and extending beyond C_{150} . At the laser spot on the graphite rod the plasma is constricted at high buffer pressure. This makes clustering reactions in the plume of the carbon vapor rapid compared with the diffusion speed and results in large molecules [20]. In an attempt to shift the distribution down to smaller masses the source body was shortened (from 20 to 5 mm) to reduce the time available for clustering and the backing pressure lowered to decrease its speed. Changing the pressure from 10 to 3.5 bar seemed to produce only slightly more C_5 . In the design used it becomes increasingly hard to keep a stable gas flow for backing pressures below 3 bar and the channel clogged quickly with soot and crystal-like structures.

While lowering the pressure did not greatly enhance the C_5 production, changing the buffer gas from Ar to Ne and further to He did increase the amount of C_3 and C_5 significantly. C_3 is well known as the major neutral loss fragmentation channel for most small to middle-sized ($4 < n < \approx 30$) cations in collision induced dissociation measurements [21, 22], metastable reactions [23], gas chromatography [24], and from anions in impact-induced fragmentation experiments [25]. Less work has been done on neutral C_n , but the recent studies on the fragmentation of highly excited $C_{5,7,9}$ report a prevalence of C_3 cleavage [26]. Carbon atoms, C_2 , and C_5 are among the other abundant fragments. The loss of C_2 units is often associated with annealing into fullerenes [27]. Intense C and C_5 loss is observed for a significant number of systems of sizes below C_{30}^+ [22, 23] with the latter reported even as the dominant fragmentation channel for some systems [22]. Next family of neutral losses which are manifested in the mass spectrum of graphite ablation - the C_{4n+2} -rings ($C_{14,18,22}$) - arises in both anion [25] and cation [23, 24, 27, 28] fragmentation when the parent ions surpass $C_{n \approx 17}$ size, and becomes the major channel after $C_{n \approx 24}$ for those that could not anneal into fullerenes. Ample production of these rings suggests the importance of fragmentation in the source. Taking into account the lower cooling efficiency of He compared to Ne or Ar, the increase in C_3 and C_5 production with He buffer gas thus could be attributed to enhanced fragmentation of large "hot" carbon systems.

The species produced by either source passed through a 2 mm skimmer into a differentially pumped region where ions were removed by a perpendicular electrical field before entering the TOF. The neutral molecules were then ionized by 10.5 eV photons of the 9th harmonic of a Nd:YAG laser. The ionizing photons, produced via a non-resonant frequency tripling xenon cell, meet the molecular beam anti-collinearly allowing for a maximum overlap. The efficiency of this non-resonant nonlinear conversion processes is

known to be around 10^{-4} – 10^{-3} [29, 30]. In spite of a slight defocusing of the fundamental light (because of chromatic dispersion property of the lens) in the TOF extraction region the energy density (50 mJ of 355 nm in ~ 5 mm spot) is high enough to cause non-resonant multiphoton ionization and fragmentation in the molecular beam, producing background in the channel of interest. To overcome this without losing precious microjoules of generated light with additional optical elements, the dispersive property of an off-axis penetrated lens was utilized. The 355 nm light was carefully aligned so that it was dumped on the ceramic beam block inside the vacuum chamber while the generated 118.2 nm light enters the interaction region only slightly off-axis. This energy is enough to ionize pure carbon molecules bigger than C_5 with one photon. Ions were extracted and accelerated towards a detector.

Excitation photons in the 210–550 nm range were delivered by an OPO system (3 cm^{-1} bandwidth in the visible and 6 cm^{-1} below 420 nm) for survey scans and by a Nd:YAG pumped dye laser (0.15 cm^{-1} bandwidth or 0.05 cm^{-1} using an intracavity etalon). The laser beam was combined on a dichroic mirror with the 3rd harmonic of a Nd:YAG laser and fed into the extraction chamber along with the generated 118.2 nm light. The beam of the excitation laser was defocused to suppress alignment dependence on the wavelength while scanning a relatively broad range.

6.4 Observations and Discussion

6.4.1 Electronic transitions of C_5 .

Figure 6.1 shows a spectrum of C_5 obtained using the REMPI method. It consists of three electronic transition systems: A, B, and C, around 511, 445, and 232 nm. Band system A, assigned in [31] as a ${}^1\Pi_u \leftarrow X{}^1\Sigma_g^+$ transition, shows the most well resolved structure and has its origin at 510.94 nm in agreement with the CRD results [13]. Features to the red of the origin are hot bands. This interpretation is based on the fact that the bands do not appear if the discharge source is used. Though the latter produces molecules much colder vibrationally, the rotational profile overlap was found to be essentially unchanged. The rotations are known to cool more efficiently in effusive beams than the vibrations [32]. Thus the slowed adiabatic expansion (backing pressure used in ablation source is 2-3 times lower) is still sufficient to cool the molecules rotationally down to ≈ 30 K.

Band system B (fig. 6.1) is another candidate suggested for the assignment to the ${}^1\Pi_u \leftarrow X{}^1\Sigma_g^+$ transition [33]. This spectral feature consists of at least three bumps each of ≈ 10 nm width. It is found to be very dependent on the intensity of resonant laser light. While A and C systems required a fraction of a mJ to appear, B required the full available laser power (> 10 mJ) to rise above the background noise. Though the predicted oscillator

strength is 0.015 [33], even a strong transition would hardly be detectable by REMPI if fast intramolecular processes deplete the excited state. The laser intensity to the blue of 420 nm drops an order of magnitude because the frequency doubling system is used. This results in the decrease in signal observed in the middle of the transition system. The dashed line in figure 6.1 represents the magnified and smoothed signal to help guide the eye for the probable band shape that would have been obtained if the higher laser power were to be used.

Band system C is the most intense in the spectrum. It exhibits vibronic structure (see section 6.4.4), shifted $\sim 65\text{ cm}^{-1}$ to the blue of the corresponding absorption in a neon matrix [31], in contrast with the ${}^1\Pi_u \leftarrow X^1\Sigma_g^+$ band at 511 nm which lies 29 cm^{-1} to the red.

6.4.2 Decay of C_5 electronic states

The bands of all three electronic transitions are broadened to a larger extent than can be expected from the spontaneous emission rates according to the calculated oscillator strengths [33]. Predissociation is not thought to be involved as they all lie below the lowest thermodynamical dissociation channel: $C_5 \rightarrow C_3 + C_2$ at 5.88 eV [34] or 5.96 eV [35]. Attention was given to avoid power broadening the narrowest spectral feature (band system A at 511 nm). Even with $50\mu\text{J}$ per 10 ns laser pulse the rotational structure is still not discernible. According to a spectral simulation this should have been resolved with the bandwidth used. Intramolecular processes are thought to cause the broadening.

The relatively slow (ns, μs) part of the intramolecular processes can be monitored using nanosecond REMPI. The fast steps, occurring on ps and fs time-scales, can only be inferred from the spectral broadening of the absorption features. In this way the depletion rates from the excited electronic states indicated in figure 6.2 were estimated. The energy of electronic excitation does not immediately get converted into ground state vibrations. It evolves somehow, likely state specific, but remains energetically accessible for the second ionizing step photons (i.e. within 10.5 eV from IP) for at least $15\mu\text{s}$ - the detection window of the set-up. The electronic state that is thought to act as a sink is a triplet state (T in fig. 6.2). Such a state, $a^3\Pi_u$, was calculated [33,36] and identified experimentally in C_5 by anion photoelectron spectroscopy to lie 1.99 eV above the ground state [37]. An alternative explanation would be that the system is trapped in highly excited vibrational levels of the ground state manifold. DFT calculations (B3LYP/6-31g(d)) for the ground state of C_5 and C_5^+ indicate only a small change in geometry ($\approx 2\%$ elongation) upon ionization. Therefore direct ionization from vibrational excited levels of C_5 is not likely to be effective because of low Franck-Condon factors. The involvement of a triplet state as shown in the scheme of fig. 6.2 would lead to a better overlap because the internal vibrational energy

excess is ≈ 2 eV less. Not all the excited C_5 molecules have to end up in the triplet state. Those in the ground state manifold could account for the experimentally observed reduction in the ion current at long delays.

None of the excited states were detected using a 7.9 eV (F_2 excimer laser) instead of 10.5 eV light for the ionization step. Because of the quickness of the first stage of decay, the absence of a two color signal does not provide information on the energy required to ionize the molecule from these states. Rather, it imposes a limitation on the energy of the "sink" state, $E_T < IP(C_5) - 7.9$ eV. *Ab initio* calculations indicate several low-lying triplet states [36]. All three electronic states accessed in this experiment may not necessarily evolve to the same "sink" state. These different states would all have to be low enough in energy to escape detection with the F_2 laser. On the other hand, internal conversion within the triplet manifold is likely to be more efficient compared to the intersystem crossing from the lowest triplet state to $X^1\Sigma_g^+$. Hence it seems reasonable to assign the state T to the lowest triplet state, namely $a^3\Pi_u$.

The decay following the excitation to the A-state with 511 nm light exhibits bi-exponential character: a relatively fast process (~ 800 ns) and slower one ($< 15 \mu s$). This can be accounted for by a conversion to lower lying singlet states, which then decays to the longer lived $a^3\Pi_u$ state.

6.4.3 The $A^1\Pi_u \leftarrow X^1\Sigma_g^+$ transition of C_5

The spectrum shown in figure 6.3 is a high resolution scan of the C_5 511 nm electronic absorption band. The approach used is mass-selective, so one can be sure that overlap due to other species has been eliminated. The spectrum is broadened according to the rotational profile simulations to about 1.0 cm^{-1} (plus 0.15 cm^{-1} due to laser bandwidth) for each line. Though at higher laser powers significant broadening was observed, the presented spectrum is free from this; no further profile narrowing was achieved by decreasing the laser intensity. The linewidths observed in the REMPI spectrum are also comparable to those obtained using CRDS [13], where power broadening is limited by the fact that the highly reflective mirrors used allow only $\sim 10^{-4}$ of the ~ 1 mJ laser intensity to enter the cavity.

Since the detection of the electronic transitions of C_5 in a neon matrix [31], new *ab initio* calculations have become available [33]. The authors found a 0.5 eV discrepancy between the calculated energy of the first allowed transition (to a $^1\Pi_u$ state) and the experimentally measured system. Thus they suggested that the observed absorption spectrum at 511 nm should be assigned to the formally forbidden $^1\Sigma_u^-$ or $^1\Delta_u$ states, becoming allowed either vibronically or due to a bent structure in the excited state. If C_5 were slightly non-linear in both the ground and excited states one should see rotational K-structure

in the electronic spectrum. This, however, is not the case. Infrared laser spectroscopy of C_5 in the gas phase has proven that C_5 is linear in its $X^1\Sigma_g^+$ ground state [1]. The excited states might be bent, and, at this stage the observed electronic spectrum cannot rule out this possibility. An attempt was made to fit the measured profile to various types of transitions. The contour could be fitted to both linear-to-linear $\Pi_u \leftarrow \Sigma_g^+$ but not $\Sigma_u^+ \leftarrow \Sigma_g^+$ (lack of Q-branch), or linear-to-bent *cis* ($A_1 \leftarrow A_1$, $B_2 \leftarrow A_1$, but not $B_1 \leftarrow A_1$) or *trans* ($A_u \leftarrow A_g$, $B_u \leftarrow A_g$). This is because the unresolved rotational profile is essentially defined by variation of the B-constant (and C), which is not very sensitive to the off-axis atoms. One conclusion can be derived from the fit: the rotational constant B must decrease in the excited state. Thus the molecule elongates upon excitation no matter whether it will bend at the same time or not.

The picture of the intramolecular dynamics (fig. 6.2) suggests the presence of another singlet state under the A-state. This is necessary to justify the fast internal conversion that occurs, suggesting that the originally proposed assignment, $^1\Pi_u \leftarrow X^1\Sigma_g^+$, is reasonable [31].

6.4.4 UV band of C_5

The UV region of the REMPI C_5 spectrum is shown in fig. 6.4 (trace *b*) in comparison with the absorption spectrum (*a*) obtained in a neon matrix [31], and the photofragment yield spectrum (*c*) taken from ref. [38]. Though the thermodynamical dissociation channel opens only above 5.88 eV [34], presence of photofragment signal at energies below indicates the importance of multiphoton processes in this case [38]. Calculations [35] predict several possible fragmentation pathways resulting in C_2+C_3 . These include the non-ground state potential surface fragmentation channel $C_5(a^3\Pi_u) \rightarrow C_2(a^3\Pi_u)+C_3(X^1\Sigma_g^+)$ which lies just 0.03 eV above the lowest thermodynamical dissociation $C_5(X^1\Sigma_g^+) \rightarrow C_2(X^1\Sigma_g^+)+C_3(X^1\Sigma_g^+)$. The observed dynamics of the excited states decay (section 6.4.2), indicating an efficient crossing to the triplet manifold, suggests that fragmentation may indeed occur from a triplet state.

The three spectra manifest the vibronic progression that was assigned to the 2_0^2 symmetric stretch within a dipole forbidden electronic transition [31]. The absence of the broad underlying continuum in the matrix absorption spectrum should not be alarming, as it is caused by a fall-off in detection sensitivity below 250 nm due to the increasing light-scatter from the matrix using the waveguide technique [31]. It is also not possible to distinguish broad peaks from the background due to scattering in this spectral region.

This broad background present in the REMPI spectrum is assigned to the $^1\Sigma_u^+ \leftarrow X^1\Sigma_g^+$ transition of C_5 . This is based upon the wavelength (onset of band system) dependence of the corresponding electronic transitions of C_{2n+1} ($n=3-7$) on the number of carbon

atoms in the chain. They shift linearly with the addition of every two carbons [31] and C_5 is thus expected to absorb at ~ 210 nm. The absorption spectra of the matrix isolated C_{2n+1} species indicate two electronic transition systems in the UV region which come closer to each other with decreasing the chain size. Then the two electronic states mix more and the relative intensity of the weak transition grows as it borrows intensity from the stronger one (${}^1\Sigma_u^+ \leftarrow X {}^1\Sigma_g^+$). At C_5 chain size the weaker band system should have an onset at 238 nm and these two transitions should overlap. Thus the vibronic progression apparent in electronic spectrum (fig. 6.4) was assigned to the weak transition (denoted as "forbidden" in [31]). However it does not have to be a forbidden one as the new *ab initio* calculations [33] predict the presence of one more dipole allowed, though quite weak ($f \sim 0.0005$), $2 {}^1\Pi_u \leftarrow X {}^1\Sigma_g^+$ electronic transition below the strong ${}^1\Sigma_u^+ \leftarrow X {}^1\Sigma_g^+$ system.

6.4.5 Electronic spectra of C_6 , C_8 , and C_9

The $2 {}^3\Sigma_u^- \leftarrow X {}^3\Sigma_g^-$ electronic transition previously observed at 237.5 nm for C_6 and at 277.2 nm for C_8 in neon matrices [39], lies energetically half-way between their ground states and the IP. Thus conventional [1+1] REMPI can be used (fig. 6.5.a). Photons delivered from the same laser allow perfect time synchronization for the two steps. The corresponding transition of C_6 , seen before only in neon matrices, is shown in figure 6.6.a. In view of the rather broad contour of the system, indicating a fast decay rate from this state, the detection of C_6 with a nanosecond laser is somewhat surprising.

Additional information on fate of the excitation can be obtained in the following way. The molecules are irradiated by the photons energetic enough to cause direct ionization. A second laser, applied before the first one and tuned in resonance with the predissociative electronic transition, will cause a depletion of the ion current for the species of interest which manifests itself as an inverse peak in the REMPI spectrum (fig. 6.5.b). This is observed in C_6 where up to 50% of the molecules are thus depleted (fig. 6.6.b) The approach shows that the loss channel is indeed a fragmentation as any other energy redistribution would not remove the molecule from interaction with the 10.5 eV light and lead to the observed dip. Furthermore, assignment of the broad features in the [1+1] REMPI spectra to a certain molecule could be confused by the signal originating from cationic products of resonant photofragmentation of a larger carbon compound. In turn the dissociative hole-burning guarantees that the electronic spectrum originates from C_6 .

Similar observations allowed the detection of the $2 {}^3\Sigma_u^- \leftarrow X {}^3\Sigma_g^-$ transition in C_8 with maximum at 270 nm. Other members of the C_{2n} homologous series have escaped detection. C_4 would absorb at ~ 195 nm, a wavelength not accessible with the equipment used. Longer C_{2n} linear chains, on the other hand, become progressively less abundant virtually disappearing beyond C_{10} where the cyclic form prevails [39].

The ${}^1\Sigma_u^+ \leftarrow X {}^1\Sigma_g^+$ transition in linear C_9 could be detected. A strong band is apparent in the depletion spectrum and virtually nonexistent in the [1+1] REMPI spectrum for either the energetic reasons (adiabatic IP/2=4.38±0.05 eV=283±3 nm) or if the internal conversion from the excited state to the one dissociating is too fast. The transition system detected in C_9 is the same as the one responsible for the intense broad onset at the blue end in the electronic spectrum of C_5 (fig. 6.1). There the photon energy used for the hole-burning is insufficient for direct ionization, so that only [1+1'] REMPI could be employed for its spectroscopic detection.

The spectrum of C_7 was not observed with either method. However, energetic considerations (based upon the 8.09±0.1 eV adiabatic IP [40] and the energy of its ${}^1\Sigma_u^+ \leftarrow X {}^1\Sigma_g^+$ electronic transition measured in neon matrix) predict this state to be accessible with both methods. On the other hand, the relatively weak C_7 peak in the mass-spectrum suggests either an inefficient production or ionization of this linear chain. In fact both reasons may contribute. The reported IP of C_7 is believed to be due to its cyclic isomer [40, 41], whereas the linear one is predicted to be ~2 eV more stable [41]. Hence the transition will not be accessible with [1+1] REMPI and the peak in mass-spectrum could be exclusively or mostly due to the cyclic isomer, thus disabling also the dissociative hole-burning approach. The longer odd chains (C_{2n+1} , $n>4$) were not monitored during the experiments. However one could expect the dissociative hole-burning to be applicable for the linear chain isomers of the few next odd-numbered carbon molecules having even lower IPs, and being still abundant in the plasma.

6.5 Concluding remarks

The current work presents the first complete gas phase electronic spectrum of the neutral linear chain C_5 from near infrared to 210 nm. Three electronic systems at 511, 445, and 232 nm are identified. Unresolved rotational structure precludes full characterization of the first excited state, but the band profile implies that the molecule elongates in the A-state. The broadened nature of the bands indicates fast (~2-5 ps) depopulation of even the first detected excited electronic state suggesting the presence of a lower lying singlet state, leaving the question of exact assignment [31, 33] of this transition open.

The strong $2 {}^3\Sigma_u^- \leftarrow X {}^3\Sigma_g^-$ UV transitions in C_6 and C_8 , and the ${}^1\Sigma_u^+ \leftarrow X {}^1\Sigma_g^+$ in C_9 were detected for the first time in the gas phase. The predissociative nature of the excited electronic states was confirmed via 'dissociative hole-burning' experiments.

The significant result of the present study is the observation of the electronic transitions of C_5 , without the overlapping bands of other carbon moieties. This will allow a better comparison with astronomical measurements through diffuse interstellar clouds

than has been hitherto possible. The rotational profile of the origin band at 511 nm (trace *a* of fig. 6.3) should be used for such a purpose. An alternative could be to use the UV system around 225 nm showing broad vibrational peaks (fig. 6.4), as the oscillator strength of this transition is predicted to be larger than for the 511 nm system. As far as C₆, C₈, and C₉ chains are concerned, the very broad absorption systems below 300 nm are not attractive for an astronomical search. Nevertheless the detection of the REMPI spectra of these chains, and C₅ in particular, opens a way to monitor these species in terrestrial environments and chemical reactions.

6.6 Acknowledgement

This work has been supported by the Swiss National Science Foundation (project 200020-100019), and the European Union project "Molecular Universe" (MRTN-CT-2004-512303).

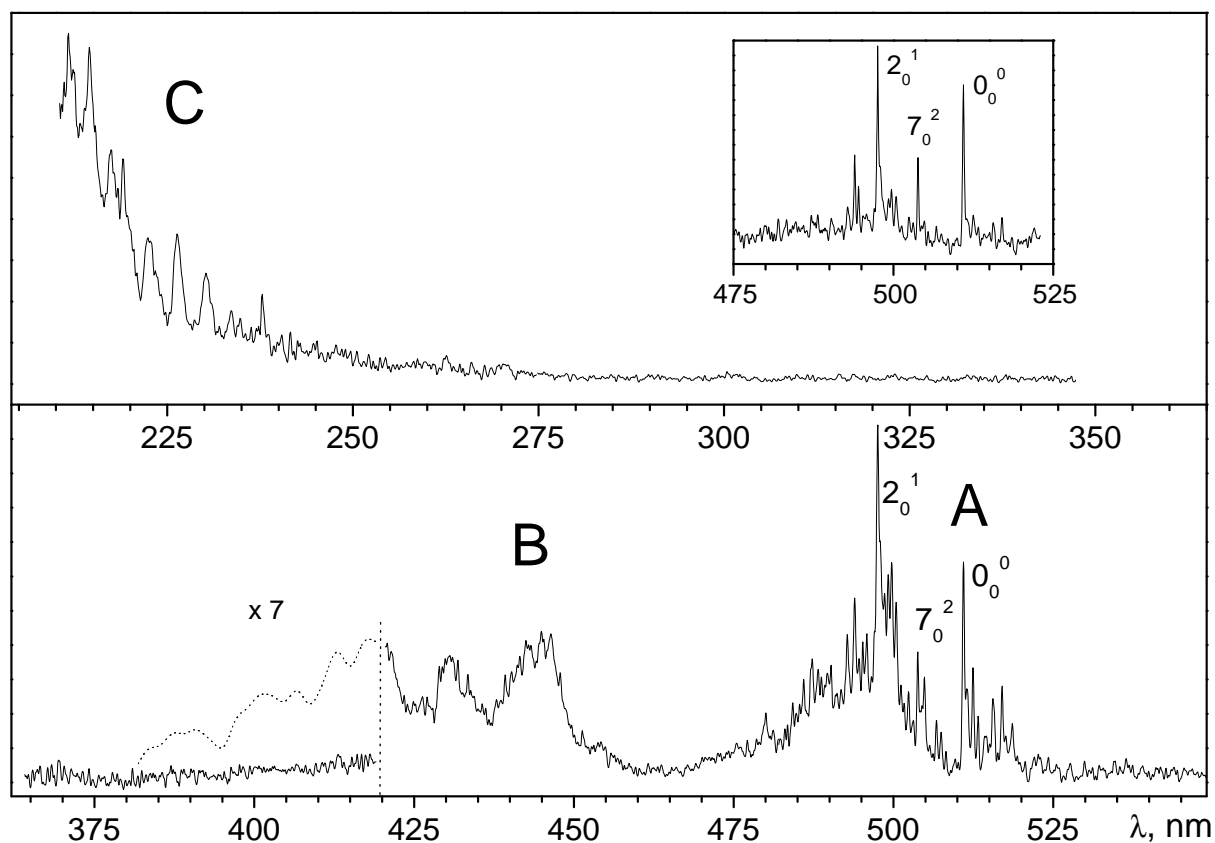


Figure 6.1: Gas phase electronic spectrum of C_5 detected using resonant two-color two-photon ionization in a supersonic free jet. The laser bandwidth was about 3 cm^{-1} in the visible and 6 cm^{-1} below 420 nm . A–C identify the electronic transition systems. The gap around 355 nm is caused by the non-transparency of the dichroic mirror used for combining the two laser beams. Discontinuity of the spectrum at 420 nm is an artifact of the doubling system used. The insert shows band system A detected using a discharge source: it is free of sequence bands, and four vibronic bands are seen (assignment is from [13]; the band near 493 nm may correspond to the 5_0^2 transition).

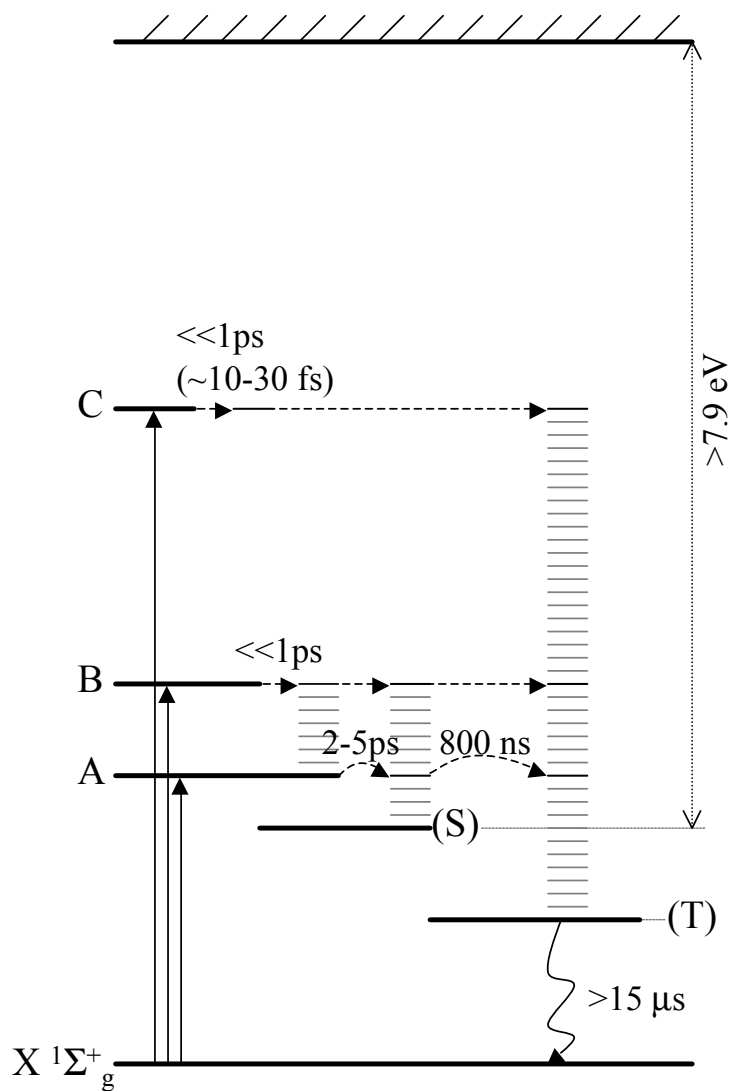


Figure 6.2: Inferred intramolecular dynamics in excited electronic states of C_5 . Dashed lines do not reflect the exact pathways of energy flow but just connect the initial and final states.

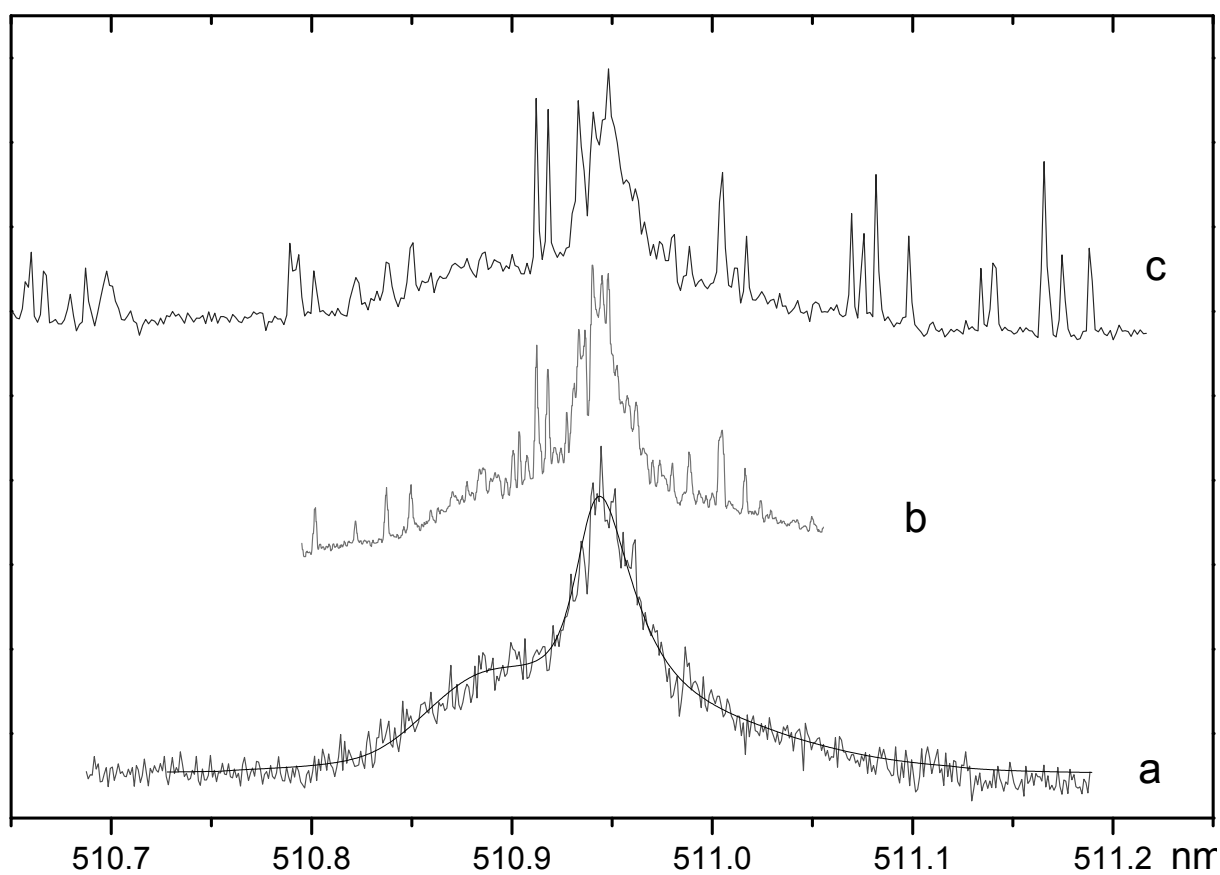


Figure 6.3: Trace *a*: Origin band of the 511 nm electronic transition system of C_5 measured with 0.15 cm^{-1} resolution (increasing it to 0.05 cm^{-1} had no influence). The simulated profile (solid line in *a*) is shown for 1.0 cm^{-1} (plus 0.15 cm^{-1} due to laser bandwidth) linewidth. Traces *b* (0.05 cm^{-1}) and *c* (0.15 cm^{-1}) recorded by CRDS are reproduced from refs. [13] and [42], respectively.

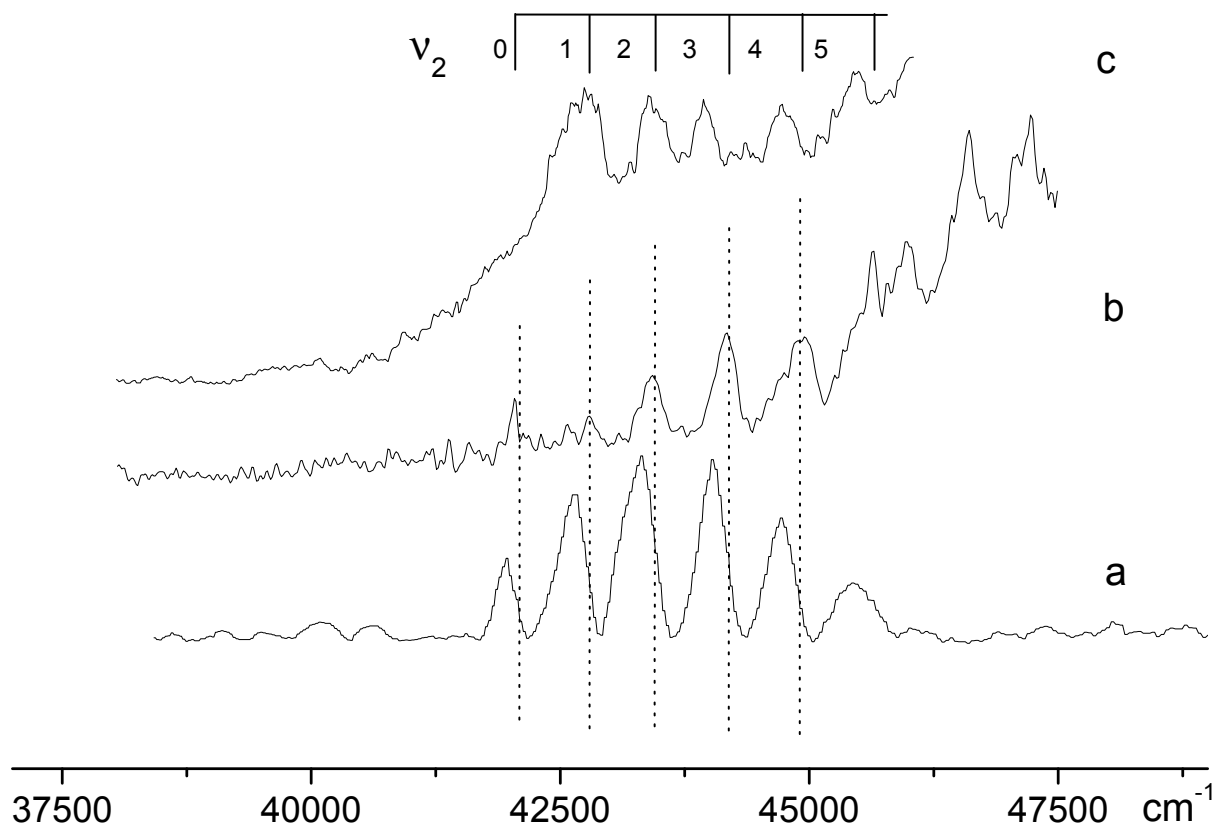


Figure 6.4: The UV region of the REMPI C_5 spectrum (trace *b*), in comparison with the absorption spectrum (*a*) obtained in a neon matrix [31], and the photofragment yield spectrum (*c*) reproduced from [38]. The spectra show the vibronic structure assigned to the 2_0^n (symmetric stretch) progression of a dipole forbidden electronic transition [31]. Absorption in the neon matrix is shifted $\sim 65 \text{ cm}^{-1}$ to the red from the gas-phase position.

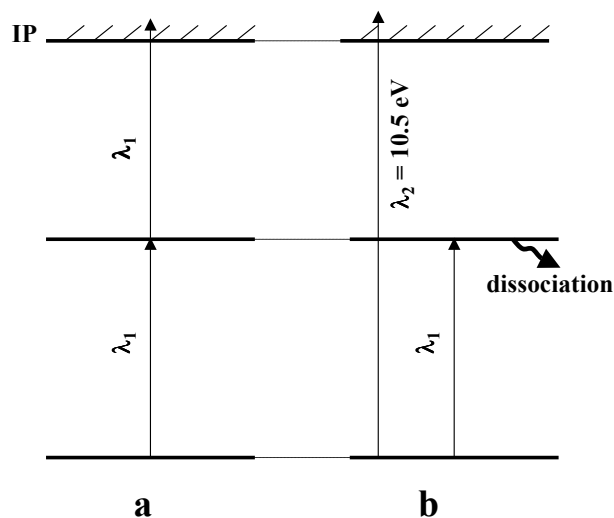


Figure 6.5: Two ways to detect the electronic transition to predissociative states in C_6 , C_8 , and C_9 . *a*) Conventional [1+1] REMPI: the number of resonantly ionized molecules is probed. *b*) Dissociative "hole-burning": the decrease of ion current due to depletion of the studied species via dissociation is monitored. The relatively fast predissociation, which could limit the efficiency of the first method, allows the hole-burning approach to be applied.

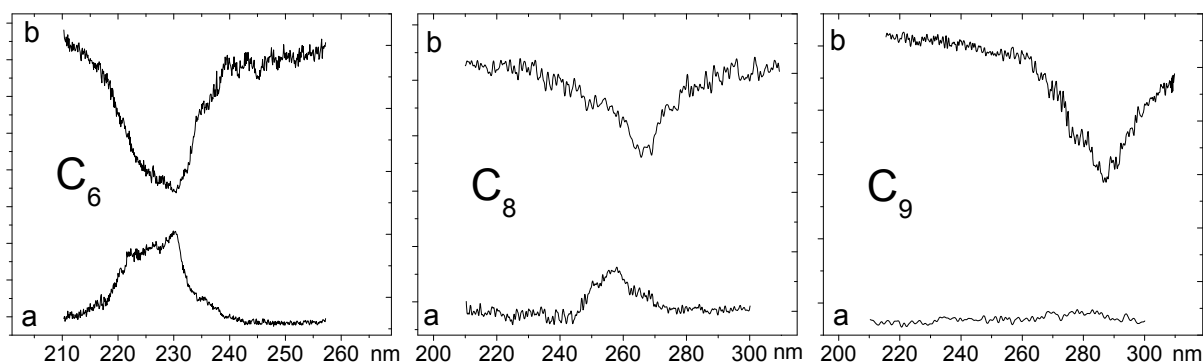


Figure 6.6: Electronic absorption band system of the $2^3\Sigma_u^- \leftarrow X^3\Sigma_g^-$ transition of C_6 and C_8 , and $1^1\Sigma_u^+ \leftarrow X^1\Sigma_g^+$ transition of C_9 in gas phase detected by [1+1] REMPI *a*) and dissociative "hole-burning" *b*) approaches.

Bibliography

- [1] A. Van Orden and R. J. Saykally. Small carbon clusters: Spectroscopy, structure, and energetics. *Chem. Rev.*, 98: 2313–2357, 1998. and references therein.
- [2] R. J. Van Zee, R. F. Ferrante, K. J. Zeringue, W. Weltner, and D. W. Ewing. Electron-spin resonance of the C_6 , C_8 and C_{10} molecules. *J. Chem. Phys.*, 88: 3465–3474, 1988.
- [3] W. Weltner and R. J. Van Zee. Carbon molecules, ions, and clusters. *Chem. Rev.*, 89: 1713–1747, 1989. and references therein.
- [4] K. W. Hinkle, J. J. Keady, and P. F. Bernath. Detection of C_3 in the Circumstellar Shell of IRC+10216. *Science*, 241: 1319–1322, 1988.
- [5] P. F. Bernath, K. H. Hinkle, and J. J. Keady. Detection of C_5 in the Circumstellar Shell of IRC+10216. *Science*, 244: 562–564, 1989.
- [6] D. W. Arnold, S. E. Bradforth, T. N. Kitsopoulos, and D. M. Neumark. Vibrationally resolved spectra of c_2 - c_{11} by anion photoelectron-spectroscopy. *J. Chem. Phys.*, 95: 8753–8764, 1991.
- [7] C. S. Xu, G. R. Burton, T. R. Taylor, and D. M. Neumark. Photoelectron spectroscopy of C_4^- , C_6^- , and C_8^- . *J. Chem. Phys.*, 107: 3428–3436, 1997.
- [8] J. P. Maier. Electronic spectroscopy of carbon chains. *Chem. Soc. Rev.*, 26: 21–28, 1997. and references therein.
- [9] S. Yang, K. J. Taylor, M. J. Craycraft, J. Conceicao, C. L. Pettiette, O. Cheshnovsky, and R. E. Smalley. UPS of 2-30-atom carbon clusters: chains and rings. *Chem. Phys. Lett.*, 144: 431–436, 1988.
- [10] Y. Achiba, M. Kohno, M. Ohara, S. Suzuki, and H. Shiromaru. Electron detachment spectroscopic study on carbon and silicon cluster anions. *J. Electron Spectrosc. Relat. Phenom.*, 142: 231–240, 2005.
- [11] G. Q. Zhang, K. S. Chen, A. J. Merer, Y. C. Hsu, W. J. Chen, S. Shaji, and Y. A. Liao. The 4051Å band of C_3 ($A^1\Pi_u < -X^1\Sigma_g^+$, 000-000): Perturbed low-J lines and lifetime measurements. *J. Chem. Phys.*, 122: 244308, 2005.
- [12] H. Linnartz, O. Vaizert, T. Motylewski, and J. P. Maier. The $^3\Sigma_u^- < -X^3\Sigma_g^-$ electronic spectrum of linear C_4 in the gas phase. *J. Chem. Phys.*, 112: 9777–9779, 2000.

- [13] T. Motylewski, O. Vaizert, T. F. Giesen, H. Linnartz, and J. P. Maier. The ${}^1\Pi_u < -X^1\Sigma_g^+$ electronic spectrum of C_5 in the gas phase. *J. Chem. Phys.*, 111: 6161–6163, 1999.
- [14] J. P. Maier, G. A. H. Walker, and D. A. Bohlender. Limits to interstellar C_4 and C_5 toward ζ Ophiuchi. *Astrophys. J.*, 566: 332–335, 2002.
- [15] J. P. Maier, G. A. H. Walker, and D. A. Bohlender. On the possible role of carbon chains as carriers of diffuse interstellar bands. *Astrophys. J.*, 602: 286–290, 2004.
- [16] A. E. Boguslavskiy, H. Ding, and J. P. Maier. Gas-phase electronic spectra of C_{18} and C_{22} rings. *J. Chem. Phys.*, 123: 034305, 2005.
- [17] R. E. Haufler, Y. Chai, L. P. F. Chibante, M. R. Fraelich, R. B. Weisman, R. F. Curl, and R. E. Smalley. Cold molecular-beam electronic-spectrum of C_{60} and C_{70} . *J. Chem. Phys.*, 95: 2197–2199, 1991.
- [18] R. Ramanathan, J. A. Zimmerman, and J. R. Eyler. Ionization-potentials of small carbon clusters. *J. Chem. Phys.*, 98: 7838–7845, 1993.
- [19] F. Guthe, H. B. Ding, T. Pino, and J. P. Maier. Diagnosis of a benzene discharge with a mass-selective spectroscopic technique. *Chem. Phys.*, 269: 347–355, 2001.
- [20] J. R. Heath, Q. Zhang, S.C. O’Brien, R. F. Curl, H. W. Kroto, and R. E. Smalley. The formation of long carbon chain molecules during laser vaporization of graphite. *J. Am. Chem. Soc.*, 109: 359–363, 1987.
- [21] M. B. Sowa, P. A. Hintz, and S. L. Anderson. Dissociation-energies for carbon cluster ions (C_{2-15}^+). A system where photodissociation is misleading. *J. Chem. Phys.*, 95: 4719–4720, 1991.
- [22] M. B. Sowa, P. A. Hintz, and S. L. Anderson. Dissociation-energies for small carbon cluster ions (C_{2-19}^+) measured by collision-induced dissociation. *J. Phys. Chem.*, 99: 10736–10741, 1995.
- [23] P. P. Radi, T. L. Bunn, P. R. Kemper, M. E. Molchan, and M. T. Bowers. A new method for studying carbon clusters in the gas-phase - observation of size specific neutral fragment loss from metastable reactions of mass selected C_n^+ , $n \leq 60$. *J. Chem. Phys.*, 88: 2809–2814, 1988.
- [24] G. von Helden, N. G. Gotts, and M. T. Bowers. Annealing of carbon cluster cation-rings to rings and rings to fullerenes. *J. Am. Chem. Soc.*, 115: 4363–4364, 1993.

- [25] R. L. Whetten, C. Yeretjian, and P. M. Stjohn. Cleavage patterns of carbon clusters from impact-induced fragmentation of C_n^- , $n=10-50$. *Int. J. Mass Spectrom.*, 138: 63–76, 1994.
- [26] G. Martinet, S. Diaz-Tendero, M. Chabot, K. Wohrer, S. Della Negra, F. Mezdari, H. Hamrita, P. Desesquelles, A. Le Padellec, D. Gardes, L. Lavergne, G. Lалу, X. Grave, J. F. Clavelin, P. A. Hervieux, M. Alcami, and F. Martin. Fragmentation of highly excited small neutral carbon clusters. *Phys. Rev. Lett.*, 93: 063401, 2004.
- [27] J. M. Hunter, J. L. Fye, and M. F. Jarrold. Annealing and dissociation of carbon rings. *J. Chem. Phys.*, 99: 1785–1795, 1993.
- [28] J. Hunter, J. Fye, and M. F. Jarrold. Carbon rings. *J. Phys. Chem.*, 97: 3460–3462, 1993.
- [29] A. H. Kung, J. F. Young, and S. E. Harris. Generation of 1182 Å radiation in phase-matched mixtures of inert-gases. *Appl. Phys. Lett.*, 22: 301–302, 1973.
- [30] A. H. Kung. Correction. *Appl. Phys. Lett.*, 28: 239–239, 1976.
- [31] D. Forney, P. Freivogel, M. Grutter, and J. P. Maier. Electronic absorption spectra of linear carbon chains in neon matrices .4. C_{2n+1} $n=2-7$. *J. Chem. Phys.*, 104: 4954–4960, 1996.
- [32] P. C. Engelking. Spectroscopy of jet-cooled ions and radicals. *Chem. Rev.*, 91: 399–414, 1991.
- [33] M. Hanrath and S. D. Peyerimhoff. The electronic spectrum of C_5 . *Chem. Phys. Lett.*, 337: 368–374, 2001.
- [34] K. A. Gingerich, H. C. Finkbeiner, and R. W. Schmude. Enthalpies of formation of small linear carbon clusters. *J. Am. Chem. Soc.*, 116: 3884–3888, 1994.
- [35] Z. X. Cao, M. Muhlhauser, M. Hanrath, and S. D. Peyerimhoff. Study of possible photodissociation channels in linear carbon clusters C_n ($n=4-6$). *Chem. Phys. Lett.*, 351: 327–334, 2002.
- [36] M. Kolbuszewski. Ab-initio study of the optical-spectra of C_3 , C_5 , and C_7 chains. *J. Chem. Phys.*, 102: 3679–3684, 1995.
- [37] M. Kohno, S. Suzuki, H. Shiromaru, and Y. Achiba. Characterization of the lowest triplet states of linear form C_{2n+1} by anion photoelectron spectroscopy. *J. Chem. Phys.*, 110: 3781–3784, 1999.

- [38] H. Choi, R. T. Bise, A. A. Hoops, D. H. Mordaunt, and D. M. Neumark. Photodissociation of linear carbon clusters C_n ($n=4-6$). *J. Phys. Chem. A*, 104: 2025–2032, 2000.
- [39] M. Grutter, M. Wyss, E. Riaplov, J. P. Maier, S. D. Peyerimhoff, and M. Hanrath. Electronic absorption spectra of linear C_6 , C_8 and cyclic C_{10} , C_{12} in neon matrices. *J. Chem. Phys.*, 111: 7397–7401, 1999.
- [40] S. B. H. Bach and J. R. Eyler. Determination of carbon cluster ionization-potentials via charge-transfer reactions. *J. Chem. Phys.*, 92: 358–363, 1990.
- [41] G. von Helden, W. E. Palke, and M. T. Bowers. The lowest energy structures of C_7^+ , C_7 and C_7^- . An ab-initio study. *Chem. Phys. Lett.*, 212: 247–252, 1993.
- [42] A. Denisov. *Electronic spectroscopy of some unsaturated carbon chains in the gas phase by cavity ringdown*. PhD thesis, University of Basel, Switzerland, 2006.

Chapter 7

Gas-phase electronic spectra of C_6NH_2 and C_8NH_2



Gas-phase electronic spectra of C_6NH_2 and C_8NH_2

A.E. Boguslavskiy, H. Ding, J.P. Maier*

Department of Chemistry, University of Basel, Klingelbergstrasse 80, CH-4056 Basel, Switzerland

Received 13 October 2005; received in revised form 10 December 2005; accepted 12 December 2005

Available online 24 January 2006

Abstract

The electronic spectra of C_6NH_2 and C_8NH_2 have been detected in the gas phase in the $16700\text{--}22000\text{ cm}^{-1}$ range by a mass selective resonant two-color two-photon ionization technique coupled to a laser ablation source. Several possible structural motifs are discussed. The production suggests to be amino radical addition to a linear carbon skeleton (C_6NH_2). Calculations indicate that a structure with hydrogens and nitrogen on opposite ends of the molecule (H_2C_6N) lies 2.8 eV lower in energy. The absence of $\sim 20\text{ cm}^{-1}$ spaced rotational K-structure indicates the presence of an off-axis carbon or nitrogen atom, but not hydrogen alone.

© 2006 Elsevier B.V. All rights reserved.

Keywords: Optical spectroscopy; Nitrogen containing hydrocarbons; Laser ablation; Electronic transitions

1. Introduction

Approximately one quarter of the interstellar and circumstellar molecules detected to date contain nitrogen. The majority of these species have only carbon and hydrogen as additional elements. It is also striking that the longest of these nitrogen containing compounds are cyanopolyynes [1]: a carbon skeleton capped by H and N atoms at opposite ends. Such an abundance invokes interest to the mechanism of their formation. As several amino-containing molecules are also detected in space, the study of C_nNH_2 moieties becomes of interest. Spectroscopic characterization of such molecules is desirable also for their identification in plasma and combustion reactions.

The conventional way to produce nitrogen capped carbon species is by applying an electrical discharge through a mixture of acetylene or diacetylene, to provide building blocks for the chains, with cyanoacetylene [2–4], cyanogen [3,5], dicyanogen [6], or even N_2 [2,7] in rare gases. This approach is not thought to be suitable for the amino-capping: introduction of ammonia or similar precursors precludes creation of long chains by blocking the growing end of the “assembly line”. Alternatively, one could

first grow a carbon skeleton and then expose the species to a reactant like NH_3 . Thus, a source that utilizes laser ablation of graphite has been adopted.

The products from graphite vaporization in reactive atmospheres have been studied mainly mass-spectroscopically. In one study it was shown that the small even carbon species are as reactive as the odd-numbered ones, but become resistant to reactions with NO , H_2 , CO , SO_2 , O_2 , and NH_3 in the 40–80 atoms range [8]. In the study of the carbon molecules comprising 6–30 atoms in the presence of H_2 , H_2O , and N_2 , the most abundant products were $C_{2n}H_2$ (and $C_{2n}N_2$ for N_2) implying linear skeleton structures [9]. At high hydrogen concentrations the peaks $C_{2n}H_{m=6,8,\dots}$ became apparent, confirming the presence of also non-linear carbon moieties in the plasma. The abundance of the $C_{2n}H_2$ products is attributed to their inert nature. In the recent study of ablated graphite in H_2 and D_2 gases, it was shown that at short delays after the laser pulse, the amount of other derivatives (C_nH_m) is significant [10]. Although mass-spectroscopic techniques give an indication as to the structure of the most abundant products, proof can be provided by spectroscopy. Recently, the cyclic and linear isomers of C_{18} and C_{22} formed by laser vaporization could be distinguished by addition of hydrogen and the subsequent identification of the electronic transition of the formed $HC_{2n}H$ chains [11].

In this contribution the gas phase electronic spectra of C_6NH_2 and C_8NH_2 created in an ammonia seeded graphite ablation are presented. Products were detected via a resonance-

* Corresponding author. Tel.: +41 61 267 3826; fax: +41 61 267 3855.

E-mail addresses: J.P.Maier@unibas.ch (J.P. Maier),

A.Boguslav@unibas.ch (A.E. Boguslavskiy)

enhanced multiphoton ionization (REMPI) scheme under supersonic molecular-beam conditions. Several possible isomers are discussed in relation to the plasma chemistry. Electronic and vibrational information is considered and the implications discussed.

2. Experiment

The apparatus consisted of a molecular beam combined with a linear time-of-flight (TOF) mass analyzer. The source relied on laser vaporization of graphite coupled to a pulsed valve. The rod was rotated and translated so that a fresh surface was continuously exposed to the laser (25 mJ/5 ns pulse of 532 nm Nd:YAG, focused to 0.3 mm) which was fired to coincide with the buffer gas flow over the target area. Vaporized carbon was swept through a 15 mm long and 3 mm diameter tube with ammonia (10%) seeded neon at 5–10 bar and expanded into a vacuum chamber. The species produced passed through a skimmer into a differentially pumped region where ions were removed by a perpendicular electrical field before entering the TOF. The neutral molecules were then ionized by 7.9 eV photons of a F_2 laser. The ionization process is more efficient when the tunable laser is resonant with a dipole-allowed electronic transition. Ions were extracted and accelerated towards a dual micro-channel plate detector. Photons in the 440–620 nm range were delivered by an OPO system ($\approx 0.25 \text{ cm}^{-1}$ bandwidth). The latter was anti-collinear to the molecular beam, while the ionization laser was perpendicular, allowing for maximum overlap. Variation of the mass-peak area as function of the laser wavelength gives the REMPI spectrum of the molecule. Separation of the ions in the drift tube after resonant excitation enables a large number of masses to be monitored simultaneously.

3. Results and discussion

3.1. Observations

Fig. 1 shows the measured electronic excitation spectra of C_6NH_2 (a) and C_8NH_2 (b) in the 17000–22000 cm^{-1} range. The maxima of the observed vibronic bands are given in Tables 1 and 2. The molecular formulae of the carriers were determined from the mass-to-charge ratio (m/z) of the ions detected. Isotopic labelled precursor was utilized to distinguish moieties like NC_5N and C_7H_4 from C_6NH_2 , which all have the same $m/z=88$. The optical spectrum moves to the $m/z=90$ channel on deuteration, confirming the presence of two hydrogens.

The spectrum of C_6NH_2 appears to have its origin at 19691 cm^{-1} . No other absorptions were observed at lower energy down to 16200 cm^{-1} . While the majority of the spectral lines are $\sim 5 \text{ cm}^{-1}$ wide, a few peaks at the blue end are noticeably broader ($\sim 30 \text{ cm}^{-1}$). Predissociation does not appear to be involved because no resonance peaks by smaller masses (down to $m/z = 40$) were observed at the same wavelength. The broadened features could have been attributed to a transition to the next electronic state, which would be expected to have a shorter lifetime due to efficient internal conversion to the underlying A-state. However, the analysis of two spectra

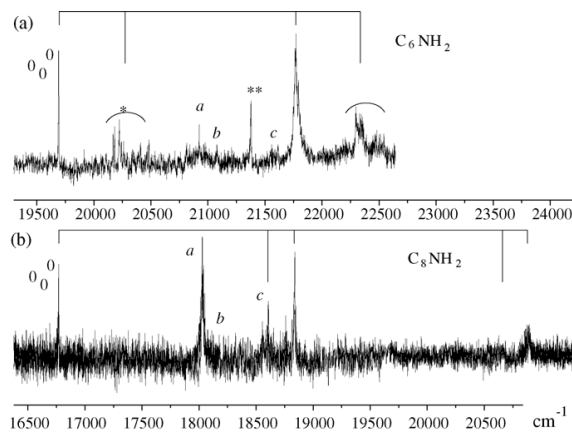


Fig. 1. Gas phase electronic spectra of (a) C_6NH_2 and (b) C_8NH_2 detected by a resonant two-color two-photon ionization technique under supersonic molecular beam conditions. Both show the excitation of $C\equiv C$ modes. Laser bandwidth increases from ≈ 0.2 to 0.3 cm^{-1} at higher energy. Letters refer to the peaks that have counterparts in both spectra, and stars—for those that do not.

traces the corresponding features for a C_8NH_2 molecule involving $\sim 2100 \text{ cm}^{-1}$ $C\equiv C$ - stretch progression. Thus, peak 19(20) is assigned to the vibronic transition $\nu_{(C=C)_0^1}$ of C_6NH_2 , and peaks 6, 9 of C_8NH_2 to $\nu_{(C=C)_0^1}$ and $\nu_{(C=C)_0^2}$. Additional bands to higher energy then appear to be due to combinations of this stretch with other lower frequency modes. There are also other similarities between the two spectra: the bands *a*, *b*, *c* in Fig. 1 seen to be common to C_6NH_2 and C_8NH_2 . Different width and pattern of the vibronic bands in the two spectra suggests

Table 1
Maxima of the vibronic bands observed in the electronic spectrum of C_6NH_2

Peak	$\nu \text{ (cm}^{-1}\text{)}$	$\Delta\nu \text{ (cm}^{-1}\text{)}$	Assignment
1	19691(1)	0	0_0^0
2	19845(2)	154	}
3	19915(2)	224	
4	20106(3)	415	
5	20169(1)	478	
6	20183(1)	492	
7	20224(2)	533	
8	20242(1)	551	
9	20261(1)	571	
10	20292(1)	601	
11	20340(1)	649	
12	20409(1)	718	
13	20484(2)	793	}
14	20922(2)	1231	
15	21078(2)	1387	ν_a
16	21375(2)	1684	ν_b
17	21547(3)	1856	ν_{**}
18	21614(2)	1923	}
19	21767(10)	2076	
20	21795(2)	2104	ν_c
21	21905(10)	2214	}
22	22297(10)	2606	
23	22341(15)	2650	}
24	22469(5)	2778	
25	22542(5)	2851	
			$(\nu_{C=C})_0^1 + \nu_*$

Table 2
Maxima of the vibronic bands observed in the electronic spectrum of C_8NH_2

Peak	ν (cm^{-1})	$\Delta\nu$ (cm^{-1})	Assignment
1	16769(1)	0	0_0^0
2	18028(2)	1259	ν_a
3	18176(2)	1407	ν_b
4	18558(4)	1789	ν_c
5	18608(3)	1839	
6	18840(4)	2071	
7	19659(15)	2890	$(\nu_{C\equiv C})_0^1$
8	20665(20)	3896	$(\nu_{C\equiv C})_0^1 + \nu_c$
9	20893(5)	4124	$(\nu_{C\equiv C})_0^2$
10	21612(15)	4843	

coupling of a “bright state” with a “dark state”. This depends on their proximity, which would be different among these two molecules.

3.2. Structural considerations

In the absence of resolved rotational structure other spectroscopic and theoretical information has to be used to infer the likely structure of the species. The mass spectra provide information on the most abundant products in the plasma and gives C_nH , C_n , C_nH_2 , C_nNH_4 , C_nH_3 , C_nH_4 . No prominent amounts of N-, NH-, or NH_2 -capped species were detected suggesting that the fragmentation $H_3N \rightarrow H_2N^\bullet + H^\bullet$ occurs without further dissociation of amidogen. Hydrogen radical makes a stronger bond with hydrocarbons than the amino radical H_2N^\bullet (see Table 2 in [12]) and is lighter and more agile. So it is expected that an H atom will react more effectively with the growing carbon chains than H_2N^\bullet . This explains the prevalence of the hydrogen capped chains in the mass-spectrum.

The apparent abundance of long chains in graphite ablation in presence of ammonia suggests that the major part of the reactions with it takes place after the growth of a carbon skeleton. Plasma at the point of the laser spot is constricted at the high buffer gas pressure and clustering reactions are rapid in the plume of carbon vapor compared with the diffusion speed [9]. Thus, the dominant products are expected to be one or both end-capped carbon moieties rather than those with a nitrogen atom inserted into the chain. This would also be in agreement with the spectro-

scopic detection of C_6NH_2 and C_8NH_2 , belonging to the same family.

Several possible structural isomers of C_6NH_2 were calculated at the DFT-B3LYP/6-31G(2df) level and the results, along with their symmetry group and relative energy, are depicted in Fig. 2. The three simplest candidates (isomers 1–3) are considered first. Isomer 1 complies with the above considerations in the most straightforward way, arising via attachment of H_2N^\bullet to a bare carbon chain in the plasma region. An unsaturated carbon chain pulls electronic density away from the nitrogen atom, forcing the molecule to flatten. The reaction mechanism for production of isomer 2 is less evident, even though it lies 2.81 eV lower in the energy than isomer 1. The formation could involve multiple collisions, which take place in the source, causing sequential H-atom additions to the opposing end of chain. Alternatively, hydrogens from one end of carbon skeleton to the other have to migrate. However, this barrier may not be crossed because of fast adiabatic cooling in the supersonic expansion. The latter is known to be efficient, sometimes freezing the reaction products before they anneal to the lowest energy conformation. An example is the detection of a C_7H_3 isomer lying 2.1 eV above the most stable form [13]. Isomer 3 (C_s) of C_6NH_2 is an intermediate form between the first two.

The absence of a clear K-structure (the rotational A constants for isomers 1 and 2 are $\approx 10\text{ cm}^{-1}$, for $3 \approx 25\text{ cm}^{-1}$) in the optical spectra restricts all measured vibronic transitions to be of A-type. As the presence of only this type of transitions seems unlikely, this leads to the consideration of structures with off-axis heavy atoms (i.e., non-hydrogen) to decrease the A-constant. If there would be just H-atoms off-axis, the K-structure would be clearly resolved (as has been observed in molecules such as H_2CCC [14]). Structures 4–8 comply with this requirement and possess an acetylenic triple bond. They also easily tolerate the addition of two carbon atoms. $(4n + 3)$ -membered rings become stabilized upon removing the excess electron from the π -orbital system, be it done by ionization, or forming a σ lone pair like in cyclopropenylidene, or delocalizing it on an adjacent unsaturated carbon chain. Different permutations of end-CH and N generate the structures 3–6. The microwave observations of the ring-chains C_nH_2 , $n = 5, 7, 9$ [15–17] and HC_nN , $n = 4, 6$ [18] further point to the existence of corresponding C_nNH_2 species.

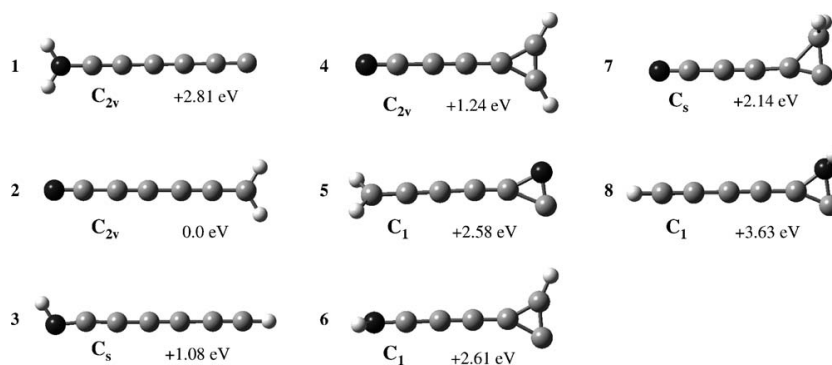


Fig. 2. Possible structural isomers of C_6NH_2 and the relative stabilities calculated at the DFT-B3LYP/6-31G(2df) level.

In isomers 7 and 8 the conjugated system will behave spectroscopically like in a linear chain. One would expect these C_6NH_2 molecules to exhibit an electronic spectrum analogous to linear C_6H , which was first measured in absorption in a neon matrix [19]. The C_6H radical absorbs in the same region as C_6NH_2 and exhibits similarities in its pattern of vibronic transitions. One can compare the acetylenic stretch vibrations 3_0^1 (1638 cm^{-1}) and 5_0^1 (2076 cm^{-1}) of C_6H with ν_{**} (1684 cm^{-1}) and $\nu_{(C=C)_0^1}$ (2076 cm^{-1}) of C_6NH_2 . The shift of the C_6NH_2 origin by $\sim 800\text{ cm}^{-1}$ to the blue of that of C_6H is probably mostly due to the $CH \rightarrow N$ substitution effects, which for linear chains are normally of the order of a thousand wavenumbers. Besides, the shift of the absorption origin upon adding two carbons C_6NH_2 to C_8NH_2 (2922 cm^{-1}) is similar to that (3016 cm^{-1}) from C_6H [20] to C_8H [21]. This shift is a normal behavior of conjugated carbon chains belonging to a homologous series.

The spectra of the “isoelectronic” series C_9H_3 , $C_{11}H_3$, $C_{13}H_3$ should be mentioned. These species were found to absorb all in the same part of the visible range [22], exhibiting remarkably similar vibrational structure and low ionization potentials ($< 6.4\text{ eV}$). However, C_6NH_2 and C_8NH_2 must possess a different structure to their isoelectronic C_mH_3 analogs since they have an ionization potential $> 7.9\text{ eV}$ and the origin band position shifts about 3000 cm^{-1} to the red upon adding two carbon atoms.

4. Concluding remarks

The electronic spectra of two nitrogen containing hydrocarbon radicals resulting from graphite ablation in the presence of NH_3/Ne are reported. The mass-spectra indicate C_6NH_2 and C_8NH_2 for their composition. While the absence of rotational structure precludes a definitive assignment of their geometry, the vibronic pattern in the electronic spectra is used as an indication of this. Candidate structures must possess a conjugated carbon chain skeleton to be consistent with the trend in the excitation energy within a homologous series. Both species have to have an off-axis carbon or nitrogen atom in a three-membered ring attached to a conjugated carbon chain and one or two hydrogens.

Although several isomers are likely to be present in the plasma, as has been shown by microwave studies of the related C_5H_2 species [15] where as many as four different conformations were identified, it seems that only one of structures is being picked out by the REMPI technique used. Apart from the existence of potential barriers between different structures and the rapid cooling capability of a supersonic jet expansion, there are specific limitations of the experimental method. Sensitivity on the ionization potential, ionization efficiency with given photon energy of an isomer, and fast intramolecular dynamics in the excited states may prevent the electronic spectra of other isomers

to be measured. The latter criterion rather than the relative abundance or lowest energy is likely the most important factor and is thought to be responsible for the non-detection of other isomers. The fact that these nitrogen containing molecules were detected implies a slow ($\sim 30\text{ ns}$ for C_6NH_2 and $\sim 5\text{ ns}$ for C_8NH_2) internal conversion from the measured excited state and hence a large energy gap above the ground state. This provides a further means to confirm their structure once good quality ab initio calculations of the excitation energies become available.

Acknowledgement

This work has been supported by the Swiss National Science Foundation (project 200020-100019).

References

- [1] M.B. Bell, P.A. Feldman, M.J. Travers, M.C. McCarthy, C.A. Gottlieb, P. Thaddeus, *Astrophys. J.* 483 (1997) 61.
- [2] V.D. Gordon, M.C. McCarthy, A.J. Apponi, P. Thaddeus, *Astrophys. J.* 540 (2000) 286.
- [3] O. Vaizert, T. Motylewski, M. Wyss, E. Riaplov, H. Linnartz, J.P. Maier, *J. Chem. Phys.* 114 (2001) 7918.
- [4] M.C. McCarthy, J.-U. Grabow, M.J. Travers, W. Chen, C.A. Gottlieb, P. Thaddeus, *Astrophys. J.* 494 (1998) 231.
- [5] H. Linnartz, O. Vaizert, P. Cias, L. Gruter, J.P. Maier, *Chem. Phys. Lett.* 345 (2001) 89.
- [6] H. Ding, A.E. Boguslavskiy, T.W. Schmidt, J.P. Maier, *Chem. Phys. Lett.* 392 (2004) 225.
- [7] M.C. McCarthy, E.S. Levine, A.J. Apponi, P. Thaddeus, *J. Mol. Spectrosc.* 203 (2000) 75.
- [8] Q.L. Zhang, S.C. O'Brien, J.R. Heath, Y. Liu, R.F. Curl, H.W. Kroto, R.E. Smalley, *J. Phys. Chem.* 90 (1986) 525.
- [9] J.R. Heath, Q. Zhang, S. O'Brien, R.F. Curl, H.W. Kroto, R.E. Smalley, *J. Am. Chem. Soc.* 109 (1987) 359.
- [10] Y. Kato, T. Wakabayashi, T. Momose, *Chem. Phys. Lett.* 386 (2004) 279.
- [11] A.E. Boguslavskiy, H. Ding, J.P. Maier, *J. Chem. Phys.* 123 (2005) 034305.
- [12] S.J. Blanksby, G.B. Ellison, *Acc. Chem. Res.* 36 (2003) 255.
- [13] H. Ding, T. Pino, F. Guethe, J.P. Maier, *J. Am. Chem. Soc.* 125 (2003) 14626.
- [14] A. Chirokolava, P. Birza, M. Araki, P. Kolek, J.P. Maier, *J. Mol. Spectrosc.* 229 (2005) 276.
- [15] C.A. Gottlieb, M.C. McCarthy, V.D. Gordon, J.M. Chakan, A.J. Apponi, P. Thaddeus, *Astrophys. J.* 509 (1998) 141.
- [16] M.C. McCarthy, M.J. Travers, C.A. Gottlieb, P. Thaddeus, *Astrophys. J.* 483 (1997) L139.
- [17] M.C. McCarthy, M.J. Travers, W. Chen, C.A. Gottlieb, P. Thaddeus, *Astrophys. J.* 498 (1998) 89.
- [18] M.C. McCarthy, J.U. Grabow, M.J. Travers, W. Chen, C.A. Gottlieb, P. Thaddeus, *Astrophys. J.* 513 (1999) 305.
- [19] P. Freivogel, J. Fulara, M. Jakobi, D. Forney, J.P. Maier, *J. Chem. Phys.* 103 (1995) 54.
- [20] M. Kotterer, J.P. Maier, *Chem. Phys. Lett.* 266 (1997) 342.
- [21] H. Linnartz, T. Motylewski, J.P. Maier, *J. Chem. Phys.* 109 (1998) 3819.
- [22] T.W. Schmidt, A.E. Boguslavskiy, T. Pino, H. Ding, J.P. Maier, *Int. J. Mass. Spectrom.* 228 (2003) 647.

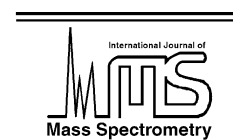
Chapter 8

**Optical detection of C_9H_3 , $C_{11}H_3$,
and $C_{13}H_3$ from a hydrocarbon
discharge source**

Available online at www.sciencedirect.com

SCIENCE @ DIRECT®

International Journal of Mass Spectrometry 228 (2003) 647–654

www.elsevier.com/locate/ijms

Optical detection of C_9H_3 , $C_{11}H_3$, and $C_{13}H_3$ from a hydrocarbon discharge source

T.W. Schmidt*, A.E. Boguslavskiy, T. Pino, H. Ding, J.P. Maier

Department of Chemistry, University of Basel, Klingelbergstrasse 80, CH-4056 Basel, Switzerland

Received 5 December 2002; accepted 20 March 2003

Abstract

Resonant two-color two-photon ionization spectra of C_9H_3 , $C_{11}H_3$, and $C_{13}H_3$ have been observed in the gas phase and are found to exhibit remarkably similar vibrational structure. All have origins in the $18,800\text{--}19,300\text{ cm}^{-1}$ region and a characteristic $\approx 40\text{ cm}^{-1}$ progression. Several pieces of spectroscopic information suggest a common moiety incorporating a strong, localized electronic transition, consistent with a low ionization potential as compared to other hydrocarbon radicals. Several possible structural motifs are discussed in relation to plasma, combustion and interstellar chemistry. © 2003 Elsevier Science B.V. All rights reserved.

Keywords: Electronic spectroscopy; Discharge plasma; Interstellar chemistry

1. Introduction

One of the unsolved problems facing physics, chemistry and astronomy is the identity of the carriers of the diffuse interstellar bands (DIBs), a series of diffuse absorption lines in the visible region observed in light having passed through the interstellar medium [1]. Candidate carriers of these features include bare carbon and hydrocarbon chains of a size and structure consistent with absorption of visible radiation [2,3]. Work over the past years, comparing the optical spectra of bare carbon chains with the DIBs, has shown that small bare carbon chains (C_n , $n \leq 10$) are not the carriers of the DIBs [4,5]. Larger species and their hydrogenated counterparts are yet to be tested thor-

oughly, though such species are incorporated into current models of interstellar chemistry [6,7]. Molecules of the generic formula C_nH_m ($m \leq n$) are abundant in flames and plasmas involving hydrocarbon precursors.

Of the molecules with formula C_nH , only one type of isomer has been observed in the laboratory: that with the hydrogen atom terminating one end of the carbon chain. Of these, $n = 1\text{--}8$ have been confirmed to exist in space [7,8]. The optical and microwave spectra are known for a variety of these species [9–11].

The C_nH_2 series exhibits a range of isomers which have been identified by a number of experimental techniques. The even polyynes, $HC_{2n}H$, have been observed in rare gas matrices by direct absorption spectroscopy, and in the gas phase by $1 + 1'$ resonance enhanced multi-photon ionization spectroscopy (REMPI) up to $HC_{26}H$ [12–14]. The band origin wavelengths show a dependence on chain length which is non-linear yet monotonically increasing.

* Corresponding author. Tel.: +41-61-267-3814;

fax: +41-61-267-3855.

E-mail address: timothy.schmidt@unibas.ch (T.W. Schmidt).

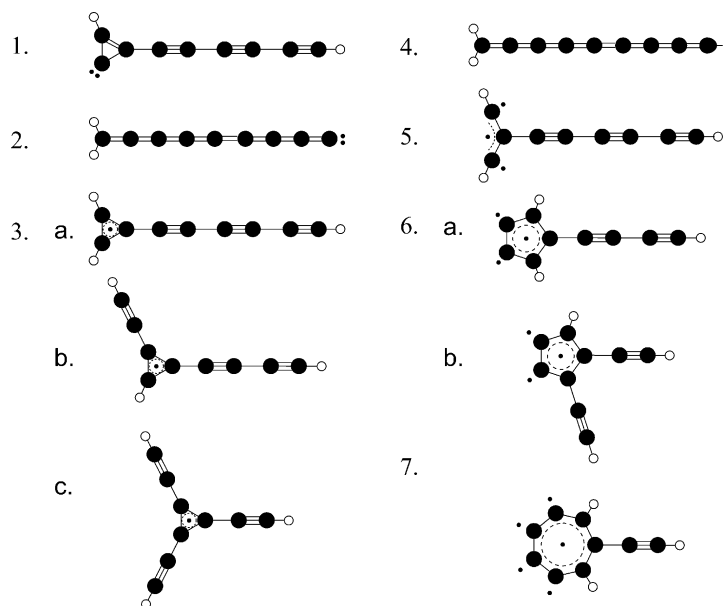


Fig. 1. Several structural isomers of C_9H_2 , 1 and 2, and C_9H_3 , 3–7. The odd-membered rings are stabilized upon ionization.

This behaviour is interpreted in terms of the persistent bond length alternation of the chromophore. The odd polyene radical chains, $HC_{2n+1}H$ ($n = 3-6$), have also been detected in matrices by direct absorption and in the gas phase by cavity ringdown spectroscopy [15] and REMPI [16]. Over the small range of chain lengths studied, these molecules exhibit a linear dependence of band origin (wavelength) with respect to their size. The dependence of the positions of the origin bands of the linear chain isomers of HC_nH on chain length can be rationalized in terms of a Hückel theory in which bond length alternation is taken into account [17].

Apart from these symmetrical isomers, a number of carbenes have been observed by microwave spectroscopy, owing to their permanent dipole moment. The observed carbene isomers of C_nH_2 fall into two main categories: those with both hydrogen atoms at the same end of a linear chain (e.g., isomer 2 in Fig. 1), and those which exhibit a three-membered ring (isomer 1) [18]. The three-membered ring species has been shown by ab initio calculations to be the more stable of the two for an odd number of carbon atoms [19].

Isomer 1 has been observed for $n = 5, 7, 9$ [20–22] and isomer 2 for $n = 5-9$, C_4H_2 and C_6H_2 having been observed in the interstellar medium [7,23]. Also detected by microwave spectroscopy are C_5H_2 where both hydrogens reside on the three-membered ring, and where the hydrogens are in the 1 and 3 positions of a linear carbon chain. The 1,3-hydrogenated isomer has also been observed for C_6H_2 [23,24].

The wide variety of C_nH_2 isomers measured by microwave spectroscopy leads one to assume that even more isomers may be observed for the corresponding C_nH_3 series, as illustrated by Mebel et al. [25]. The C_7H_3 radical had been recently observed in our laboratory by $1 + 1'$ REMPI [26]. Calculations at the DFT level employing a B3-LYP functional indicate that the ring-chain isomer (analogous to isomer 3a in Fig. 1) lies second lowest in energy (to isomer 4). Analysis of the rotational structure revealed the identity of the carrier as a ring-chain isomer.

The C_nH_3 species are a major product of hydrocarbon discharge sources and are found to be most abundant for $n \geq 7$ and up to $n = 29$. Similar distributions are observed for the cations and anions. Laser

pyrolysis of acetylene [27] and studies of fuel rich hydrocarbon flames [28] give similar results. While these species are clearly important in combustion processes, so far little is known about their structure and formation. In this article, we present the REMPI spectra of C_9H_3 , $C_{11}H_3$, and $C_{13}H_3$. Electronic and vibrational information is considered and their implications discussed.

2. Experimental

Spectra were obtained utilizing an apparatus which consisted of a molecular beam combined with a linear time-of-flight (TOF) mass analyzer (resolution of 900 at mass 200). The source was a pulsed valve coupled to an electric discharge. This discharge source was the same as that used for detection of the $HC_{2n}H$ species ($n = 8–13$) [12]. A pulse of a gas mixture of 0.5% butadiyne ($HCCCCH$) in Ar (backing pressure of 5 bar) was expanded through the ceramic body

of the source which held two steel electrodes with a ≈ 1 mm hole separated by a ceramic spacer of 4 mm. A high voltage pulse (600–1200 V) was applied between the electrodes. Ions were removed after the skimmer, and before entering the pulsed extraction zone of the TOF mass spectrometer, by an electric field perpendicular to the molecular beam. The neutral beam was then ionized and ions extracted. The signal from the multichannel plate (MCP) detector was fed into a fast oscilloscope after preamplification. Data acquisition was carried out using Labview programs.

Resonant two-color two-photon ionization was used in the 650–450 nm range. Excitation photons were delivered by a commercial OPO system (bandwidth 0.05 cm^{-1}) pumped by the third harmonic of a Nd:YAG laser. The ionizing photons at 212 nm (5.85 eV) were produced by sum frequency generation of the second harmonic and fundamental of the 637 nm output of a dye laser pumped by the second harmonic of a Nd:YAG laser. The energy per pulse was ≈ 10 mJ for the first color and a few hundred

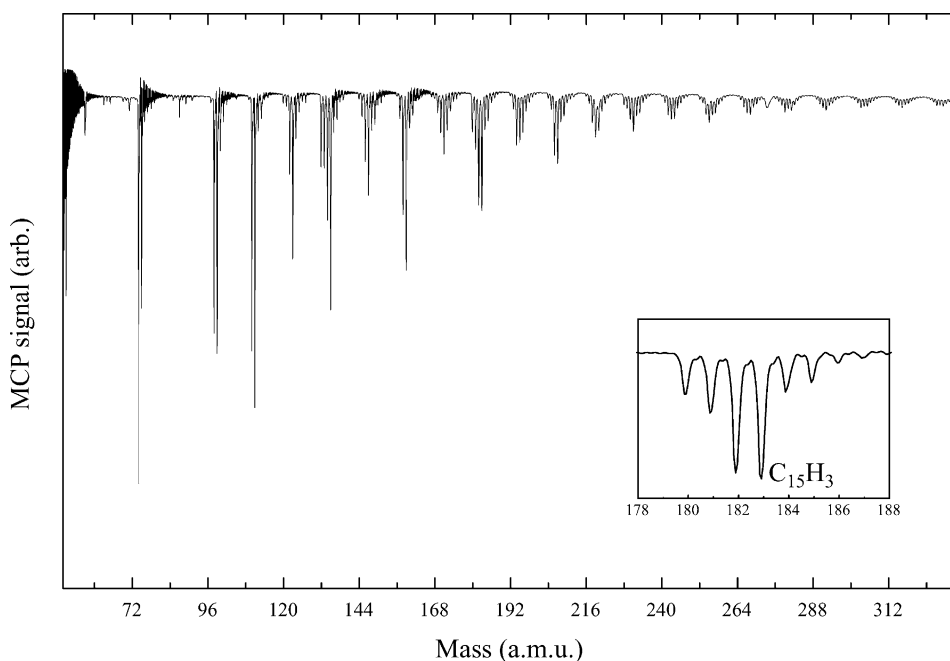


Fig. 2. A typical mass spectrum of the products of a butadiyne discharge irradiated by 157 nm light for $n \geq 4$. From $n = 7$ the most abundant species are the C_nH_3 radicals.

microjoules for the second. Both beams were anti-collinear to the molecular beam, being combined with a dichroic mirror, and aligned optimally in time and space. The mass spectrum obtained upon irradiation of the products of the plasma discharge source with 7.9 eV photons was used to optimize the experimental conditions. Such a mass spectrum is shown in Fig. 2.

3. Results and discussion

3.1. Overview of vibronic structure

Fig. 3 shows the electronic excitation spectra of C_9H_3 , $C_{11}H_3$, and $C_{13}H_3$ from 18,800 to 22,700 cm^{-1} . Immediately noticeable is the similarity between the three species. All have what appears to be their origin in the 18,800–19,300 cm^{-1} range, with no particular trend with system size. All possess a short, harmonic, vibrational progression of lines spaced by $\approx 40\text{ cm}^{-1}$. Additional features at 200, 600–700, and 2100 cm^{-1} to the blue of the origin band are common to all three species. The last of these can be assigned as the characteristic acetylenic stretch. Additional structures to

Table 1

Observed band systems of the C_nH_3 species

Species	T_0	$\nu_{C\equiv C}$	$\nu_{\approx 650\text{ cm}^{-1}}$	$\nu_{\approx 200\text{ cm}^{-1}}$	$\nu_{\approx 40\text{ cm}^{-1}}$
C_9H_3	18,881	+2113	+664	+190	+39
$C_{11}H_3$	19,313	+2039	+651	+186	+36
$C_{13}H_3$	19,246	+2147	+580	+189	+39

Vibrational frequencies are given relative to the origin band (T_0) in cm^{-1} ($\pm 1\text{ cm}^{-1}$ precision), as measured to the largest band in that system.

higher energy than the acetylenic stretch appear to be due to combinations of this stretch with the other lower frequency modes. The analogous band positions for the three species are listed in Table 1.

The spectrum of C_9H_3 is the clearest of the three. The vibrational structure near the origin is repeated throughout the spectrum. The acetylenic stretch is broadened with respect to the origin, yet maintains the 40 cm^{-1} progression. Inspection of the individual bands that make up this region reveals a splitting into at least two and as many as three bands, as illustrated in Fig. 4. This indicates the presence of a corresponding number of triple bonds in the molecular structure. The other features in the spectrum are left unassigned.

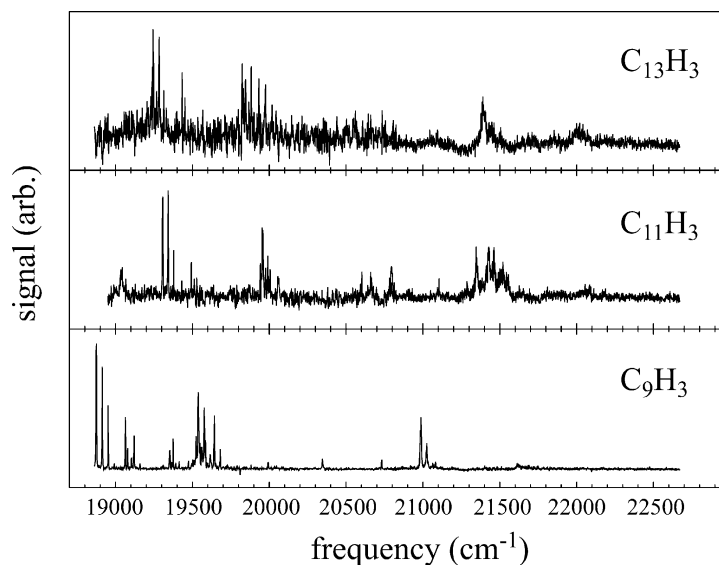


Fig. 3. The electronic spectra of the species C_9H_3 , $C_{11}H_3$, and $C_{13}H_3$. All have remarkably similar vibronic structure and exhibit the characteristic acetylenic stretch.

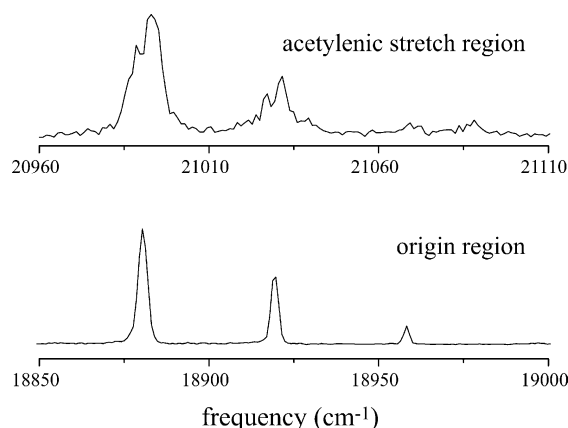


Fig. 4. The origin and acetylenic stretch regions of the electronic spectrum of C_9H_3 . The acetylenic stretch region possesses broader peaks, split into three sub-peaks. It is suggested that this splitting is due to weak interactions between three separated triple bonds.

The spectrum of $C_{11}H_3$ is similar to C_9H_3 , yet exhibits some differences. The vibrational frequency of the characteristic low frequency mode is reduced by 3 cm^{-1} upon the addition of two carbon atoms (Table 1). The section between the origin and the $\approx 650\text{ cm}^{-1}$ feature is not more complicated than C_9H_3 , yet the acetylenic stretching region shows a great deal more structure. The broad feature to the red of the origin is not thought to originate from the same electronic transition, if from the same isomer. The presence of this broad feature at $19,040\text{ cm}^{-1}$ may hint at the origin of the differences between the eleven-carbon species and the nine-carbon species. The complicated nature of the acetylenic stretching region indicates the presence of at least two but probably more triple bonds in this structure. In contrast to $C_{11}H_3$, $C_{13}H_3$ appears more similar to C_9H_3 .

3.2. Structural considerations

As of yet there is no clear rotational information with which to assign the structures of these species. Comparison with the C_7H_3 molecule recently detected in our laboratory shows that it has a different structure compared to those being discussed here [26]. C_7H_3 was found to exhibit a three-membered ring-chain

carbon skeleton with one hydrogen atom terminating the acetylenic chain, and the other two bound to the same carbon atom of the ring. This species exhibited clear K structure with an A constant of 0.88 cm^{-1} and thus it is expected that in the present case the A rotational constant should be no greater than this. A calculated and tentatively assigned splitting in the acetylenic stretch due to the interaction of two triple bonds on the same chain was found to be about 170 cm^{-1} [26].

It is the normal behaviour of conjugated carbon chains that they absorb at longer wavelengths upon increasing the length of the chain [10,12,15], be it a linear relationship or otherwise. The absence of clear K structure ($A \approx 10\text{ cm}^{-1}$), and the stability of the transition energy with system size rules out the H_2C_nH chain isomers (e.g., isomer 4) as carriers of the observed spectra. As shown above, C_9H_3 , $C_{11}H_3$, and $C_{13}H_3$ have a remarkably similar vibrational structure, and all absorb in the same part of the visible region. This behaviour is similar to that seen for other species, in which the chromophore is not a chain, but a localized electronic transition on a carbon ring [29]. It is clear from the vibrational structure that the C_9H_3 , $C_{11}H_3$, and $C_{13}H_3$ species possess at least one acetylenic bond. This leaves seven carbon atoms with which to build a structural motif common to all three species. Worthy of note is the spectrum of $C_{10}H_5$ [30], which absorbs in the same region as the other species mentioned, and possesses the characteristic low frequency progression. We suppose that where the C_nH_3 species terminate a polyynic chain with a hydrogen atom, $C_{10}H_5$ does likewise with a methyl group. For the purposes of attaining a stable transition energy with growing polyynic chain, the chromophore should possess a molecular orbital of a different symmetry to the chain. This may be affected through the construction of a three-, five- or seven-membered ring (see isomers 3, 6, and 7 in Fig. 1), or a branched chain structure in C_{2v} symmetry (isomer 5). There are many possibilities, yet candidate structures must be consistent with the other available experiment evidence. In the case of a three-membered ring-chain isomer such as 3a, the electronic transition should be

of the B or C type, to avoid strong dependence on system size, and thus exhibit *K* structure.

The characteristic low frequency mode is a special feature of this class of species. Such a low frequency which changes little from C₉H₃ to C₁₃H₃ may be indicative of a flat- or double-well potential, perhaps arising from a ring distortion mode. It should be noted that isomer 3c is expected to exhibit Jahn–Teller distortion. Others may experience similar effects, leading to interesting potential energy surfaces governing the ring geometry.

It may be tempting to assign the low frequency mode in to a bending progression of a long carbon chain constituent. Even without symmetry considerations, a mode must be found which exhibits a frequency as low as 40 cm⁻¹ in the excited state. From density functional calculations of the ground states of long linear HC_{2n+1}H chains (*n* = 4–9), such low frequency modes (π_u) have been calculated to exist [31]. Although these modes were not evidenced in their REMPI spectra [16], it is likely that the excited states have similar vibrational frequencies. Their behaviour as a function of chain length is systematic, decreasing from 52 cm⁻¹ for HC₉H to 10 cm⁻¹ for HC₁₉H. For the present species, no clear size-dependent behaviour is observed (see Table 1), and thus the mode responsible for the observed low frequency progression most likely involves the ring structure to some degree.

It may be seen in Fig. 4 that the acetylenic stretch region of C₉H₃ has a more complicated structure as compared to the origin region. While exhibiting the low frequency ($\approx 40^{-1}$) progression, each peak seems split into at least two and as many as three sub peaks (the third being of reduced intensity), with a splitting of ≈ 5 cm⁻¹. Such a small splitting indicates a weak coupling between several acetylenic stretching modes, as compared to C₇H₃, in which the splitting of the acetylenic stretches was found to be as much as 170 cm⁻¹. In isomer 3c, due to D_{3h} symmetry, the acetylene stretching modes should exhibit only two frequencies, two modes being degenerate. Isomers 3a and 3b are expected to exhibit three vibrational frequencies in this region.

Several isomers of C₁₁H₃ are consistent with the identity of C₉H₃ being one of isomers 3a, 3b, or 3c. Two of these are of C_{2v} symmetry and one is of C_s symmetry (assuming planar structures). The structures of C_{2v} symmetry would exhibit only two acetylenic stretching frequencies, the antisymmetric mode not being active. The complexity of the acetylenic stretching region of C₁₁H₃ suggests an asymmetric structure possessing several triple bonds. The slight simplification of this region on going to C₁₃H₃ suggests an increase in symmetry to C_{2v}.

The ionization potentials (IPs) of the observed species are seen to be particularly low as compared to the C_nH₂ species of similar size. Upon irradiation of the products of the butadiyne/Ar discharge with a 193 nm (6.4 eV) excimer laser, mass 111, corresponding to C₉H₃ is seen to be the most abundant ion. Masses 125 (C₁₀H₅), 135 (C₁₁H₃) and 159 (C₁₃H₃) are also prominent. The C_nH₃ peaks in the mass spectrum are also the most prominent upon irradiation with 157 nm (7.9 eV). At 127 nm (9.75 eV), the C_nH₂ species are the most prominent, a reflection of their ionization potentials and relative abundance as products of a butadiyne/Ar discharge. Such low IPs (≤ 6.4 eV) are typical of species in which the ion is stabilized through aromaticity, such as tropylium (C₇H₇⁺) [32,33]. The ionized three-, and seven-membered rings are all aromatic, and the neutrals should thus exhibit low IPs. As pointed out, the three-membered ring-chain isomers are particularly stable and thus their corresponding neutrals should have low IPs [22]. The three-membered ring-chain isomer of C₅H₃⁺ has been shown to be the most stable [34].

3.3. Chemical implications

The identity of the structure of the C_nH₃ radicals has implications for interstellar, combustion and plasma chemistry. They are a dominant product in acetylene, benzene, and diacetylene discharges, and also result in fuel rich flames [28] and from laser pyrolysis of acetylene [27]. While the C_nH₂ chemistry is dominated by those species with linear carbon skeletons, it is clear

from the results presented here that the case is very different for the C_nH_3 species.

It is postulated that the chemistry in plasmas and flames is dominated by cations and thus neutrals formed in abundance are those whose corresponding cation is particularly stable. It has been shown that the largest peak in the mass spectrum of the species resulting from a benzene discharge is the tropy radical [35]. The tropylium cation ($C_7H_7^+$) is aromatic and thus extremely stable. The expected stability of the three-membered ring-chain cations (isomers 3) suggests their production in our discharge source. The observation of the ring-chains C_nH_2 , $n = 5, 7$ and 9 [20–22] further points to the existence of the corresponding trihydrogenated species. Indeed McCarthy et al. suggest the formation of C_9H_2 from $C_9H_3^+$. Despite the expected aromatic stability of the cations of the five- and seven-membered rings, they are expected to be more reactive than the three-membered ring-chains due to their unpaired, localized electrons. It thus seems that addition of a third hydrogen to a growing carbon chain radical facilitates the formation of the first ring-bearing species in a hydrocarbon plasma. These species are therefore of paramount importance in the formation of polycyclic aromatic hydrocarbons and subsequent soot formation.

4. Concluding remarks

The electronic species of three new hydrocarbon radicals resulting from a butadiyne/Ar discharge have been reported. From the recorded mass spectra, the formulae are given as C_9H_3 , $C_{11}H_3$, and $C_{13}H_3$. While the absence of clear rotational information precluded definitive assignment of their geometrical structure, the vibronic structure give clues as to their identity. Candidate structures must possess a low frequency mode of approximately 40 cm^{-1} , and a strong localized electronic transition. All three species possess triple bonds. The C_9H_3 and $C_{13}H_3$ structures seem to have a closer relationship with each other than with $C_{11}H_3$. All species have a low IP and thus likely incorporate an odd-membered carbon ring in their structure.

Whereas most homologous hydrocarbon series exhibit definite trends in their excitation energy, the C_nH_3 series is different. Their prominence as products in the mass spectra of hydrocarbon discharges reinforces their importance in hydrocarbon chemistry. Their structures have implications as far ranging as astrophysics and combustion science. This completely new class of hydrocarbon radical has been observed in the gas phase for the first time by electronic spectroscopy. Spectroscopic evidence suggests that these molecules are the seeds of ring-bearing species produced in flames, plasmas and the interstellar medium.

Acknowledgements

This work has been supported by the Swiss National Science Foundation (project no. 20-63459.00).

References

- [1] G.H. Herbig, *Annu. Rev. Astron. Astrophys.* 33 (1995) 19.
- [2] A.E. Douglas, *Nature* 269 (1977) 130.
- [3] J. Fulara, D. Lessen, P. Freivogel, J.P. Maier, *Nature* 366 (1993) 439.
- [4] J.P. Maier, G.A.H. Walker, D.A. Bohlender, *Astrophys. J.* 566 (2002) 332.
- [5] J.P. Maier, *J. Phys. Chem. A* 102 (1998) 3462.
- [6] R.P.A. Bettens, E. Herbst, *Int. J. Mass. Spectrom.* 150 (1995) 321.
- [7] B.E. Turner, E. Herbst, R. Terzieva, *Astrophys. J. Suppl. S* 126 (2000) 427.
- [8] M. Guelin, J. Cernicharo, M.J. Travers, M.C. McCarthy, C.A. Gottlieb, P. Thaddeus, M. Ohishi, S. Saito, *Astron. Astrophys.* 317 (1997) L1.
- [9] M.C. McCarthy, W. Chen, A.J. Apponi, C.A. Gottlieb, P. Thaddeus, *Astrophys. J.* 520 (1999) 158.
- [10] H. Ding, T. Pino, F. Güthe, J.P. Maier, *J. Chem. Phys.* 117 (2002) 8362.
- [11] D.A. Kirkwood, H. Linnartz, M. Grutter, O. Dopfer, T. Motylewski, M. Pachkov, M. Tulej, M. Wyss, J.P. Maier, *Faraday Discuss.* 109 (1998) 109.
- [12] T. Pino, H. Ding, F. Güthe, J.P. Maier, *J. Chem. Phys.* 114 (2001) 2208.
- [13] E. Kloster-Jensen, H.-J. Haink, H. Christen, *Helv. Chim. Acta* 57 (1974) 1731.
- [14] M. Grutter, M. Wyss, J. Fulara, J.P. Maier, *J. Phys. Chem. A* 102 (1998) 9785.
- [15] C.D. Ball, M.C. McCarthy, P. Thaddeus, *J. Chem. Phys.* 112 (2000) 10151.

- [16] The $1 + 1'$ REMPI spectra of HC_7H , HC_9H , and HC_{11}H have been obtained in our laboratory utilizing either 157 nm or 212 nm as the ionizing wavelength.
- [17] L. Salem, *The Molecular Orbital Theory of Conjugated Systems*, W.A. Benjamin, New York, 1966.
- [18] A.J. Apponi, M.C. McCarthy, C.A. Gottlieb, P. Thaddeus, *Astrophys. J.* 530 (2000) 357.
- [19] K. Aoki, S. Ikuta, *J. Mol. Struct. (Theochem.)* 310 (1994) 229.
- [20] M.J. Travers, M.C. McCarthy, C.A. Gottlieb, P. Thaddeus, *Astrophys. J.* 483 (1997) L135.
- [21] M.C. McCarthy, M.J. Travers, C.A. Gottlieb, P. Thaddeus, *Astrophys. J.* 483 (1997) L139.
- [22] M.C. McCarthy, M.J. Travers, W. Chen, C.A. Gottlieb, P. Thaddeus, *Astrophys. J.* 498 (1998) L89.
- [23] P. Thaddeus, M.C. McCarthy, *Spectrochim. Acta A* 57 (2001) 757.
- [24] M.C. McCarthy, P. Thaddeus, *Astrophys. J.* 569 (2002) L55.
- [25] A.M. Mebel, S.H. Lin, X.M. Yang, Y.T. Lee, *J. Phys. Chem. A* 101 (1997) 6781.
- [26] H. Ding, T. Pino, F. Güthe, J.P. Maier, in preparation.
- [27] M. Schnaiter, T. Henning, H. Mutschke, B. Kohn, M. Ehbrecht, F. Huisken, *Astrophys. J.* 519 (1999) 687.
- [28] A.B. Fialkov, K.-H. Homann, *Combust. Flame* 127 (2001) 2076.
- [29] J.B. Hopkins, D.E. Powers, R.E. Smalley, *J. Chem. Phys.* 72 (1980) 5039.
- [30] This spectrum was recorded in our laboratory under the same conditions as the others reported in this paper and will be presented in a future publication.
- [31] H. Ding, T.W. Schmidt, T. Pino, A.E. Boguslavskiy, F. Güethe, J.P. Maier, *J. Chem. Phys.*, in press.
- [32] T. Pino, F. Güthe, H. Ding, J.P. Maier, *J. Phys. Chem. A* 106 (2002) 10022.
- [33] T. Koenig, J. Chang, *J. Am. Chem. Soc.* 100 (1978) 2240.
- [34] B. Weiner, C.J. Williams, D. Heaney, M.C. Zerner, *J. Phys. Chem.* 94 (1990) 7001.
- [35] F. Güthe, H. Ding, T. Pino, J.P. Maier, *Chem. Phys.* 269 (2001) 347.

Chapter 9

Appendix

Sellmeier formula and refraction indices for Ar, Kr, and Xe in the 100–250 nm range.

The refractive indices of gases can be related to the dielectric polarizability α and to the absorption oscillator strengths f_i for transitions of wavelength λ_i by means of dispersion relation

$$\frac{n^2 - 1}{n^2 + 2} = \frac{\widetilde{N}\alpha}{3\epsilon_0} = \frac{\widetilde{N}e^2}{12\pi^2\epsilon_0 mc^2} \sum_i \frac{f_i}{\lambda_i^{-2} - \lambda^{-2}} \quad (9.1)$$

where \widetilde{N} is the number density of atom or molecules, e and m are the charge and mass of electron respectively, and ϵ_0 is the vacuum permittivity. For rare gases where the refractive index is close to 1, the simplified Sellmeier expression could be used [1]

$$n - 1 \simeq \frac{\widetilde{N}e^2}{8\pi^2\epsilon_0 mc^2} \sum_i \frac{f_i}{\lambda_i^{-2} - \lambda^{-2}} \quad (9.2)$$

At the standard conditions (0°C, 760 torr):

$$\widetilde{N} = \frac{P}{kT} = \left/ \begin{array}{l} P = 760 \text{ torr} = 101.325 \text{ kPa} \\ T = 0^\circ\text{C} = 273.15 \text{ K} \\ k = 1.38 \cdot 10^{-23} \text{ JK}^{-1} \end{array} \right/ = 2.7 \cdot 10^{25} \text{ m}^{-3} \quad (9.3)$$

$$\frac{\widetilde{N}e^2}{12\pi^2\epsilon_0 mc^2} = \left/ \begin{array}{l} \epsilon_0 = 8.85 \cdot 10^{-12} \text{ J}^{-1}\text{C}^2\text{mol}^{-1} \\ e = 1.602 \cdot 10^{-19} \text{ C} \\ m = 9.11 \cdot 10^{-31} \text{ kg} \end{array} \right/ = 1.21 \cdot 10^{-2} (\mu\text{m})^{-2}$$

the formula 9.2 can be written as (here λ_i is in μm)

$$n - 1 = 1.21 \cdot 10^{-2} \sum_i \frac{f_i}{\lambda_i^{-2} - \lambda^{-2}} \quad (9.4)$$

Using the data on absorption wavelength λ_i and the corresponding oscillator strengths f_i from Table 9.1, the following curves for the refractive indices of neon, argon, krypton, and xenon could be plotted for $\lambda > 100$ nm. As can be seen from equations 9.2 and 9.3, the $(n - 1)$ can be manipulated by pressure P or temperature T of a gas. Moreover, certain given values of refractivity and dispersion of a gas medium can be achieved (although not at every wavelength) by mixing two or more different gases.

A short glance at these curves is enough to realize why tunable tripling is virtually impossible. Phase matching condition ($n_{3\omega} = n_\omega$) dictates certain value of the refractive index $n_{3\omega}$. The latter, however, is very sensitive to the wavelength, and even in those regions where the tripling is possible, scanning λ would require continuous variation of P and/or T of the gas in the cell in order to fulfill the phase matching conditions.

Ne		Ar		Kr		Xe	
λ [$\times 10^{-3} \mu m$]	f	λ [$\times 10^{-3} \mu m$]	f	λ	f	λ	f
074.37	0.149	106.66	0.0609	123.58	0.214	146.96	0.273
073.59	0.0118	104.82	0.25	116.49	0.193	129.56	0.186
...		089.43	(0.01)	103.00	(0.1)	125.02	0.0098
		100.36	(0.1)	119.20	0.4
				100.11	(0.1)	117.04	0.099
				96.333	(0.05)	112.93	0.0025
				...		111.07	0.083
						109.97	0.0236
						108.54	0.0217
						107.86	
						107.04	
						106.82	0.205
						106.13	0.0096
						105.61	0.123
						105.50	
						105.11	0.0042
						...	

Table 9.1: Atomic lines data (absorption wavelengths λ_i and corresponding oscillator strengths f_i) for neon, argon, krypton, and xenon inert gases. Data compiled from NIST database [2]. Only lines with $\lambda > 100$ nm are presented here.

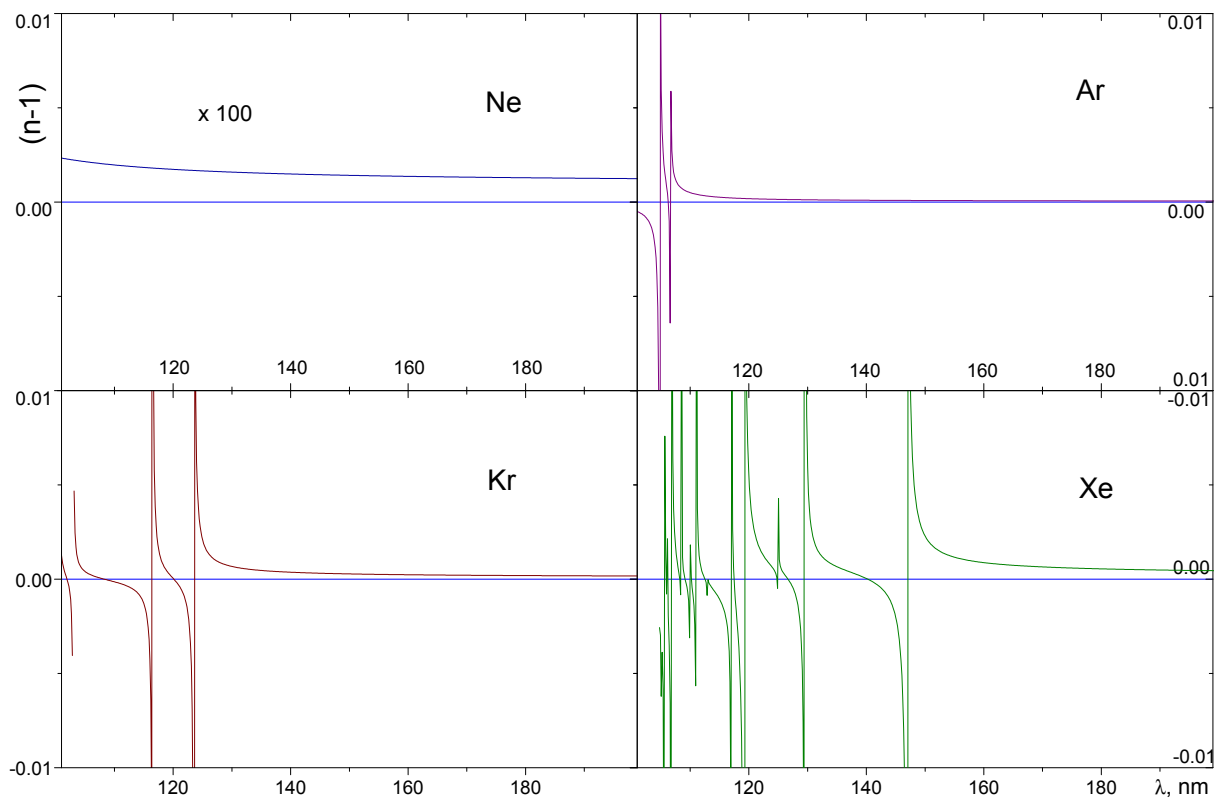


Figure 9.1: Neon, argon, krypton, and xenon refractivities at normal conditions in the 100–200 nm range calculated using formula 9.2 and atomic lines data from Table 9.1.

Bibliography

- [1] A. Bideau-Mehu, Y. Guern, R. Abjean, and A. Johannin-Gilles. Measurement of refractive-indexes of neon, argon, krypton and xenon in the 253.7-140.4 nm wavelength range. Dispersion-relations and estimated oscillator-strengths of the resonance lines. *J. Quant. Spectrosc. Radiat. Transfer*, 25(5):395–402, 1981.
- [2] NIST. Atomic Spectra Database. http://physics.nist.gov/cgi-bin/AtData/main_asd.

Other publications contributed during PhD study

Electronic spectra of carbon chains, rings, and ions of astrophysical interest

A. Boguslavskiy, A. Dhzonson, and J.P. Maier¹

*Department of Chemistry, University of Basel,
Klingelbergstrasse 80, CH-4056 Basel, Switzerland.*

Abstract. On the basis of a comparison of the electronic spectra of a number of carbon chains measured in the laboratory with diffuse interstellar band (DIB) absorptions, it is concluded that carbon chains and related systems comprising up to a handful of carbon atoms can not be the carriers, as originally suggested by Douglas. However, the detection of the weak absorptions in diffuse clouds due to C_3 enables arguments to be brought forward why certain larger carbon chains remain viable candidates. Specifically the odd-numbered carbon chains, C_{17} , C_{19} , ... have special spectroscopic properties: their lowest electronic transitions lie in the 400–900 nm DIB range, as is known from observation in neon matrices, and manifest very large oscillator strengths. An attempt to measure these in the gas phase was unsuccessful, but the electronic spectrum of a bare C_{18} ring could be observed. Particularly striking is the similarity of its origin band profile at temperatures in the 20–100 K range with some DIB measurements at high resolution, though at other wavelengths. The peak structure of the DIBs and the laboratory band is almost superimposable, suggesting that other plate-like species, with electronic transitions in the visible with high oscillator strengths, could be some of the DIB carriers.

In order to measure the electronic spectra of larger cations under conditions relevant to diffuse interstellar clouds, an ion trap instrument has been set-up. In this ions are held in a 22-pole trap, where the vibrational and rotational degrees of freedom are equilibrated to temperatures down to 20 K by collisions with cryogenically cooled helium. The analysis of the vibrational pattern and of the rotational K-structure in the electronic spectrum of 2,4-hexadiyne cation, detected by a one photon predissociation process, shows that the relaxation to such low temperatures has taken place. Measurement of the electronic spectrum of 1,4-dichlorobenzene cation illustrates a scheme to detect the electronic spectra for bound excited states using two photon absorption.

Keywords: carbon-chains, carbon-rings, cations, electronic spectra, diffuse interstellar bands

PACS: 98.38.Dq, 33.20.-t, 42.62.Fi

The article by A. Douglas published in 1977 proposing that carbon chains are good candidates as carriers of some diffuse interstellar band absorptions [1] has continued to be cited. His arguments were based on their likely spectroscopic and photophysical properties; i.e. leading to electronic transitions in the visible part of the spectrum and possible broadenings of the absorptions due to intramolecular processes. In order to test this hypothesis, gas phase electronic spectra of the systems he was alluding to, e.g. the bare carbon chains C_n $n=5, 7 \dots 15$ were required. Thus as part of our research activity dealing with the development and application of the methods to study the electronic spectra of radicals and ions we set ourselves the goal of measuring these spectra in the gas phase.

As a first step the electronic absorption spectra were obtained in neon matrices at 6 K. This was achieved using a cesium sputter source to produce the carbon anions, C_n^- , then codeposit the mass-selected species with excess of neon to trap the anions in the matrix thus formed, and finally the neutral entities were generated by photodetachment of the electrons. By this means the electronic spectra of the carbon chain anions, C_n^- $n=3-13$, neutrals C_n $n=4-21$ [2], and most recently of cations, C_n^+ $n=6-9$ [3], could be observed and identified. With this information in hand gas phase spectra of those species possessing electronic transitions in the DIB range [4], 400–900 nm, were aimed for. These were obtained for a number of carbon cation, neutral and anion chains using supersonic free jets through which a discharge runs. With acetylene seeded in a rare gas numerous such carbon chains can be produced as diagnosed by mass-spectrometry. The electronic transitions were then observed in absorption with pulsed and cw cavity ringdown methods for the cations and neutrals and photodetachment processes for the anions. This in turn allowed for the first time a direct comparison of laboratory spectra with astronomical measurements [5].

All the comparisons proved negative, including those for the bare carbon chains C_4 , C_5 , [6] and for species which are known to be present in the diffuse medium, e.g., C_3H [7]. However the upper limits to the column densities derived,

¹ Corresponding author: e-mail: J.P.Maier@unibas.ch, Tel.: +41 61 267 3826, Fax: +41 61 267 3855

	EW (Å)	f	N (cm ⁻²)
C ₃	~10 ⁻⁴	~10 ⁻²	10 ¹⁰
C _{n~21}	~10 ⁻¹	~10	10 ¹¹

FIGURE 1. Estimation of the column density of a longer carbon chain based on the expected oscillator strength of its ${}^1\Sigma_u^+ \leftarrow X {}^1\Sigma_g^+$ transition and the observations made for a rotational line in the ${}^1\Pi_u \leftarrow X {}^1\Sigma_g^+$ system of C₃ in diffuse clouds (ref. [10]).

typically $<10^{12}$ cm⁻², are consistent with the values obtained for the species detected by rotational spectroscopy [8]. Thus even though species with column densities around the latter values can be detected in the *mm*-range, the relatively modest values of the oscillator strengths of the electronic transitions, e.g. around 0.004 for C₃H with origin band near 521 nm [7], would lead to a DIB with an equivalent width (EW) of less than 1 mÅ, a hardly detectable DIB. Several such comparisons, lead to the conclusion that Douglas's hypothesis that carbon chains C_n with n lying in the range 5–15 are good DIB candidates can be excluded [9]. More generally, this statement applies not only to the bare carbon chains but to also to their derivatives such as those containing a hydrogen, C_nH, comprising up to around a dozen of atoms.

The consequences of this are illustrated with reference to the study which detected C₃ in diffuse clouds [10] and summarized in Fig. 1. The rotational lines identified corresponded to interstellar absorption lines with EW of 0.1 mÅ and summing over all the rotational lines gave a total column density of around 10¹² cm⁻²; (the N value given in Fig. 1 is for an individual rotational level of C₃). The electronic transition detected, the origin band of the ${}^1\Pi_u \leftarrow X {}^1\Sigma_g^+$ Comet band system, has an oscillator strength of ~ 0.02 . Thus to observe one of the stronger, narrower DIBs, with EW of 0.1 Å and FWHM around 1 Å, either the column density of the species has to be two orders of magnitude larger than for C₃ or the oscillator strength, f , has to be correspondingly larger. The latter is the situation with the C_{2n+1} chains for their ${}^1\Sigma_u^+ \leftarrow X {}^1\Sigma_g^+$ transition. This is found around 170 nm for C₃ with a f value of around unity [11]. The wavelength of the transition shifts by regular increments with the length of the chain as can be seen in Fig. 2 and f scales quasilinearly with n . Thus these odd-numbered chains C₁₇, C₁₉... to, say, C₃₁ have these electronic transitions in the 400-900 nm DIB region with f values in the 1–10 range. Their spectra have been observed in absorption in 6 K neon matrices for up to C₂₁ [12]. In Fig. 1 C₂₁ is taken as the example: to obtain a DIB with EW of 0.1 Å would require a column density of 10¹¹ cm⁻², not an excessive amount. As consequence the current goal is obtain the spectra of the chains of this size, as yet unsuccessfully.

The approach we have used for this purpose is resonance enhanced two photon ionization (RE2PI) combined with a laser vaporization source as illustrated by Fig. 3. A tunable laser (λ_1) scans the region where the electronic transitions are expected in view of the spectra observed in neon matrices, and subsequently ionization is induced with a F₂ 157 nm laser (λ_2). As the mass-spectrum in Fig. 4 shows, the sought after C₁₇, C₁₉... species are formed. However the RE2PI approach using nanosecond lasers failed to detect the transitions suggesting that the lifetimes of the excited electronic states are in the picosecond range. On the other hand the electronic spectra of C₁₈ and C₂₂ could be observed [13].

As this is the first gas phase detection of a large bare carbon chain, both an analysis of the spectrum and a comparison with DIB data were carried out. The electronic absorption spectrum of C₁₈ is seen in Fig. 5. It comprises several

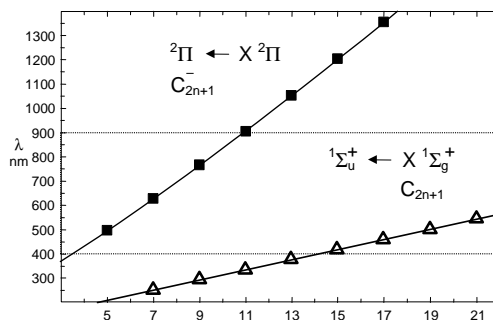


FIGURE 2. Wavelength dependence of the electronic transition (origin band) on the number of carbon atoms for two series of carbon chains. The 400–900 nm DIB range is indicated.

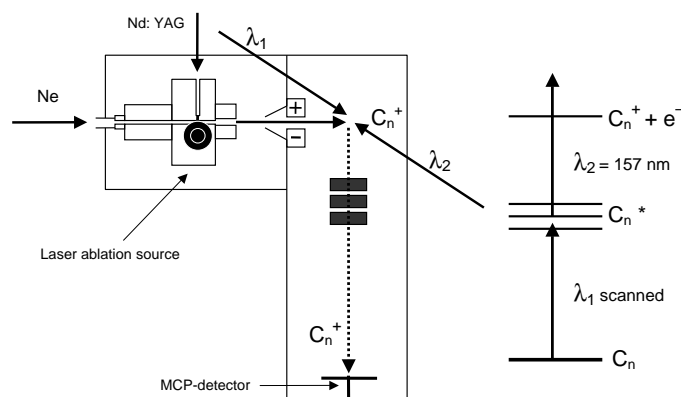


FIGURE 3. Technique used to measure the electronic spectra of the C_{18} ring in the gas phase involving a two colour excitation-ionization scheme.

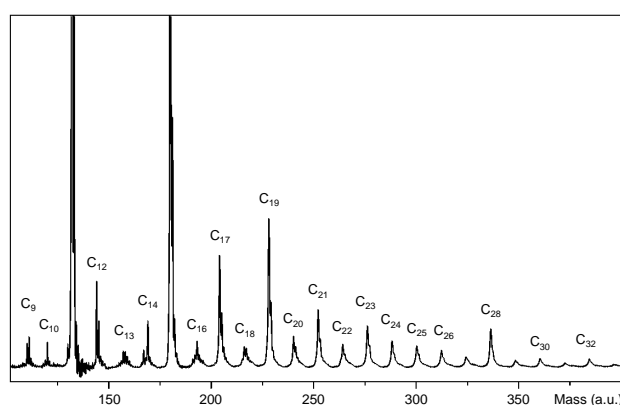


FIGURE 4. Typical mass-spectrum obtained from the laser vaporization source, using an 157 nm laser for the two photon ionization.

electronic transitions; the first one with origin band near 593 nm shows relatively narrow bands, few cm^{-1} broad but going up in the energy manifold the peaks progressively broaden. This is caused by lifetime shortening of the excited electronic states as result of intramolecular processes. Thus as far as a comparison with DIBs is concerned it is only interesting for the origin band at 593 nm. This has been done in a recent collaborative study with astronomers, leading once again merely to upper limit $2 \times 10^{11} \text{cm}^{-2}$ in the column density [14]. The results are consistent with the conclusions drawn on the basis of the data comparison with the small linear carbon chains, C_n $n=3-5$, that the transition should have a large oscillator strength, which is in the case of C_{18} not the case ($f \approx 0.02$). The structure

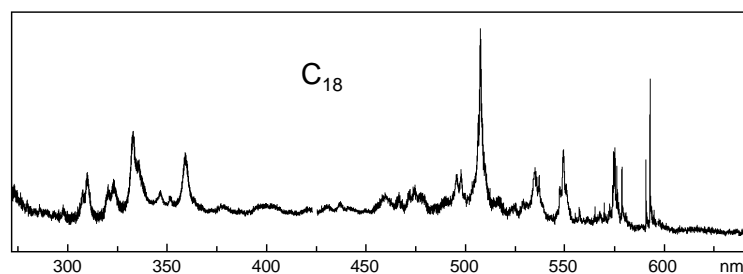


FIGURE 5. Electronic absorption spectrum of cyclic C_{18} measured in the gas phase using the two photon scheme shown in Fig. 3. It comprises several electronic transitions and the bands broaden with increase in internal excitation energy.

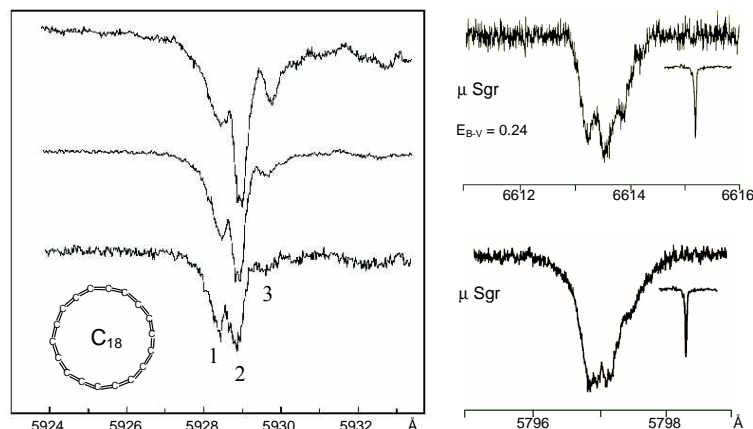


FIGURE 6. The origin band of the first electronic transition of cyclic C_{18} measured in the laboratory (left plot). The temperature ranges from around 100 K in the top trace to 20 K at bottom. The right plots show the profiles of two diffuse interstellar absorption features measured at high resolution, reproduced from ref. [15].

of the observed C_{18} species is shown in Fig. 6: it is the cyclic form which has been detected. This conclusion could be drawn on the basis of experimental observations: one can distinguish linear and cyclic forms from the behavior of the absorptions on addition of hydrogen to the plasma discharge while simultaneously monitoring the produced linear $HC_{18}H$ species whose absorption spectrum is known, knowledge where the linear isomer absorbs and the comparison with the calculated excitation energies for the cyclic isomer [13]. Though the finer details whether the symmetry is D_{9h} or C_{9h} can not be resolved, that a cyclic isomer is observed is certain.

In Fig. 6 is seen the origin band of the C_{18} ring at 593 nm recorded in the laboratory at three different temperatures, achieved by using different expansion conditions. It drops roughly from 100 K (top trace) to 20 K (bottom). The three peaks are interpreted as follows. Bands 1 and 3 are sequence transitions from vibrationally excited levels in the ground state of the ring. Peak 1 which persists even at 20 K probably arises from the residual population of the lowest frequency vibration ($\approx 56 \text{ cm}^{-1}$) whereas that associated with peak three is of higher frequency as it can be depopulated at low temperatures. Peak 2, the 0–0 origin band also changes intensity with respect to 3 because of the overlap. The residual width, $1\text{--}2 \text{ cm}^{-1}$, of peak 1 is due to the unresolved rotational profile. Simulation of the profile for such a C_{18} ring with the theoretically calculated ground state geometry, temperature of 20–80 K typical of the diffuse cloud environment, and for a parallel transition, leads to a slightly asymmetric profile with widths as observed.

Particularly striking is the comparison of the laboratory measurement for the C_{18} ring with the high resolution measurements of DIBs, though at other wavelengths. In Fig. 6 two such results have been selected; the triplet structure observed for the 661.4 nm and the doublet for the 579.7 nm DIB, measured towards μ Sgr with a resolving power of $300\,000$ [15]. It is seen that the triplet DIB structure when shifted to the same wavelength as the C_{18} band at ≈ 100 K is almost superimposable, as is the case with the bottom doublet trace for the laboratory recording at 20 K. Thus it is rather tempting to suggest that the two observed DIBs are indeed due to plate-like molecules with sizes something like C_{20} to C_{100} with the requirement that the electronic transition responsible has a considerable f value. The central peak would be the origin band and the accompanying bands could be the sequence transitions involving the lowest frequency modes which remain populated even down to 20 K.

Of interest with this suggestion is the relation to PAH studies and the arguments for their cations as possible DIB carriers [16]. It has been shown that the intermediate size rings, as discussed here, are likely to lose all their hydrogens in the UV radiation field, whereas the larger systems will rather end up in the protonated form [17]. Thus the similarity of the C_{18} origin band profile to the DIBs may suggest that one should look also for the laboratory spectra of the cyclic ring cations with large oscillator strengths. For such a purpose we have built up an ion trap instrument to measure such spectra of bare carbon cations which have been collisionally equilibrated to the 20–40 K temperatures pertinent to the diffuse interstellar clouds.

The set-up of the approach is indicated in Fig. 7: ions produced in an electron impact ion source are mass selected with a quadrupole filter and then fed during 10 ms into a 22-pole radio-frequency trap. The latter has been designed according to the principles given [18] and typically 1000 ions are trapped. During the next 70 ms the ions' rotational and vibrational degrees of freedom are equilibrated to low temperatures by collisions with cryogenically cooled helium

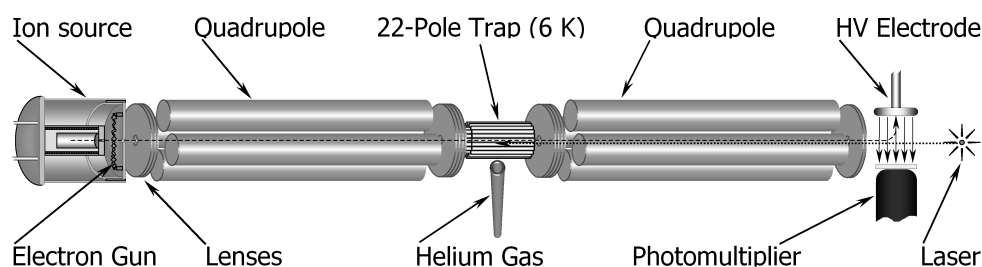


FIGURE 7. A schematic sketch of the instrument used to measure the electronic spectra of cations which have been collisionally equilibrated to 20–30 K in a 22-pole trap.

gas. Subsequently an electronic transition of the ion is induced by excitation with tunable, nanosecond lasers using one or two colour schemes to produce fragment ions. The trap is then opened and the fragment ions are mass selected by a further quadrupole and detected.

The first measurements with this instrument were to demonstrate that both the rotations and vibrations have been relaxed. Low rotational temperatures are more easily obtained in supersonic free jets, but the vibrational modes are not always cooled. However this is an important aspect for the study of larger ions, e.g. C_{60}^+ , so that the electronic spectra are measured under conditions comparable to the interstellar medium. The ion chosen to test this was 2,4-hexadiyne, a benzene isomer, which has been well studied by emission and other spectroscopies [19]. The situation for this ion is that the first excited electronic state A^2E_u , which lies 2.5 eV above the X^2E_g ground state, decays by competing mechanisms: radiative decay as well as by dissociation to produce fragment ions. So for example, on production of the $v=0$ level in the A^2E_u state 3/4 of the time a visible photon is emitted and the ion lands back in the X^2E_g ground state and in 1/4 of the events mainly the $C_6H_5^+$ fragment is produced, with smaller probabilities for the formation of $C_6H_4^+$ or $C_4H_4^+$ [20]. Thus the $A^2E_u - X^2E_g$ electronic spectrum can simply be measured by a one photon excitation process. This can be seen in Fig. 8 where the $C_4H_4^+$ fragments were monitored while the laser wavelength was scanned [21]. As can be seen the origin band at 20553 cm^{-1} stands isolated with no evidence of hot band transitions in the vicinity. This is to be contrasted with the spectrum recorded in supersonic free jets with rotational temperatures down to 20 K where however the sequence transitions near the origin band are still apparent [19]. As the lowest frequency mode is around 120 cm^{-1} the vibrational temperature of the ions collisionally cooled in the 22-pole trap is below 30 K. The rest of the spectrum shows the population of the vibrationally excited levels in the upper state. Their intensities depend on the laser power used and by this means the vibrational manifold can be lit up as even weak transitions, involving multi-quanta excitations of the degenerate modes, are then readily observed.

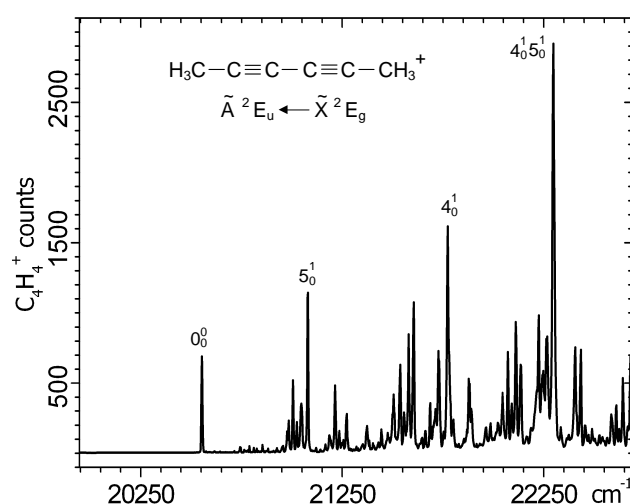


FIGURE 8. The $A^2E_u - X^2E_g$ electronic spectrum of 2,4-hexadiyne cation, relaxed to 20–30 K, in the region of the origin band measured in the gas phase by monitoring the $C_4H_4^+$ fragment ions produced.

The additional reason for choosing 2,4-hexadiyne cation as the test molecule is that its K-rotational structure can

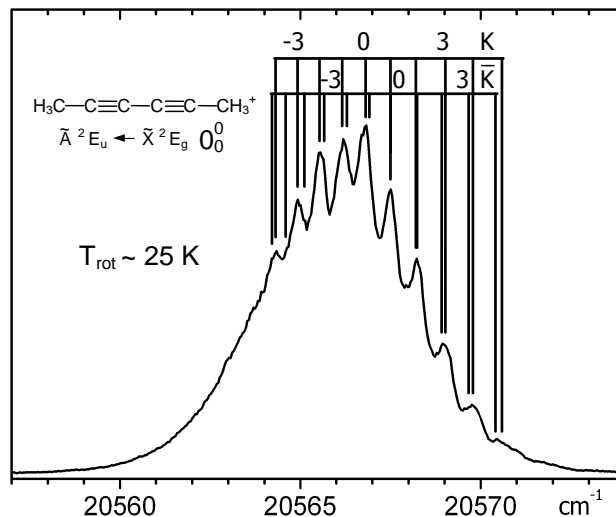


FIGURE 9. The origin band of the $A\ ^2E_u - X\ ^2E_g$ transition of 2,4-hexadiyne cation recorded with a laser bandwidth of 0.15 cm^{-1} . The peaks discernible are due to the rotational structure in the K-manifold and their intensity pattern fits a temperature in the 20–30 K range.

be observed with modest laser resolution. In larger cations, even if linear, special Doppler free methods would have to be used to resolve the P, Q, R lines. However the presence of the light hydrogens off the central carbon axis in the hexadiyne species leads to the formation of the K-structure, i.e. due to rotation about the internuclear axis. Thus when the origin band in the $A\ ^2E_u - X\ ^2E_g$ transition is recorded with a laser-band width of 0.15 cm^{-1} , the K-structure is seen (Fig. 9). The pattern has already been analyzed earlier in the emission spectrum of this cation and the labels given are taken from there [19]. The intensity pattern of the K-stacks is a measure of the temperature and simulations of this, or experimentally achieved by variation of the expansion conditions, lead to the conclusion that in the presently observed spectrum it corresponds to a rotational temperature around 20 K. This and the absence of the vibrational sequence band proves that the rotational and vibrational degrees of freedom have been relaxed to the low temperatures, as typical in diffuse interstellar clouds.

With this established the challenge is to find ways of measuring the electronic spectra of the astrophysically relevant ions whose excited electronic states are not subject to predissociation. This requires two photon, two colour schemes and the first such successful measurement is illustrated on 1,4-dichlorobenzene cation, another species whose electronic spectrum is known. Specifically, the $B\ ^2B_{3u} - X\ ^2B_{2g}$ transition has been studied in emission in an effusive jet [22]. The origin band lies at 19622 cm^{-1} , around 1 eV below the threshold for fragmentation. This is seen in Fig. 10 where the electronic states of relevance and the dissociation thresholds are indicated. To observe this electronic transition for

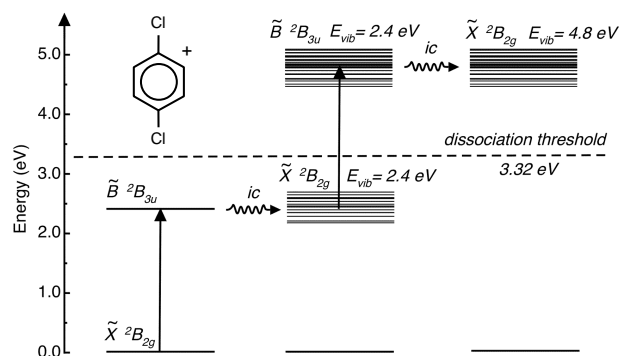


FIGURE 10. The excitation scheme for the detection of the $B\ ^2B_{3u} - X\ ^2B_{2g}$ electronic spectrum of 1,4-dichlorobenzene cation using resonant two-photon excitation involving internal conversion and subsequent dissociation.

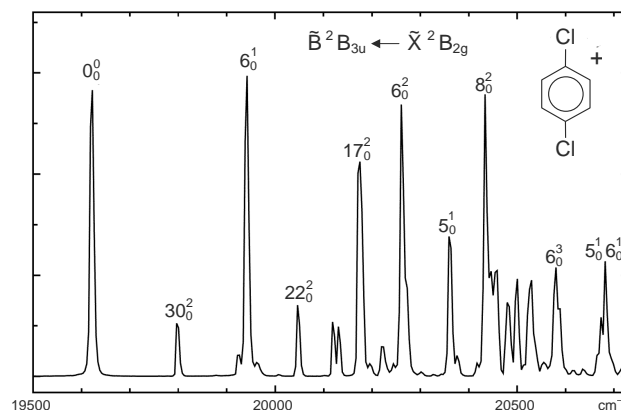


FIGURE 11. The $B^2B_{3u}-X^2B_{2g}$ electronic spectrum of 1,4-dichlorobenzene cation measured in the gas phase using the excitation and detection scheme shown in Fig. 10. The rotational and vibrational degrees of freedom were equilibrated to 20–30 K by collisions with cryogenically cooled helium.

the 1,4-dichlorobenzene cations which have been collisionally cooled to 20 K a two photon scheme was used [23]. This involved the same photon frequency as for the population of the excited electronic state. The diagram suggests the likely pathway. Resonant excitation of the $B^2B_{3u}-X^2B_{2g}$ transition is followed by internal conversion to the ground state vibrational manifold, which is in competition with the radiative decay evaluated to proceed at 10^{11} s^{-1} [22]. The vibrationally excited ions on the X^2B_{2g} surface then absorb a second photon of the same frequency as the first to populate highly excited levels in the upper B^2B_{3u} state which again internally convert to leave the ions with nearly 5 eV of internal energy. This is then sufficient for fragmentation to take place (loss of a chlorine atom) and the $C_6H_4Cl^+$ ion is detected. Ion-electron coincidence measurements of 1,4-dichlorobenzene cation indicate that this fragmentation rate is in the 10^4 to 10^5 s^{-1} range [24]. The resulting spectrum is seen in Fig. 11.

As in the case of 2,4-hexadiyne cation, there is no evidence of hot band transitions in the region of the origin band indicative of a successful collision relaxation to below 30 K. Furthermore the bands are much sharper than observed earlier in the emission spectrum [22] because of the low vibrational temperature. An analysis can be made leading to the frequencies of many of the modes in the excited B^2B_{3u} electronic state [23].

Thus having established that not only the rotational but also the vibrational degrees of freedom of larger organic cations can be efficiently cooled to low temperatures, 20–30 K, characteristic of the diffuse interstellar clouds, the measurement of unknown electronic spectra of astrophysically interesting ions can be undertaken. Among the spectra aimed for are of the bare carbon chains, rings and fullerenes as well as their derivatives including H, N, O. Some such experiments involving two photon excitation schemes, as illustrated for 1,4-dichlorobenzene cation, but instead using a second colour for the dissociation process have now proven to be successful for the species such as C_nH^+ .

ACKNOWLEDGMENTS

The research has been financed by the Swiss National Science Foundation (200020-100019) and is also part of the European Union “Molecular Universe” project (MRTN-CT-2004-512302). The 22-pole instrument was built with the help and guidance of Prof. Dieter Gerlich, Technical University of Chemnitz, Germany.

REFERENCES

1. A. E. Douglas, *Nature* **269**, 130 (1977).
2. J. P. Maier, *J. Phys. Chem. A* **102**, 3462 (1998).
3. J. Fulara, I. Shnitko, A. Batalov, and J. P. Maier, *J. Chem. Phys.* **125**, 44305 (2005).
4. G. H. Herbig, *Annu. Rev. Astrophys.* **33**, 19 (1995).
5. T. Motylewski, H. Linnartz, O. Vaizert, J. P. Maier, G. A. Galazutdinov, F. A. Musaev, J. Krelowski, G. A. H. Walker, and D. A. Bohlender, *Astrophys. J.* **531**, 312 (2000).

6. J. P. Maier, G. A. H. Walker, and D. A. Bohlender, *Astrophys. J.* **566**, 332 (2002).
7. H. Ding, T. Pino, F. Güthe, and J. P. Maier, *J. Chem. Phys.* **115**, 6913 (2001).
8. H. S. Liszt, and R. Lucas, *Astron. Astrophys.* **358**, 1069 (2000).
9. J. P. Maier, G. A. H. Walker, and D. A. Bohlender, *Astrophys. J.* **602**, 286 (2004).
10. J. P. Maier, N. M. Lakin, G. A. H. Walker, and D. A. Bohlender, *Astrophys. J.* **553**, 267 (2001).
11. G. Monninger, M. Förderer, P. Gürtler, S. Kalhofer, S. Petersen, L. Nemes, P. G. Szalay, and W. Krätschmer, *J. Phys. Chem. A.* **106**, 5779 (2002).
12. D. Forney, P. Freivogel, M. Grutter, and J. P. Maier, *J. Chem. Phys.* **104**, 4954 (1996).
13. A. E. Boguslavskiy, H. Ding, and J. P. Maier, *J. Chem. Phys.* **123**, 034305 (2005).
14. J. P. Maier, A. E. Boguslavskiy, H. Ding, G. A. H. Walker, and D. A. Bohlender, *Astrophys. J.* **in press** (2006).
15. P. J. Sarre, J. R. Miles, T. H. Kerr, R. E. Hibbins, S. J. Fossey, and W. B. Sommerville, *Mon. Not. R. Astron. Soc.* **277**, L41 (1995).
16. A. G. G. M. Tielens, and T. P. Snow, editors, *The Diffuse Interstellar Bands*, vol. 202 of *Astrophysics and space science library*, Dordrecht, Kluwer, 1995, ISBN 0-7923-3629-1.
17. V. Le Page, T. P. Snow, and V. M. Bierbaum, *Astrophys. J.* **584**, 316 (2003).
18. D. Gerlich, *Adv. Chem. Phys.* **82**, 1 (1992).
19. D. Klapstein, R. Kuhn, S. Leutwyler, and J. P. Maier, *Chem. Phys.* **78**, 167 (1983).
20. J. Dannacher, *Chem. Phys.* **29**, 339 (1978).
21. A. Dzhonson, and J. P. Maier, *Int. J. Mass Spectrom.* **in press** (2006).
22. J. P. Maier, and O. Marthaler, *Chem. Phys.* **32**, 419 (1978).
23. A. Dzhonson, D. Gerlich, E. J. Bieske, and J. P. Maier, *J. Mol. Struct.* **in press** (2006).
24. S. Olesik, T. Baer, and J. C. Morrow, *J. Phys. Chem.* **90**, 3563 (1986).

THE ASTROPHYSICAL JOURNAL, 640:369–372, 2006 March 20
 © 2006. The American Astronomical Society. All rights reserved. Printed in U.S.A.

THE GAS PHASE SPECTRUM OF CYCLIC C_{18} AND THE DIFFUSE INTERSTELLAR BANDS

JOHN P. MAIER, ANDREY E. BOGUSLAVSKIY, AND HONGBIN DING

Department of Chemistry, University of Basel, Klingelbergstrasse 80, Basel CH-4056, Switzerland; j.p.maier@unibas.ch

GORDON A. H. WALKER

1234 Hewlett Place, Victoria, BC V8S 4P7, Canada; gordonwa@uvic.ca

AND

DAVID A. BOHLENDER¹

National Research Council of Canada, Herzberg Institute of Astrophysics, 5071 West Saanich Road,
 Victoria, BC V9E 2E7, Canada; david.bohlender@nrc-cnrc.gc.ca

Received 2005 September 22; accepted 2005 November 28

ABSTRACT

The gas phase spectrum of the cyclic C_{18} molecule recorded in the laboratory at a temperature typical of diffuse interstellar clouds is compared with absorption features toward ζ Oph and HD 204827 in the 5730–5934 Å region. For the origin band at 5928.5 Å an upper limit to the column density of $\leq 1.8 \times 10^{11}$ cm⁻² is inferred. The origin band pattern in the laboratory spectrum changes on lowering the internal temperature in the 100–20 K range and bears a striking resemblance to the observed structure of a number of DIBs at other wavelengths. This suggests that platelike molecules or ions, comprising a couple of dozen to hundred carbon atoms, could be responsible for some of the latter absorptions.

Subject headings: ISM: general — ISM: lines and bands — ISM: molecules — stars: individual (ζ Oph, HD 204827)

1. INTRODUCTION

It has long been recognized that gas-phase electronic absorption spectra of carbon-dominated molecular systems are of interest in the identification of the diffuse interstellar absorption bands (DIBs; Herbig 1995). Of particular interest have been carbon chains, the hydrogenated rings (PAHs), and fullerenes. It has been conjectured that carbon chains C_n of the size $n = 5$ –15 may be responsible for some DIBs (Douglas 1977). However, only in the last few years has it proved possible to obtain the gas phase electronic spectra of C_4 and C_5 in the laboratory, the comet band system of C_3 having long been known. No other such gaseous spectra of polyatomic bare carbon species are available except of the fullerenes, C_{60} and C_{70} (Haufler et al. 1991). In neon matrices the knowledge of the electronic transitions of bare carbon species is more extensive, and the location of the transitions of linear carbon chains, C_{2n+1} ($n = 2$ –12), C_{2n} ($n = 2$ –4), and a few cyclic systems, C_{10} , C_{12} , and C_{14} , have been identified (Maier 1998).

The electronic spectra of C_4 and C_5 have transitions in the visible region, thereby allowing a comparison with known DIBs (Maier et al. 2002). Although no matches were found, upper limits to the column density of these molecules in diffuse interstellar clouds could be inferred (see also Adamkovic et al. 2006). In this connection, C_3 could be detected via its comet tail origin band at 4050 Å (Maier et al. 2001). The general conclusion of these studies was that the smaller carbon chains—of up to a dozen atoms—and the related species containing hydrogen or nitrogen atoms cannot be responsible for the stronger DIBs (Maier et al. 2004). Further arguments were presented to explain why larger systems remain viable candidates and indicating the species that should be the subject of laboratory studies. Among

these are the longer bare chains with an odd number of carbon atoms, C_{17} , C_{19} , . . . , C_{31} , because they have electronic transitions in the 4000–8000 Å range with very large oscillator strengths. Thus, their laboratory gas phase spectra are required. This led to the observation of the gas phase spectra of the first larger bare carbon species, C_{18} and C_{22} , but in their cyclic forms (Boguslavskiy et al. 2005).

The cyclic C_{18} molecule, which shows absorptions in the visible, was obtained by laser vaporization of carbon, collisionally cooling the synthesized molecules to temperatures typical of the diffuse clouds (e.g., 50 K) in a supersonic expansion. The electronic spectra were detected by a resonant two laser photon ionization technique. In this, the first photon induces the transition, whereas the second, higher energy photon ionizes the species, and the C_{18}^+ cation is detected by mass spectroscopy. A spectroscopic analysis and theoretical calculations indicate a cyclic-like structure (Boguslavskiy et al. 2005). From the astrophysical point of view, the significance is that one can compare the laboratory and DIB spectral signatures directly for the first time for a bare carbon species of such a size, at temperatures pertinent to the interstellar medium. The origin band near 5930 Å has a triple-component pattern reminiscent of structure seen in some DIBs.

2. OBSERVATIONS AND DATA REDUCTION

High signal-to-noise (S/N) spectra of the reddened stars ζ Oph (HD 149757) and HD 204827 were obtained on 2005 May 19 UT with the Canada-France-Hawaii 3.6 m telescope (CFHT) and the high-resolution bench-mounted ESPaDOnS echelle spectrograph, fiber-fed from the telescope's Cassegrain focus. The fiber is continually agitated at a high frequency close to the entrance of the spectrograph to mitigate modal noise. ESPaDOnS was used in the “object only” spectroscopic mode, and thus its 40 echelle orders and the EEV1 CCD (with 13.5 μm^2 pixels) provided nearly complete wavelength coverage from 3700 to 10050 Å at a resolution $\sim 80,000$. To avoid saturation of the detector in any

¹ Visiting Astronomer, Canada-France-Hawaii Telescope, operated by the National Research Council of Canada, the Centre National de la Recherche Scientifique of France, and the University of Hawaii.

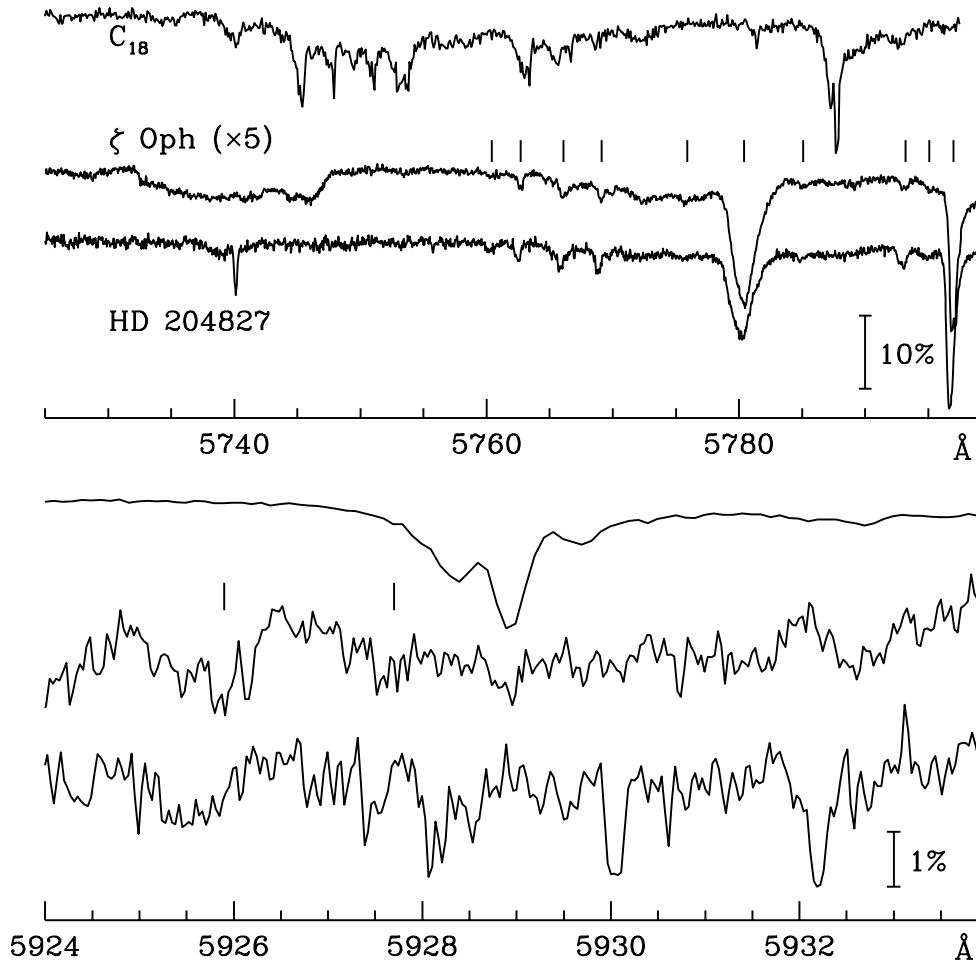


FIG. 1.—Comparison of the laboratory C_{18} gas-phase spectrum with high-S/N, high-resolution spectra of the reddened stars ζ Oph and HD 204827. A vertical bar in each panel indicates the relative intensity scale for the HD 204827 spectra, and in both cases this scale is multiplied by 5 for ζ Oph. The positions of known diffuse interstellar bands are indicated by tick marks. HD 204827 is a spectroscopic binary, and the weak, narrow features $\lambda\lambda$ 5740, 5930, and 5932.2 are photospheric lines of the secondary star.

order, 25×90 s exposures of ζ Oph and 4×20 minute exposures of HD 204827 were acquired in succession and combined after processing. Nine 30 s exposures of the rapidly rotating B9 V star α Leo (HD 87901) were obtained to allow identification and removal of telluric lines. The usual Th/Ar comparison arc spectra, flat-field spectra of the spectrograph's twin tungsten lamps, and bias exposures were acquired at the start and end of the night.

The trimming, bias subtraction, flat-fielding, optimal extraction, and wavelength calibration of the individual spectra was carried out with the data reduction package provided for ESPaDOnS users, Libre-ESPRIT.² Spectra were averaged, telluric lines removed, and continuum levels rectified by using appropriate IRAF³ packages. The final interstellar components of the spectra discussed here were placed on a laboratory scale by

applying velocity corrections of -14.53 and -4.0 km s^{-1} for ζ Oph and HD 204827, respectively. Portions of the final spectrum for each star are shown in Figure 1 along with the laboratory gas-phase spectrum of cyclic C_{18} (Boguslavskiy et al. 2005). There are a number of known DIBs (Galazutdinov et al. 2000) within the region, as shown by the tick marks in Figure 1.

For the origin band at 5929 Å, the 3σ detection limits for interstellar C_{18} are derived from the relation

$$W_{\max} = 3(wd)^{1/2}(S/N)^{-1},$$

where the 3σ limiting equivalent width, W_{\max} , and the FWHM of the laboratory feature, w , are both measured in Å, the spectrograph dispersion, d , is in Å pixel $^{-1}$, and S/N is the signal-to-noise ratio per pixel. Here $w = 1.6$ was adopted for the core of the laboratory C_{18} band at 5929 Å and $w = 16$ at 5749 Å. For the reduced ESPaDOnS data, $d = 0.0358$. At 5929 Å, the spectra of ζ Oph and HD 204827 have S/N of 1600 and 300, respectively, giving $W_{\max} = 0.0004$ and 0.002 Å. The ζ Oph and HD 204827 spectra near 5729 Å have S/N levels of 2050

² The ESPaDOnS data reduction software package Libre-ESPRIT was written by J.-F. Donati (Observatoire Midi-Pyrénées) and provided by CFHT.

³ IRAF is distributed by the National Optical Astronomy Observatory, which is operated by the Association of Universities for Research in Astronomy (AURA), Inc., under cooperative agreement with the National Science Foundation.

and 270 pixel^{-1} and in turn give $W_{\text{max}} = 0.001$ and 0.008 \AA , respectively.

3. DISCUSSION

The aim was to compare the first gas phase laboratory spectrum of a bare carbon ring, C_{18} , with DIB observations. Apart from such investigations for the linear C_3 , C_4 , and C_5 chains, this has also been carried out for the fullerene C_{60} , but no match is apparent (Herbig 2000).

There are two interesting aspects of this laboratory and astronomical comparison for cyclic C_{18} : determination of an upper limit to the column density and the similarity of the band structure measured in the laboratory to observation of the DIB profiles at higher resolution and seen through single clouds.

In the determination of the upper limit to the column density, the main uncertainty is in the oscillator strength of the electronic transition. This can be estimated as $f \sim 10^{-2}$ from experimental observations concerning the lifetime of the excited state. Taking an equivalent width, W_{max} for the detection as 0.4 m\AA (§ 2), the column density in the diffuse cloud is estimated from

$$N_{\text{max}} = \frac{1.13 \times 10^{20} W_{\text{max}}}{\lambda^2 f}$$

to be $\leq 1.84 \times 10^{11} \text{ cm}^{-2}$. This latter value is comparable to the upper limits inferred for linear C_5 toward ζ Ophiuchi ($\leq 2 \times 10^{11} \text{ cm}^{-2}$; Maier et al. 2002).

In a recent article discussing the possible role of carbon chains as carriers of DIBs, and excluding the smaller ones say up to 10 atoms, arguments were presented about which systems should be the focus of laboratory studies (Maier et al. 2004). The two primary criteria were that the species must have electronic transitions in the DIB region, but in addition, the oscillator strength should be in the range 1–10 to stand any chance of corresponding to some of the stronger DIBs. The odd-numbered linear chains in size C_{15} to C_{31} satisfy these requirements.

The present study shows that the C_{18} molecule does have electronic transitions in the DIB range and may even be large enough to be at least partly stable to photodissociation in the interstellar radiation field, but the oscillator strength is too low, even though estimates favor larger species (Le Page et al. 2003). The electronic spectrum of the cyclic C_{18} molecule was observed by chance during attempts to measure the spectra of the C_{15} to C_{31} chains. Because these could so far not be detected in the laboratory measurements using nanosecond lasers, an additional criterion for the sort of molecules that could be responsible for DIBs has materialized, the lifetime of the excited electronic state. The processes that limit this are intramolecular in nature. Thus, if the excited state has a lifetime of picoseconds, this would correspond to a lifetime broadened line width of around 5 \AA , implying that these transitions would not be related to the narrower DIBs with FWHM of 1 \AA . It remains to be established whether the lifetimes of the excited states of C_{15} to C_{31} chains are indeed 1 ps or less.

Another interesting aspect of the study of the bare carbon C_{18} ring is the relation to PAH studies. These, or rather their ions, have often been considered as possible DIB carriers (Tielens & Snow 1995). The most recent efforts in this area, the gas phase studies of the electronic transitions of some PAH cations, such as those of naphthalene (Romanini et al. 1999) and anthracene (Sukhorukov et al. 2004), have led to negative results. However, studies of $C_{24}H_{12}^+$ among other PAH^+ in an ion trap have

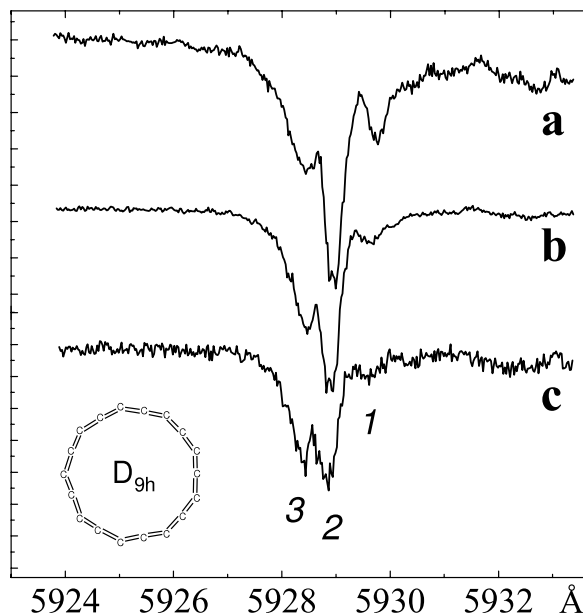


FIG. 2.—Close-up of the origin band of C_{18} . The intensity ratio of the three peaks depends on the internal temperature. The internal temperature is reduced on going from trace *a* to *c* in the 100–20 K range by different buffer gases in the supersonic expansion. *Inset*: the geometric structure of C_{18} in D_{9h} symmetry. According to calculations, the bond lengths are equal, 1.285 \AA , while the bond angles alternate between 168° and 152° .

shown that on UV irradiation, complete dehydrogenation takes place (Ekern et al. 1998), suggesting that some bare neutral and ionic carbon rings of this size may be prevalent in the diffuse medium. Hence the relevance of the current study on cyclic C_{18} .

Cyclic C_{18} is essentially a dehydrogenated PAH, also with singlet ground state, but is perhaps photochemically more robust because the hydrogens have already been removed and the $4n + 2$ ring shows enhanced stability. The ionization potential of cyclic C_{18} can be bracketed in the 8–10 eV range according to the experiments (Boguslavskiy et al. 2005). Thus, depending on the degree of ionization in diffuse clouds, cyclic C_{18}^+ could also be of interest, although it would be less stable than its neutral counterpart. However, no laboratory spectral information on such cations is available.

The structure of the C_{18} origin band (Fig. 2) is rather similar to some of the DIBs (but at other wavelengths) such as those at 6614 , 6379 , and 5797 \AA recorded at high resolution (e.g., Sarre et al. 1995; Walker et al. 2000, 2001). It is tempting to speculate that the carriers responsible have structural and size characteristics similar to C_{18} . In order to draw inferences on this, the peaks and profiles seen around the origin band of the spectrum recorded in the laboratory (Fig. 2) has to be explained. The interpretation is based on the relative intensity changes on cooling the C_{18} molecule (Fig. 2) in the laboratory experiment (Boguslavskiy et al. 2005). The temperature of the laboratory spectrum shown in Fig. 2 changes from around 100 K (trace *a*) to 20 K (trace *c*), typical of a nonpolar molecule in the diffuse clouds. The analysis of the rotational structure in the electronic spectrum of C_3 yielded $\sim 70 \text{ K}$ (Maier et al. 2001) and the studies of the infrared transitions of H_3^+ values in the 30–50 K range (McCall et al. 2002). For polar molecules the temperatures are likely to be lower.

Peak 1 is probably a sequence transition originating from the lowest frequency vibration ($\sim 56\text{ cm}^{-1}$) in the ground electronic state. Peaks 2 and 3 also change in intensity, and thus there is an overlap of the 0–0 transition with another sequence band. Thus, it is seen that at $\sim 40\text{ K}$ the transitions originating from low ($< 100\text{ cm}^{-1}$) frequency vibrational modes of molecules will contribute to the pattern around the origin band, in addition to the rotational profile, which itself may show splitting according to simulations (Cossart-Magos & Leach 1990).

Simulation of the rotational profile for the observed electronic band of a cyclic C_{18} molecule, with the ground state geometry shown in Figure 2, leads to slightly asymmetric profile with FWHM $\sim 1\text{--}2\text{ cm}^{-1}$ for temperatures of 20–80 K, i.e., comparable to the observed widths of the individual peaks in the laboratory spectrum. In fact, a similar simulation has been carried out (Kerr et al. 1996) to reproduce the fine structure observed in the high-resolution profile of the 5797 and 6614 Å DIBs (Sarre et al. 1995). Curiously, this fitted reasonably to a ring of 18 atoms; the general conclusion being that the DIB structures can be compatible with electronic transitions of ring molecules with 14–30 carbons. Indeed, the laboratory-measured pattern for the C_{18} molecule (Fig. 2) at 5930 Å resembles the 6614 Å DIB (Fig. 1 of Sarre et al. 1995) or other DIB profiles with splittings (Walker et al. 2001).

However, the simulations described by Kerr et al. (1996) were for a perpendicular transition, and the three peaks observed were just the rotational profile. Changing the temperature does not lead to the intensity changes as observed in the experiment on C_{18} (Fig. 2). In the case of a parallel transition, which is the assignment of the 5929 Å laboratory band, two of the peaks have to be vibrational sequences, whose intensity ratios vary with temperature.

Thus, the implication would be that the observed profiles of DIBs with structures similar to that seen in Figure 2 could be of platelike nonpolar molecules, with sizes C_{20} to C_{100} rings. The subsidiary peaks surrounding the origin band under which the rotational lines are hidden would be contributed by transitions between the lowest frequency modes that are still sufficiently populated at, say, 40 K.

This work was supported by the Swiss National Science Foundation (project 200020-100019) and the European Union project “Molecular Universe” (MRTN-CT-2004-512302) (J. P. M.), the Canadian Natural Sciences and Engineering Research Council (G. A. H. W.), and the National Research Council of Canada (D. A. B.).

REFERENCES

- Adamkovic, M. A., Blake, G. A., & McCall, B. J. 2006, in 60th International Symposium on Molecular Spectroscopy, Abstract FA07, in press
- Boguslavskiy, A. E., Ding, H., & Maier, J. P. 2005, *J. Chem. Phys.*, 123, 4305
- Cossart-Magos, C., & Leach, S. 1990, *A&A*, 233, 559
- Douglas, A. E. 1977, *Nature*, 269, 130
- Ekern, S. P., Marshall, A. G., Szczepanski, J., & Vala, M. 1998, *J. Phys. Chem. A*, 102, 3498
- Galazutdinov, G. A., Musaev, F. A., Krelowski, J., & Walker, G. A. H. 2000, *PASP*, 112, 648
- Hauffer, R. E., Chai, Y., Chibante, L. P. F., Fraelich, M. R., Weisman, R. B., Curl, R. F., & Smalley, R. E. 1991, *J. Chem. Phys.*, 95, 2197
- Herbig, G. H. 1995, *ARA&A*, 33, 19
- . 2000, *ApJ*, 542, 334
- Kerr, T. H., Hibbins, R. E., Miles, J. R., Fossey, S. J., Somerville, W. B., & Sarre, P. J. 1996, *MNRAS*, 283, L105
- Le Page, V., Snow, T. P., & Bierbaum, V. M. 2003, *ApJ*, 584, 316
- Maier, J. P. 1998, *J. Phys. Chem. A*, 102, 3462
- Maier, J. P., Lakin, N. M., Walker, G. A. H., & Bohlender, D. A. 2001, *ApJ*, 553, 267
- Maier, J. P., Walker, G. A. H., & Bohlender, D. A. 2002, *ApJ*, 566, 332
- . 2004, *ApJ*, 602, 286
- McCall, B. J., et al. 2002, *ApJ*, 567, 391
- Romanini, D., Biennier, L., Salama, F., Kachanov, A., Allamandola, L. J., & Stoeckel, F. 1999, *Chem. Phys. Lett.*, 303, 165
- Sarre, P. J., Miles, J. R., Kerr, T. H., Hibbins, R. E., Fossey, S. J., & Somerville, W. B. 1995, *MNRAS*, 277, L41
- Sukhorukov, O., Staicu, A., Diegel, E., Rouille, G., Henning, Th., & Huisken, F. 2004, *Chem. Phys. Lett.*, 386, 259
- Tielens, A. G. G. M., & Snow, T. P., ed. 1995, *The Diffuse Interstellar Bands* (Dordrecht: Kluwer)
- Walker, G. A. H., Bohlender, D. A., & Krelowski, J. 2000, *ApJ*, 530, 362
- Walker, G. A. H., Webster, A. S., Bohlender, D. A., & Krelowski, J. 2001, *ApJ*, 561, 272

Gas phase electronic spectra of two C_5H_5 radical isomers

H. Ding, A. E. Boguslavskiy and J. P. Maier

Department of Chemistry, University of Basel, Klingelbergstrasse 80, CH-4056 Basel, Switzerland

Received 5th October 2004, Accepted 12th December 2004
First published as an Advance Article on the web 18th January 2005

Gas phase electronic spectra of two C_5H_5 radical isomers have been observed in the 440–470 nm spectral region. The technique was a mass selective resonant two-color two-photon ionization coupled to a supersonic plasma source. Structures, relative energies and vertical electronic transition energies of six isomers of C_5H_5 have been calculated. Based on an analysis of the rotational profiles of the observed bands and theoretical calculations, the spectra are assigned as the $\tilde{A}^2A'' \leftarrow \tilde{X}^2A''$ electronic transition of isomer **1** and $\tilde{A}^2A_2 \leftarrow \tilde{X}^2B_1$ of **6** with origin band at 461.8 nm and 456.1 nm, respectively. Isomer **1**, 1,3-vinylpropargyl, has C_s symmetry, while **6**, a planar zig-zig chain with one hydrogen on each carbon, has C_{2v} symmetry.

I. Introduction

Unsaturated hydrocarbons are reactive intermediates in combustion processes¹ and play a role in the chemical evolution of the interstellar medium (ISM).^{2–6} The near UV electronic absorption spectrum of the $\tilde{A}^2A_2'' \leftarrow \tilde{X}^2E_1''$ system of cyclopentadienyl radical C_5H_5 (with origin band at ~ 338.1 nm) was reported in 1956⁷ and studied subsequently.^{8–10} Cyclopentadienyl radical was proposed as a potential key intermediate for the formation of polycyclic aromatic hydrocarbons in the outflow of carbon-rich stars.¹¹ A striking match between a laboratory absorption band at 442.9 nm in a benzene plasma and the strongest diffuse interstellar band (DIB) around 442.9 nm has been reported.¹² This initiated a discussion whether radical fragments of aromatic rings might be present in the diffuse interstellar medium.¹³ These authors attributed the observed laboratory band to C_5H_5 or C_3H_5 , or their cations, based on a deuteration analysis, but an unambiguous assignment of the carrier could not be given. The supplementary laboratory data obtained by combination of cavity ringdown absorption and mass-selective resonant two-color two-photon ionization (R2C2PI) techniques indicated that a C_5H_5 isomer, with a planar but non linear structure is the absorber.¹⁴ It was also pointed out that it is unlikely that the DIB and the absorption band at 442.9 nm are related due to differences in their profiles. In this paper the electronic spectra of two other C_5H_5 isomers are reported, also detected via a mass-selective R2C2PI in combination with a supersonic discharge source. *Ab initio* calculations are used to help the assignment of the observed transitions.

II. Experiment

The experiment consisted of a molecular beam combined with a linear time of flight mass-analyzer.¹⁵ The plasma source used to produce the C_5H_5 radical was a pulsed valve coupled to an electric discharge. A gas mixture of 0.3% of benzene in Ar (backing pressure 8 bar) was expanded through the ceramic body of the source. A 100–200 μ s, 500–800 V voltage pulse was applied between the electrodes. The current was limited to ~ 100 mA. The emerging C_5H_5 radical beam entered the ionization region through a 2 mm diameter skimmer. Ions produced in the source were removed by an electric field perpendicular to the molecular beam after the skimmer and before entering the extraction zone of the mass-spectrometer.

The neutral radicals were ionized by R2C2PI and then extracted into a two-stage acceleration setup towards a micro-channel plate detector. The signal was fed into an ultrafast oscilloscope after pre-amplification and transferred to a computer. Gates were set on different ion masses.

In R2C2PI spectroscopy, the first color pump laser is tuned over the (ro)vibrational level of the excited electronic state while the second, fixed wavelength, is used to ionize the excited molecules. The spectrum was recorded by monitoring the ion current as a function of the wavelength of the pump laser. Pump photons were delivered by a tunable dye laser (bandwidth ~ 0.1 cm^{-1}), with typically 5–10 mJ pulse⁻¹. The 212 nm photons for the ionization (~ 1 mJ pulse⁻¹) came from the frequency tripled output of a dye laser pumped by the second harmonic of a Nd:YAG laser. Both the pump and probe lasers were unfocused.

III. Results

The observed R2C2PI spectrum of C_5H_5 (with $m/z = 65$) is shown in Fig. 1. The intensities of bands A_0 and A_1 vary in a large way relative to the B_0 , B_1 and B_2 bands as the plasma conditions are changed (Fig. 2). The stronger vibronic bands A_0 and A_1 have been scanned with higher resolution (~ 0.03 cm^{-1}), but the rotational structure could not be resolved. The

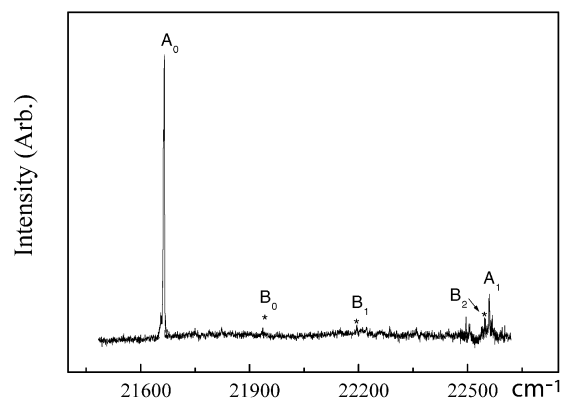


Fig. 1 Gas phase electronic spectrum of C_5H_5 in the 440–470 nm region detected by a resonant two-color two-photon approach with 212 nm ionisation.

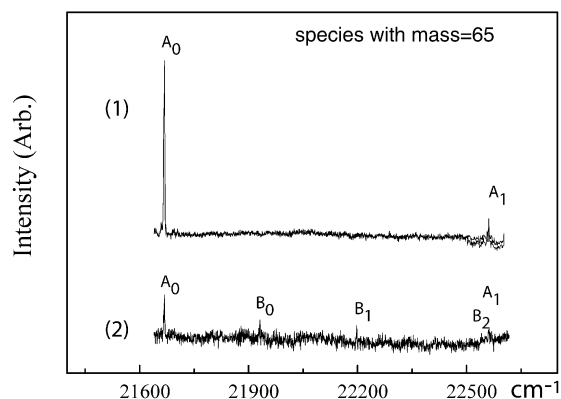


Fig. 2 The intensities of bands A_0 and A_1 vary relative to B_0 to B_2 as the plasma conditions are changed. Trace 1 was observed using C_5H_6/Ar discharge at 8 bar with a voltage of ~ 800 V (~ 150 mA); trace 2 with ~ 500 V (~ 80 mA).

profile of band A_0 is shown for comparison with the computed contours (Figs. 4–6), described in next section. The wavelengths of the maxima of the five bands seen in Fig. 1 are given in Table 1.

IV. Discussion

A. Theoretical calculations

Theoretical calculations were carried out using the GAUSSIAN 98 programs¹⁶ and the MOLPRO package.¹⁷ Full geometry optimization and harmonic frequency calculations used the hybrid density functional B3LYP method¹⁸ with Dunning's correlation consistent basis sets cc-pVDZ.¹⁹ Six isomers of C_5H_5 with chain, three-membered, four-membered and five-membered ring forms are predicted with the optimized geometries as shown in Fig. 3. The cyclopentadienyl radical was not included in our calculations because its first electronic transition system lies in the 325–338 nm range and there are no other states lying below 6 eV.⁷ It is ruled out as carrier of the bands in Fig. 1. The calculated energies (E) with zero point vibrational energies correction, relative energies (ΔE), total dipole moments (D_{total}), rotational constants (A , B , C) in the ground states and the vertical transition energies for the first three lowest dipole-allowed electronic transition systems of the isomers 1–6 are given in Table 2. The calculations show that the isomers in Fig. 3 are local minima at the B3LYP/cc-pVDZ level of theory (all possessing real harmonic frequencies²⁰). Isomer 1, 1,3-vinylpropargyl radical, is the most stable structure.

Calculations of electronically excited states were carried out using the time-dependent density functional theory (TD-DFT)²¹ with hybrid B3LYP functional with cc-pVDZ basis sets. The oscillator strengths ($f_{a,b,c}$) and transition-types are also given, where the subscripts a , b and c correspond to the transition dipole moment along the a -, b -, c -axes. The a -axis is defined to be the long-axis of the molecular top for near prolate

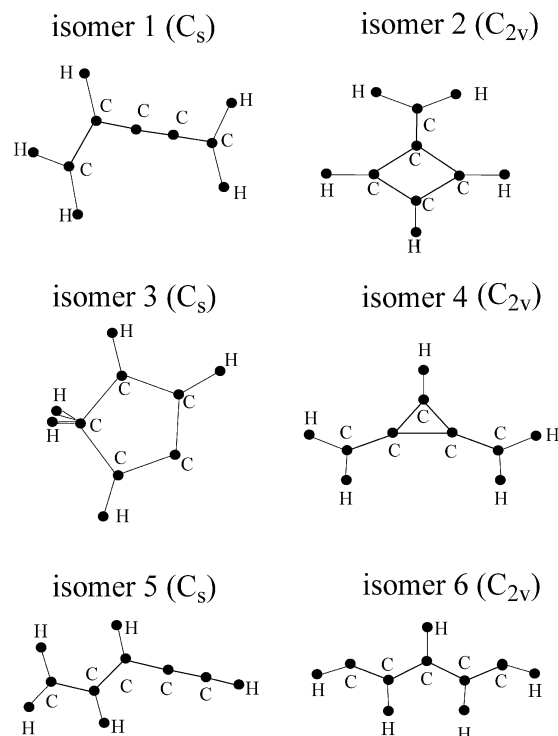


Fig. 3 Optimized geometries of the C_5H_5 isomers in the ground states using DFT-B3LYP/cc-pVDZ level of theory.

molecules, while the c -axis is the shortest one for near oblate molecules.

Because the TD-DFT calculated transition energies 2.95 eV for isomer 1 and 3.02 eV for 6 are close to the observation and 1 has the right transition dipole moment direction (along the a -axis), *ab initio* calculations with multi-configuration electron correlation method have been carried out at the CASPT2 level of theory²² using cc-pVDZ basis sets. The CASPT2 calculations used an active space CAS(9,7) with nine electrons in three a' and four a'' orbitals for isomer 1 and CAS(7,7) with seven electrons in two a_1 , two b_1 , one b_2 and two a_2 for isomer 6. Isomer 1 has a \tilde{X}^2A'' ground state with $\dots(14a')^2(5a')^2(1a'')^2(2a'')^2(3a'')^1$ electronic configuration. Electron promotion from the $2a''$ to the $3a''$ orbital leads to the \tilde{A}^2A'' excited state. Isomer 6 has a \tilde{X}^2B_1 ground state dominated by two electronic configurations $\dots(9a_1)^2(1b_1)^2(6b_2)^2(7b_2)^0(1a_2)^2(2b_1)^1$ and $\dots(9a_1)^0(1b_1)^2(6b_2)^2(7b_2)^2(1a_2)^2(2b_1)^1$.

The $1a_2 \rightarrow 2b_1$ and $2b_1 \rightarrow 2a_2$ double electron excitations lead to the \tilde{A}^2A_2 state. The calculated vertical electronic transition energies are summarized in Table 3.

B. Electronic transitions

The assignment of the observed electronic transitions is guided by examination of the vertical transition energies, oscillator

Table 1 Maxima of the vibronic bands observed in the gas phase electronic spectrum of C_5H_5 and the suggested assignment

Label	λ/nm	ν/cm^{-1}	$\Delta\nu/cm^{-1}$	Assignment
A_0	461.77	21 649.7	0.0	Isomer 1 $0_0^0(\tilde{A}^2A'' \leftarrow \tilde{X}^2A'')$
A_1	443.50	22 541.6	892	$13_0^1(a')$
B_0	456.12	21 917.9	0.0	Isomer 6 $0_0^0(\tilde{A}^2A_2 \leftarrow \tilde{X}^2B_1)$
B_1	450.77	22 178.0	260	$9_0^0(a_1)$
B_2	443.74	22 529.4	612	$7_0^0(a_1)$

Table 2 Calculated energies, dipole moments and rotational constants in the ground states and the vertical transition energies for the first three lowest dipole-allowed electronic transitions of the C₅H₅ isomers using DFT and TD-DFT theories at the B3LYP/cc-pVDZ level

Isomer	1	2	3	4	5	6
$E + 193(\text{h})$	-0.352 660	-0.342 908	0.342118	-0.323 700	-0.308 105	-0.230 905
$\Delta E/\text{kJ mol}^{-1}$	0.0	25.6	27.7	75.9	116.9	319.4
$D_{\text{total}}/\text{D}$	0.347	0.566	1.44	0.477	0.297	1.29
A/cm^{-1}	1.2681	0.4669	0.3135	0.4360	0.6589	1.4373
B/cm^{-1}	0.0751	0.1682	0.2691	0.1345	0.1135	0.0797
C/cm^{-1}	0.0709	0.1237	0.1489	0.1028	0.0968	0.0755
$T_{1\leftarrow X}/\text{eV}$	2.89	3.00	2.06	2.18	1.57	0.71
$f_{1\leftarrow X}$	$f_c < 10^{-5}$	$f_b \approx 10^{-4}$	$f_c \approx 7 \times 10^{-4}$	$f_a \approx 0.07$	$f_a \approx 0.002$	$f_c \approx 4 \times 10^{-4}$
$T_{2\leftarrow X}/\text{eV}$	2.95	3.12	2.84	3.81	3.94	2.56
$f_{2\leftarrow X}$	$f_a \approx 0.003$	$f_a < 10^{-4}$	$f_{a,b} \approx 0.0001$	$f_c < 10^{-5}$	$f_a \approx 0.001$	$f_c \approx 0.001$
$T_{3\leftarrow X}/\text{eV}$	4.45	3.36	4.15	4.38	4.64	3.02
$f_{3\leftarrow X}$	$f_a \approx 0.33$	$f_b \approx 0.01$	$f_c \approx 0.001$	$f_b \approx 0.02$	$f_b < 10^{-4}$	$f_a \approx 0.003$

strengths and transition dipole moment direction among the candidate isomers.

The information on the transition dipole moment direction of the observed bands can be decoded by analysis of their contours even for unresolved rotational lines.²³ The program Wang²⁴ was used to simulate the band contours and a Lorentzian profile with 0.1 cm⁻¹ (fwhm) was taken for the rotational lines. The *ab initio* rotational constants in Table 2 were used for the ground state. For the excited state, *A'*, *B'* and *C'* were taken as those in the ground state and then increased from 0.1% to 5%. Previous experiments indicate that the rotational temperature in our molecular beam is in the range 10–17 K^{25,26} and therefore $T = 13$ K was used in the computations. The simulations indicate that contours with b-type and c-type transitions (Figs. 4 and 5) have an open subband structure and a wider distribution compared with the experimental profile of band A₀, while the computed a-type contours for isomers 1–6 have a similar pattern to that of observed band A₀ (Fig. 6). This indicates that the transition dipole moment is along the *a*-axis. The computed a-type contours of isomers 1 and 6 are the most similar to the observed profile. In addition, the calculations show that only the isomers 1 and 6 have large transition dipole moments in the observed region. These two isomers are therefore considered as the likely carriers.

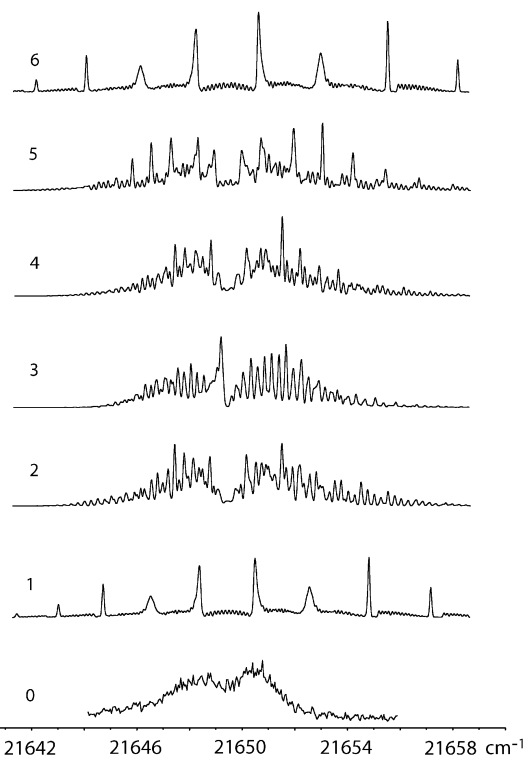
The observed spectra lie in the 2.68–2.79 eV region. The CASPT2 calculations (Table 3) predict an $\tilde{A}^2A'' \leftarrow \tilde{X}^2A''$ electronic transition of isomer 1 at 2.55 eV and an $\tilde{A}^2A_2 \leftarrow \tilde{X}^2B_1$ system of isomer 6 at 2.45 eV. The strong band A₀ is assigned as the origin of the $\tilde{A}^2A'' \leftarrow \tilde{X}^2A''$ system of isomer 1 and the weak band B₀ as the one of the $\tilde{A}^2A_2 \leftarrow \tilde{X}^2B_1$ transition of isomer 6 in view of their relative energy stability (320 kJ mol⁻¹ at DFT/cc-pVDZ level and 254 kJ mol⁻¹ at RCCSD(T)/cc-pVDZ//DFT/cc-pVDZ level). Band A₁ is then assigned to the 13₀¹ transition implying a frequency of 892 cm⁻¹ for the ν_{13} (*a'*) mode in the upper electronic state. The bands B₁ and B₂ are assigned to the 9₀¹ and 7₀¹ vibronic transitions within the electronic system of isomer 6. This is guided by the calculated

Table 3 Calculated vertical transition energies (in eV) at CASPT2/cc-pVDZ level of theory at the optimized ground state geometries for the C₅H₅ isomers 1 and 6. The oscillator strengths were calculated with CASPT2 transition energies but CASSCF transition dipole moments

	Isomer		Experiment
	1(C _s)	6(C _{2v})	
	CASPT2	CASPT2	
\tilde{X}	0.0 (${}^2A''$)	0.0 (2B_1)	
A	2.55 (${}^2A''$)	2.45 (2A_2)	2.68
$f_{A\leftarrow X}$	$f_a = 0.004$	$f_a = 0.003$	a-type

harmonic frequencies in the ground states.²⁰ The deduced vibrational frequencies are given in Table 1.

The TD-DFT calculations (Table 2) predict that the electronic transition of isomer 3 lies at 2.82 eV with a-type vibronic bands. However, the calculated oscillator strength of the transition is ten times smaller than those of isomers 1 and 6. Thus the contribution of isomer 3 to the observed spectrum is expected to be minor. The most stable isomer 1 could be expected to have a higher concentration in our source than that of the less stable 6. The main evidence for the assignment of the observed spectrum to two distinct isomers is that the intensities of bands A₀ and A₁ vary, in a large way relative to the B₀, B₁ and B₂ bands as the plasma conditions are changed. The B-bands have been observed with a small discharge voltage and current (~500 V and ~80 mA) while the A-bands favor large values (~800 V and ~150 mA). Increasing the

**Fig. 4** Computed *b*-type contours (traces 1–6) for isomers 1–6 in comparison to the experimental profile (trace 0) of the A₀ vibronic band. The open sub-structure in *b*-type contours 1–6 is dominated by the value of $2(A' - (B' + C')/2)$.

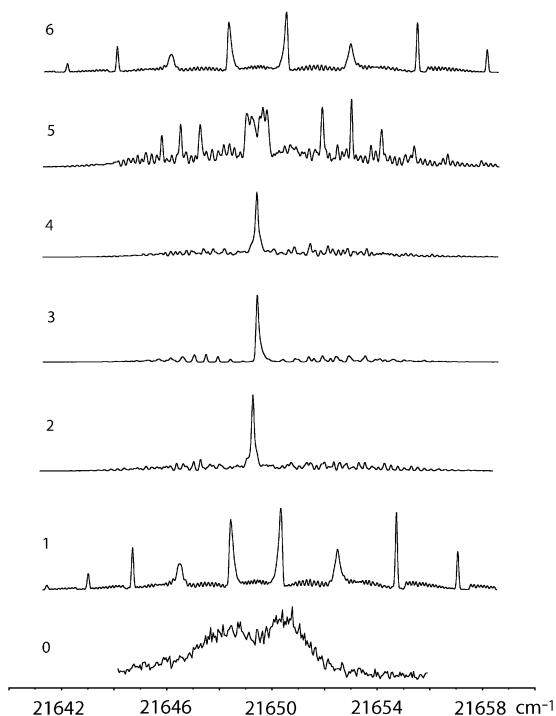


Fig. 5 Computed *c*-type contours (traces 1–6) for isomers 1–6 in comparison to the experimental profile (trace 0) of the A_0 vibronic band. The significant Q-branch in the contours 2–4 is dominated by the rotational lines with $K''_a = 0, 1, J''$ and $K''_c = 4, 5, 6, \Delta J = 0, \Delta K_a = \pm 1, \Delta K_c = 0$ transitions. This is due to isomers 2–4 being near the limiting oblate top.

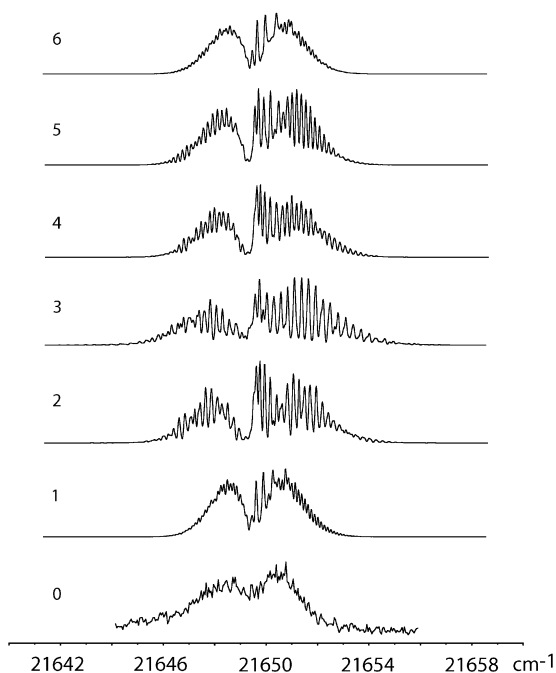


Fig. 6 Computed *a*-type contours (traces 1–6) for isomers 1–6 in comparison to the experimental profile (trace 0) of the A_0 vibronic band. Close sub-structure in *a*-type contours 1–6 is dominated by the value of $(B' + C')/2$.

voltage the A-bands became about 10 times more intense, but the B-bands completely disappeared (Fig. 2). This seems reasonable in view of the plasma chemistry in the discharge source. Isomer 6 could be produced by CH elimination following the benzene ring opening at an early stage. A high voltage (current) causes 6 fragment further and rearrange. Isomer 6 decomposes on increasing the discharge voltage (current) and 1 favors a large voltage (current).

V. Conclusion

The measured R2C2PI spectra are assigned as the $\tilde{A}^2A'' \leftarrow \tilde{X}^2A''$ electronic transitions of isomer 1 and $\tilde{A}^2A_2 \leftarrow \tilde{X}^2B_1$ of isomer 6. Isomer 1 with C_s symmetry is the most stable while 6 with C_{2v} symmetry lies ~ 254 kJ mol $^{-1}$ to higher energy. The observed gas phase electronic spectra of these two C_3H_5 radicals provide a database for their study and identification in chemical processes such as combustion, plasmas and interstellar space.

Acknowledgements

This work has been supported by the Swiss National Science Foundation (project no. 200020-100019).

References

- 1 K.-H. Homann, *Angew. Chem. Int. Ed. Engl.*, 1998, **37**, 2434.
- 2 T. Henning and F. Salama, *Science*, 1998, **282**, 2204.
- 3 H. W. Kroto, J. R. Heath, S. C. O'Brien, R. F. Curl and R. E. Smalley, *Astrophys. J.*, 1987, **314**, 352.
- 4 R. I. Kaiser, C. Ochsenfeld, M. Head-Gordon, Y. T. Lee and A. G. Suits, *Science*, 1996, **274**, 1508.
- 5 E. Buonomo and D. C. Clary, *J. Phys. Chem. A*, 2001, **105**, 2694.
- 6 H. Ding, T. W. Schmidt, T. Pino, A. E. Boguslavskiy, F. Güthe and J. P. Maier, *J. Chem. Phys.*, 2003, **119**, 814.
- 7 B. A. Thrush, *Nature (London)*, 1956, **178**, 155.
- 8 G. Porter and B. Ward, *Proc. R. Soc. London, Ser. A*, 1968, **303**, 139.
- 9 J. R. Engleman and D. A. Ramsey, *Can. J. Phys.*, 1970, **48**, 964.
- 10 B. E. Applegate, A. J. Bezzant and T. A. Miller, *J. Chem. Phys.*, 2001, **114**, 4869.
- 11 R. I. Kaiser, H. Y. Lee, A. M. Mebel and Y. T. Lee, *Astrophys. J.*, 2001, **548**, 852.
- 12 C. D. Ball, M. C. McCarthy and P. Thaddeus, *Astrophys. Lett.*, 1999, **523**, L89.
- 13 P. Thaddeus and M. C. McCarthy, *Spectrochimica Acta Part A*, 2001, **57**, 757.
- 14 M. Araki, H. Linnartz, P. Kolek, H. Ding, A. Boguslavskiy, A. Denisov, T. W. Schmidt, T. Motylewski, P. Cias and J. P. Maier, *Astrophys. J.*, 2004, **616**, 1301.
- 15 F. Güthe, H. Ding, T. Pino and J. P. Maier, *Chem. Phys.*, 2001, **269**, 347.
- 16 M. J. Frisch, *et al.*, *GAUSSIAN 98 (Revision A.7)*, Gaussian, Inc., Pittsburgh, PA, 1998.
- 17 *MOLPRO* version 2002.3 is a package of *ab initio* programs written by H.-J. Werner and P. J. Knowles, with contributions from others: see <http://www.molpro.net/>.
- 18 A. D. Becke, *J. Chem. Phys.*, 1993, **98**, 5648.
- 19 D. E. Woon and T. H. J. Dunning, *J. Chem. Phys.*, 1993, **98**, 1358.
- 20 The calculated bond lengths and bond angles and the harmonic vibrational frequencies in the ground states of the isomers 1–6 are available from the authors.
- 21 R. E. Stratmann, G. E. Scuseria and M. J. Frisch, *J. Chem. Phys.*, 1998, **109**, 8218.
- 22 P. Celani and H.-J. Werner, *J. Chem. Phys.*, 2000, **112**, 5546.
- 23 J. M. Hollas, *J. Chem. Soc., Faraday Trans.*, 1998, **94**, 1527.
- 24 D. Luckhaus and M. Quack, *Mol. Phys.*, 1989, **68**, 745.
- 25 H. Ding, T. Pino, F. Güthe and J. P. Maier, *J. Chem. Phys.*, 2001, **115**, 6913.
- 26 H. Ding, T. Pino, F. Güthe and J. P. Maier, *J. Am. Chem. Soc.*, 2003, **125**, 14626.

Available online at www.sciencedirect.com

SCIENCE @ DIRECT®

Chemical Physics Letters 392 (2004) 225–228

CHEMICAL
PHYSICS
LETTERSwww.elsevier.com/locate/cplett

Gas phase electronic spectrum of the nitrogen terminated nanowire NC_{16}N

H. Ding, A.E. Boguslavskiy, T.W. Schmidt¹, J.P. Maier**Department of Chemistry, University of Basel, Klingelbergstrasse 80, CH-4056, Basel, Switzerland*

Received 14 April 2004; in final form 11 May 2004

Available online 10 June 2004

Abstract

The UV electronic spectrum of NC_{16}N has been measured by means of a mass selective resonant two-color two-photon ionization technique. The observed bands are assigned to the dipole allowed, $\text{B}^1\Sigma_u^+ \leftarrow \text{X}^1\Sigma_g^+$, electronic transition. The electronic structures of NC_{2n}N ($n = 2\text{--}8$) in the ground and excited states have been investigated using density functional theory. The calculated transition energies of the $\text{A}^1\Delta_u(1\Sigma_u^-) \leftarrow \text{X}^1\Sigma_g^+$ and the $\text{B}^1\Sigma_u^+ \leftarrow \text{X}^1\Sigma_g^+$ systems decrease monotonically with increasing chain size and slowly converge to the HOMO–LUMO gap of the long chain limit. The present studies imply that a long carbon nanowire terminated with nitrogen will be semiconducting due to π -electron localization and bond-length alternation.

© 2004 Elsevier B.V. All rights reserved.

1. Introduction

The development of a variety of experimental methods in recent years has made it possible to produce materials with lower dimensionality than those usually encountered in nature. The properties and electronic structure of, for example, a 1D nanowire, may differ significantly from that of 3D materials and show strong quantum behavior [1]. One-dimensional carbon-based materials like nanotubes [2], Pt-containing polyynes [3], and hydrogen terminated polyynes [4] have become of significant scientific and technological interest. One of the central questions is if the material is a semiconductor with π -electrons around the Fermi level, and whether the electrons are delocalized over the complete carbon backbone. In our previous publications, the gas phase electronic spectra of hydrogen terminated carbon nanomolecular wires such as HC_{2n}H [4,5] and HC_{2n+1}H [6] were studied by a mass selective resonant two-color two-photon ionization (R2C2PI) technique in a supersonic molecular beam. For the closed shell even chains HC_{2n}H

it was found that convergence to bulk behavior was slow and that a significant optical band-gap of 3.3 eV persisted in chains as long as 3 nm (HC_{26}H).

Molecular wires likely to find employment in technological applications are modified at their ends such that they may bind covalently to gold electrodes or other materials. An example is the use of the lone-pair bearing nitrogen atom in pyridine as a molecular ‘alligator clip’ [7]. It is therefore of interest to investigate the effects of chemical substitution on the electronic structure of the hydrogen-terminated nanowires studied previously.

In this Letter, the gas phase electronic spectrum of the nitrogen terminated nanowire NC_{16}N is presented and analyzed. The results of theoretical calculations using time-dependent density functional theory (TD-DFT) of the band gaps of the nitrogen terminated carbon nanowires are presented and discussed in terms of the electronic structure of these species.

2. Experiment

The experimental set-up has been described in detail elsewhere [8]. It consisted of a molecular beam combined with a linear time of flight mass-analyzer. The source used to produce NC_{16}N was a pulsed valve

* Corresponding author.

E-mail address: t.schmidt@chem.usyd.edu.au (T.W. Schmidt).¹ Present address: School of Chemistry, University of Sydney 2006, Building F11, Australia. Fax: +61-2-9351-3329.

coupled to an electric discharge through which a gas mixture comprising 0.5% dicyanoacetylene (NCCCCN) in argon (backing pressure 8 bar) was expanded. A 100–200 μs pulse (600–900 V) was applied between the electrodes resulting in a current of 100 mA. The emerging molecular beam containing the NC_{16}N dicyanopolyne entered the ionization region through a 2 mm skimmer. Ions were removed prior to the skimmer by an electric field. The neutral molecules were then ionized by the R2C2PI method and the ions extracted towards a detector. The mass resolution of the instrument was ≈ 900 . The ion signal of a large number of masses was simultaneously recorded as a function of the wavelength.

R2C2PI spectra were recorded in the near UV range. The excitation photons were produced by the frequency doubled output of a dye laser (bandwidth $\sim 0.1 \text{ cm}^{-1}$) pumped by the second harmonic of a Nd:YAG laser. The ionizing photons at 157 nm were produced by a F_2 excimer laser with the energy of a few mJ/pulse. Both lasers were unfocused. The excitation laser beam was anti-collinear to the molecular beam while the F_2 laser beam was perpendicular to the molecular beam. The temporal sequence of the two lasers was optimized to maximize the R2C2PI signal, the F_2 laser pulse usually passing through the molecular beam a few ns after the dye laser.

The bands observed in the spectrum were due to a $1 + 1'$ resonance. This was confirmed by the absence of signal at the appropriate mass-to-charge ratio in the absence of either laser pulse. Transitions from $2 + 1'$ resonances were not expected to be seen because the molecular density in the source is low and the small laser power ($\sim 10^7 \text{ W cm}^{-2}$) did not favor multiphoton processes.

3. Results and discussion

3.1. Spectroscopy

The observed R2C2PI spectrum of NC_{16}N is shown in Fig. 1. The corresponding transition of the isoelectronic HC_{18}H molecule is reproduced from [5] in the bottom trace. The wavelength maxima of the observed vibronic transitions and the suggested assignments are given in Table 1. Because the spectrum was recorded under the low temperature conditions of a supersonic molecular beam, vibrational hot bands are not expected. The band observed $\sim 209 \text{ cm}^{-1}$ to the blue of the origin is attributed to the excitation of the lowest frequency σ_{g}^+ vibration, which corresponds to a stretching vibrational mode as suggested by ab initio calculation [9]. This value is near identical to the lowest σ_{g}^+ vibrational frequency of the isoelectronic HC_{18}H molecule (Table 1). The observed vibronic bands of the NC_{16}N chain are due to the dipole-allowed $\text{B}^1\Sigma_{\text{u}}^+ \leftarrow \text{X}^1\Sigma_{\text{g}}^+$ electronic transition.

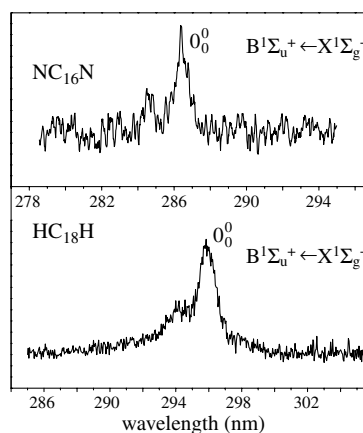


Fig. 1. Gas phase electronic spectrum of NC_{16}N detected by a resonant two-color two-photon ionization technique. The corresponding spectrum of the isoelectronic HC_{18}H molecule is given for comparison.

The oscillator strength of the $\text{B}^1\Sigma_{\text{u}}^+ \leftarrow \text{X}^1\Sigma_{\text{g}}^+$ system may be calculated using the formula $f = \frac{2}{3} \Delta E \times [R_{\ell\ell'}]^2$, where ΔE is the vertical transition energy (in Hartree) of the $\text{B}^1\Sigma_{\text{u}}^+ \leftarrow \text{X}^1\Sigma_{\text{g}}^+$ transition and $R_{\ell\ell'}$ is the transition dipole moment (in a.u.). For a single electron, by definition, the sum of all transitions yields a combined oscillator strength of unity. For an N -electron atom, the Thomas–Reiche–Kuhn rule states that the sum of oscillator strengths for all transitions is N [10]. Static electron correlation, which allows mixing of formal one-electron transitions, is responsible for oscillator strengths of individual transitions greater than unity but not greater than N . In many electron systems, the transition energy and transition moment values are often calculated without sufficiently accounting for the effects of dynamic electron correlation. Also, the basis sets implemented are designed to describe that part of the wavefunction of highest electron density. In the length formalism, the transition dipole moment calculation may suffer from the regions of the wavefunction far from the nuclei being described poorly (yet sufficiently well for calculation of energy). For the HC_{2n+1}H series [6] where the behavior of the oscillator strength was seen to be of great importance to astrophysics, the calculated f -value for a given (strong) transition was seen to vary by nearly a factor of two between CASSCF and MRCI levels of theory. The errors associated with both the calculated transition energy and transition moment values allow for calculated oscillator strengths much greater than expected. Such calculated values, while overestimated, indicate substantial *actual* oscillator strengths.

The calculated oscillator strength of the $\text{B}^1\Sigma_{\text{u}}^+ \leftarrow \text{X}^1\Sigma_{\text{g}}^+$ transition at the TD-DFT level of theory in the length formalism is ~ 7 . This may be compared to the value of ~ 9 taken from [9] (ZINDO). It has been shown

Table 1
Observed band maxima in the $\text{B}^1\Sigma_u^+ \leftarrow \text{X}^1\Sigma_g^+$ electronic transition of NC_{16}N and HC_{18}H

	λ (nm)	ν (cm^{-1})	$\Delta\nu$ (cm^{-1})	Assignment	T_0 (observed) (eV)	T_0 (calculated) (eV)	f_{cal}
NC_{16}N	286.4	34906(5)	0.0	0_0^0	4.33	3.717	7.1
	284.5	35115(5)	209(5)	$\nu(\sigma_g^+)$			
HC_{18}H	295.9	33784(5)	0.0	0_0^0	4.18	3.480	7.4
	294.1	33994(5)	210(5)	$\nu(\sigma_g^+)$			

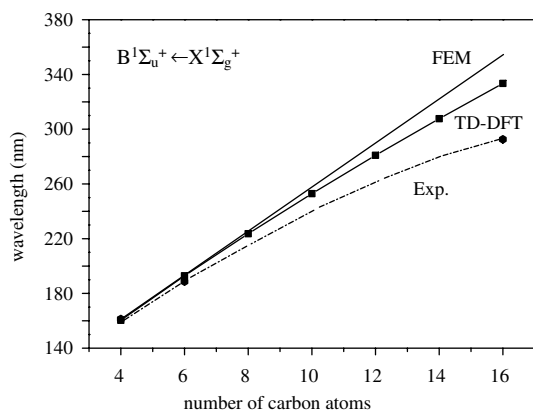


Fig. 2. The wavelength of the origin band in the $\text{B}^1\Sigma_u^+ \leftarrow \text{X}^1\Sigma_g^+$ transitions observed experimentally here and in [15], and predicted by TD-DFT theory and the free-electron model (FEM) as function of the length of carbon chains NC_{2n}N ($n = 2-8$).

that in some cases the value calculated within the gradient (momentum) formalism is more accurate [7]. In this case, the oscillator strength in the momentum formalism is ~ 5 . It has been suggested that as the formalisms should agree for an accurate wavefunction, a reasonable value can be obtained by taking the geometric mean of the two.

3.2. Electronic structure: size dependence of NC_{2n}N

3.2.1. HOMO–LUMO gap

The $\text{X}^1\Sigma_g^+$ ground state electronic configuration of NC_{16}N is dominated by the configuration $\dots [18\sigma_u]^2 [19\sigma_g]^2 [4\pi_g]^4 [5\pi_u]^4$. The HOMO is $5\pi_u$ and the LUMO is $5\pi_g$. Calculations of the HOMO–LUMO gap (Fig. 3) were carried out using the GAUSSIAN 98 suite of programs [11] at the hybrid density functional (B3LYP) level of theory [12] with Dunning's correlation consistent basis sets cc-pVDZ [13] in the optimized ground state geometries taken from [9]. The HOMO–LUMO gap is seen to decrease with increasing chain length, as expected, and the discrepancy between this value and the observed transition energies is seen to decrease (Fig. 4).

3.2.2. Band gaps

Calculations of vertical electronic excitation energies (band gaps) were undertaken using TD-DFT [14]. To a

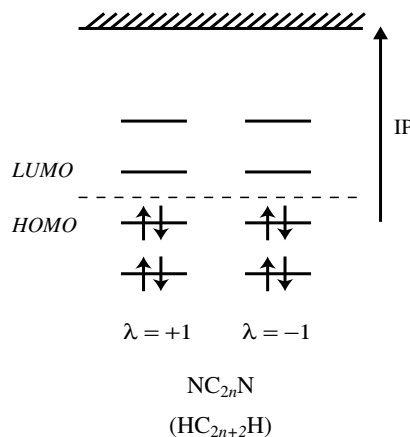


Fig. 3. An MO description of the electronic ground states of NC_{2n}N and HC_{2n+2}H . λ is the projection of orbital angular momentum onto the molecular axis. The Fermi level is indicated by the dotted line.

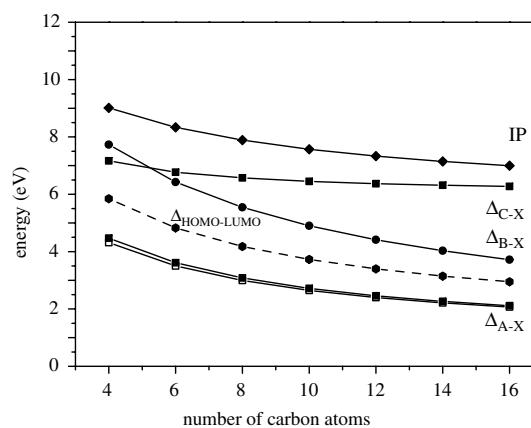


Fig. 4. The calculated HOMO–LUMO gap and the bands gaps Δ (electronic transition energies) as a function of the length of carbon chains NC_{2n}N ($n = 2-8$).

first approximation, the $\text{A}^1\Sigma_u^-$ and $\text{A}^1\Delta_u$ states of NC_{16}N , arise from the same configuration produced by excitation from $5\pi_u(x,y)$ to $5\pi_g(y,x)$. Excitation from $5\pi_u(x,y)$ to $5\pi_g(x,y)$ results in the $\text{B}^1\Sigma_u^+$ excited state. The $\text{C}^1\Pi_u$ state corresponds to $5\pi_u$ to $19\sigma_g$ electron promotion. The calculated band gaps, $\Delta_{\text{A-X}}$, $\Delta_{\text{B-X}}$ and

Δ_{C-X} , are shown in Fig. 4 as a function of the size of the carbon chains.

The band gaps Δ_{A-X} and Δ_{B-X} decrease with increasing chain size and should converge to $\Delta_{\text{HOMO-LUMO}}$ in the limit of long chains. However, the plots in Fig. 4 show that the convergence is very slow, as observed for the hydrogenated chains [4]. The chain NC_{16}N (~ 2 nm in length) is still far away from exhibiting bulk properties. In contrast, the band gap Δ_{C-X} converges to the IP of the chain rather than to $\Delta_{\text{HOMO-LUMO}}$. This is probably due to the electronic state $\text{C}^1\Pi_u$ being Rydberg in character as is the case for NC_4N [15].

For bare C_{2n} chains the bonding structures in the ground state were predicted to be of the cumulene type [16]. The calculated bond length alternation [9] in the ground state for the nitrogen terminated carbon chains highlights the important role of the end-capped nitrogen atoms. It has been pointed out that the very slow convergence to bulk is due to the slow decay of the bond length alternation induced by the symmetry and quantum effects of the terminal atoms [4]. Bond length alternation between single and triple carbon-carbon bonds is due to π -electron localization [5]. Ab initio calculations show that the alternation in the ground state of HC_{2n}H is more pronounced compared to that in excited state; in the latter, a cumulenic-like carbon skeleton is favored [8]. For example, the calculations for HC_6H indicate that the ratios of $\frac{r_{C-C}}{r_{C\equiv C}}$ are $\frac{1.3873 \text{ \AA}}{1.2105 \text{ \AA}} = 1.146$ for the $X^1\Sigma_g^+$ ground state, $\frac{1.2860 \text{ \AA}}{1.2580 \text{ \AA}} = 1.022$ for the $A^1\Sigma_u^-$ state and $\frac{1.3217 \text{ \AA}}{1.2474 \text{ \AA}} = 1.059$ for the $B^1\Sigma_u^+$ state, respectively. The structure changes from acetylene-like in the ground state to cumulene-like in the electronic excited states have been experimentally demonstrated by the observed dominant progression involving the $\text{C}\equiv\text{C}$ stretch vibrational motion in the $B^1\Sigma_u^+ \leftarrow X^1\Sigma_g^+$ transition system (see Fig. 2 of [5]). Other theoretical studies have also revealed that the hypothetical infinite polyene would have a structure of alternating shorter (triple) and longer (single) bonds in the ground state, and would be a semiconductor with orbitals of π symmetry around the Fermi level [17]. Experimental evidence for the alternation is found in the plot of the wavelengths of the origin bands of the $B^1\Sigma_u^+ \leftarrow X^1\Sigma_g^+$ transitions against the number of carbon atoms. This is not exactly linear as predicted by the free electron model (FEM, complete delocalization of π -electrons). The wavelength seemingly converges to a finite value in the long chain limit due to π -electron localization (Fig. 2). The similarity between the NC_{2n}N and HC_{2n}H series (see Fig. 3 of [5]) indicates that the dicyanopolyene nanowires in the ground state are semiconductors but could exhibit metallic characteristics in the excited electronic state.

4. Conclusion

The gas-phase $B^1\Sigma_u^+ \leftarrow X^1\Sigma_g^+$ electronic spectrum of NC_{16}N has been observed in a supersonic molecular beam. The 0_0^0 band position and nearby vibrational structure was observed to be extremely similar to the isoelectronic HC_{18}H molecule, indicating comparable electronic structure.

The electronic excited states of these chains were also calculated using time-dependent density-functional theory. The slow convergence of the band gap highlighted the important role of the end-capped nitrogen atoms which induce localization of the π -electrons in the ground state configuration, effectively the same as the effect of $-\text{CH}$ termination. The present studies indicate that a long carbon nanowire terminated with nitrogen should be a semiconductor in the ground state but exhibit metallic properties in the excited electronic states due to enhanced π -electron delocalization.

Acknowledgements

This work has been supported by the Swiss National Science Foundation (Grant 200020-100019) and the NCCR (Basel) on ‘Nanoscale Science’.

References

- [1] M. Springborg, J. Solid State Chem. 176 (2003) 311.
- [2] S. Iijima, Nature 354 (1991) 56.
- [3] H.F. Wittmann, R.H. Friend, M.S. Khan, J. Lewis, J. Chem. Phys. 101 (1994) 2693.
- [4] H. Ding, T.W. Schmidt, T. Pino, F. Güthe, J.P. Maier, Phys. Chem. Chem. Phys. 5 (2003) 4772.
- [5] T. Pino, H. Ding, F. Güthe, J.P. Maier, J. Chem. Phys. 114 (2001) 2208.
- [6] H. Ding, T.W. Schmidt, T. Pino, A.E. Boguslavskiy, F. Güthe, J.P. Maier, J. Chem. Phys. 119 (2003) 814.
- [7] A. Bilic, J.R. Reimers, N.S. Hush, J. Phys. Chem. B 106 (2002) 6740.
- [8] H. Ding, Spectroscopy of hydrogenated carbon clusters in the gas phase, PhD Thesis, University of Basel, 2003.
- [9] A. Scemama, P. Chaquin, M.-C. Gazeau, Y. Bénilan, J. Phys. Chem. A 106 (2002) 3828.
- [10] see for example E. Merzbacher, Quantum Mechanics, second edn., Wiley, New York, 1970, p. 458.
- [11] M.J. Frisch et al., GAUSSIAN 98, Revision A.7, Gaussian Inc., Pittsburgh, PA, 1998.
- [12] A.D. Becke, J. Chem. Phys. 98 (1993) 5648.
- [13] D.E. Woon, T.H.J. Dunning, J. Chem. Phys. 98 (1993) 1358.
- [14] R.E. Stratmann, G.E. Scuseria, M.J. Frisch, J. Chem. Phys. 109 (1998) 8218.
- [15] R.E. Connors, J.L. Roebber, K. Weiss, J. Chem. Phys. 60 (1974) 5011.
- [16] Q. Fan, G.V. Pfeiffer, Chem. Phys. Lett. 162 (1989) 472.
- [17] M. Springborg, J. Phys. C 19 (1986) 4473.

NEW LABORATORY DATA ON A MOLECULAR BAND AT 4429 Å

M. ARAKI, H. LINNARTZ,¹ P. KOLEK, H. DING, A. BOGUSLAVSKIY, A. DENISOV, T. W. SCHMIDT,
T. MOTYLEWSKI, P. CIAS, AND J. P. MAIERDepartment of Chemistry, University of Basel, Klingelbergstrasse 80, CH-4056 Basel, Switzerland; mitsunori.araki@unibas.ch,
linnartz@few.vu.nl, p.kolek@unibas.ch, hongbin.ding@unibas.ch, a.boguslav@unibas.ch, alexey.denisov@unibas.ch,
t.schmidt@chem.usyd.edu.au, t.motylewski@bfad.de, pawel@stan.chemie.unibas.ch, j.p.maier@unibas.ch

Received 2004 April 13; accepted 2004 July 30

ABSTRACT

New laboratory data are presented for the previously reported molecular absorption band at 4429 Å observed in a benzene plasma matching the strongest diffuse interstellar band (DIB) at 4428.9 Å. Gas-phase absorption spectra are presented for rotational temperatures of ~15 and 200 K. The observations indicate that it is unlikely that the laboratory band and the 4429 Å DIB are related. Eleven isomers of C₅H₅⁽⁺⁾ and C₆H₅⁽⁺⁾, both neutral and cationic, were considered as possible carriers of the laboratory band in view of the observed rotational profiles and deuterium isotope shifts. The experimental data and theoretical calculations (CASPT3, MRCI) indicate that the HCCHCHCH radical, a planar but nonlinear chain with one hydrogen on each carbon, is the most probable candidate causing the 4429 Å laboratory absorption.

Subject headings: ISM: lines and bands — ISM: molecules — line: identification — methods: laboratory — molecular data

1. INTRODUCTION

Recent progress with sensitive optical spectroscopic techniques allows the detection of gas-phase spectra of molecules that have been considered as potential carriers of diffuse interstellar bands (DIBs). The DIBs are observed as absorption features toward reddened stars (Herbig 1975). Up to now over 200 such features have been reported (Jenniskens & Désert 1994; Tuairisg et al. 2000), varying in width and intensity. It is a long-standing problem to explain their origin. Various forms of matter have been proposed, but none have resulted in an unambiguous assignment (Tielens & Snow 1995). The report in this journal (Ball et al. 2000) of a striking match between a laboratory band at 4429 Å measured through an expanding benzene plasma and the strongest DIB, centered at 4428.9(1.4) Å, has attracted attention, initiating a discussion on whether radical fragments of aromatic rings might be present in the diffuse interstellar medium (Thaddeus & McCarthy 2001).

In their thorough spectroscopic study of a hydrocarbon plasma, Ball et al. find a strong molecular band at 4429.27(4) Å consisting of an unresolved *P*-, an unresolved *Q*-, and an unresolved *R*-branch, matching in wavelength to a few parts in 10⁴ the 4429 DIB. They conclude from partial and complete deuteration of the precursor gas benzene that the laboratory carrier is a hydrocarbon of the form C_nH₅⁽⁺⁾ with two pairs of equivalent hydrogen atoms plus a single hydrogen. They discuss a series of possible radicals and propose as most likely candidates the quasi-linear benzene fragments C₃H₅⁺ and C₅H₅, for which optical data have not been reported.

While the match in wavelength between the laboratory and astronomical spectra is striking, there is no agreement in their line widths; the 4429 DIB feature is about 17 times wider than the band observed in the jet. In two recent studies of the intrinsic profile of the 4429 DIB (Snow 2002; Snow et al. 2002), the lack of fine structure is attributed to an electronic transition of a

gaseous molecule with the upper state undergoing a rapid internal conversion, or alternatively a system consisting of overlapping rotational lines. The first explanation implies that the laboratory and astronomical spectra are identical both in wavelength and in line width, which is not the case. The second explanation leaves space for the proposition by Ball et al. that the mismatch in line width may be due to a substantial difference in rotational temperature of the carrier in a supersonic beam (a few K), where collisional cooling is the main relaxation mechanism, and in interstellar space (a few hundred K), where radiative cooling might be very inefficient for weakly polar species. Hence measuring the same spectrum at different temperatures will give additional information on the astrophysical relevance of the 4429 Å molecular band. Moreover, the discussion will benefit from the identification of the carrier of the laboratory spectrum.

2. EXPERIMENT

The results of two complementary laboratory experiments are described. The first is similar to that reported by Ball et al. (2000); the 4429 Å band has been recorded through a benzene plasma generated in a planar supersonic jet at rotational temperatures of 15–40 K. In the second a hollow cathode discharge cell is used instead, resulting in a substantially higher rotational temperature of about 200 K. In both experiments, cavity ring-down (CRD) spectroscopy is used as a sensitive detection technique to observe signals in direct absorption (O’Keefe & Deacon 1988). Very long absorption path lengths are obtained by confining the light tens of microseconds in the cavity.

In the first experiment a cooled planar plasma is generated by applying a 500 μs voltage pulse (–700 to –900 V) to a 1 ms gas pulse of a 0.3% C₆H₆/Ar (C₆D₆/Ar) mixture that is expanded through a 3 cm × 300 μm slit with a backing pressure of about 10 bars. This setup has been used in the study of over 20 hydrocarbon radicals and cations up to now (see, e.g., Motylewski et al. 2000) and combines high molecular densities with an effective adiabatic cooling. The resolution is increased

¹ Current address: Laser Centre and Department of Physical Chemistry, De Boelelaan 1083, NL-1081 HV, Amsterdam, Netherlands.

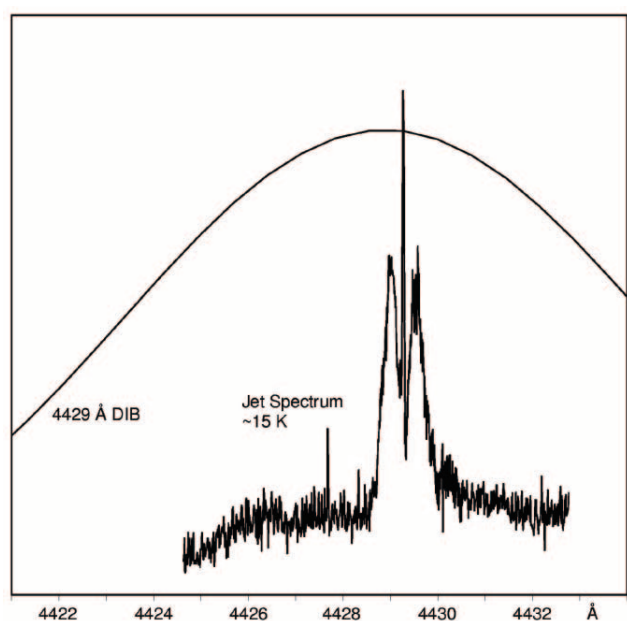


FIG. 1.—The 4429 Å absorption band observed through a planar benzene plasma expansion using a CRD approach. The band coincides in wavelength with the 4429 Å DIB (taken from Jenniskens & Désert 1994 as shown in part above), but the line widths of the laboratory and astronomical spectra differ significantly.

compared to pinhole expansions as used by Ball et al. (2000) because of reduced Doppler broadening parallel to the slit that allows spectroscopy at the limit of the laser resolution. Rotational temperatures are slightly higher, typically 15–40 K.

A much warmer plasma is obtained in the second experiment by applying a 500 μ s voltage pulse (–1000 V) to gas mixtures identical to those used in the jet, but in an 84 cm long hollow cathode discharge cell, running at a pressure of a few mbar. The spectroscopy is not Doppler-free, and with liquid nitrogen cooling, rotational temperatures are typically 150–200 K (Kotterer et al. 1996).

3. RESULTS AND DISCUSSION

3.1. Comparison between the 4429 Å DIB and Laboratory Bands

Figure 1 shows the CRD spectrum obtained through the supersonic planar plasma. Although the signal-to-noise ratio is good, no rotational structure is observed that could provide structural information that is necessary to identify the carrier. This indicates either that the separation between adjacent lines is smaller than 0.03 cm^{-1} or that a lifetime broadening exists. The absorption profile is in the middle of the strong 4429 Å DIB as seen from the synthetic spectrum shown in Figure 1. As discussed by Ball et al. (2000), there is a clear difference in spectral width of both features, and this has to be explained before a correlation between the laboratory and astronomical spectra can be established. Ball et al. correctly argue that for the proposed nearly symmetric prolate top molecules, a spectrum consisting of a *P*-, a *Q*-, and an *R*-branch is expected similar to the one observed, under the explicit condition that only the lowest *K* ladder in the ground state is populated. The many subbands from the higher *K* ladders of the ground state may fill out the contour at higher temperatures, causing the observed spectrum to broaden symmetrically, as observed recently for the nonlinear carbon chain C_6H_4^+ (Araki et al.

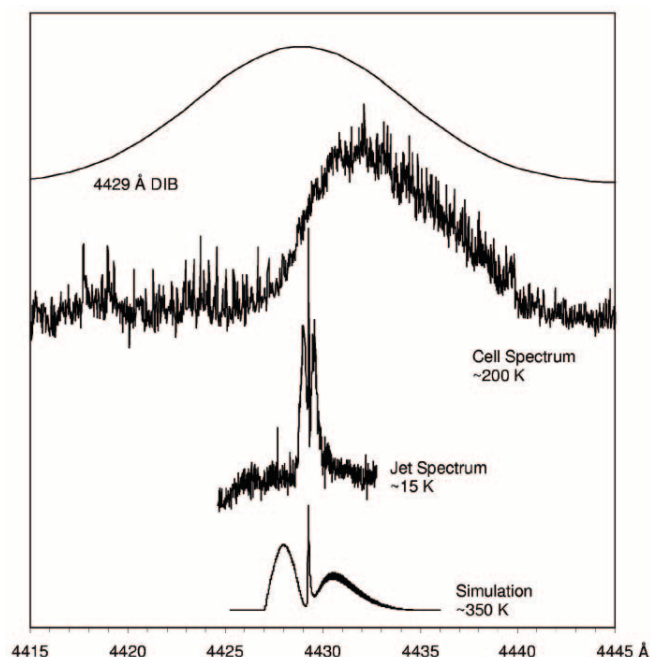


FIG. 2.—The 4429 Å absorption band measured in a jet and liquid nitrogen cooled hollow cathode discharge cell and compared to the 4429 Å DIB (taken from Jenniskens & Désert 1994). At the higher temperature a clear broadening is observed. A simulated rotational profile at 350 K, using the same constants as in Fig. 3, is clearly different from the observed cell spectrum.

2003). Therefore the same spectrum was recorded under warmer conditions than in the jet expansion. Decreasing the backing pressure, increasing the benzene/mixing ratio, measuring closer to the jet, and using higher discharge voltages generally increases the rotational temperature from 15 to 30–40 K. Indeed, we observed a small shift in the Boltzmann maximum to higher *J*-values, but no broadening could be observed. Consequently, a cell discharge was then used to obtain a much higher temperature.

In Figure 2 the absorption spectrum recorded in a liquid nitrogen cooled hollow cathode cell is shown. The rotational temperature under these conditions is about 200 K. A band broadened asymmetrically to the red is now observed (Fig. 2, with the jet spectrum shown as a reference). Such a broadening is typical for a hot-band progression and quite possible at the high ambient temperatures in the cell. Nevertheless, the spectrum does not fill up the 4429 Å DIB. In order to be sure that the cell and jet spectra are due to the same carrier, the experiment was repeated with fully deuterated benzene as precursor; the absorption feature shifts $123(1) \text{ cm}^{-1}$ to higher energy, which is identical to the shift observed in the jet study: 122.8 cm^{-1} (Ball et al. 2000). These observations seem to indicate that the laboratory band and the 4429 Å DIB originate from different carriers.

In order to compare the laboratory and astronomical spectra it would be helpful to know more about the vibrational temperature (T_{vib}) in the cell plasma, but without the detection of a resolved transition from a vibrationally excited level in the ground state it is hard to determine this value. Generally, vibrational temperatures in a cooled cell discharge vary from a few hundred to a thousand kelvins according to similar discharge systems (Zelinger et al. 2003; Greenberg & Hargis 1990). The determination of rotational temperatures (T_{rot}), e.g., 200 K for N_2^+ (Kotterer et al. 1996) and 500–600 K for D_3O^+ (Araki et al. 1999) put a lower limit to T_{vib} . Such values are indeed

sufficiently high to excite low-frequency vibrational modes in molecules the size of C_5H_5 . A broadening due to a series of hot-band progressions is therefore reasonable to assume.

On the other hand, in the plasma jet expansion such bands are not expected. It has been shown that these low rotational temperatures at high vibrational temperatures are obtained for small (diatomic) molecules (Bazalgette Courrèges-Lacoste et al. 2001), but for larger species with smaller vibrational spacings, rotational and vibrational temperatures will be more similar. As a consequence, hot-band progressions are not observed. Nevertheless, because the cooling and heating mechanisms in space are completely different from those in the laboratory, care has to be taken when comparing the CRD spectrum with the 4429 Å DIB.

3.2. Comparison between the 4429 Å DIB and the Simulated Spectrum

We have made a substantial effort to identify the carrier of the laboratory band by combining experimental and theoretical information. The 4429 Å absorption band has been reproduced using the program WANG (Luckhaus & Quack 1989). It is found that an “*a*-type transition” of a nearly prolate top with rotational constants $A \sim 1$ and $B \approx C \sim 0.1 \text{ cm}^{-1}$ reproduces the observed spectrum under the assumption that the molecular geometry change upon electronic excitation is small and that differences of rotational constants in the two electronic states are less than 1%. A simulated spectrum for 15 K is shown in Figure 3. For B and C values larger than 0.1 cm^{-1} , a resolved rotational profile is expected, which is not the observation. As a consequence, molecules with less than five carbon atoms are not considered. Furthermore, the production of molecules with more than six carbon atoms or with a four-membered ring is not favored in the benzene discharge. Additional information is available from the observation of deuterium isotope shifts by Ball et al. (2000) that indicates that the carrier contains five hydrogen atoms, including two pairs of equivalent ones. These considerations result in 11 isomers of $C_5H_5^{(+)}$ and $C_6H_5^{(+)}$ (Fig. 4), both neutral and cationic, as the most probable carriers of the laboratory spectrum. Anions are not considered since their production is not favored under the conditions used in the CRD experiment.

We have simulated the profile with $T_{\text{rot}} = 350 \text{ K}$ (Fig. 2). This indicates that our cell spectrum cannot be reproduced by a rotational profile of the origin-band alone. This is consistent with the proposed explanation that the cell spectrum is the result of overlap of such rotational profiles for various vibrational hot-band transitions. Furthermore, the simulation at $T_{\text{rot}} = 350 \text{ K}$ indicates the profile of the 4429 Å DIB cannot be reproduced by a rotational profile of the origin-band alone. In the jet spectrum the intensity of the *R*-branch is stronger than that of *P*, because the ground-state rotational constant $(B + C)/2$ is larger than in the excited state. At high temperatures the intensity difference between the *R*- and *P*-branches increases and the rotational profile becomes asymmetric, although the 4429 Å DIB has a symmetric Lorentzian profile (Snow et al. 2002).

As vibrational frequencies in excited electronic states are generally lower than in the ground state, the hot-band transitions are usually to the red of the origin band. This is as seen in the cell spectrum at $T_{\text{vib}} = 200 \text{ K}$, where the profile extends asymmetrically to the red. Thus it does not seem realistic that the profile to the blue of the origin band could be filled by hot-band transitions even at very high values of T_{vib} . Our conclusion is that the laboratory band and the 4429 Å DIB are unlikely to originate from the same carrier.

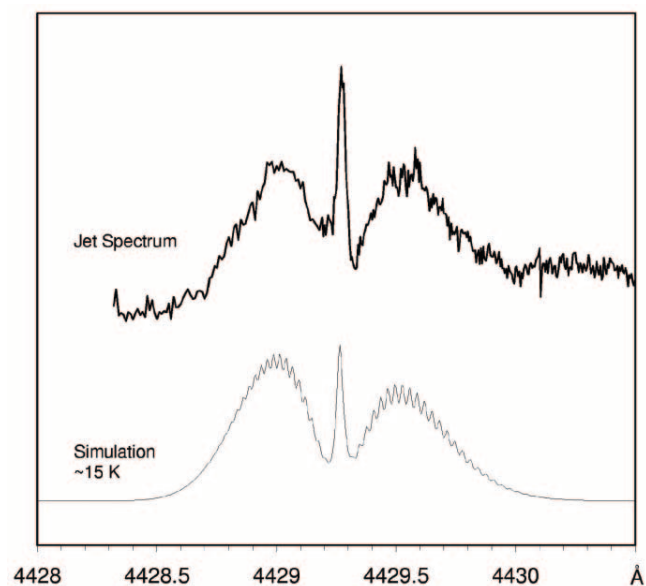


FIG. 3.—Simulated *a*-type rotational profile of the 4429 Å electronic transition for a prolate molecule at 15 K compared to the laboratory absorption spectrum.

3.3. Identification of the 4429 Å Laboratory Band

Calculations of vertical excitation energies and transition moments were carried out for various C_5H_5 and C_6H_5 species (Fig. 4) using the TD-DFT (B3LYP) method with the Gaussian program (Frisch et al. 2003). For selected molecules, higher accuracy excitation energies (vertical and adiabatic) and rotational constants in the ground and excited states were computed with the CASSCF, CASPT3, and MRCI methods, with the MOLPRO 2002.3 package (Werner & Knowles 2003); see Appendix for the computational details. The cc-pVDZ basis set was used in all calculations.

The electronic transition must fulfill four conditions for the molecule to be regarded as a possible carrier for the laboratory band: (1) it must have excitation energy close to the experimental value of 2.80 eV, (2) it must have a nonzero oscillator strength, (3) the transition dipole moment must be predominantly along the *a*-axis ($|\mu_a| \gg |\mu_b|$ and $|\mu_a| \gg |\mu_c|$), and (4) it must have small differences of rotational constants between the ground and excited states. At the TD-DFT stage of calculations, a vertical excitation energy around 2.8–3.1 eV is required. Conditions 1–3 are fulfilled by the neutral radical $5a^N$ and the cation $5b^+$, but they are not fulfilled by any of the C_6H_5 species, either neutral or cationic (Table 1). The TD-DFT method was found useful because it gives vertical excitation energies with a reasonable accuracy (including dynamical correlation) at relatively low computational cost. However, this method is not applicable for $5d$ and $5e$ because of the complicated electronic structures (§ A2). CASSCF calculations for the $5d$ species [doublet $5d^N(D)$ and quartet $5d^N(Q)$ for neutral and singlet $5d^+(S)$ and triplet $5d^+(T)$ for cation] are presented in the Appendix. Calculated electronic structures and spectroscopic parameters of $5d$ and $5e$ are almost the same.

In order to judge whether the carrier of the 4429 Å band is a neutral or a cation, an additional experiment has been carried out. In this the 4429 Å transition was searched for in a benzene plasma with a resonant two-color two-photon ionization (R2C2PI) approach (Ding et al. 2003), capable of measuring the masses of the neutral radicals selectively. The discharge systems used in the R2C2PI and CRD setups are

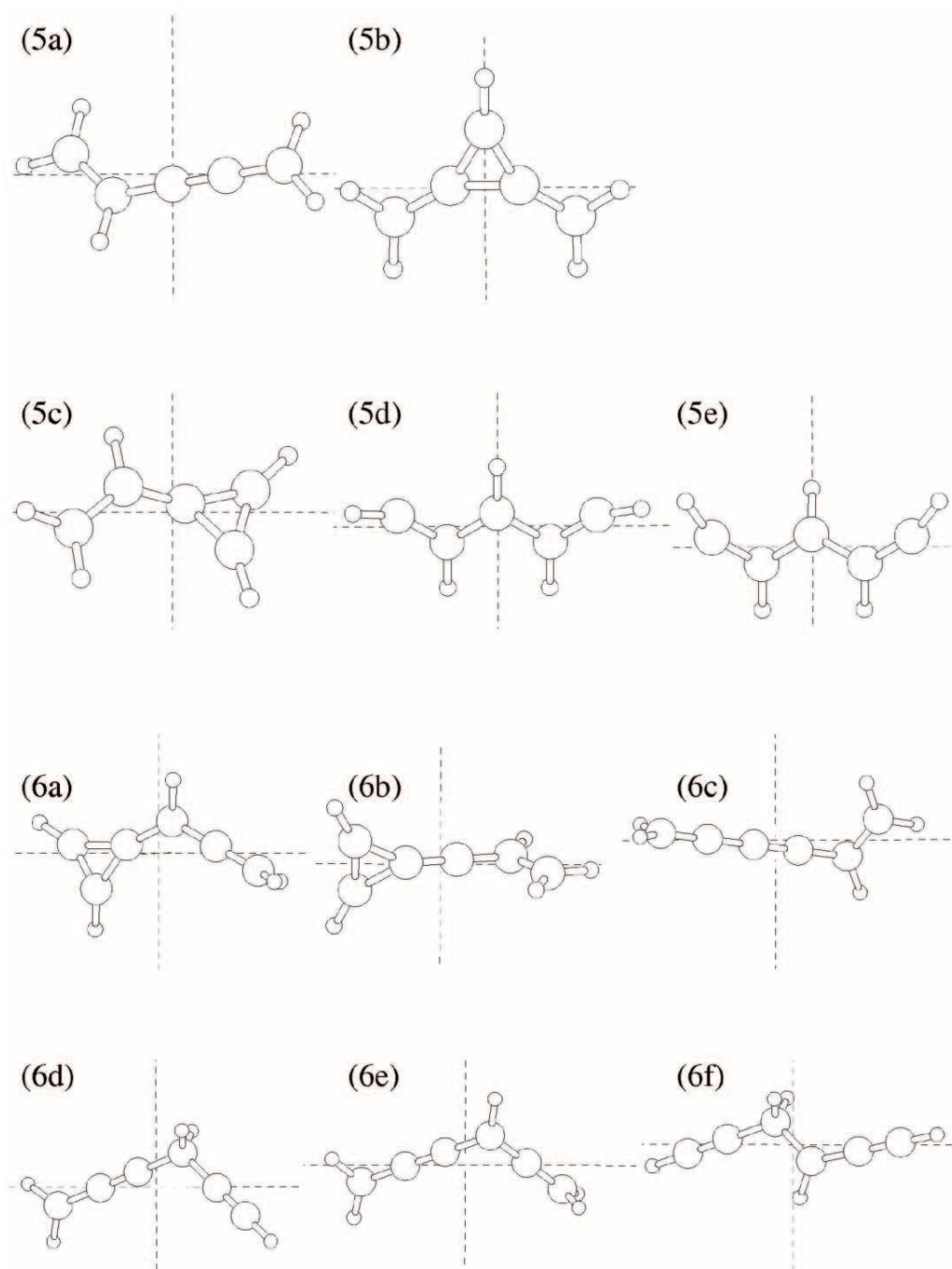


FIG. 4.—Eleven possible C_5H_5 and C_6H_5 isomers with two pairs of equivalent hydrogen atoms and a prolate structure. The horizontal dashed line indicates the a -axis, the vertical one the b -axis; the c -axis is perpendicular to the plane formed by a and b .

comparable, and experiments have been performed using similar conditions. A 0.4% C_6H_6/Ar mixture (backing pressure 5 bars) was discharged between two stainless steel electrodes mounted in the ceramic body of a pinhole source. The excitation laser was scanned around 4429 Å, and intense radiation from an F_2 laser (157 nm) or Nd:YAG (212.5 nm) was used for the ionization. Neutral species with an ionization potential of less than 10.7 eV are detected in this way. All species with a mass of less than 200 amu have been monitored simultaneously.

A weak band of neutral C_5H_5 was observed at 4435 Å, but no band at 4429 Å could be seen (Fig. 5). This suggests

that the carrier of the 4429 Å laboratory band either is a charged species, or a neutral one with an ionization potential higher than 10.7 eV, or has a very short upper electronic state lifetime. It is also possible that the species is destroyed by chemical reactions before reaching the mass spectrometer because in the R2C2PI experiment the molecular beam is probed 30 cm downstream, but only 2 mm downstream in the CRD experiment.

The profiles of the 4429 Å CRD absorption (Fig. 1) and the R2C2PI C_5H_5 band (Fig. 5) are similar, indicating that the molecules probably have similar geometries. The R2C2PI band can be reproduced by a simulation of the rotational profile based

TABLE 1
 VERTICAL ELECTRONIC TRANSITIONS OF C₅H₅ AND C₆H₅ CALCULATED USING TD-DFT METHOD

ISOMER ^a	NEUTRAL					CATION				
	ΔE^b (eV)	f^c	Transition Moment (D)			ΔE^b (eV)	f^c	Transition Moment (D)		
			μ_a	μ_b	μ_c			μ_a	μ_b	μ_c
5a.....	2.93	0.000	0.000	0.000	0.012	2.36	0.000	0.000	0.000	0.022
	2.98 ^d	0.003	-0.514	-0.016	0.000	4.37	0.498	5.475	0.281	0.000
5b.....	2.22	0.073	2.948	0.000	0.000	3.09 ^d	0.190	-4.032	0.106	0.000
	3.86	0.000	0.000	0.000	-0.065	3.36	0.000	0.000	0.000	-0.105
5c.....	1.57	0.002	-0.097	0.576	0.000	5.62	0.102	-1.861	-1.145	0.000
	3.94	0.001	0.065	-0.272	0.000	5.86	0.391	-4.071	-1.019	0.000
6a.....	1.35	0.002	0.260	0.557	0.000	4.05	0.000	0.000	0.000	-0.007
	2.72	0.000	0.000	0.000	-0.004	5.35	0.000	0.001	0.000	0.007
6b.....	2.34	0.000	0.000	-0.019	0.000	1.89	0.000	0.000	0.027	0.000
	2.93	0.000	-0.008	0.000	-0.069	5.03	0.430	4.692	0.000	-0.729
6c.....	2.38	0.000	-0.002	0.000	-0.008	2.05	0.000	0.008	-0.002	-0.014
	2.70	0.000	0.002	-0.001	0.017	4.07	0.245	3.943	-0.568	0.000
6d.....	3.15	0.000	0.000	-0.001	0.036	1.39	0.000	0.002	0.001	0.121
	4.16	0.041	-1.547	0.483	0.000	1.72	0.068	3.226	-0.004	-0.001
6e.....	3.05	0.000	0.001	0.000	-0.001	2.56	0.000	0.000	0.000	0.005
	3.07	0.001	0.271	-0.184	0.000	2.98	0.000	0.000	0.000	-0.045
6f.....	3.35	0.000	0.000	0.000	-0.004	1.40	0.000	0.007	-0.002	-0.124
	4.02	0.028	-1.353	-0.081	0.000	1.73	0.070	3.235	-0.379	0.001

NOTE.—B3LYP hybrid functional and the cc-pVDZ basis set were used.

^a See Fig. 4.

^b The observed adiabatic transition energy is 2.80 eV (=4429 Å).

^c Oscillator strength.

^d For higher level calculations see Tables 2 and 3.

on the assumptions that the transition is *a*-type and that the carrier is a nearly prolate C₅H₅ molecule at 7 K, a typical temperature of the molecules produced in this apparatus. Simulation at 15 K with the same molecular constants can reproduce the profile of the 4429 Å CRD band. Thus it appears that both the carrier of the 4429 Å CRD and the 4435 Å resonance-

enhanced multiphoton ionization (REMPI) band have five carbon atoms, but are different isomers.

The 5*e* isomer cannot convert to cyclic pentadienyl radical as easily as 5*d* because additional cis-trans isomerizations are difficult. The isomer does not decay as fast and may be one of the possible candidates for the REMPI band. For the same reason production of 5*d* should be favored and a larger abundance of this isomer could be expected immediately after the discharge through benzene. Therefore 5*d* would be a better candidate for the carrier of the CRD band.

Higher level theoretical calculations were carried out for the 5*a*^N, 5*b*⁺, 5*d*^N(*D*), 5*d*^N(*Q*), 5*d*⁺(*T*), 5*e*^N(*D*), 5*e*^N(*Q*), and 5*e*⁺(*T*) species with the CASPT3 (Werner 1996; Celani & Werner 2000) and MRCI methods (Werner & Knowles 1988; Knowles & Werner 1988). The 5*d*⁺(*S*) and 5*e*⁺(*S*) isomers were not considered at this stage because the CASSCF results indicate too-high excitation energies of 4.6 eV for the lowest *a*-type transitions (see § A1). The active space, including seven orbitals (five π -orbitals perpendicular to the molecular plane, and two in-plane orbitals), was used with seven electrons for a neutral radical and six for a cation. The vertical and adiabatic transition energies are given in Table 2. The transitions $2^2A_2 \leftarrow 2^2B_1$ of 5*d*^N(*D*) and $3^3A_1 \leftarrow 3^3B_2$ of 5*d*⁺(*T*) (both in C_{2v} symmetry) have adiabatic excitation energies of 2.72 and 2.75 eV, respectively, at the CASPT3 level of theory, which are close to the experimental value of 2.80 eV. The same transitions of 5*e*^N(*D*) are 0.02 eV lower than those of 5*d*^N(*D*) (CASPT3). This is an additional reason for the assignment of the 4429 Å CRD band. The smallest differences between vertical and adiabatic excitation energies predicted for 5*d*^N(*D*), 5*e*^N(*D*), 5*d*⁺(*T*), and 5*e*⁺(*T*) are consistent with the analysis of the rotational profile and may suggest a small geometry change upon electronic excitation. We searched for a transition up to 2400 cm⁻¹ to the blue

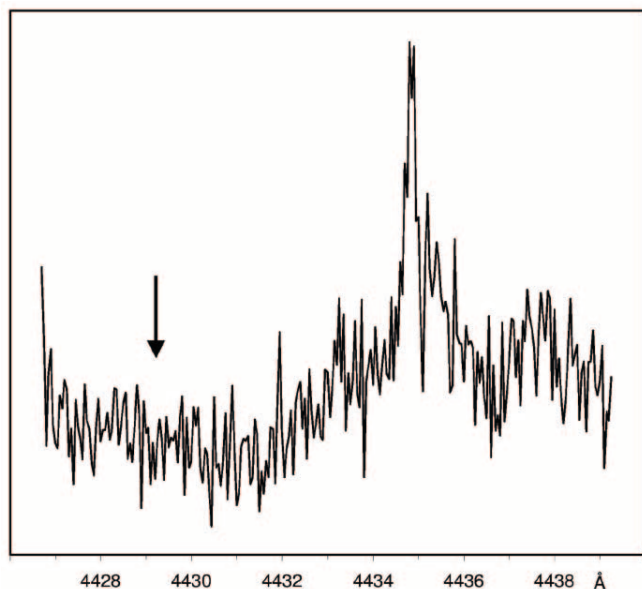


FIG. 5.—Absorption spectrum recorded through a benzene plasma at mass 65 amu (C₅H₅) in the 4429 Å region using a two-laser photon excitation scheme. A 2125 Å laser was used for the ionization step. The 4435 Å band detected has a profile similar to that of the 4429 Å band in the CRD spectrum of Fig. 1. Position of the 4429 Å band in the CRD spectrum is indicated by the arrow.

TABLE 2
ELECTRONIC TRANSITION ENERGY CALCULATED AT THE MRCI AND CASPT3 LEVEL OF THEORY FOR THE A-TYPE TRANSITION

Isomer ^a	Transition	Method	Adiabatic ^b (eV)	Vertical (eV)	(Vertical) – (Adiabatic) (eV)
Observed	2.80
$5a^N$	$2A''-2A''$	CASPT3	2.39	2.64	0.25
	...	MRCI	2.42	2.69	0.27
	...	MRCI+D	2.40	2.66	0.26
$5d^N(D)$	$2^2A_2-2B_1$	CASPT3	2.72	2.87	0.15
	...	MRCI	2.68	2.84	0.16
	...	MRCI+D	2.65	2.84	0.19
$5d^N(Q)$	$4B_1-4A_2$	CASPT3	2.62	2.84	0.22
	...	MRCI	2.61	2.83	0.22
	...	MRCI+D	2.62	2.84	0.22
$5d^+(T)$	$3A_1-3B_2$	CASPT3	2.75	2.93	0.18
	...	MRCI	2.86	3.06	0.20
	...	MRCI+D	2.81	2.98	0.17
$5e^N(D)$	$2^2A_2-2B_1$	CASPT3	2.70	2.87	0.17
	...	MRCI	2.64	2.81	0.17
	...	MRCI+D	2.62	2.81	0.21
$5e^N(Q)$	$4B_1-4A_2$	CASPT3	2.63	2.85	0.22
	...	MRCI	2.63	2.85	0.22
	...	MRCI+D	2.63	2.86	0.23
$5e^+(T)$	$3A_1-3B_2$	CASPT3	2.72	2.89	0.17
	...	MRCI	2.82	2.97	0.15
	...	MRCI+D	2.78	2.95	0.17
$5b^+$	$1B_2-1A_1$	CASPT3	3.06	3.39	0.33
	...	MRCI	3.20	3.51	0.31
	...	MRCI+D	3.02	3.31	0.29

NOTE.—The geometries are optimized at the CASPT3 level of theory. For computational details see Appendix.

^a See Fig. 4.

^b Adiabatic transition energies without zero vibrational level correction.

of the 4429 Å band using the CRD spectrometer. However, no band that would correspond to vibrational excitation in the upper electronic state was observed in this region either by us or in the study of Ball et al. (2000). Thus the origin band dominates the transition, and the geometry change appears to be small.

Rotational constants in the ground and excited states were calculated at the CASPT3 level of theory by numerical geometry optimization and are given in Table 3. The simulation of the rotational profile of the 4429 Å band suggests that the rotational constants change less than 1% between the two states. The calculated differences in the cases of $5d^N(D)$, $5e^N(D)$ and $5d^N(Q)$, $5e^+(T)$ agree with the simulation within the errors, and the

values of ΔA in the cases of $5a^N$, $5b^+$, $5d^+(T)$, and $5e^+(T)$ are too large.

Good agreement with the experimental data of the 4429 Å CRD band is predicted for the $2^2A_2 \leftarrow 2B_1$ transitions of $5d^N(D)$ and $5e^N(D)$, although it is slightly better for the first one with all considered criteria. From the candidates discussed we conclude that the $5d^N(D)$ isomer, “planar W structure” with five carbons in C_{2v} symmetry (Fig. 4), a doublet radical, is the most likely carrier of the 4429 Å laboratory band.

This work has been supported by the Swiss National Science Foundation (project 200020-100019).

TABLE 3
ROTATIONAL CONSTANTS CALCULATED AT THE CASPT3 LEVEL OF THEORY

Isomer ^a	Transition	A (cm ⁻¹)	B (cm ⁻¹)	C (cm ⁻¹)	ΔA^b (%)	ΔB^b (%)	ΔC^b (%)
$5a^N$	$2A''-2A''$	1.235	0.0742	0.0700	-16	1	0
$5d^N(D)$	$2^2A_2-2B_1$	1.381	0.0792	0.0749	-5	-2	-2
$5d^N(Q)$	$4B_1-4A_2$	1.378	0.0793	0.0750	-4	-3	-3
$5d^+(T)$	$3A_1-3B_2$	1.201	0.0828	0.0775	11	-4	-5
$5e^N(D)$	$2^2A_2-2B_1$	1.079	0.0827	0.0768	-4	-2	-2
$5e^N(Q)$	$4B_1-4A_2$	1.082	0.0827	0.0768	-4	-2	-2
$5e^+(T)$	$3A_1-3B_2$	0.963	0.0865	0.0794	13	-6	-4
$5b^+$	$1B_2-1A_1$	0.452	0.1288	0.1003	-21	2	11

NOTE.—For computational details see Appendix. Rotational constants A , B , and C are in the ground state.

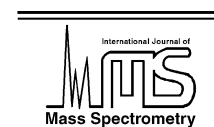
^a See Fig. 4.

^b Differences of rotational constants between the ground and excited states.

Available online at www.sciencedirect.com

SCIENCE @ DIRECT®

International Journal of Mass Spectrometry 233 (2004) 131–136

www.elsevier.com/locate/ijms

Sulfur terminated nanowires in the gas phase: laser spectroscopy and mass spectrometry

A. Denisov, T.W. Schmidt, A.E. Boguslavskiy, H. Ding, M. Araki, J.P. Maier*

Department of Chemistry, University of Basel, Klingelbergstrasse 80, CH-4056 Basel, Switzerland

Received 28 September 2003; accepted 19 December 2003

Dedicated to Prof. Tilmann Märk on the occasion of his 60th birthday.

Abstract

The products of a CS₂-hydrocarbon discharge are elucidated through a combination of mass spectrometry and laser spectroscopy. Sulfur containing species are identified and their structures proposed using spectroscopic considerations. The resonant 2-color 2-photon ionization A²Π ← X²Π spectrum of HC₆S is presented, confirming previous non-mass selective identification. The origin band of the A²Π ← X²Π transitions of HC₈S and HC₁₀S were measured at 14838.4(1) and 13333.7(5) cm⁻¹ by cavity ringdown spectroscopy. The near linear relationship of absorption wavelength and chain length characterizes these species as molecular nanowires exhibiting cumulenic bonding. From these data HC₁₂S is estimated to absorb at 820 ± 5 nm.

© 2004 Elsevier B.V. All rights reserved.

Keywords: Discharge; Optical spectroscopy; Carbon chains; Diffuse interstellar bands; Sulfur; Nanowires

1. Introduction

Sulfur-bearing conjugated carbon systems are of interest to many fields of scientific enquiry ranging from molecular electronics to astrophysics. As molecular electronic devices they are invoked due to the propensity of the sulfur terminal to bond to a gold surface [1]. Single sulfur-bearing conjugated molecules have been placed between gold electrodes with voltages applied between them, thereby allowing the measurement of current passing through a single molecule [2]. The current–voltage characteristics observed depends critically upon the electronic structure of the bridging sulfur-bearing conjugated carbon system [3].

It is known that sulfur plays an important part in the chemistry of the interstellar medium [4]. Sulfur-bearing carbon chains such as C₃S and C₅S have been discovered in space by rotational spectroscopy [5–7]. Sulfur heteroatoms terminating carbon chains cause strong polarization of the π-electron cloud and increases the oscillator strength of its electronic transitions. As such, despite the lower abundance of sulfur in the interstellar medium as compared to carbon,

the sulfur terminated carbon chains can absorb strongly and may be considered as candidate carriers of the diffuse interstellar bands. Confirmation as carriers of diffuse interstellar bands can only come from a direct comparison with gas-phase optical laboratory spectra. As sulfur-bearing carbon chains such as C_nS and HC_nS are radicals, they must be produced as transient species. This is usually performed with a sulfur-seeded hydrocarbon discharge.

Such discharges have been utilized to produce laser-induced fluorescence spectra of the transient species HC_{2n}S (*n* = 1–3) and the SCCS⁻ anion [8–11], and pure rotational spectra of HC_nS (*n* = 2–8) [12,13] and C_nS (*n* = 4–9) [14]. Despite the importance of this discharge system for the production of sulfur-bearing species relevant to astrophysics, it has never been studied by a mass-selective technique.

The paper is arranged as follows. The CS₂/C₄H₂ discharge is analyzed by time-of-flight (TOF) mass spectrometry. The sulfur-bearing species are identified and structures are proposed. Mass-selective resonant 2-colour 2-photon ionization (R2C2PI) spectroscopy is used to confirm the previous assignment of the optical spectrum of HC₆S by laser-induced fluorescence spectroscopy [10]. The origin bands of HC₈S and HC₁₀S and their deuterated analogs are presented for the first time, measured by cavity ringdown spectroscopy (CRDS). The results obtained by various techniques are

* Corresponding author. Tel.: +41-61-267-38-07;

fax: +41-61-267-38-55

E-mail address: j.p.maier@unibas.ch (J.P. Maier).

combined to provide a diagnosis of the chemistry taking place in the $\text{CS}_2/\text{C}_4\text{H}_2$ discharge.

2. Experiment

2.1. R2C2PI TOF spectroscopy

The R2C2PI TOF experimental set-up has been described elsewhere [15]. It consisted of a molecular beam coupled to a linear TOF mass analyzer. The source used to produce sulfur-bearing carbon chains was a pulsed valve coupled to an electric discharge. A gas mixture pulse of 0.5% of butadiyne (HCCCCH) in Ar (backing pressure 8 bar) was passed through an ice-cooled reservoir of CS_2 and subsequently expanded through the ceramic body of the source. A high voltage pulse (600–900 V) from a home-built pulse generator was applied between the electrodes placed either side of the ceramic spacer. The emerging beam entered the ionization region through a 2 mm skimmer. The neutral molecules were then ionized and the ions extracted in a two-stage acceleration setup towards a multichannel plate detector. The signal from the detector was fed into an oscilloscope after pre-amplification and transferred to a computer.

R2C2PI spectra were recorded in the near UV and visible range. Excitation photons in the UV range came from the frequency doubled output of a dye laser (bandwidth $\sim 0.1 \text{ cm}^{-1}$) pumped by the second harmonic of a Nd:YAG laser. Visible photons were produced by an excimer pumped dye laser. The ionizing photons at 157 nm were produced by an F_2 excimer laser with the energy of a few mJ/pulse. Photons of wavelength 193 nm were produced by an ArF excimer laser with pulse energies of 100 mJ. The excitation laser was anticollinear while the excimer laser was perpendicular to the molecular beam. Since the laser beams were unfocused, multiphoton transitions were not expected.

2.2. CRD spectroscopy

The experiment is composed of a cavity ringdown (CRD) spectrometer sampling a supersonic planar plasma. The plasma was generated by a discharge through a gas pulse (–600 V, 30 Hz repetition rate) of a premixed precursor gas passing through a $3 \text{ cm} \times 300 \mu\text{m}$ multilayer slit nozzle (backing pressure 10 bar). For production of HC_8S (DC_8S) a 0.5% C_2H_2 (and/or C_2D_2) with 0.1% CS_2 mixture in argon was used while for production of HC_{10}S (DC_{10}S), C_2H_2 was substituted by 0.4% C_4H_2 (and/or C_4D_2). Rotational temperatures of the order of 20–40 K were routinely achieved. The nozzle was mounted in an optical cavity where the expansion was intersected approximately 2 mm downstream by the pulsed beam of a tunable dye laser (resolution 0.15 cm^{-1}). The light leaking out of the cavity was detected with a photodiode, the resulting ringdown event being used as input for standard ringdown analysis [16]. The spectra were recorded by determining an aver-

aged ringdown time as a function of the laser frequency, calibrated by a wavemeter.

3. Ab initio calculations

Quantum chemical calculations were performed using the GAMESS computational package [17]. The basis set employed for all calculations was the double-zeta basis of Dunning and Hay [18]. Ground state equilibrium geometries of HC_nS ($n = 2–6$) were calculated at the multi-configuration quasi-degenerate perturbation theory (MCQDPT) level of theory [19] with a minimal self-consistent field (SCF) reference wavefunction. Single point calculations for the neutral HC_nS species and their ions were then performed by MCQDPT using SCF and multi-configuration self-consistent field (MCSCF) reference wavefunctions. The latter calculations were performed with a complete active space comprising six orbitals with five electrons for $n = 3, 5$ and seven electrons for $n = 2, 4, 6$. Estimates of the vertical ionization potentials (IPs) of these species were made by taking the difference between the energy of the neutral and ionic species at the same level of theory.

4. Results and discussion

4.1. Mass spectrometry

Time-of-flight mass spectra recorded at ionization wavelengths of 157 and 193 nm are presented in Fig. 1. The 57 nm spectrum exhibits many more peaks than the 193 nm spectrum. This is a reflection of the number of species produced in the discharge for which the IP is lower than the photon energy. While the energy of a 193 nm photon is quite low (6.4 eV), it is sufficient to ionize the $\text{C}_{2n+1}\text{H}_3$

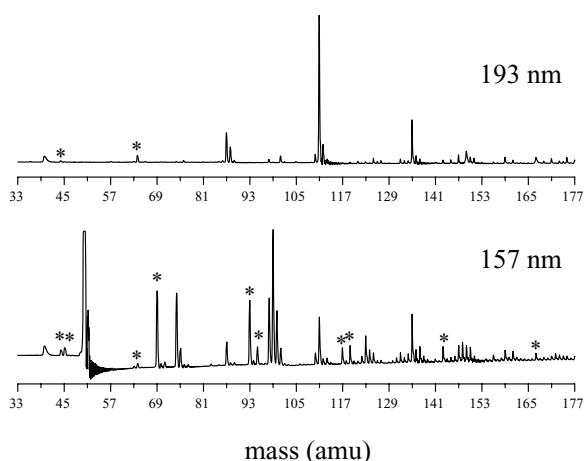


Fig. 1. Typical mass spectra from a $\text{CS}_2/\text{C}_4\text{H}_2$ discharge at two ionization wavelengths. Peaks determined to be sulfur-bearing are marked with ‘*’

Table 1
Selected mass peaks observed in the CS₂/C₄H₂/Ar discharge irradiated with either 193 or 157 nm

Mass	Molecular formula
40	Ar
44	CS
45	HCS
50	HCCCCH
64	S ₂
69	HCCCS
74	HC ₆ H
87	C ₇ H ₃
93	HCCCCCS
95	H₂CCCCCSH
111	C ₉ H ₃
117	HCCCCCCCS
119	H₂CCCCCCSH
135	C ₁₁ H ₃
143	H₂CCCCCCCCSH
167	H₂CCCCCCCCCSH

Sulfur-bearing carbon chains are emboldened. The formulae ascribed to masses 95, 119, 143 and 167 are tentative and are discussed in the text.

series [20] which dominates the mass spectrum. The structure of these species has not been unambiguously identified yet it is probable that they comprise a three-membered ring which possesses aromatic stability in its ionic form. While the intensity of the 193 nm radiation was two orders of magnitude larger than that of the 157 nm beam, the large peaks in the mass spectrum are not believed to arise from two-photon ionization. Some of the smaller peaks (certainly mass 40, Ar⁺) derive from ionization of molecules trapped in long lived metastable states.

Variation of the concentration of CS₂ in the discharge made it possible to determine the sulfur containing species. Assignments of prominent peaks to molecular formulae are given in Table 1. On increasing the ionization photon energy from 6.4 eV (193 nm) to 7.9 eV (157 nm), many more species are observed. Two notable series are the HC_{2n+1}S (*n* = 1–3) chains and another 14 mass units heavier.

The appearance of the HC_{2n+1}S series as strong peaks under irradiation at 7.9 eV suggests quite low IPs. This is predicted by ab initio calculations and may be justified by invoking simple Hückel considerations. The terminal sulfur atom is capable of taking part in the π-bonding network. As such, after taking account of one electron for the sigma-bond to its neighbouring carbon atom, and two electrons for a lone pair, this leaves three electrons to allocate to the delocalized π-system. Because the π-system is more than half filled for odd numbers of carbon atoms, the IP will be low (see Fig. 2). However, since the peaks are not observed in the 193 nm mass spectrum, the IPs of these chains must lie above 6.4 eV. This situation does not arise for the HC_{2n}S chains. Since HC₆S was not observed strongly in the spectrum presented in Fig. 1, it is supposed that the IP of this species lies above 7.9 eV. Since the excitation spectrum of HC₆S was measured by R2C2PI spectroscopy utilizing 193 nm as the ionizing laser, its IP must lie below

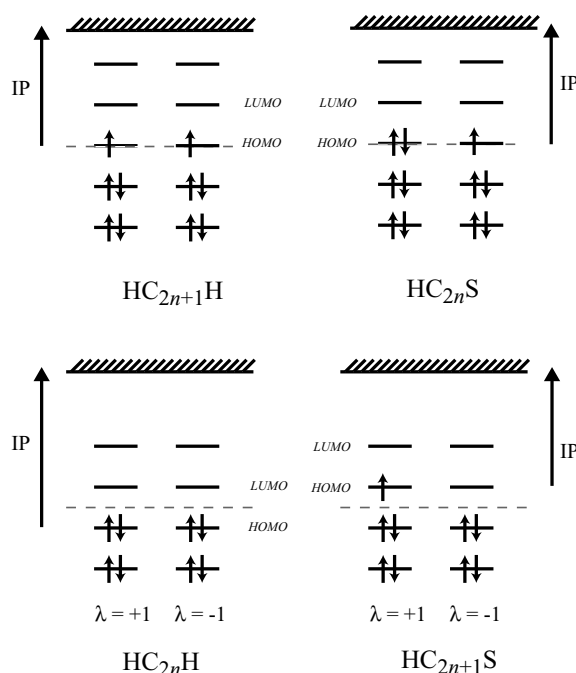


Fig. 2. A cartoon description of the electronic ground states of HC_nH and HC_nS. Indicated is the IP and λ , the projection of orbital angular momentum onto the molecular axis. It is seen that the HC_{2n+1}S species possess electrons occupying orbitals above the Fermi level (dotted line) of the corresponding all-carbon π-system (HC_{2n}H). This accounts for these species' low IPs.

8.5 eV, as discussed below. The results of quantum chemical calculations are presented in Fig. 3. Overall, the calculated values seem low, yet all levels of theory are in agreement with respect to the odd–even alternation.

The second series, 14 mass units heavier, commences at 95 a.m.u., which would correspond to a molecule of formula C₅H₃S. The addition of CH₂ to the HC_nS chains may result in methyl-terminated chains. It has been shown that

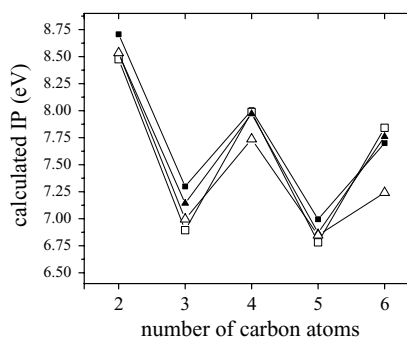


Fig. 3. The calculated vertical IPs for the HC_nS (*n* = 2–6) carbon chains. MCQDPT values are given as open symbols and those of MCSCF as filled ones. The SCF (squares) and (5, 7/6) MCSCF reference wavefunctions (triangles) both indicate odd–even alternation of IPs as justified in the text.

methyl substitution for a hydrogen is prevalent in a hydrocarbon discharge [21]. However, in this case the pattern of substitution seems unlikely. While the peak corresponding to C_7H_3S could be caused by CH_3C_6S , this species should have an IP and excitation spectrum similar to the unsubstituted species, HC_6S . As will be shown below, such a spectrum is not observed. In order to have low IPs, similar to the $HC_{2n+1}S$ series, the π -system must contain an even number of atoms (including the $-S$ moiety). Moving one hydrogen from the methyl group of $CH_3C_{2n}S$ to the sulfur terminal, results in species of formula $H_2C_{2n+1}SH$, which will behave in a similar way to the $HC_{2n+1}S$ series with respect to IP. The structurally similar cumulenethiones H_2C_nS ($n = 4-7$) have been observed by rotational spectroscopy [12], but were not observed by mass spectrometry of the discharge source.

In addition to the species discussed above, numerous others were observed. Those easily identifiable by their R2C2PI spectra included CS, HCS, S_2 , CCS and CS_2 .

4.2. Ionization spectroscopy

The mass spectrometry detailed above was used as a tool to tune the discharge conditions to produce desired carbon chain species. Fig. 4 shows the origin band and one hot band of HC_6S . The mass-selective measurement of this band confirms the observation of this species by laser-induced fluorescence [10]. One new band of this molecule was obtained 782.9 cm^{-1} to lower energies than the origin. The $C=S$ stretch is observed to be around 500 cm^{-1} in these $HC_{2n}S$ species [8–10], yet as high as 863 cm^{-1} for CCS. Since the $C=S$ stretches in the ground states of similar molecules lie much lower than the 782.9 cm^{-1} energy difference observed here, the band is assigned as a hotband starting from double excitation of a bending mode in the ground state.

The spectrum of HC_6S was obtained readily utilizing 193 nm as the ionizing wavelength. This places the IP of HC_6S below 8.5 eV. Despite 157 nm photons being energetic enough to ionize electronically excited HC_6S ,

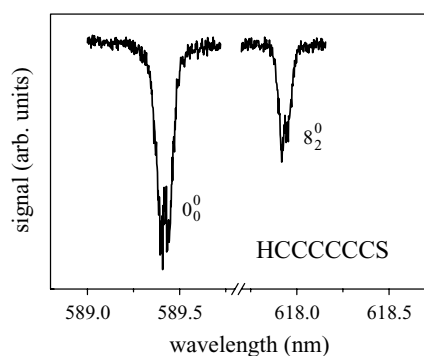


Fig. 4. Bands of HC_6S measured by R2C2PI spectroscopy. The mass-selective measurement confirms the identification by LIF spectroscopy (Ref. [10]). The hotband 782.9 cm^{-1} to the red is assigned to doubly excited bending in the ground state (8_2^0)

the intensity of this wavelength was about two orders of magnitude weaker than that at 193 nm and in this case not intense enough to produce observable signal. (The spectrum of HC_6S utilizing 157 nm as the ionizing wavelength has been subsequently observed in our laboratory.)

A search for HC_8S using R2C2PI spectroscopy was unsuccessful. Utilization of 193 nm as the ionizing wavelength while exciting HC_8S around 677 nm produces a combined photon energy of 8.26 eV. It is possible that the IP of HC_8S lies above this value, yet it should lie below 8.5 eV (the upper limit for HC_6S) assuming the normal trend of IP to decrease with chain length. The non-observation is suggested to be caused by a short lifetime (\approx ps) in the upper state. Observation of HC_8S was also unsuccessful using 157 nm, for the reasons outlined above.

Also observed by 2-colour and 1-colour ionization spectroscopy in this discharge were the S_2 , CS, CCS and C_3 molecules. The $E^3\Sigma^- \leftarrow X^3\Sigma^-$ spectrum of CCS was measured for the first time in the gas phase, following the identification of the band system in a neon matrix [22]. However, rotational profiles were not obtained, and thus a test of the predicted bond lengths was not possible.

Since the peak in the mass spectrum for mass 119 was observed to be strong, it is assumed that the molecule responsible for this peak is abundant in the discharge. Were this molecule to be a methyl-substituted version of HC_6S , namely CH_3C_6S , then one would expect to have observed a R2C2PI spectrum under the same conditions as that for which HC_6S was observed. The negative result and observation of low IPs for the $H_3C_{2n+1}S$ series suggests an alternative identity for this series as discussed in Section 4.1.

4.3. Cavity ringdown spectroscopy

Fig. 5 shows the measured origin bands of HC_8S and DC_8S measured by CRDS. The origin position of HC_8S ,

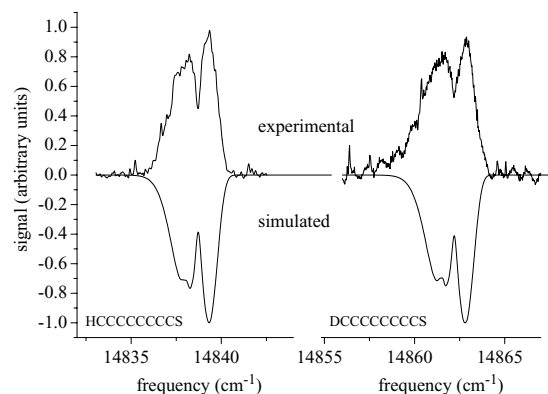


Fig. 5. The origin band of HC_8S (left) and DC_8S (right) measured by CRDS. The origin of HC_8S lies 80 cm^{-1} to the blue of the prediction in Ref. [5], based on a linear relationship of the absorption wavelength and chain length. Simulations were performed using the spectroscopic constants listed in Table 2.

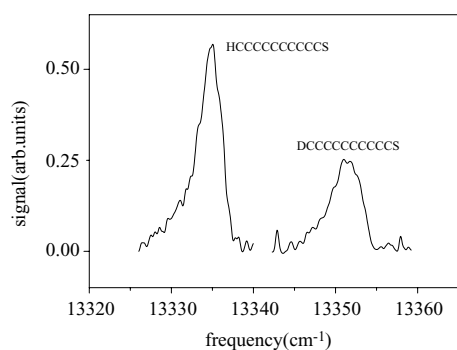


Fig. 6. Origin bands of HC₁₀S (left) and DC₁₀S (right) measured by CRDS. From the broadening of the bands the excited state lifetime is estimated to be about 2.6 ps.

14838.4 cm⁻¹, is only 80 cm⁻¹ to the blue of that predicted by a linear relationship between chain length and origin wavelength, extrapolated from the smaller species, HC₂S, HC₄S, and HC₆S [9,10]. The slight deviation from linearity is continued for HC₁₀S and its deuterated analog, DC₁₀S. The broad spectra of these species are shown in Fig. 6. The origin positions of HC₁₀S and DC₁₀S cannot be estimated better than the laser resolution (0.15 cm⁻¹) due to the severe lifetime broadening. Spectroscopic constants for HC₈S, DC₈S, HC₁₀S and DC₁₀S are given in Table 2.

The strongly linear relationship between absorption wavelength and chain size is a reflection of the cumulenic bonding structure in the HC_{*n*}S species induced by the carbon–sulfur double bond. The bonding pattern was confirmed by the quantum chemical calculations described above. This relationship is also seen in the C_{*n*}H⁻ anions [23], where one end of the chain exhibits cumulenic bonding which merges smoothly to acetylenic character on moving to the terminal hydrogen. It is this acetylenic

Table 2
The origins and the effective rotational constants (in cm⁻¹) of the vibronic bands of the HC₈S and HC₁₀S radicals, and their deuterated analogs

	<i>T</i> ₀	<i>B</i> ''	<i>B</i> '	Δ <i>A</i> _{SO}
HC ₈ S	14838.4(1)	0.00958 ^a	0.00954(2) ^b	0.7
DC ₈ S	14861.9(1)	0.00938(2) ^c	0.00935(3) ^b	0.7
HC ₁₀ S	13333.7(5)	0.00551(1) ^d	0.00542(5) ^b	2.5
DC ₁₀ S	13350.8(5)	0.00541(1) ^{c,d}	0.00535(5) ^b	2.5

Spin orbit constants are in the vicinity of 25 cm⁻¹. Only the change in *A*_{SO} could be determined accurately by the fitting procedure.

^a Previously determined by microwave spectroscopy [12].

^b Rotational constants in the excited state were extrapolated using the rotational constant ratio *B*'/*B*' of HC₆S and HC₄S. Reported errors were estimated during the fitting procedure.

^c The rotational constants of the deuterated species in the ground state were calculated according to the assumption that the structure of deuterated species is unchanged upon isotopic substitution.

^d The rotational constant of HC₁₀S in the ground state was estimated under consideration of increasing chain length.

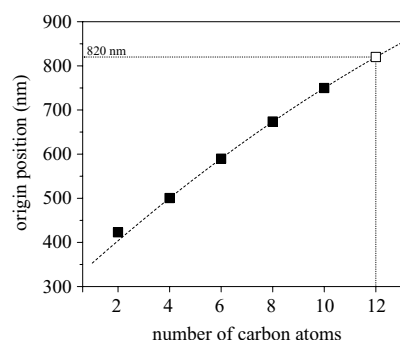


Fig. 7. A plot of the origin band wavelength of the HC_{2*n*}S series as a function of the number of carbon atoms in the chain, 2*n*. The relationship is remarkably linear, a reflection of the cumulenic bonding in these systems. A quadratic fit to the points measured for *n* = 2–5 yields an estimate for the absorption position of HC₁₂S of 820 nm.

character, induced at the hydrogen terminal, which explains (at the Hückel level of theory) the deviation from linearity. It has been shown that for the long carbon chains, HC_{2*n*}H, the relationship between chain length and absorption wavelength is strongly non-linear [15]. As the near-linear relationship is expected to continue, a prediction can be made for the origin position of HC₁₂S. Based on the present data (making a small correction due to non-linearity), this species is expected to absorb at 820 ± 5 nm. (See Fig. 7.)

The shift in origin band position upon deuterium substitution is caused by the difference in zero-point energies in the ground and excited states. This is 23 cm⁻¹ to higher energies for HC₈S and 17 cm⁻¹ for HC₁₀S. This compares with 35 cm⁻¹ for HC₆S and 54 cm⁻¹ for HC₄S. The decreasing deuterium shift upon increasing the chain size reflects the decreasing effect that the electronic excitation has on the vibrational modes involving motion of the hydrogen (deuterium) moiety. With this in mind, it is expected that the origin band position of DC₁₂S will lie about 12 cm⁻¹ to the blue of the HC₁₂S band position.

It has been noted that the excited state lifetimes of the HC_{2*n*}S series decrease with increasing chain length. Laser-induced fluorescence work has estimated the lifetimes of HC₄S and HC₆S to be 30 ns and 270 ps, respectively [9,10]. The lifetime of HC₈S is thus expected to be shorter still. Due to lack of resolution, the lifetime could not be estimated from the spectrum displayed in Fig. 5. The line width used in the simulated spectra was that of the laser resolution used, 0.15 cm⁻¹. If the lifetime broadening is no more than this order of magnitude, a conservative lower limit for the lifetime can be made of 70 ps. From spectral simulation, the lifetime of the A²Π excited state of HC₁₀S is estimated to be 2.6 ps. Short excited state lifetimes have implications for selecting the energy of the second photon when measuring R2C2PI spectra.

5. Conclusions

By time-of-flight mass spectrometry it was found that a sulfur-seeded hydrocarbon discharge produces a range of hydrogen and sulfur-bearing carbon chains, and that these species dominate the discharge chemistry. This is in accord with previous detection of sulfur-bearing chains as products of CS₂/hydrocarbon discharges. The dominant series appearing in the mass spectrum under irradiation by 157 nm light are the HC_{2n+1}S series and another 14 a.m.u. higher for which the identity is suggested to be H₂C_{2n+1}SH. The low IPs for the HC_{2n+1}S series were predicted semi-quantitatively by quantum chemical calculations. The production of the even chains HC_{2n}S was confirmed by R2C2PI spectroscopy and cavity ringdown spectroscopy. The spectrum of HC₈S was measured for the first time and was found to lie within 80 cm⁻¹ of the prediction according to an extrapolation from smaller members of the same series [8–10]. The extremely broad origin band of HC₁₀S was measured for the first time and confirmed the slight deviation from linearity of the relationship between chain size and absorption position. This measurement provided an updated estimate for the position of the HC₁₂S origin band, which is expected to be found near 820 nm. The near linear relationship between the absorption wavelength and the length of the carbon chain is indicative of cumulenic bonding. There is no evidence for a bandgap developing for long HCC...CCS chains and thus they are expected to exhibit conducting properties if employed as molecular wires. None of the spectra of the HC_{2n}S chains match those of the DIBs. The predicted position of the origin band of HC₁₂S does not lie nearby any DIBs and thus these species can be ruled out as carriers thereof.

Acknowledgements

This work has been supported by the Swiss National Science Foundation (project no. 200020-100019) and is part of the NCCR on nanoscale science in Basel.

References

- [1] M.G. Samant, C.A. Brown, J.G. Gordon, *Langmuir* 8 (1992) 1615.
- [2] M.A. Reed, C. Zhou, C.J. Muller, T.P. Burgin, J.M. Tour, *Science* 278 (1997) 252.
- [3] V. Mujica, A. Nitzan, S. Datta, M.A. Ratner, C.P. Kubiak, *J. Phys. Chem. B* 107 (2003) 91.
- [4] R. Lucas, H.S. Liszt, *Astron. Astrophys.* 384 (2002) 1054.
- [5] T.J. Millar, J.R. Flores, A.J. Markwick, *Mon. Not. R. Astr. Soc.* 327 (2001) 1173.
- [6] M.B. Bell, L.W. Avery, P.A. Feldman, *Astrophys. J.* 417 (1993) L37.
- [7] J. Cernicharo, M. Guelin, H. Hein, C. Kahane, *Astron. Astrophys.* 181 (1987) L9.
- [8] S.L.N.G. Krishnamachari, T.V. Venkitachalam, *Chem. Phys. Lett.* 55 (1978) 116;
S.L.N.G. Krishnamachari, D.A. Ramsay, *Faraday Discuss. Chem. Soc.* 71 (1981) 205.
- [9] M. Nakajima, Y. Sumiyoshi, Y. Endo, *Chem. Phys. Lett.* 351 (2002) 359.
- [10] M. Nakajima, Y. Sumiyoshi, Y. Endo, *Chem. Phys. Lett.* 355 (2002) 116.
- [11] M. Nakajima, Y. Yoneda, Y. Sumiyoshi, T. Nagata, Y. Endo, *J. Chem. Phys.* 119 (2003) 7805.
- [12] V.D. Gordon, M.C. McCarthy, A.J. Apponi, P. Thaddeus, *Astrophys. J. Supp. Ser.* 138 (2002) 297.
- [13] Y. Hirahara, Y. Oshima, Y. Endo, *J. Chem. Phys.* 101 (1994) 7342.
- [14] V.D. Gordon, M.C. McCarthy, A.J. Apponi, P. Thaddeus, *Astrophys. J. Supp. Ser.* 134 (2001) 311.
- [15] T. Pino, H. Ding, F. Güthe, J.P. Maier, *J. Chem. Phys.* 114 (2001) 2208.
- [16] A. O'Keefe, D.A.G. Deacon, *Rev. Sci. Instrum.* 59 (1988) 2544.
- [17] M.W. Schmidt, K.K. Baldrige, J.A. Boatz, S.T. Elbert, M.S. Gordon, J.J. Jensen, S. Koseki, N. Matsunaga, K.A. Nguyen, S. Su, T.L. Windus, M. Dupuis, J.A. Montgomery, *J. Comput. Chem.* 14 (1993) 1347.
- [18] T.H. Dunning Jr., P.J. Hay, in: H.F. Schaefer III (Ed.), *Methods of Electronic Structure Theory*, Plenum Press, New York, 1977, Chapter 1, p. 1.
- [19] H. Nakano, *J. Chem. Phys.* 99 (1993) 7983.
- [20] T.W. Schmidt, A.E. Boguslavskiy, H. Ding, T. Pino, J.P. Maier, *Int. J. Mass. Spectrom.* 248 (2003) 647.
- [21] T.W. Schmidt, H. Ding, A.E. Boguslavskiy, T. Pino, J.P. Maier, *J. Phys. Chem. A* 107 (2003) 6550.
- [22] E. Riaplov, M. Wyss, J.P. Maier, D. Panten, G. Chambaud, P. Rosmus, J. Fabian, *J. Mol. Spectrosc.* 222 (1) (2003) 15.
- [23] D.A. Kirkwood, M. Tulej, M.V. Pachkov, M. Schnaiter, F.Güthe, M. Grutter, M. Wyss, J.P. Maier, G. Fischer, *J. Chem. Phys.* 111 (1999) 9280.

Methyl Substitution in Hydrocarbon Discharge Chemistry: Diagnosis by Laser Spectroscopy

T. W. Schmidt, H. Ding, A. E. Boguslavskiy, T. Pino, and J. P. Maier*

Department of Chemistry, University of Basel, Klingelbergstrasse 80, CH-4056 Basel, Switzerland

Received: April 10, 2003; In Final Form: June 18, 2003

The spectra of C_8H_4 and $C_{10}H_5$ were observed in a butadiyne/argon discharge under the same conditions as those whereby C_7H_2 and C_9H_3 have been found to dominate the spectroscopy. It is shown that the species C_8H_4 and $C_{10}H_5$ most likely originate from methyl substitution of a hydrogen in C_7H_2 and C_9H_3 such as not to significantly disturb the chromophore. Assuming comparable oscillator strengths for the substituted species, it is found that the ratio of abundances of the unsubstituted and substituted species is around 27:1. This is discussed in relation to the chemistry of plasmas and the interstellar medium.

1. Introduction

The study of highly unsaturated hydrocarbon molecules produced from discharge sources is partly motivated by the search for the carriers of the diffuse interstellar bands (DIBs).¹ While these are yet to be identified, many highly unsaturated hydrocarbon species have been observed in dark interstellar clouds by rotational spectroscopy.² These observations allow one to characterize the chemistry of the interstellar medium and build models which attempt to explain relative abundances of species found therein.

Molecules of the generic formula C_nH_m ($m \leq n$) are abundant in flames and plasmas involving hydrocarbon precursors. One type of isomer of the C_nH formula has been observed in the laboratory, the linear species. The first eight members of this series have been confirmed to exist in space.^{2,3} Optical and microwave spectra have been measured for several of these species.^{4,5}

The spectra of several of the HC_nH series have been observed in rare gas matrixes,^{6–8} and in the gas phase by resonant two-color two-photon ionization spectroscopy (R2C2PI)⁹ and cavity ringdown spectroscopy (CRDS).¹⁰ Of this class of molecules, HC_4H and HC_6H have been observed in space by infrared spectroscopy.¹¹

A number of H_2C_n carbenes have been observed by microwave spectroscopy, owing to their permanent dipole moment,^{12–14} with H_2C_3 , H_2C_4 , and H_2C_6 having been observed in space.^{15–17} Less symmetric isomers^{18,19} and ring–chain²⁰ species have also been observed.

Recently, the spectra of $C_{2n+1}H_3$ ($n = 3–6$) molecules were observed by R2C2PI spectroscopy.²¹ These species were found to incorporate at least one ring structure. In the case of C_7H_3 , this was found to be a three-membered ring, whereas for C_9H_3 , $C_{11}H_3$, and $C_{13}H_3$, it was supposed that the ring structure was also three-membered.²¹

Under the same conditions as C_9H_3 was observed, it was found that the most dominant spectrum measurable in the range 650–440 nm was that of linear C_7H_2 . While these two molecules easily dominated the spectroscopy, a number of other species

were observed with significantly lower signal-to-noise (S/N). Two of these belonged to the same series as C_9H_3 and are discussed elsewhere.²¹ The other species observed, C_8H_4 , $C_{10}H_5$, and $C_{11}H_7$, appear at first glance rather arbitrary. It is shown in this paper that the most likely structures of these species are those arising from methyl substitution of the dominant C_7H_2 and C_9H_3 isomers. This is discussed with reference to the chemistry of plasmas and the interstellar medium.

2. Experimental Section

Spectra were obtained utilizing an apparatus which consisted of a molecular beam combined with a linear time-of-flight (TOF) mass analyzer (resolution of 900 at mass 200). The source, a pulsed valve coupled to an electric discharge, was the same as that used for detection of the $C_{2n+1}H_3$ species ($n = 4–6$).²¹ A pulse of a gas mixture of 0.5% butadiyne (HCCCCH) in Ar (backing pressure of 5 bar) was expanded through the ceramic body of the source which held two steel electrodes with an ≈ 1 mm hole separated by a ceramic spacer of 4 mm. A high voltage pulse (600–1200 V) was applied between the electrodes. Any resulting ions were removed after the skimmer, and before entering the pulsed extraction zone of the TOF mass spectrometer, by an electric field perpendicular to the molecular beam. The neutral beam was then ionized and ions were extracted into the TOF tube. The signal from the multichannel plate detector was fed into a fast oscilloscope after preamplification. Data acquisition was carried out using Labview programs.

R2C2PI was used in the 650–440 nm range. Excitation photons were delivered by a commercial OPO system (bandwidth 0.05) pumped by the third harmonic of a Nd:YAG laser. The ionizing photons at 212 nm (5.85 eV) were produced by sum frequency generation of the second harmonic and fundamental of the 637 nm output of a dye laser pumped by the second harmonic of a Nd:YAG laser. The energy per pulse was ≈ 5 mJ for the first color and a few hundred microjoules for the second. Both beams were anticollinear to the molecular beam, being combined with a dichroic mirror, and aligned optimally in time and space. The mass spectrum obtained upon irradiation of the products of the plasma discharge source with 7.9 eV photons from an F_2 excimer laser was used to optimize the discharge conditions.

* Author to whom correspondence should be addressed. E-mail: j.p.maier@unibas.ch.

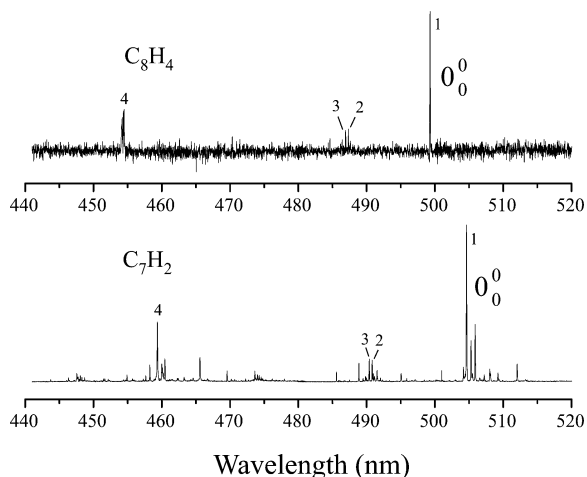


Figure 1. Comparison of resonant two-color two-photon ionization spectra of C_7H_2 and C_8H_4 . Analogous features are listed in Table 1.

3. Results and Discussion

3.1. Overview of Vibronic Structure. Figure 1 compares the electronic excitation spectra of C_7H_2 and C_8H_4 . The spectrum of C_7H_2 exhibits sequence or hot-band structure near the origin (band 1) which is repeated throughout the spectrum for each vibronic band. C_7H_2 is linear (HC_7H) with the electronic transition arising from $A^3\Sigma_u^- \leftarrow X^3\Sigma_g^-$ excitation. This spectrum has been discussed previously.^{8,10} The origin band of C_8H_4 appears nearby that of C_7H_2 , and exhibits similar vibronic structure. Bands 2 and 3 lie 493 cm^{-1} and 509 cm^{-1} to the blue of the origin band. The analogous bands in C_7H_2 are assigned to the excitation of double quanta of bending modes and are located 558 cm^{-1} and 575 cm^{-1} to the blue of the origin.⁸ Band 4 is split into two features, respectively, located at 1992 cm^{-1} and 1977 cm^{-1} . This feature in the HC_7H spectrum is located 1952 cm^{-1} to the blue of the origin.

Figure 2 compares the origin regions of C_9H_3 and $C_{10}H_5$. No other bands were observed for $C_{10}H_5$. It is striking that these spectra appear so close spectrally, both possessing a low-frequency progression. In $C_{10}H_5$ this progression is reduced from 39 cm^{-1} to 33 cm^{-1} . The positions of the origin bands of these electronic transitions are extremely close in energy. The relevant band positions may be found in Table 1. Only one band was observed for $C_{11}H_7$, and is listed in Table 1.

3.2. Structural Considerations. Without clear rotational resolution the structure of C_8H_4 may be deduced by a number of electronic and vibrational considerations. The most symmetric structure, the cumulene $H_2C_8H_2$, can be ruled out immediately since it is expected to absorb in the deep ultraviolet, and possesses no acetylenic stretch. It is argued here that the structure of the C_8H_4 isomer observed in the spectrum in Figure 1 is $(CH_3)C_7H$. Substituting a methyl group for one of the terminal hydrogens in HC_7H (Figure 3a) results in a molecule with a near identical chromophore, since the π -bonding system is left unaltered (to a first approximation). Indeed, it is expected that such a molecule would absorb in the same region as HC_7H . As seen in Figure 1, this is so. Methyl substitution increases the reduced mass for any bending motions and thus it is expected that the frequencies of such modes would decrease. Again, this is observed. Another piece of evidence consistent with the $(CH_3)C_7H$ structure is the splitting of the acetylenic stretch into two bands. There are two strong, triple bonds in HC_7H , yet only one acetylenic stretch is observed due to the $D_{\infty h}$ symmetry (only the totally symmetric modes may be populated with single

TABLE 1: Comparison of Features Observed in the R2C2PI Spectra of HC_7H , $(CH_3)C_7H$, C_9H_3 , $C_{10}H_5$, and $C_{11}H_7$ in the Gas Phase

label	λ (nm)	ν (cm^{-1})	$\Delta\nu$ (cm^{-1})	assignment
HC_7H				$A^3\Sigma_u^- \leftarrow X^3\Sigma_g^-$
1	504.5	19818	0	0_0^0
2	490.7	20376	558	$2\nu_\alpha$
3	490.2	20393	575	$2\nu_\beta$
4	459.2	21770	1952	2_0^1
$(CH_3)C_7H$				$A^3A_1 \leftarrow X^3A_1$
1	499.1	20035	0	0_0^0
2	487.2	20528	493	$2\nu_\alpha$
3	486.8	20544	509	$2\nu_\beta$
4	454.3	22012	1977	$\nu_{C=C}$
	454.0	22026	1992	$\nu_{C=C}$
C_9H_3	529.5	18886	0	0_0^0
	528.4	18925	39	low-frequency mode
$C_{10}H_5$	528.7	18914	0	0_0^0
	527.8	18947	33	low-frequency mode
$C_{11}H_7$	522.5	19139	0	0_0^0

quanta). Lifting this symmetry to C_{3v} for the $(CH_3)C_7H$ structure allows both acetylenic stretching modes to be populated upon electronic excitation. The absence of hot or sequence-band structure in $(CH_3)C_7H$ may be due to the mixing of modes upon reduction symmetry allowing more efficient cooling.

No signature specific to a methyl substituent is observed in the spectrum of $(CH_3)C_7H$. The extent of vibrational excitation of the “umbrella” motion of the $-CH_3$ group ($\approx 1300\text{ cm}^{-1}$) would depend on the Franck–Condon factor for this mode. Since the methyl group does not couple strongly to the chromophore it is probable that the potential curve for this mode in both states is similar. The Franck–Condon factor for excitation of the umbrella mode would thus be small. By analogy with the lowest transition of HC_7H , $^3\Sigma_u^- \leftarrow ^3\Sigma_g^-$, the symmetry of the lowest electronic transition of $(CH_3)C_7H$ is $^3A_1 \rightarrow ^3A_1$. Since this represents a parallel band of a symmetric top molecule, no structure is expected from transitions arising from $\Delta K \neq 0$ (change in rotation about the molecular axis). The A rotational constant of this species is expected to be near 5 cm^{-1} , but it should not change significantly upon electronic excitation. Clear rotational structure was not observed in the spectrum of $(CH_3)C_7H$, consistent with a parallel transition.

The structure of C_9H_3 was not unambiguously determined,²¹ yet the spectra of this species and the related $C_{11}H_3$ and $C_{13}H_3$ species pointed to a ring–chain system. The fact that this isomer of $C_{10}H_5$ is seen under the same conditions as C_9H_3 , that they are related by addition of CH_2 , that they absorb at a near identical frequency, and that they both possess a characteristic low-frequency mode indicates that this isomer of $C_{10}H_5$ is likely a methyl-substituted version of the dominant C_9H_3 isomer (for example, see Figure 3b). It is clear that if this is the case then the $-CH_3$ group will not be found near the chromophore of the molecule. Substitution of a further $-CH_3$ group results in a molecule of molecular formula $C_{11}H_7$. An extremely weak band was found for this mass at 522.48 nm , only a few nm to higher energy than $C_{10}H_5$. If this molecule arises from a structure related to C_9H_3 and $C_{10}H_5$, then the second substitution must perturb the chromophore more strongly than the first. Such a scenario is illustrated in Figure 3b.

In the present experimental setup, over 200 masses were monitored simultaneously. However, with 212 nm as the ionizing wavelength, the most dominant spectra observed in the spectral range $650\text{--}440\text{ nm}$ were those of C_7H_2 and C_9H_3 . The

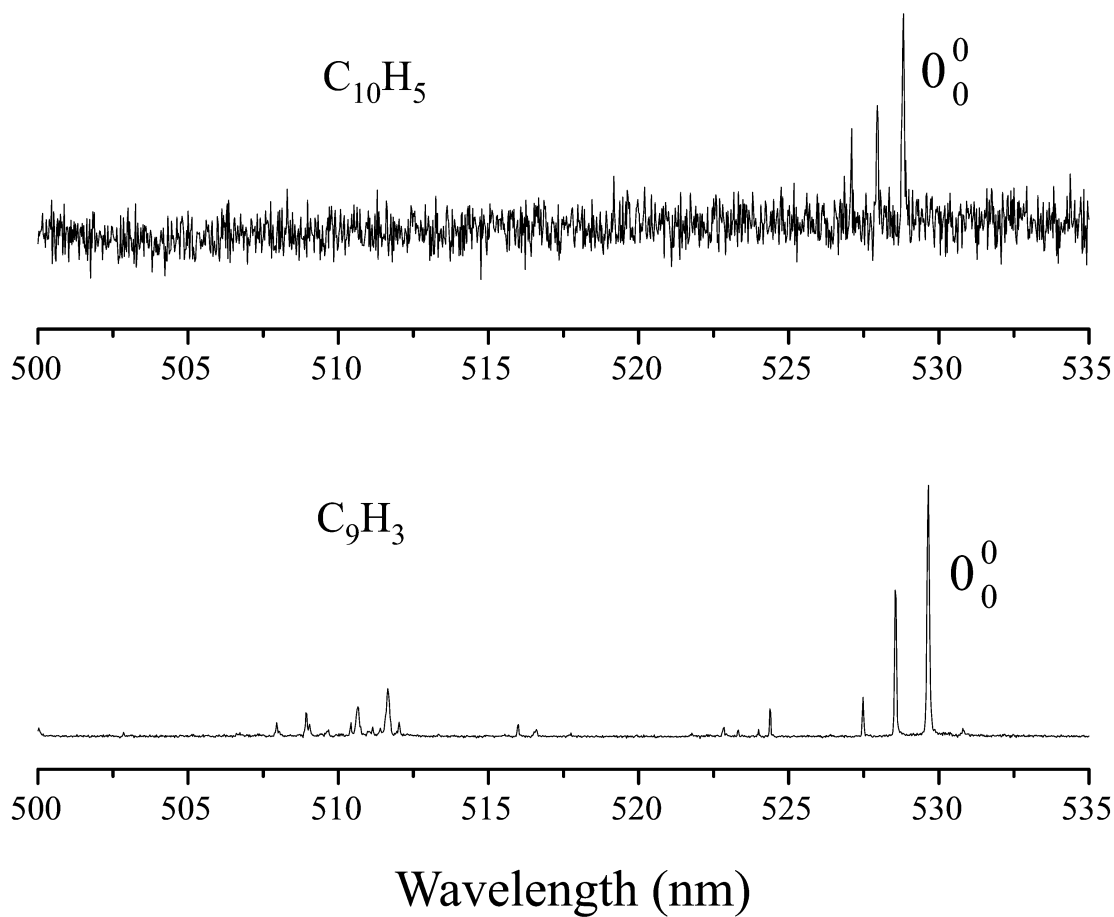


Figure 2. Comparison of resonant two-color two-photon ionization spectra of C_9H_3 and $C_{10}H_5$. Analogous features and band origin of $C_{11}H_7$ are listed in Table 1.

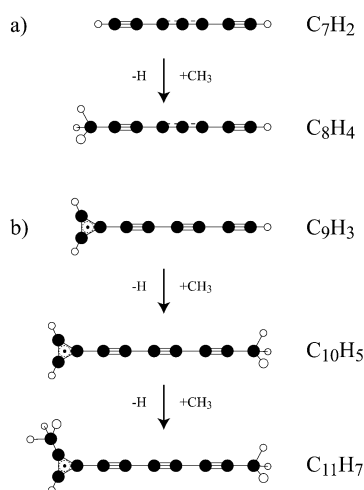


Figure 3. (a) A cartoon representation of the isomers of C_7H_2 and C_8H_4 described in the text. (b) An example of a ring–chain isomer of C_9H_3 , and the resulting isomers of $C_{10}H_5$ and $C_{11}H_7$ upon methyl substitution.

S/N of the former is conservatively estimated to be 1700, while that of the latter was found to be 700. Also observed under these conditions are C_9H_2 , $C_{11}H_3$, and $C_{13}H_3$ with S/N 10, 12, and 6, respectively. The facts that C_8H_4 and $C_{10}H_5$ are observed under these conditions and that they have spectra similar to those of the dominant species, C_7H_2 and C_9H_3 , strongly suggests that they are related molecules. That they are related by an extra 14 mass units suggests methyl substitution in place of a hydrogen.

For C_8H_4 the most likely structure is $(CH_3)C_7H$. As the structure of C_9H_3 is not unambiguously determined, one can only assume that $C_{10}H_5$ is related by a methyl substitution in such a way as to decrease the frequency of the low-frequency mode. The $C_{11}H_7$ spectrum obtained indicated only one band and was extremely weak. It is thought that its relationship to $C_{10}H_5$ is similar to the relationship of that molecule to the very strongly evident C_9H_3 isomer. In benzene discharges, styrene and methylstyrene have been observed, exhibiting spectra with near identical origin positions.²² That such behavior has been observed before in hydrocarbon discharges strengthens the assertions made here. No other species other than those indicated in this text were observed with excitation between 440 and 650 nm using 212 nm as the ionizing laser.

4. Chemical Implications

Because the transition positions move by less than 5 nm upon methyl substitution, it may be safe to assume that the oscillator strengths of the species HC_7H and $(CH_3)C_7H$ are similar. Given equal oscillator strengths and the fact that the spectra of HC_7H and $(CH_3)C_7H$ were recorded simultaneously, one may estimate that the ratio of abundances of the species is 27:1 in favor of HC_7H . Performing the same calculation for C_9H_3 and $C_{10}H_5$, their ratio of abundance is also found to be 27:1 in favor of the unsubstituted species. If this is taken as a general rule, then one expects to experimentally observe the methyl-substituted carbon chain (or ring–chain) only if the “parent” molecule is observed with a S/N above 30 or so. Since $C_{10}H_5$ is observed with S/N of about 6, it is perhaps fortunate to have observed

$C_{11}H_7$ at all. Indeed, this spectrum was only reproduced with great difficulty.

The methyl polyynes $CH_3(C\equiv C)_4H$ and $CH_3(C\equiv C)_5H$ have been observed by microwave spectroscopy of the products of a mixed methylacetylene/butadiyne discharge.²³ The shorter member $CH_3(C\equiv C)_3H$ has also been observed in the laboratory by microwave spectroscopy.²⁴ The choice of methylacetylene as a precursor suggests the importance of the methyl radical in the growth of these species. In space, the CH_3 radical is a fundamental intermediate in the growth of larger hydrocarbons and is closely related to the interstellar chemistry of methane.²⁵ The methyl substituent is also seen in carbonaceous grains in the interstellar medium by infrared absorption.²⁶ Indeed, the methyl radical and ion are integral to models of highly unsaturated hydrocarbon chemistry.^{2,27} The importance of methyl substitution in the hydrocarbon chemistry of a discharge source in the laboratory and the interstellar medium reinforces the link between the two.

Methyl-substituted chains are observed in the interstellar medium due to their permanent dipole moment. The acetylenic derivatives CH_3C_2H and CH_3C_4H have been observed in translucent molecular clouds² and in the atmospheres of moons and planets.²⁸ It is difficult to estimate how their abundances compare to the "parent" unsubstituted chains in the interstellar medium due to their absence of dipole moment. It is known that acetylene and butadiyne are components of the atmosphere of Titan,^{29,30} and due to their size and simplicity are expected to be found in the interstellar medium. Indeed, the polyynes C_4H_2 and C_6H_2 have been detected in the protoplanetary nebula CRL 618.¹¹ In the atmosphere of Titan, the ratio of acetylene to methylacetylene is estimated to be 240:1.³¹ The relative abundances of these species depend on the proportions of various elements in the medium, as well as chemical factors. In the source used in the present experiments, it is clear that where one species is strongly observed, the methyl-substituted species may be detected also.

5. Concluding Remarks

The observation of methyl-substituted species from a butadiyne discharge provides a benchmark for those modeling such systems. The observation of molecules with similar or equal transition moments simultaneously provides a way of comparing the relative abundances of those species. In this paper, it was shown that the ratios of $C_9H_3/C_{10}H_5$ and $HC_7H/(CH_3)_C_7H$ were both about 27:1. Any model of the chemistry involved in a butadiyne/Ar discharge must either support these observations or provide an alternative explanation. Because the level of unsaturation of hydrocarbons found in plasma discharges and the interstellar medium is similar, it is expected that the present work should have implications for astrochemical models.

Acknowledgment. This work has been supported by the Swiss National Science Foundation (Project No. 200020-100019).

References and Notes

- (1) Herbig, G. H. *Annu. Rev. Astron. Astrophys.* **1995**, *33*, 19.
- (2) Turner, B. E.; Herbst, E.; Terzieva, R. *Astrophys. J. Suppl. S* **2000**, *126*, 427, and references therein.
- (3) Guelin, M.; Cernicharo, J.; Travers, M. J.; McCarthy, M. C.; Gottlieb, C. A.; Thaddeus, P.; Ohishi, M.; Saito, S. *Astron. Astrophys.* **1997**, *317*, L1.
- (4) McCarthy, M. C.; Chen, W.; Apponi, A. J.; Gottlieb, C. A.; Thaddeus, P. *Astrophys. J.* **1999**, *520*, 158.
- (5) Ding, H.; Pino, T.; Güthe, G.; Maier, J. P. *J. Chem. Phys.* **2002**, *117*, 8362.
- (6) Kloster-Jensen, E.; Haink, H.-J.; Christen, H. *Helv. Chim. Acta* **1974**, *57*, 1731.
- (7) Grutter, M.; Wyss, M.; Fulara, J.; Maier, J. P. *J. Phys. Chem. A* **1998**, *102*, 9785.
- (8) Fulara, J.; Freivogel, P.; Forney, D.; Maier, J. P. *J. Chem. Phys.* **1995**, *103*, 8805.
- (9) Pino, T.; Ding, H.; Güthe, F.; Maier, J. P. *J. Chem. Phys.* **2001**, *114*, 2208.
- (10) Ball, C. D.; McCarthy, M. C.; Thaddeus, P. *J. Chem. Phys.* **2000**, *112*, 10151.
- (11) Cernicharo, J.; Heras, A. M.; Tielens, A. G. G. M.; Pardo, J. R.; Herpin, F.; Guélin, M.; Waters, L. B. F. M. *Astrophys. J.* **2001**, *546*, L123.
- (12) Travers, M. J.; McCarthy, M. C.; Gottlieb, C. A.; Thaddeus, P. *Astrophys. J.* **1997**, *483*, L135.
- (13) McCarthy, M. C.; Travers, M. J.; Gottlieb, C. A.; Thaddeus, P. *Astrophys. J.* **1997**, *483*, L139.
- (14) McCarthy, M. C.; Travers, M. J.; Chen, W.; Gottlieb, C. A.; Thaddeus, P. *Astrophys. J.* **1998**, *498*, L89.
- (15) Cernicharo, J.; Gottlieb, C. A.; Guélin, M.; Killian, T. C.; Paubert, G.; Thaddeus, P.; Vrtilek, J. M. *Astrophys. J.* **1991**, *368*, L39.
- (16) Cernicharo, J.; Gottlieb, C. A.; Guélin, M.; Killian, T. C.; Thaddeus, P.; Vrtilek, J. M. *Astrophys. J.* **1991**, *368*, L43; Kawaguchi, K.; Kaifu, N.; Ohishi, M.; Ishikawa, S.; Hirahara, Y.; Yamamoto, S.; Saito, S.; Takano, S.; Murakami, A.; Vrtilek, J. M.; Gottlieb, C. A.; Thaddeus, P.; Irvine, W. M. *Publ. Astron. Soc. Jpn.* **1991** *43* (4), 607.
- (17) Langer, W. D.; Velusamy, T.; Kuiper, T. B. H.; Peng, R.; McCarthy, M. C.; Travers, M. J.; Kovács, A.; Gottlieb, C. A.; Thaddeus, P. *Astrophys. J.* **1997**, *480*, L63.
- (18) Thaddeus, P.; McCarthy, M. C. *Spectrochim. Acta A* **2001**, *57*, 757.
- (19) McCarthy, M. C.; Thaddeus, P. *Astrophys. J.* **2002**, *569*, L55.
- (20) Apponi, A. J.; McCarthy, M. C.; Gottlieb, C. A.; Thaddeus, P. *Astrophys. J.* **2000**, *530*, 357.
- (21) Schmidt, T. W.; Boguslavskiy, A. E.; Ding, H.; Pino, T.; Maier, J. P. *Int. J. Mass Spectrom.* **2003**, *228*, 647–654.
- (22) Güthe, F.; Ding, H.; Pino, T.; Maier, J. P. *Chem. Phys.* **2001**, *269*, 347.
- (23) Travers, M. J.; Chen, W.; Grabow, J.-U.; McCarthy, M. C.; Thaddeus, P. *J. Mol. Spectrosc.* **1998**, *192*, 12.
- (24) Alexander, A. J.; Kroto, H. W.; Maier, M.; Walton, D. R. M. *J. Mol. Spectrosc.* **1978**, *70*, 84.
- (25) van Dishoeck, E. F.; Blake, G. A. *Annu. Rev. Astron. Astrophys.* **1998**, *36*, 317.
- (26) Pendleton, Y. J.; Allamandola, L. J. *Astrophys. J. Suppl. S* **2002**, *138*, 75.
- (27) Richter, H.; Howard, J. B. *Prog. Energ. Combust.* **2000**, *26*, 565.
- (28) MacGuire, W. C.; Hanel, R. A.; Jennings, D. E.; Kunde, V. G.; Samuelson, R. E. *Nature* **1981**, *292*, 683.
- (29) Stahl, F.; Schleyer, P. V.; Schaefer, H. F.; Kaiser, R. I. *Planet Space Sci.* **2002**, *50*, 685.
- (30) Kunde, V. G.; Aikin, A. C.; Hanel, R. A.; Jennings, D. E.; MacGuire, W. C.; Samuelson, R. E. *Nature* **1981**, *292*, 686.
- (31) Taylor, F. W.; Coustenis, A. *Planet Space Sci.* **1998**, *35*, 1085.

Gas phase electronic spectra of the linear carbon chains HC_{2n+1}H ($n=3-6,9$)

H. Ding, T. W. Schmidt, T. Pino, A. E. Boguslavskiy, F. Güthe, and J. P. Maier

Department of Chemistry, University of Basel, Klingelbergstrasse 80, CH-4056, Basel, Switzerland

(Received 7 April 2003; accepted 9 April 2003)

The $B^3\Sigma_u^- \leftarrow X^3\Sigma_g^-$ transitions of HC_{13}H and HC_{19}H have been measured in the gas phase, exhibiting broad, Lorentzian shaped bands. More extensive $A^3\Sigma_u^- \leftarrow X^3\Sigma_g^-$ spectra have been observed for HC_{2n+1}H ($n=3-6$) than before with many new vibronic bands identified. The spectra were obtained by means of a mass selective resonant two-color two-photon ionization technique coupled to a supersonic plasma source. The electronic structures of this series of molecules ($n=2-9$) in both the ground and excited states have been investigated using DFT, MP2, and state-averaged CASSCF theories. The three lowest dipole allowed electronic transition systems are $A^3\Sigma_u^- \leftarrow X^3\Sigma_g^-$, $B^3\Sigma_u^- \leftarrow X^3\Sigma_g^-$, and $C^3\Pi_u \leftarrow X^3\Sigma_g^-$, located, for the smaller members of the series, in the visible, UV and VUV range, respectively. The $A^3\Sigma_u^- \leftarrow X^3\Sigma_g^-$ system is found to be of medium intensity and the $B^3\Sigma_u^- \leftarrow X^3\Sigma_g^-$ transition is predicted to be very strong. This is a result of configuration mixing in the excited states. The oscillator strength of the lowest energy transition is not strongly dependent on the length of the chain, but that of the $B^3\Sigma_u^- \leftarrow X^3\Sigma_g^-$ system increases monotonically with size. The $C^3\Pi_u$ state is Rydberg in character. The astrophysical implications are considered and an upper limit of the column densities of these carbon chains in diffuse clouds has been estimated as 10^{13} cm^{-2} , based on calculated oscillator strengths. © 2003 American Institute of Physics. [DOI: 10.1063/1.1578476]

I. INTRODUCTION

Unsaturated hydrocarbon chains are important intermediates in combustion processes,¹ plasma chemistry² and play an important role in the chemistry of the interstellar medium (ISM).^{3,4} Following the unsuccessful attempts to detect C_4 and C_5 in diffuse interstellar clouds, arguments were presented for much longer carbon chains to be of relevance as carriers of the diffuse interstellar bands (DIBs).⁵ This proposal assumes that the oscillator strengths of low-lying electronic transitions of these chains increase in proportion to the chain length. While this is the case for the lowest electronic transitions of some classes of carbon chain, for others the transition of interest must be chosen carefully, as this article shows.

Bare carbon clusters, C_2 (Ref. 6) and C_3 ,⁷ have been detected in diffuse interstellar clouds by their optical absorption spectra. Carbon chains such as the C_nH ($n=2-8$) radicals have been detected in dark interstellar molecular clouds and in envelopes of evolved stars by radioastronomy.⁸⁻¹⁰ Small members ($n=1, 2$) of the HC_{2n}H series have also been detected in the atmosphere of planets¹¹ and moons.^{12,13} The odd chains, HC_{2n+1}H , are believed to exist in the ISM because their C_{2n+1}H ($n=0-3$) counterparts have been detected. The existence of highly unsaturated and reactive species is an essential characteristic of the ISM chemistry.

Recently the gas phase electronic spectra of even polyynes HC_{2n}H ($n=8-13$) and $l\text{-C}_{2n+1}\text{H}$ ($n=1-4$) radicals have been studied in a molecular beam by a mass selective resonant two-color two-photon ionization (R2C2PI) spectroscopic technique.¹⁴⁻¹⁶ Compared to the even HC_{2n}H chains, the odd series is more reactive and cannot be

synthesized in macroscopic quantities. They can only be detected in low temperature matrices or under supersonic molecular beam conditions. The electronic spectra of the $A^3\Sigma_u^- \leftarrow X^3\Sigma_g^-$ transitions of HC_{2n+1}H ($n=2-7$) have been observed in neon gas matrices.¹⁷ The origin and strong $\nu_{\text{C}\equiv\text{C}}$ stretching vibronic bands (for $n=3-6$) were subsequently observed by gas-phase cavity-ring-down (CRD) spectroscopy.¹⁸ High quality *ab initio* calculations on electronic states for small members (HC_5H to HC_9H) of this series have been carried out at the MRCI level of theory.¹⁹⁻²¹ In addition to the first dipole-allowed electronic transitions, $A^3\Sigma_u^- \leftarrow X^3\Sigma_g^-$, which have been measured, the calculations predict that there is a much stronger electronic transition, $B^3\Sigma_u^- \leftarrow X^3\Sigma_g^-$ in the VUV at 170 nm (7.31 eV) for HC_5H (Ref. 19) moving into the far UV at 210 nm (5.91 eV) for HC_9H .²¹ The prediction by that the $B^3\Sigma_u^- \leftarrow X^3\Sigma_g^-$ system carries the oscillator strength, expected (albeit naively) for $A^3\Sigma_u^- \leftarrow X^3\Sigma_g^-$, implies that it is this system which is of astrophysical interest in relation to the carriers of the DIBs.

In this paper the observation of the $B^3\Sigma_u^- \leftarrow X^3\Sigma_g^-$ transition of HC_{13}H and HC_{19}H in the UV region in the gas phase is reported. *Ab initio* calculations extending from small to large members of this series (HC_5H to HC_{19}H) have been carried out in order to guide the assignment. Geometry optimizations, harmonic frequencies, electronic vertical transition energies and oscillator strengths were investigated by *ab initio* calculations at the DFT-B3LYP, MP2, and CASSCF levels of theory.

In addition to the $B^3\Sigma_u^-$ state data, some new gas-phase vibronic bands of the $A^3\Sigma_u^- \leftarrow X^3\Sigma_g^-$ transitions of HC_{2n+1}H ($n=3-6$), which were not observed in previous

neon matrix or CRD experiments, have been observed using the R2C2PI technique.

II. EXPERIMENT

The experimental set-up has been described.¹⁴ It consisted of a molecular beam combined with a linear time of flight mass-analyzer (TOF). A gas mixture pulse of 0.3% of acetylene or diacetylene in Ar (backing pressure 8 bar) was expanded through the ceramic body of the source comprising two steel electrodes to which a discharge voltage was applied. The emerging beam containing HC_{2n+1}H chains entered the ionization region through a 2 mm skimmer. The neutral molecules were then ionized by the R2C2PI method and the ions extracted in a two-stage acceleration setup towards a multichannel plate (MCP) detector.

R2C2PI spectra were recorded in the UV (282–350 nm) and visible (410–740 nm) ranges. Excitation photons were delivered by the frequency doubled output of a dye laser (bandwidth ~0.1 cm⁻¹) pumped by a Nd:YAG laser or a commercial OPO system (bandwidth 0.05 cm⁻¹). The ionizing photons of wavelength 157 nm (or 193 nm) were delivered by an F₂ (or ArF) excimer laser or 212 nm produced by sum frequency generation of the second harmonic and fundamental of the 637 nm output of a dye laser pumped by the second harmonic of a Nd:YAG laser. Both excitation and ionizing lasers were unfocused.

III. THEORETICAL CALCULATIONS

A. Ground states

Ab initio calculations were carried out using the GAUSSIAN 98 suite of programs²² at the MP2 (Ref. 23) and DFT-B3LYP (Ref. 24) levels of theory using the 6-31G* basis set.²⁵ These calculations show bond-length alternation for both the MP2 and DFT-B3LYP levels of theory. In the MP2 calculations the alternation between bond-lengths is more pronounced in comparison to the DFT-B3LYP calculations. The harmonic frequencies in the ground states for HC_{2n+1}H ($n=2-6$) were calculated using MP2/6-31G* and DFT-B3LYP/6-31G*.²⁶

B. Excited states

Ab initio calculations of the electronically excited states were undertaken using the MOLPRO package.²⁷ The $X^3\Sigma_g^-$ ground states of HC_{2n+1}H are dominated by the $\cdots[(n-1)\pi_g]^4[n\pi_u]^2$ electronic configuration for $n=2,4,\dots,8$ and $\cdots[(n-1)\pi_u]^4[(n-1)\pi_g]^2$ for $n=3,5,\dots,9$.

Two configurations dominate the excited state wave functions. To a first approximation, the $A^3\Sigma_u^-$ state and $B^3\Sigma_u^-$ state are admixtures of configurations which arise from excitation from the fully occupied levels, $(n-1)\pi_g$ (or $(n-1)\pi_u$) to the semioccupied molecular orbitals (SOMO), $n\pi_u$ (or $(n-1)\pi_g$), and excitation from the SOMO, to the lowest unoccupied molecular orbital (LUMO), $n\pi_g$ (or $n\pi_u$). Excitation from the SOMO to the second lowest unoccupied molecular orbital (SLUMO), σ_g (or σ_u), results in

TABLE I. Calculated vertical excitation energies (eV) for the HC_{2n+1}H ($n=2-9$) at the CASSCF level. MRCI values from Refs. 19–21 are given in parentheses.

State	HC ₅ H	HC ₇ H	HC ₉ H	HC ₁₁ H
$X^3\Sigma_g^-$	0.0	0.0	0.0	0.0
$A^3\Sigma_u^-$	3.47 (2.76)	3.07 (2.55)	2.74 (2.38)	2.45
$B^3\Sigma_u^-$	9.34 (7.31)	7.81 (6.66)	6.80 (5.91)	6.09
$C^3\Pi_u$	6.95 (7.70)	8.22 (8.41)	8.43 (8.38)	8.78

State	HC ₁₃ H	HC ₁₅ H	HC ₁₇ H	HC ₁₉ H
$X^3\Sigma_g^-$	0.0	0.0	0.0	0.0
$A^3\Sigma_u^-$	2.28	2.13	2.04	1.96
$B^3\Sigma_u^-$	5.74	5.37	5.20	5.06
$C^3\Pi_u$	9.10	9.48	9.75	9.93

the $C^3\Pi_u$ excited states. The calculated ordering in energy for HC₅H is reversed for the $B^3\Sigma_u^-$ and $C^3\Pi_u$ states, yet this notation is retained for clarity.

Vertical electron excitation energies were calculated at the ground state geometry for the triplet multiplicity only. These were obtained at the state-averaged CASSCF/6-31G* level of theory,^{28,29} in the D_{2h} group of symmetry. The calculations implemented an active space including 10 electrons in 12 orbitals for HC₅H to HC₁₉H. The calculated vertical excitation energies are listed in Table I. For the smaller members of the series, the $A^3\Sigma_u^-$, $B^3\Sigma_u^-$, and $C^3\Pi_u$ excited states are located in the visible, UV, and VUV spectral range, respectively. A comparison of the calculated transition energies with available experimental data is given in Fig. 1. The values calculated at the CASSCF level of theory are systematically high by ~0.5 eV for the $A^3\Sigma_u^- \leftarrow X^3\Sigma_g^-$ transition and ~1.3 eV for $B^3\Sigma_u^- \leftarrow X^3\Sigma_g^-$ system compared to the available experimental values. For comparison the transition energies for HC₅H to HC₉H calculated at the MRCI level of theory^{19–21} have also been given in Fig. 1. Good qualitative agreement between the theoretical and experimental results, with respect to behavior with system size, have been achieved in the present calculations (Fig. 1).

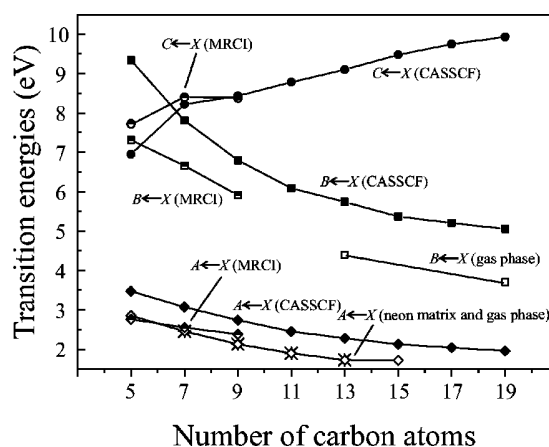


FIG. 1. The calculated and observed electronic transition energies of the first three dipole allowed electronic transition systems as the function of the size of carbon chains of HC_{2n+1}H ($n=2-9$). The values for the neon matrix are taken from Ref. 17. The MRCI values are taken from Refs. 19–21.

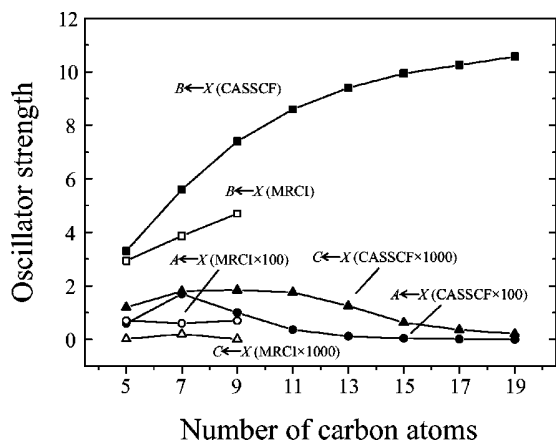


FIG. 2. The calculated oscillator strength (f -value) for the first three dipole allowed electronic transitions as the function of the size of the carbon chains of $HC_{2n+1}H$ ($n=2-9$). The MRCI values are taken from Refs. 19–21.

Both the transition energies of the $A^3\Sigma_u^- \leftarrow X^3\Sigma_g^-$ and $B^3\Sigma_u^- \leftarrow X^3\Sigma_g^-$ systems decrease with the chain size. The $B^3\Sigma_u^- \leftarrow X^3\Sigma_g^-$ transitions have very large oscillator strengths (f -values). They increase monotonically with the size of the chains while the much smaller f -values of the $A^3\Sigma_u^- \leftarrow X^3\Sigma_g^-$ system first increase from HC_5H to HC_7H and then slightly decrease with the chain size (Fig. 2). This behavior may be rationalized in terms of the configurations and wave functions generated by the Hückel theory. According to the Hückel theory, the excited configurations which lead to the $A^3\Sigma_u^-$ and $B^3\Sigma_u^-$ states have the same energy. In addition, if these configurations alone were to represent different electronic states, then the oscillator strengths of their respective transitions from the ground state would also be equal. That the lowest transitions of odd-numbered alternant, conjugated hydrocarbon systems arise through strong mixing of two configurations was shown analytically by Dewar and Longuet-Higgins,³⁰ and extended to self-consistent orbitals by Longuet-Higgins and Pople.³¹ At the MRCI (Refs. 19–21) and CASSCF levels, the two leading configurations are seen to mix in approximately equal proportions, the $A^3\Sigma_u^-$ and $B^3\Sigma_u^-$ states resulting from even and odd combinations. Accordingly one of the transitions loses oscillator strength while the other gains oscillator strength. At the CASSCF and MRCI levels of theory, it is the general behavior of the $HC_{2n+1}H$ series that the $B^3\Sigma_u^- \leftarrow X^3\Sigma_g^-$ system carries the oscillator strength, as predicted. This increases with the size of the molecule while the $A^3\Sigma_u^- \leftarrow X^3\Sigma_g^-$ oscillator strength does not.

IV. RESULTS AND DISCUSSION

A. The $B^3\Sigma_u^- \leftarrow X^3\Sigma_g^-$ transition system

Spectra of the second dipole-allowed electronic transition, the $B^3\Sigma_u^- \leftarrow X^3\Sigma_g^-$ system, are shown in Fig. 3. Since experimental measurement is difficult in the far UV, just a few of the larger chains were studied.

In contrast to those of the $A^3\Sigma_u^- \leftarrow X^3\Sigma_g^-$ system, these have broad band profiles. In the case of $HC_{13}H$, the spectrum was recorded with different pulse energies, from 1 mJ up to

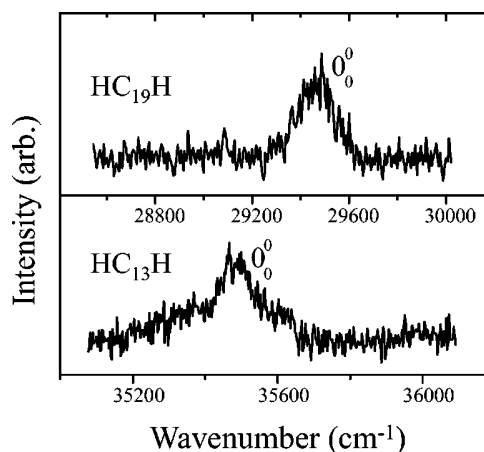


FIG. 3. Electronic spectra of the strong $B^3\Sigma_u^- \leftarrow X^3\Sigma_g^-$ transitions of $HC_{13}H$ and $HC_{19}H$ measured by the resonant 2-color 2-photon ionization (R2C2PI) technique.

5 mJ. No significant power broadening was observed. Thus the line shape is intrinsic and Lorentzian in nature. The full width at half maximum (FWHM) is about 160 cm^{-1} , indicating a ~ 60 fs lifetime for the excited state. Predissociation can be excluded because mass-selective detection is used and no fragment peaks were observed at the same wavelength for species of mass < 158 . Internal conversion is responsible for this electronic relaxation and is efficient due to the number of high-lying electronic states and number of vibrational degrees of freedom. After excitation into the $B^3\Sigma_u^-$ state, the energy is converted into vibrational energy in the ground state on a subpicosecond time scale. Experimental evidence for this was observed: the ion signal did not change when the delay between the excitation and ionization laser was varied from a few nanoseconds up to $10\ \mu\text{s}$ and one color signal could not be detected although the energy of two UV photons is higher than the IP of $HC_{13}H$ (< 8.15 eV). Unlike in the one-color scheme, the two color signal was detected because the Franck–Condon factor for the ionization step ($\hbar\omega = 7.9$ eV) becomes favorable upon crossing to the ground state.

The transition energies of the $B^3\Sigma_u^- \leftarrow X^3\Sigma_g^-$ system decrease and the oscillator strengths increase with the chain size. It can be predicted that for larger members of this series, the spectra of the $B^3\Sigma_u^- \leftarrow X^3\Sigma_g^-$ system will be located in the visible region. The large predicted oscillator strength of the $B^3\Sigma_u^- \leftarrow X^3\Sigma_g^-$ transition suggests that they may be observable by absorption spectroscopy. If it is assumed that the theoretical values are on the order of 1.3 eV too high, then an extrapolation to long chains reveals that this transition of the $HC_{2n+1}H$ may enter the visible region near $HC_{25}H$. Of particular interest is the prediction that the spectra of the $B^3\Sigma_u^- \leftarrow X^3\Sigma_g^-$ transition is extrapolated to near the $4428\ \text{\AA}$ DIB between $HC_{29}H$ and $HC_{31}H$. Recently high-quality spectra of the $4428\ \text{\AA}$ DIB have been reported.³³ The intrinsic profile of this DIB is Lorentzian, with an average FWHM being $17.25\ \text{\AA}$ ($\sim 90\text{ cm}^{-1}$).³³ The central wavelength and depth and FWHM of the $4428\ \text{\AA}$ DIB are invariant with the color excess. These points imply that a molecular carrier in the gas phase is responsible. The upper

state lifetime is estimated as 10^{-13} s. This means that the molecule must have very rapid internal conversion for relaxation from this upper state. There is a similarity of the profile of the $B^3\Sigma_u^- \leftarrow X^3\Sigma_g^-$ transition of long polyynes chains to that of the 4428 Å DIB. Thus the laboratory study of the $B^3\Sigma_u^- \leftarrow X^3\Sigma_g^-$ transitions of the HC_{2n+1}H chains which fall in this wavelength range is desirable.

B. Importance of configuration interaction in excited states of open shell π -systems

As demonstrated for small odd polyynes^{19–21} and confirmed in the present study for larger systems, configuration interaction is of the utmost importance in describing the lowest dipole allowed transitions and has a profound effect upon the calculated oscillator strengths of these transitions. This effect was predicted for odd-numbered, alternant, radical conjugated systems,³⁰ such as those studied in the present paper. For other systems where the first two excited configurations are not, in general, degenerate, the effect is of second order.

The behavior of the oscillator strengths seen in the odd polyynes is also seen in a variety of other open shell π -systems. The oscillator strengths of linear C_4 were investigated in detail.³⁴ Linear C_4 possesses only six π electrons and therefore has a $^3\Sigma_g^-$ ground state, similar to the molecules presented here. A node was found on the transition moment surface of the lowest $^3\Sigma_u^- \leftarrow ^3\Sigma_g^-$ transition near the equilibrium geometry, highlighting the difficulty of predicting small oscillator strengths. Upon distortion of the geometry, the oscillator strength of the higher energy $^3\Sigma_u^- \leftarrow ^3\Sigma_g^-$ transition was seen to be robust. It may be concluded, therefore, that only the strong calculated oscillator strength may be taken as a reliable prediction of spectral intensity. The strong configuration mixing is also seen in C_6 , which is of a similar electronic configuration to C_4 .³⁵ Removal of one electron from this system leaves the cation in a doublet state. It has been shown that the C_6^+ system possesses analogous transitions to the neutral species with similar behavior with respect to their oscillator strengths.³⁶ The odd, bare carbon chains, C_{2n+1} , do not exhibit this effect, since they are closed shell.

The monohydrogenated even chains, C_{2n}H , have doublet ground states with an unpaired electron (hole) residing in the π system. A study of C_6H (Ref. 37) showed that the two relevant electronically excited configurations do not strongly mix. The resulting transitions ($2\pi \rightarrow 3\pi$ and $3\pi \rightarrow 4\pi$) are computed to be at 2.556 eV and 3.43 eV, both possessing medium oscillator strengths. The difference between this system and the bare carbon chains is the size of the HOMO–LUMO gap. A widening of the HOMO–LUMO gap is a signature of the bond-length alternation induced by the hydrogen end group. The HC_6H^+ cation behaves in a similar way to C_6H .³⁷ Of the odd monohydrogenated chains C_5H ,³⁸ which has a ground state configuration $\cdots 3\pi^1$, configuration mixing is exhibited for states resulting from the $2\pi \rightarrow 3\pi$ and $3\pi \rightarrow 4\pi$ electron promotions. This is not strong, though, which may be a reflection of the differing bond length alter-

nation pattern between the monohydrogenated and dihydrogenated series.

It may be seen that the systems affected by the configurational mixing are those which possess two electronically excited π configurations of near identical orbital energy. Those systems are the cumulenic even carbon chains and their cations, and the odd polyyne species. Following this logic, the $\text{HC}_{2n+1}\text{H}^+$ cations should exhibit the same effect, but this is yet to be shown.

C. Other electronic states

The positions of the electronic states $1^3\Delta_u$ and $1^3\Sigma_u^+$ were predicted to be close to that of $A^3\Sigma_u^-$, but these two states are dipole forbidden for optical transition. The third dipole allowed electronic transition is the $C^3\Pi_u \leftarrow X^3\Sigma_g^-$ system. The energies of the $C^3\Pi_u \leftarrow X^3\Sigma_g^-$ system are predicted to slightly increase with the chain size and the f -values decrease only slightly (Fig. 2). This is because it is a valence to Rydberg transition while $A^3\Sigma_u^- \leftarrow X^3\Sigma_g^-$ and $B^3\Sigma_u^- \leftarrow X^3\Sigma_g^-$ systems are valence to valence transitions. The CASSCF calculations for HC_7H show that the matrix element $\langle C^3\Pi_u | z^2 | C^3\Pi_u \rangle$ is 60.5 (a.u.)², much larger than 6.8 (a.u.)², the value of $\langle X^3\Sigma_g^- | z^2 | X^3\Sigma_g^- \rangle$. The wave function of $\langle C^3\Pi_u |$ is thus much more diffuse (i.e., comprises a Rydberg orbital). The calculations show that the $C^3\Pi_u$ states of HC_{2n+1}H are of $ns\sigma$ Rydberg character, similar to the $C^1\Pi_u$ Rydberg state of acetylene.³⁹

D. New vibronic bands in the $A^3\Sigma_u^- \leftarrow X^3\Sigma_g^-$ system

New bands were observed in the $A^3\Sigma_u^- \leftarrow X^3\Sigma_g^-$ transition system measured previously in the gas phase by cavity ringdown spectroscopy.¹⁸ While many of these are assigned as hot-bands, several new members of acetylenic progressions were observed. In particular, the spectrum of HC_7H was observed with a signal to noise ratio of ≈ 1700 , allowing many hot-bands and bending vibrations to be identified.

1. HC_7H

The HC_7H R2C2PI spectrum has a complicated structure (Fig. 4). The origin region shows a number of additional peaks on the low energy side which are assigned to sequence bands. This structure is repeated for all other identifiable vibronic bands in the spectrum and thus arises from the same structural isomer and electronic state. Bands in Fig. 4 are labeled sequentially from the origin to higher energy. Bands to lower energy than the origin are labeled with a prime.

Bands 2 and 3 are assigned to C–C–H bending modes with π_u (or π_g symmetries), which are denoted $2\nu_\alpha$ and $2\nu_\beta$. This assignment is based on neon matrix spectra of the deuterated analogs of HC_7H .¹⁷ Band 4 is assigned as the 4_0^1 transition. The ν_α mode is the lowest σ_g vibrational mode, with a frequency of 638 cm^{-1} . These bands and other new observations are listed in Table II. Based on the R2C2PI observations, an upper limit of 8.3 eV can be placed on the ionization potential of HC_7H .

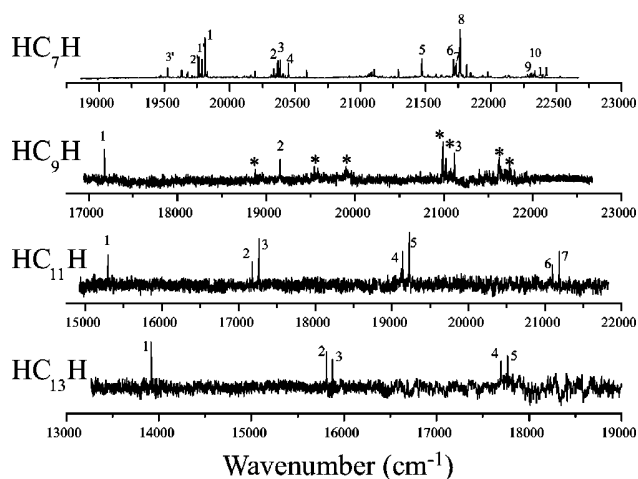


FIG. 4. The electronic spectrum of HC_7H , HC_9H , $HC_{11}H$, and $HC_{13}H$ detected by the resonant 2-color 2-photon ionization (R2C2PI) technique. The peaks marked * are from fragments of photodissociation of C_9H_3 (Ref. 32).

2. HC_9H

The R2C2PI spectrum of HC_9H is shown in Fig. 4. Only three bands were observed. Of these band 3 has been observed for the first time in the gas phase and is assigned to the 3_0^2 transition, corresponding to acetylenic stretching motion. The observed bands are listed in Table II. This spectrum was only observed using 212 nm as the ionizing wavelength

TABLE II. Maxima of selected vibronic bands observed in the electronic spectrum of HC_9H , $HC_{11}H$, $HC_{13}H$, and $HC_{19}H$ in gas phase.

Label	λ (nm)	ν (cm^{-1})	$\Delta\nu$ (cm^{-1})	Assignment
HC_7H				$A^3\Sigma_u^- \leftarrow X^3\Sigma_g^-$
1	504.45	19818.2	0.0	0_0^0
2	490.65	20375.8	558	$2\nu_\alpha$
3	490.23	20393.2	575	$2\nu_\beta$
4	488.71	20456.5	638	4_0^1
8	459.19	21770.4	1952	2_0^2
9	447.92	22325.9	2508	$2_0^1 + 2\nu_\alpha$
10	447.42	22349.3	2531	$2_0^2 + 2\nu_\beta$
11	446.20	22412.8	2595	$2_0^1 4_0^1$
...	421.45	23727.6	3909	2_0^2
HC_9H				$A^3\Sigma_u^- \leftarrow X^3\Sigma_g^-$
1	581.75	17185.4	0.0	0_0^0
2	521.77	19160.4	1975	3_0^1
3	473.15	21127.1	3942	3_0^2
$HC_{11}H$				$A^3\Sigma_u^- \leftarrow X^3\Sigma_g^-$
1	653.67	15293.4	0.0	0_0^0
3	579.03	17265.3	1972	3_0^1
5	519.91	19229.5	3936	3_0^2
7	471.88	21185.9	5893	3_0^3
$HC_{13}H$				$A^3\Sigma_u^- \leftarrow X^3\Sigma_g^-$
1	718.36	13916.7	0.0	0_0^0
3	629.70	15874.5	1958	4_0^1
5	562.68	17767.3	3851	4_0^2
	281.82	35473	0.0	$B^3\Sigma_u^- \leftarrow X^3\Sigma_g^-$
$HC_{19}H$				$B^3\Sigma_u^- \leftarrow X^3\Sigma_g^-$
	339.20	29481	0.0	0_0^0

due to excessive background with 157 nm or 193 nm. An upper limit of 8.0 eV may thus be placed on the IP of this species.

3. $HC_{11}H$

The R2C2PI spectrum of $HC_{11}H$ is shown in Fig. 4. There is a vibrational progression to higher energy of three quanta. Each band is twinned with a smaller counterpart 90 cm^{-1} to the red. This structure was not observed in the origin region, and thus its assignment is not clearly a hot-band.

Bands 5 and 7 have not been observed before and are assigned to the 3_0^n progression. The observed position of band 3, 3_0^1 , (579.04 nm) differs by nearly 1 nm from that observed by CRD spectroscopy [579.907(10) nm].¹⁸ The IP of $HC_{11}H$ is expected to be lower than that of HC_9H , but it likely to be greater than 7.9 eV (157 nm).

4. $HC_{13}H$

The R2C2PI spectrum of $HC_{13}H$ is similar to that of $HC_{11}H$ and is shown in Fig. 4. There is a stretching progression consisting of twin peaks, as above. The spacing in this case is 65 cm^{-1} , the lower energy peak assumed to be a hot-band. Band 5 is observed for the first time in the gas phase and is assigned to 4_0^2 , the acetylenic stretch. An upper limit of 8.15 eV may be placed on the IP of $HC_{13}H$ since its $A^3\Sigma_u^- \leftarrow X^3\Sigma_g^-$ spectrum could be measured using 193 nm as the ionizing wavelength. Most likely, though, it is below the 8.0 eV limit determined for HC_9H .

V. ASTRONOMICAL IMPLICATIONS

The visible electronic spectra in the gas-phase provide a database for an astronomical search. However, the observed electronic spectra do not precisely match any known DIBs.⁴⁰ This does not necessarily mean that these species do not exist in the ISM. An upper limit of the column density can be estimated for the molecules in diffuse clouds. The oscillator strengths of the 0–0 band of the observed $A^3\Sigma_u^- \leftarrow X^3\Sigma_g^-$ electronic transitions have been calculated to be in the range 0.02–0.001. Assuming an equivalent width of $1\text{ m}\text{\AA}$ (sensitivity limit of DIB's detection),⁴¹ the upper limit of column densities of $HC_{2n+1}H$ in such diffuse clouds would be 10^{13} cm^{-2} . Since the column density of $l\text{-C}_3H$ is determined as $5 \times 10^{12}\text{ cm}^{-2}$ in a dark cloud (TMC-1) and $< 8.7 \times 10^{11}\text{ cm}^{-2}$ in diffuse clouds⁴² and those of $l\text{-C}_5H$ and $l\text{-C}_7H$ in TMC-1 have been reported as $\sim 5.8 \times 10^{12}\text{ cm}^{-2}$ and $< 1.5 \times 10^{11}\text{ cm}^{-2}$, respectively,^{8,43,44} and if one assumes that the $l\text{-C}_{2n+1}H$ chains are produced by photodissociation of $HC_{2n+1}H$, the estimated upper limit of column densities of $HC_{2n+1}H$ ($n=3-6$) seem to be reasonable.

The similarity between the band profile of the $B^3\Sigma_u^- \leftarrow X^3\Sigma_g^-$ transition and that of 4428 \AA DIB band shows that the $B^3\Sigma_u^- \leftarrow X^3\Sigma_g^-$ transitions of the long odd polyene chains fit the constraints imposed by the profile of some broad strong DIBs. The larger members of the odd polyene chains may be considered candidates as carriers of some of the broad and strong DIBs.

ACKNOWLEDGMENT

This work has been supported by the Swiss National Science Foundation (Project No. 20-100019).

- ¹K.-H. Homann, *Angew. Chem., Int. Ed. Engl.* **37**, 2434 (1998).
- ²T. Fujii and M. Kareev, *J. Appl. Phys.* **89**, 2543 (2001).
- ³T. Henning and F. Salama, *Science* **282**, 2204 (1998).
- ⁴H. W. Kroto, J. R. Heath, S. C. O'Brian, R. F. Curl, and R. E. Smalley, *Astrophys. J.* **314**, 352 (1987).
- ⁵J. P. Maier, G. A. H. Walker, and D. A. Bohlender, *Astrophys. J.* **566**, 332 (2002).
- ⁶E. F. van Dishoeck and J. H. Black, *Astrophys. J., Suppl. Ser.* **62**, 109 (1986).
- ⁷J. P. Maier, N. M. Lakin, G. A. H. Walker, and D. A. Bohlender, *Astrophys. J.* **553**, 267 (2001).
- ⁸M. B. Bell, P. A. Feldman, J. K. G. Watson, M. C. McCarthy, M. J. Travers, C. A. Gottlieb, and P. Thaddeus, *Astrophys. J.* **518**, 740 (1999), and references therein.
- ⁹M. C. McCarthy, M. J. Travers, A. Kovacs, C. A. Gottlieb, and P. Thaddeus, *Astrophys. J., Suppl. Ser.* **113**, 105 (1997).
- ¹⁰M. C. McCarthy, W. Chen, M. J. Travers, and P. Thaddeus, *Astrophys. J., Suppl. Ser.* **129**, 611 (2000), and references therein.
- ¹¹S. J. Kim, J. Caldwell, R. A. Rivolo, R. Wagener, and S. G. Orton, *Icarus* **64**, 233 (1985).
- ¹²F. Stahl, P. V. Schleyer, H. F. Schaefer, and R. I. Kaiser, *Planet. Space Sci.* **50** (2002).
- ¹³V. G. Kunde, A. C. Aikin, R. A. Hanel, D. E. Jennings, W. C. Maguire, and R. E. Samuelson, *Nature (London)* **292**, 686 (1981).
- ¹⁴T. Pino, H. Ding, F. Güthe, and J. P. Maier, *J. Chem. Phys.* **114**, 2208 (2001).
- ¹⁵H. Ding, T. Pino, F. Güthe, and J. P. Maier, *J. Chem. Phys.* **115**, 6913 (2001).
- ¹⁶H. Ding, T. Pino, F. Güthe, and J. P. Maier, *J. Chem. Phys.* **117**, 8362 (2002).
- ¹⁷J. Fulara, P. Freivogel, D. Forney, and J. P. Maier, *J. Chem. Phys.* **103**, 8805 (1995).
- ¹⁸C. Ball, M. C. McCarthy, and P. Thaddeus, *Astrophys. Lett.* **525**, L61 (2000).
- ¹⁹A. Mavrandonakis, M. Mühlhäuser, G. E. Froudakis, and S. D. Peyerimhoff, *Phys. Chem. Chem. Phys.* **4**, 3318 (2002).
- ²⁰G. Mpourmpakis, M. Mühlhäuser, G. E. Froudakis, and S. D. Peyerimhoff, *Chem. Phys. Lett.* **356**, 398 (2002).
- ²¹M. Mühlhäuser, J. Haubrich, and S. D. Peyerimhoff, *Chem. Phys.* **280**, 205 (2002).
- ²²M. J. Frisch *et al.*, GAUSSIAN 98, Revision A.7, Gaussian, Inc., Pittsburgh, PA, 1998.
- ²³M. Head-Gordon and T. Head-Gordon, *Chem. Phys. Lett.* **220**, 122 (1994); M. J. Frisch, M. Head-Gordon, and J. A. Pople, *ibid.* **166**, 275 (1990); **166**, 281 (1990); J. A. Pople, R. Krishnan, H. B. Schlegel, and J. S. Binkley, *Int. J. Quantum Chem., Quantum Chem. Symp.* **13**, 325 (1979); N. C. Handy and H. F. Schaefer III, *J. Chem. Phys.* **81**, 5031 (1981); C. Moller and M. S. Plesset, *Phys. Rev.* **46**, 618 (1934).
- ²⁴A. D. Becke, *J. Chem. Phys.* **98**, 5648 (1993); **97**, 9173 (1992); **96**, 2155 (1992); C. Lee, W. Yang, and R. G. Parr, *Phys. Rev. B* **37**, 785 (1988).
- ²⁵G. A. Petersson and M. A. Al-Laham, *J. Chem. Phys.* **94**, 6081 (1991); G. A. Petersson, A. Bennett, T. G. Tensfeldt, M. A. Al-Laham, W. A. Shirley, and J. Mantzaris, *ibid.* **89**, 2193 (1988).
- ²⁶The equilibrium ground state geometries and harmonic vibrational frequencies of HC_{2n+1}H ($n=2-9$) are available from the authors on request.
- ²⁷MOLPRO is a package of *ab initio* programs written by H.-J. Werner and P. J. Knowles, with contributions from others, see www.tc.bham.ac.uk/molpro
- ²⁸H. J. Werner and P. J. Knowles, *J. Chem. Phys.* **82**, 5053 (1985).
- ²⁹P. J. Knowles and H. J. Werner, *Chem. Phys. Lett.* **115**, 259 (1985).
- ³⁰M. J. S. Dewar and H. C. Longuet-Higgins, *Proc. Phys. Soc., London, Sect. A* **67**, 795 (1954).
- ³¹H. C. Longuet-Higgins and J. A. Pople, *Proc. Phys. Soc., London, Sect. A* **68**, 591 (1955).
- ³²T. W. Schmidt, A. E. Boguslavskiy, H. Ding, T. Pino, and J. P. Maier, *Int. J. Mass Spectrom. (in press)*.
- ³³T. P. Snow, D. Zukowski, and P. Massey, *Astrophys. J.* **578**, 877 (2002).
- ³⁴M. Jungen and R. Xu, *Z. Phys. Chem. (Munich)* **217**, 105 (2003).
- ³⁵M. Hanrath, S. D. Peyerimhoff, and F. Grein, *Chem. Phys.* **249**, 121 (1999).
- ³⁶J. Haubrich, M. Mühlhäuser, and S. D. Peyerimhoff, *Phys. Chem. Chem. Phys.* **4**, 2891 (2002).
- ³⁷Z. X. Cao and S. D. Peyerimhoff, *Phys. Chem. Chem. Phys.* **3**, 1403 (2001).
- ³⁸J. Haubrich, M. Mühlhäuser, and S. D. Peyerimhoff, *J. Phys. Chem. A* **106**, 8201 (2002).
- ³⁹M. Jungen, *Chem. Phys.* **2**, 367 (1973).
- ⁴⁰S. Ó. Tuairisg, J. Cami, B. H. Foing, P. Sonnentrucker, and P. Ehrenfreund, *Astron. Astrophys., Suppl. Ser.* **142**, 225 (2000).
- ⁴¹L. Spitzer, *Physical Processes in the Interstellar Medium* (Wiley, New York, 1978).
- ⁴²R. Lucas and H. S. Liszt, *Astron. Astrophys.* **358**, 1069 (2000).
- ⁴³J. Cernicharo, C. Kahane, J. Gomez-Gonzalez, and M. Guélin, *Astron. Astrophys.* **167**, L5 (1986).
- ⁴⁴M. Guélin, J. Cernicharo, M. J. Travers, M. C. McCarthy, C. A. Gottlieb, P. Thaddeus, M. Ohishi, S. Saito, and S. Yamamoto, *Astron. Astrophys.* **317**, L1 (1997).

List of publications during PhD study

- [1] A. E. Boguslavskiy and J. P. Maier. Gas phase electronic spectra of the carbon chains C_5 , C_6 , C_8 , and C_9 . *J. Chem. Phys.*, 125, 2006. in press.
- [2] A. E. Boguslavskiy, A. Dzhonson, and J. P. Maier. Electronic spectra of carbon chains, rings and ions of relevance to astrophysics. In *Proceeding Pacificchem Symposium "Astrochemistry"*, 2006. in press.
- [3] A. E. Boguslavskiy, H. Ding, and J. P. Maier. Gas-phase electronic spectra of C_6NH_2 and C_8NH_2 . *Int. J. Mass Spectrom.*, 249: 317–320, 2006.
- [4] J. P. Maier, A. E. Boguslavskiy, H. B. Ding, G. A. H. Walker, and D. A. Bohlender. The gas phase spectrum of cyclic C_{18} and the diffuse interstellar bands. *Astrophys. J.*, 640: 369–372, 2006.
- [5] A. E. Boguslavskiy, H. Ding, and J. P. Maier. Gas-phase electronic spectra of C_{18} and C_{22} rings. *J. Chem. Phys.*, 123: 034305, 2005.
- [6] H. Ding, A. E. Boguslavskiy, and J. P. Maier. Gas phase electronic spectra of two C_5H_5 radical isomers. *Phys. Chem. Chem. Phys.*, 7: 888–891, 2005.
- [7] H. Ding, A. E. Boguslavskiy, T. W. Schmidt, and J. P. Maier. Gas phase electronic spectrum of the nitrogen terminated nanowire $NC_{16}N$. *Chem. Phys. Lett.*, 392: 225–228, 2004.
- [8] M. Araki, H. Linnartz, P. Kolek, H. Ding, A. Boguslavskiy, A. Denisov, T. W. Schmidt, T. Motylewski, P. Cias, and J. P. Maier. New laboratory data on a molecular band at 4429 Å. *Astrophys. J.*, 616: 1301–1310, 2004.
- [9] A. Denisov, T. W. Schmidt, A. E. Boguslavskiy, H. Ding, A. Araki, and J. P. Maier. Sulfur terminated nanowires in the gas phase: laser spectroscopy and mass spectrometry. *Int. J. Mass Spectrom.*, 233: 131–136, 2004.
- [10] T. W. Schmidt, H. Ding, A. E. Boguslavskiy, T. Pino, and J. P. Maier. Methyl substitution in hydrocarbon discharge chemistry: Diagnosis by laser spectroscopy. *J. Phys. Chem. A*, 107: 6550–6553, 2003.
- [11] T. W. Schmidt, A. E. Boguslavskiy, T. Pino, H. Ding, and J. P. Maier. Optical detection of C_9H_3 , $C_{11}H_3$, and $C_{13}H_3$ from a hydrocarbon discharge source. *Int. J. Mass Spectrom.*, 228: 647–654, 2003.
- [12] H. Ding, T. W. Schmidt, T. Pino, A. E. Boguslavskiy, F. Guthe, and J. P. Maier. Gas phase electronic spectra of the linear carbon chains $HC_{2n+1}H$ ($n=3-6,9$). *J. Chem. Phys.*, 119: 814–819, 2003.

Curriculum vitae of the author

Personal details:

Name: Andrey E. Boguslavskiy
Born: January 30, 1978, Novosibirsk, Russia
Current address: Muelhauserstrasse 86, CH-4056 Basel, Switzerland
Phone: +41 77 417 6203
e-mail: A.Boguslav@unibas.ch

Education:

2001-06 Doctorate Degree (Ph.D.) in Physical Chemistry, July 2006

Chemistry Department, University of Basel, Switzerland

Thesis title: "Gas-phase electronic spectroscopy of highly unsaturated hydrocarbons by resonance enhanced multiphoton ionization."

Supervisor: Prof. John P. Maier FRS

1999-01 Master degree (M.Sc.) in Physics, Summer 2001

Physics Department, Novosibirsk State University, Russia.

Thesis title: "Experimental study of nonlinear resonances in Rb atoms in multiple lasers field"

Supervisor: Dr. Igor I. Ryabtsev.

Work passed in: Laboratory of Nonlinear Resonant Processes and Laser Diagnostics in Quantum Division of Institute of Physics of Semiconductors (ISP), Novosibirsk, Russia

1994-99 Bachelor degree(B.Sc.) in Physics, Summer 1999

Physics Department, Quantum optics speciality, Novosibirsk State University, Russia

Thesis title: "Investigation of the sub-doppler resonances in spectroscopy of Rb D₂-line in weak magnetic fields."

Supervisors: Vasily M. Entin and Prof. Igor M. Beterov.

Work passed in: Laboratory of Nonlinear Resonant processes and Laser Diagnostics in Quantum Division of Institute of Physics of Semiconductors (ISP), Novosibirsk, Russia

1984-94 Secondary school 162 in Novosibirsk, Russia

Teaching experience

Laboratory course instructor of Physical Chemistry, Department of Chemistry, University of Basel, 2003-present.

Languages

English - spoken, written. Russian - native.

Experience with

Time-of-Flight mass spectrometry, high vacuum apparatus, range of ns-pulsed lasers (YAGs, excimer, dye, OPO), cw semiconductor lasers, VUV generation (in cell), discharge and ablation molecular sources

Computer skill

Software experience: Gaussian 98, Origin 6.1, CorelDraw, LaTeX, Mathematica, MS Office;

Programming: LabView, C